University of Bath

PHD

Metallic glasses for pulse compression

Sheard, Simon M.

Award date:
1989

Awarding institution:
University of Bath

Link to publication

Alternative formats
If you require this document in an alternative format, please contact:
openaccess@bath.ac.uk

Copyright of this thesis rests with the author. Access is subject to the above licence, if given. If no licence is specified above, original content in this thesis is licensed under the terms of the Creative Commons Attribution-NonCommercial 4.0 International (CC BY-NC-ND 4.0) Licence (https://creativecommons.org/licenses/by-nc-nd/4.0/). Any third-party copyright material present remains the property of its respective owner(s) and is licensed under its existing terms.

Take down policy
If you consider content within Bath's Research Portal to be in breach of UK law, please contact: openaccess@bath.ac.uk with the details. Your claim will be investigated and, where appropriate, the item will be removed from public view as soon as possible.

Download date: 04. May. 2023

METALLIC GLASSES FOR PULSE COMPRESSION

Submitted by Simon M. Sheard

for the degree of PhD

of the University of Bath

1989

COPYRIGHT

Attention is drawn to the fact that copyright of this thesis rests with its author. This copy of the thesis has been supplied on condition that anyone who consults it is understood to recognise that its copyright rests with its author and that no quotation from the thesis and no information derived from it may be published without the prior written consent of the author.

This thesis may be made available for consultation within the University Library and may be photocopied or lent to other libraries for the purposes of consultation.

UMI Number: U020215

All rights reserved

INFORMATION TO ALL USERS
The quality of this reproduction is dependent upon the quality of the copy submitted.

In the unlikely event that the author did not send a complete manuscript
and there are missing pages, these will be noted. Also, if material had to be removed,
a note will indicate the deletion.

UMI U020215
Published by ProQuest LLC 2014. Copyright in the Dissertation held by the Author.
Microform Edition © ProQuest LLC.
All rights reserved. This work is protected against
unauthorized copying under Title 17, United States Code.

ProQuest LLC
789 East Eisenhower Parkway
P.O. Box 1346
Ann Arbor, MI 48106-1346

UNIVERSITY OF BATH
LIBRARY
24 12 FEB 1990
Ph.D.
5037469

To Christine

Everything that happens, happens as it should, and if you observe carefully, you will find this to be so.

Marcus Aurelius Antonius, 121-180

PREFACE

This document describes work carried out in the School of Physics at Bath University, between July 1986 and July 1989. The project was wholly funded by British Aerospace and was supervised by Dr M.R.J. Gibbs. The work described in this document is original and is my own work, except where credited to others.

My chief thanks are due to my supervisor Dr Mike Gibbs for all his patience, enthusiasm, encouragement and trust. I would also like to thank Drs R.K. Avery and N. Seddon of British Aerospace, Ken for the initial work on the ac and pulse measurement systems and Nigel for arranging access to the pulse equipment and for helpful discussion regarding the pulse measurements. Additional thanks are due to Prof. K. Overshott, Mr P.T. Squire, Mr. D.W Rees, Mr A.P. Thomas, Mr M. Tatar and to Miss C. Swain.

Parts of this work have been presented at the following conferences and in the following papers:

Sheard, S.M., Gibbs, M.R.J. and Avery, R.K., J. Magn. Magn. Mat. 75, (1988), 397.

Sheard, S.M., Gibbs, M.R.J. and Avery, R.K., J. Appl. Phys. 64(10), (1988), 6035.

Squire, P.T., Sheard, S.M., Carter, C.H. and Gibbs, M.R.J., J. Phys. E: Sci. Instrum. 21, (1988), 1167.

Sheard, S.M., Gao Wei, Gibbs, M.R.J. and Cantor, B., J. Magn. Magn. Mat. 78, (1989), 347.

Sheard, S.M., Gibbs, M.R.J., Avery, R.K. and Seddon, N. Submitted to EMMA 1989.

Informal Rapid Solidification Conference, Surrey, September, 1986.

UK Informal Conference on Rapid Solidification, Cambridge, 1988.

4th Joint MMM-Intermag Conference, Vancouver, 1988.

IEEE Current Research in Applied Magnetism Meeting, Preston, 1988.

UK Magnetics Club Meeting, Sheffield, 1988.

ABSTRACT

The project concerns the optimisation of metallic glasses for use as saturable inductors in a pulse compression system. This thesis briefly describes the history of metallic glasses and outlines the possible advantages offered by this class of materials under ac and pulse conditions. The principles of operation of a Melville pulse compression line are also discussed.

In contrast to much of the work in the literature, the emphasis in this project was on understanding the effects of various post production treatments on the fundamental magnetic properties of metallic glasses, and using this information to determine what treatments should be used to attain the best possible pulse performance from a given alloy. To this end, magnetic characterisation was carried out under three measurement regimes - dc, sinusoidal field ac and resonant charging pulse conditions. Two metallic glass alloys were studied, one magnetostrictive and one non-magnetostrictive (METGLAS 2605-SC and VAC 6030 respectively). The results obtained on both materials indicate that, although the ideal dc loop shape required for Saturating Wave-type reversal may be approached by longitudinally field annealing the toroidal cores, the effect of this on the pulse behaviour is to reduce the number of walls available for the reversal and thus increase the pulse loss and decrease the pulse permeability. Several other post production treatments were investigated with the objective of improving the pulse characteristics of these alloys.

The effects of core resonances on the ac and dc behaviour of metallic glass toroids and the effects of controlled oxidation and crystallisation on the dc properties of straight strip samples were also investigated.

NOMENCLATURE

a	.. Domain Wall Spacing
A	.. Exchange Constant / Area
b	.. Shape Factor for H Waveform
B	.. Induction
ΔB	.. Flux Swing
C	.. Capacitance
d	.. thickness
E	.. Young's Modulus / Energy Loss
E_m	.. Magnetisation Energy
F	.. Force
g	.. Gain per stage
G	.. Total Gain
H	.. Field
H_c	.. Coercivity
I	.. Current
K	.. Anisotropy
L	.. Inductance
M	.. Magnetisation
n	.. Number of Compression Stages
N	.. Number of Wraps of Ferromagnetic Tape
N_p	.. Number of Primary Turns
N_s	.. Number of Secondary Turns
q	.. Charge
r	.. Core Radius
R	.. Resistance / Domain Radius
T	.. Temperature / Resonant Charging Time
T_c	.. Curie Temperature
T_x	.. Crystallisation Temperature
t	.. Time
V	.. Voltage
v	.. Core Volume
w	.. Ribbon Width
Z	.. Impedance

Δ	.. Change in..
ω	.. Angular Resonant Charging Frequency
σ	.. Electrical Conductivity / Stress
ρ	.. Electrical Resistivity / Density
λ	.. Magnetostriction
ϕ	.. Flux / General Angle
θ	.. General Angle
μ	.. Permeability

SUBSCRIPTS

bd	.. Bar Domains
m	.. Maximum
p	.. Pulse
pr	.. Probe
r	.. Remanent
s	.. Saturation
sw	.. Saturating Wave (Sandwich Domains)

CONTENTS

CHAPTER 1

1 An Introduction to Metallic Glasses

This chapter will give a brief history of amorphous alloys and will describe some of the production techniques available. Some of the unique properties, both magnetic and non-magnetic, exhibited by these materials will also be discussed. Finally, current and possible future applications will be reviewed.

1.1 A Brief History

The first reported production of an amorphous metallic alloy seems to be in some doubt. O'Handley (1987) refers to the observations of Brill (1930) while other authors (Luborsky,1983) claim that the production of a range of amorphous metallic alloys was first reported in 1934 by Kramer. Brenner and Riddell (1946), and Brenner, Couch and Williams (1950) subsequently reported the production of electro-deposited Ni-P alloys. Two years later, Buckel and Hilsch (1952) reported the first production of superconducting amorphous films. However, although high phosphorous amorphous alloys have subsequently been used for wear and corrosion resistent coatings, little interest in the amorphous metallic state was

stimulated until 1960. In this year, a method of producing these materials in 'bulk' by direct quenching from the melt was discovered by Klement, Willens and Duwez (1960). The technique used involved impacting a small drop of molten alloy onto a cold surface. This was later to become known as 'splat-cooling'. It was also in 1960 that Gubanov (Gubanov,1960) predicted, theoretically, that ferromagnetic amorphous alloys were possible. Until then it had been thought that the absence of long range order precluded the existence of magnetic ordering. The predicted ferromagnetic properties were confirmed five years later when Mader and Norwick (1965) successfully produced a vacuum deposited ferromagnetic Co-Au alloy.

There followed an enormous research effort into the production and study of amorphous metallic alloys. The following sections will describe briefly the production routes now available and some of the important magnetic and mechanical characteristics of these materials.

1.2 Production Methods

The routes available for the production of amorphous metals can be divided into three categories

- direct quenching, deposition techniques and local melting/rapid resolidification.

The first amorphous alloys reported were produced by vapour and electro-deposition techniques. These techniques, however, are useful only where small volumes of material are required or when high effective quench rates are needed. The high quench rates attainable (greater than 10^{8}°C/s (Liebermann, 1983)) allow the production of amorphous alloy compositions which cannot be produced by direct quenching. These techniques also allow the production of multi-layered structures.

Higher quench rates still (up to 10^{14}°C/s can be attained using laser or electron beam glazing or ion bombardment techniques (Liebermann,1983). These techniques involve the melting of a small area of sample surface followed by rapid resolidification. This is primarily a surface treatment and bulk amorphous samples can only be produced for very thin specimens.

Amorphous metals produced by the routes described above are simply referred to by the generic labels amorphous metals or amorphous alloys. Alloys produced by direct quenching from the melt are usually termed

metallic glasses. The production process used for the formation of a metallic glass sample, varies depending on the final sample geometry required. Techniques range from atomisation and spark erosion for the production of powder samples to planar flow casting for the production of continuous, uniform ribbons and tapes. The melt spinning technique is the basis for most amorphous ribbon production and will be described below.

The melt spinning technique was patented by Strange and Pim in 1908 (cited by O'Handley, 1987) and was proposed for amorphous ribbon production by Pond and Maddin (1969). A schematic of the melt spinning wheel arrangement is shown in figure 1.1. Briefly, the production process is as follows. The required alloy is placed in a crucible and melted using induction or radio frequency heating. Gas pressure is then applied to the open end of the crucible to force the molten alloy though a hole or slit in the base of the container onto a rapidly rotating wheel. The melt puddle formed on the moving substrate acts as an alloy reservoir from which the ribbon is drawn. Cooling rates of up to 10^{6} °C/s can be achieved using this arrangement.

The ribbon geometry depends primarily upon that of

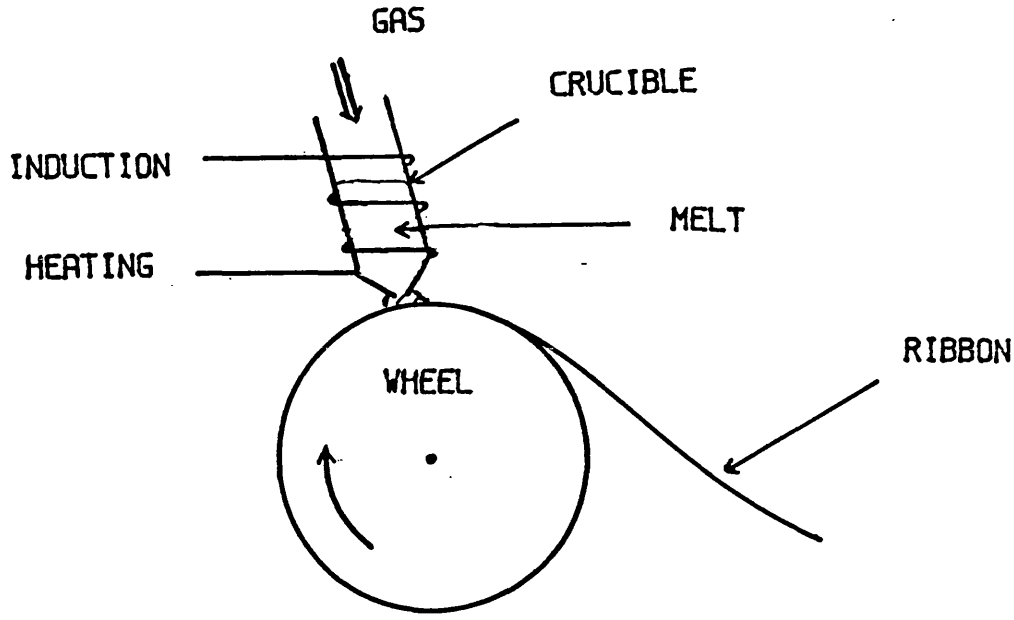

Figure 1.1 A SCHEMATIC OF THE MELT SPINNING APPARATUS

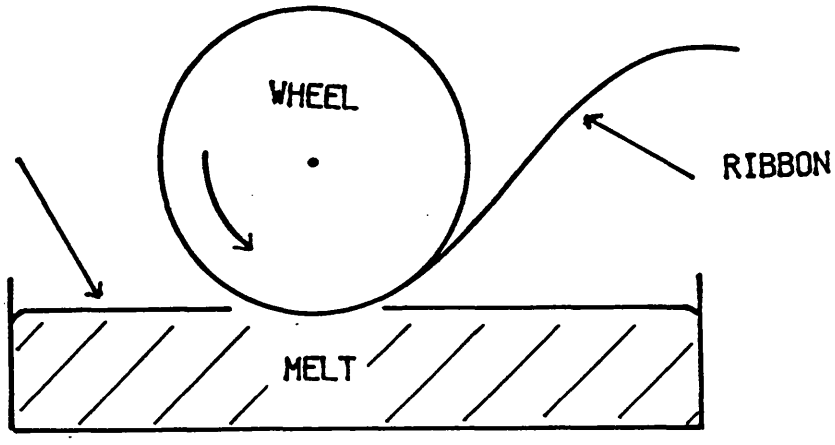

Figure 1.2 A SCHEMATIC ON THE MELT EXTRACTION APPARATUS

the melt puddle and hence that of the orifice through which the alloy is ejected. In order to produce wide ribbons, a rectangular orifice is used. The formation of a stable melt puddle then requires that the nozzle be kept in close proximity to the wheel. This is termed planar flow casting and is the technique responsible for the majority of commercially produced ribbons. Using this technique and with the nozzle-wheel separation, the ejection pressure and the wheel speed under computer control, uniform ribbons with widths of up to 25cm have been produced (Vacuumschmelze Data Sheets).

Several variations on this basic technique exist. These include the use of a double roller to produce higher initial quench rates, and the use of belts or the inside of drums as the moving substrate.

Melt extraction is a similar but little used technique. Here, the wheel skims the surface of a molten alloy bath. A thin layer of alloy solidifies on contact with the wheel and is removed from the bath in ribbon form by the spinning motion of the wheel (figure 1.2).

Further information on production techniques described here can be found in Amorphous Metallic

Alloys (ed, Luborsky,1983) and Magnetic Glasses (ed, Moorjani and Coey,1984). The samples used in this investigation were all produced by the planar flow casting technique.

1.3 Structure and Material Properties

No attempt is made here to review the large volume of information available on the structure of metallic glasses or on the attempts at modelling amorphous metals. The purpose of this section is simply to point out the special mechanical, electrical and magnetic properties of this group of materials which arise as a consequence of the absence of long range order.

The absence of long range order has two important consequences. Firstly, there can be no grain boundaries in an amorphous material. Secondly, there are many properties including the electrical resistivity and the magnetic anisotropy which are affected strongly by the crystal lattice in a conventional material. These are consequently quite different in an amorphous material. These points are discussed below.

1.3.1 Mechanical Properties

The absense of grain boundaries in metallic glasses result in a solid which is mechanically extremely hard (Davis,1976), with very high yield stresses (Cahn,1980) and high wear resistance (Whang and Giessen,1982). These materials also exhibit low coefficients of friction (Lee and Evetts,1984) and, due to the formation of a passivating surface oxide layer, good corrosion resistance (Naka, Nishi and Masumoto,1978). The initial commercial interest in these new materials was centred around these unique mechanical properties. However, for two main reasons the promise of these materials in this area has to date, not been fulfilled. The first of these is the relatively low resistance to cyclic fatigue exhibited by amorphous metals under tension (Davis,1976). The second is due to the high cooling rates required to retain the amorphous 'structure' of the liquid phase. This limits the maximum thickness of the sample to a few tens of microns, obviously excluding amorphous alloys from certain potential uses. Recently high undercooling production techniques with cooling rates of the order of $1^{\circ}C/s$ have yielded fully amorphous samples of $Pd_{40}Ni_{40}P_{20}$ with a minimum dimension of 1cm (Kui, Greer and Turnbull,1984). This method, however has not been widely reported and it is unlikely that

bars or rods made in this way will be available in the forseable future. It should also be noted that this alloy is non-magnetic.

The many magnetic applications of these materials (Raskin and Smith,1983) are now of far greater commercial interest than their mechanical properties and in several areas metallic glasses are now replacing silicon iron, ferrites and the permalloys.

1.3.2 Magnetic properties

One of the main advantages of metallic glasses over conventional magnetic materials is that the magnetic properties vary considerably and smoothly with the composition of the glass, the production technique and parameters and the post production history of the glass. Thus it is possible to 'tailor' the magnetic behaviour to those required for a particular application (Boll, Hilzinger and Warlimont, 1983). In particular, the absence of magneto-crystalline anisotropy means that the magnetic anisotropy of metallic glass samples, can be largely controlled by simple heat treatments. This will be discussed further in section 1.4.3. In addition to this versatility, metallic glasses have a number of other advantages over conventional magnetic materials.

These include very high electrical resistivities - typically twice those of crystalline alloys resulting in lower eddy current losses in ac applications (Boll, Hilzinger and Warlimont,1983). The strength and general physical form of the metallic glasses produced by the melt spinning process can also be an advantage. For example, the thin strip form of the as-received alloy is advantageous in ac applications, again because of the associated decrease in the eddy current losses.

1.4 Control of the magnetic properties

Having indicated that the magnetic properties of this class of materials are potentially superior to those of conventional crystalline alloys, it is important to know what controls these properties. The properties of metallic glasses can be divided roughly into three groups:-

i) Those which are determined by the alloy composition and are affected little by subsequent sample treatments. For example, the Curie temperature, the saturation magnetisation and the crystallisation temperature.

ii) Those whose maximum value is determined by the composition but whose measured value depends upon the sample treatment, eg, the magnetostriction and the sample anisotropy.

iii) Those parameters which depend purely on the sample history. These include the remanence ratio, the coercivity, the magnetisation energy and the static loss.

The control of the parameters listed in groups (ii) and (iii) will be discussed in section 1.7 and 1.8. First, however, a basic knowledge of the domain theory of ferromagnetism and of the factors controlling the magnetisation process are required. These are presented below and in more detail in Cullity (1972).

1.4.1 Domains

Under conditions of zero applied field, it is rare for a ferromagnetic sample to be magnetised to saturation in any given direction - this would lead to a large magnetostatic energy. The exchange force between neighbouring moments, however acts to keep them aligned. In addition, magnetic materials are generally not isotropic (see section 1.4.3), ie, magnetisation is easier in some directions than in

others. Thus, exchange energy is stored in the sample if neighbouring moments are not parallel and anisotropy energy is stored if the sample is magnetised away from an easy direction. It is found that a reduction in the total energy of the sample can be achieved if the material divides into separate regions, each of which is magnetically saturated in a given direction. These regions are termed magnetic domains (or simply domains). Separating these regions are domain walls across which the magnetisation direction changes in a number of steps. In a real sample the position and width of the walls will depend upon energy considerations. Having divided up into domains, the sample can respond to an applied field in one of two ways - moment rotation or wall motion. Moment rotation, as its name suggests is simply the rotation of individual atomic moments from their equilibrium position towards that of the applied field. Wall motion is somewhat more complex and is described in section 1.5.

1.4.2 Magnetostriction

Fundamentally magnetostriction is caused by the asymmetry of the electron orbit of an atom in a solid. There are two models for magnetostriction - the single

and two ion models, proposed by Callen and Callen (1963,1965). A detailed knowledge of the mechanisms involved is not required here and the simple model illustrated in figure 1.3 is sufficient for the present purpose. Here, the asymmetry is depicted schematically by the ellipsoidal electron orbits. It can be seen that as the sample is magnetised, the rotation of the moments into the direction of the field produces a change in length. Two important results can be seen from this simple picture. Firstly, that the maximum value of the length change will occur if all of the atoms are initially perpendicular to the applied field direction. Secondly, if the magnetisation process takes place only by 180° domain wall motion, then the magnetostriction will be zero.

1.4.3 Anisotropy

In a conventional crystalline material, the ease of magnetisation is not the same in all directions - the material is anisotropic. There are five sources of anisotropy:- crystal, exchange, shape, stress and induced. In an amorphous material the crystal anisotropy is absent and exchange anisotropy is present only in exceptional circumstances. The anisotropy of magnetisation is therefore governed largely by the remaining three.

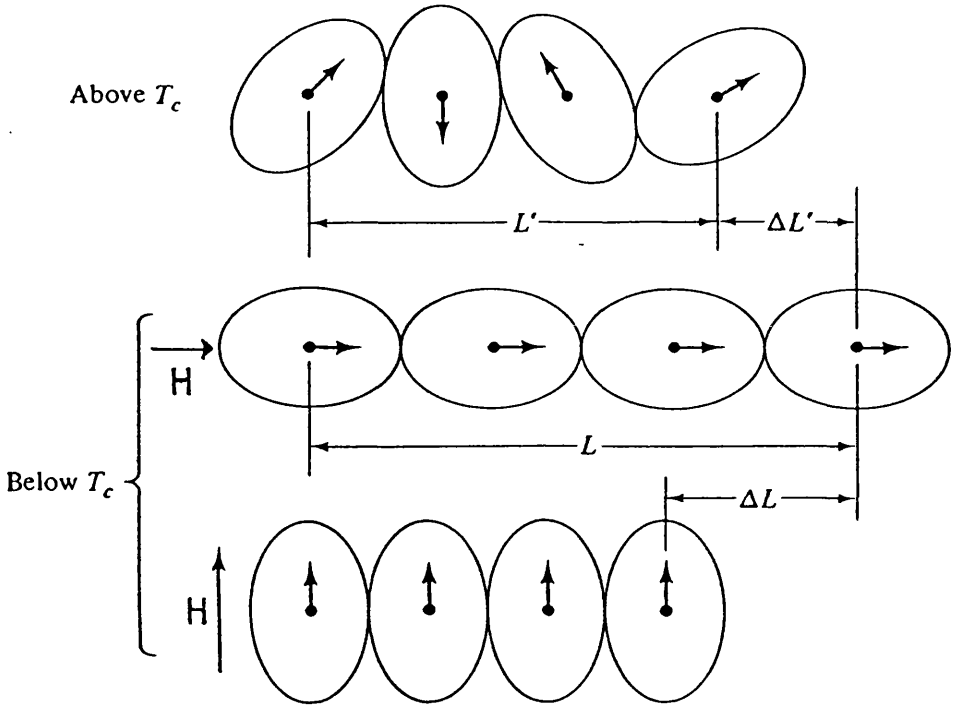

Figure 1.3 A SIMPLE MODEL OF MAGNETOSTRICTION

(after Cullity)

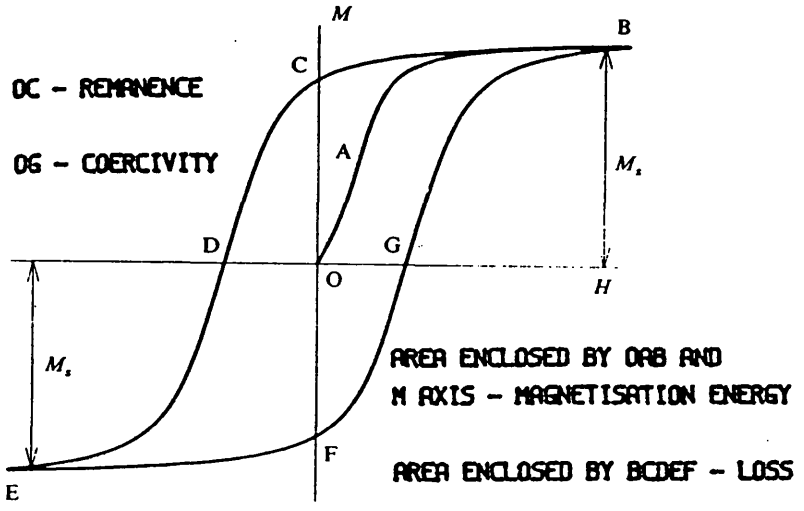

Figure 1.4 THE M-H LOOP

Shape anisotropy is related to the magnetostatic energy discussed above. When a sample is magnetised, the free poles formed at ends of the sample set up an internal field from North to South. This field acts to demagnetise the sample and is more important the closer the poles are together. Thus for any non-spherical sample this effect will produce easy and hard directions of magnetisation.

Stress anisotropy is related to the magneto-striction effect discussed in section 1.4.2. It will be remembered that a change in magnetisation can result in a length change. Conversely, an internal or externally applied strain will affect the magnetic state of a sample, creating local easy directions either parallel or perpendicular to the stress direction depending upon the sign of the magneto-striction. It should be noted that the magneto-strictive strain caused by the magnetisation of a sample will affect the sample behaviour in this way and that the magnitude of this effect depends upon the absolute value of the magnetostriction.

The final category is the externally induced anisotropy. This can be produced in several ways, for example magnetic field annealing or stress annealing. These treatments and the mechanism involved will be

discussed further in sections 1.7.2 and 1.8.1-1.8.3.

The sections above present some of the parameters which affect the magnetisation process. The following sections describe how these parameters affect the dc and ac magnetic response of a given material.

1.5 The dc M-H loop

Figure 1.4 shows a schematic of a dc hysteresis loop with the important parameters marked. The origin of these parameters will now be discussed.

Consider a sample divided by a single 180-degree domain wall (figure 1.5). If a field is applied parallel to the magnetisation direction of one of the domains, the wall will move in such a way that this domain increases in volume at the expense of the other. The static hysteresis loss and dc coercivity are caused by the irreversible jumps in magnetisation as the domain wall moves through the material (Cullity,1972). These Barkhausen jumps are caused by the variations in domain wall energy (E_w) as the wall propagates through the sample. Consider the simplified E_w-x curve for one domain wall shown in figure 1.6. The maxima and minima in the domain wall energy are caused by stresses and inhomogeneities in the material

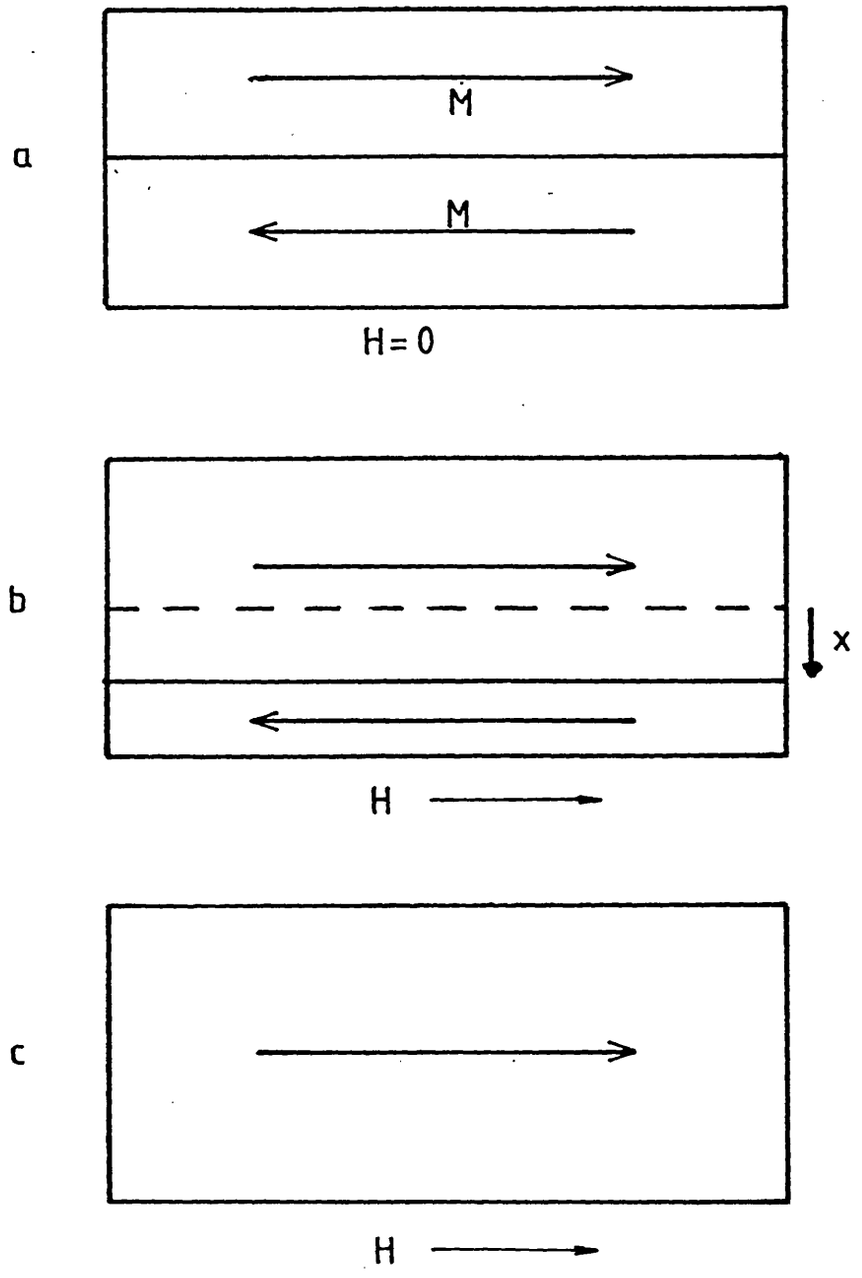

Figure 1.5 A SIMPLE SCHEMATIC ILLUSTRATING MAGNETISATION BY DOMAIN WALL MOTION

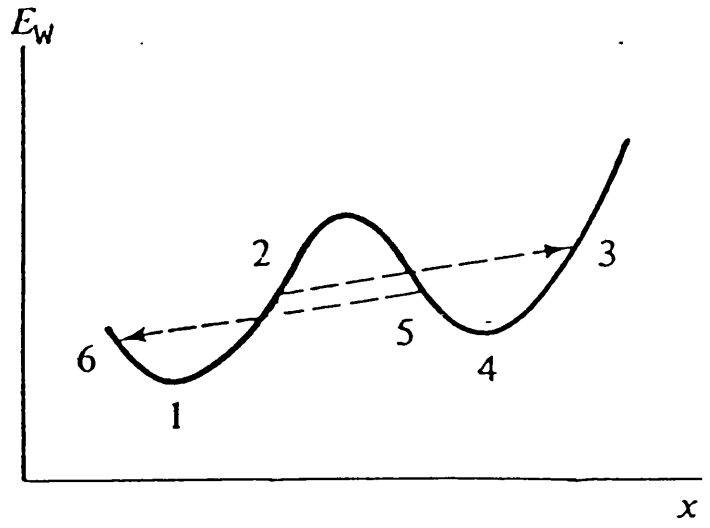

Figure 1.6 DOMAIN WALL ENERGY vs DISTANCE

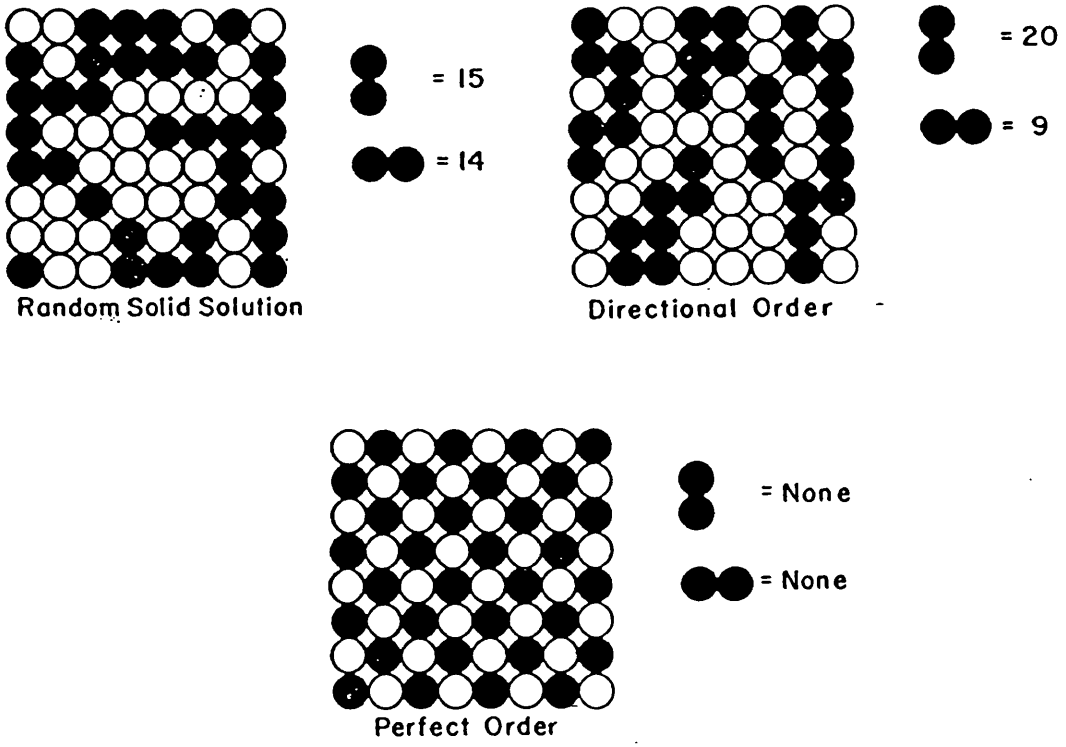

Figure 1.7 DIRECTIONAL ORDER (after Graham)

and affect the magnetisation of the sample as follows. As the applied field is increased from zero, the domain wall will move from position (1) to position (2). If the field were removed at any point in this range, the wall would move reversibly back to (1). Point (2), however, is a position of maximum energy gradient and, if this point is exceeded, the system becomes unstable and an irreversible jump to position (3) will occur. If the field were now removed the wall would return not to position (1) but to (4), the nearest position of minimum energy. A reverse field will now drive the wall via another Barkhausen jump back from (5) to (6). A hysteresis loop is therefore produced. The dc coercivity of the material, in such a simple model, is determined by the maximum energy gradients present in the material (Chen,1986) and the dc loss is caused by the eddy current loss associated with each of these tiny irreversible jumps.

The magnetisation energy is the energy required to magnetise the sample from M=0 to the saturated state, in a given direction. This is governed largely by the anisotropy of the material. For example, if a uniaxial anisotropy is assumed and, the anisotropy direction is parallel to the subsequent magnetisation direction, then a 'square' hysteresis loop will be seen and the magnetisation energy will be small. If, however, the

sample exhibits a transverse anisotropy, then a larger field is required for any given flux change, the loop will therefore be linear (or 'canted over') and hence the sample will exhibit a larger magnetisation energy.

The remanent induction is also controlled by the anisotropy and will be high if the anisotropy is parallel to the direction of magnetisation and smallest if the two are perpendicular.

1.6 The ac M-H loop

An alternating magnetic field, when applied to any electrically conducting material, will cause eddy currents to be induced in that material in such a way that the field produced by the eddy currents themselves opposes the applied field. In a non-magnetic material these eddy currents will be uniformly distributed and the ac eddy current loss can be calculated (Golding and Widdis,1933). Attempts to calculate the ac loss of a magnetic material have been made assuming total flux penetration. The total ac loss would then be the static hysteresis loss plus the macroscopic eddy current loss calculated as in the case of a non-magnetic material. It was found, however, that the sum of the so-called classical eddy current loss and the static hysteresis loss did not

account for the measured losses in magnetic materials. The difference between the two is generally referred to as the anomalous loss. It is now generally accepted that the local modification of the applied field due to microscopic eddy currents in the region of the domain walls is the principle cause of the anomalous (or excess eddy current) loss (Luborsky,1983). Some attempts have been made (Pry and Bean,1958) to calculate the energy lost assuming a simple domain structure and no wall bowing. These calculations have yielded results in better agreement with observed values. Therefore, the division of the total loss into a classical eddy current component and an anomalous component is misleading. In a real magnetic material, the concept of a classical eddy current component is no longer valid and the losses are determined by the domain structure. The exception to this occurs under ideal moment rotation conditions where the magnetisation reversal is uniform thoughout the sample.

Just as the ac loss is dependent not only on the domain wall pinning, but also on the number and distribution of walls present in the sample, so the ac coercivity and remanence ratio cannot be ascribed to a single cause. The number and orientation of walls, the anisotropy, and the wall pinning all contribute.

1.7 The effect of post production heat treatments

It has already been stated that one of the important advantages of amorphous alloys over their crystalline counterparts is that many of the magnetic properties of amorphous metals respond strongly to simple heat and mechanical treatments. Examples of these are the dc coercive field, remanence magnetisation energy and loss, the ac loss and the magnetostriction (Boll, Hilzinger and Warlimont,1983). At a fundamental level, the changes seen in these parameters are due to changes in the material anisotropy and hence the domain configuration. It should be noted that many of these parameters are strongly affected by the sample composition and sample shape (via the demagnetising effect). The magnetic properties of any given sample, however, can be tailored by various post production treatments. The effect of post-production treatments on some of the above will now be reviewed.

1.7.1 Stress relief anneal

In an as-received sample the domain geometry can be very complex (Kronmüller and Fernengel,1981). Inhomogeneities and internal stresses caused by the rapid quench (and from deformation of the sample e.g.

winding into a toroid) couple to the magnetic properties of the alloy via the magnetostriction and act as pinning centres for the domain walls making magnetisation of the sample difficult. This is reflected in the relatively high coercivities of as-cast amorphous ribbons. Luborsky, Becker and McCary (1975) were the first to show that a simple anneal can reduce this and they demonstrated that the observed changes in H_c correlated with the relief of the internal stresses. It has also been shown by direct observation (Kronmüller, Schäfer and Schroeder,1977) that annealing significantly simplifies the domain structure.

The effect of annealing on the dc properties is therefore to decrease the sample coercivity and magnetisation energy and to increase the remanence.

Under ac conditions, the remanence is again increased but the simplified domain structure and the reduction in domain wall pinning have opposite affects on the ac loss and coercivity. In a material where magnetisation reversal takes place by domain wall motion, it has been shown that the eddy current loss associated with a single moving domain wall is proportional to the wall velocity squared (Chen,1986). It is thus easy to see that under fixed dB/dt

conditions, the effect of a reduction in the number of walls will be to increase average wall velocity and hence the eddy current loss. This is also true under controlled H conditions. The reduction in loss and ac coercive field due to a reduction in the wall pinning are therefore often masked by the increase in loss caused by the reduction in walls available. This becomes worse as the excitation frequency is increased.

1.7.2 Field anneal

A more sophisticated form of heat treatment is the field anneal. If a magnetic field is applied to the sample during an anneal (below T_c), a preferential direction of magnetisation is introduced. Several mechanisms have been proposed to explain this effect. The directional ordering theory (developed by Snoek,1938,1939a,1939b,1941 and Néel,1950,1951; cited by Graham,1958) is, however, generally accepted as the dominant mechanism (Graham, 1958). This is explained below.

Consider first a two-atom solution (black and white in figure 1.7). Figure 1.7a shows a random arrangement of atoms. In this configuration, there are equal numbers of black-black and white-white neighbours.

Moreover, there are the similar numbers of vertical and horizontal black-black and white-white pairs. This should be compared with figure 1.7b which shows a perfectly ordered structure. Figure 1.7c again shows a random distribution of the 64 atoms. There are again, 29 black-black pairs but these now exhibit a definite directional order. There are 20 vertical pairs of this type but only 9 horizontal.

The effect of this type of directional ordering on the magnetic properties of a sample can be understood as follows.

If it is assumed that each atom pair has a magnetic energy which depends on the orientation of that pair, then, in the presence of a field and at temperatures below T_c but high enough for significant atom diffusion, certain atom pairs will align preferentially in the direction of the local magnetisation. This preferential arrangement will be frozen in as the temperature is decreased and will thus result in an induced anisotropy.

The effect of this treatment on the B-H loop depends on the relative directions of the anisotropy and the subsequent magnetisation (Boll, Hilzinger and Warlimont,1983). If these are uniaxial and parallel

then the resulting loop is squared up with a reduced H_c, if perpendicular, then magnetisation reversal will take place by moment rotation alone and, in the ideal case, there will be no hysteresis (Jacubovics, 1987). Some reports, however, indicate that the loop will be canted over and H_c will be larger than in the as-cast state (Boll, Hilzinger and Warlimont,1983) - see figure 1.8.

It was noted above, that a field anneal is only effective below the Curie temperature of the sample. This effect can also be observed, however, in samples annealed above T_c but cooled slowly from the anneal. In this case, the magnitude of the induced anisotropy is determined by the cool rate and the kinetics of the process. Kronmüller, Guo, Fernengel, Hofmann and Moser, (1985) and Guo, Kronmüller, Moser and Hofmann, (1986) have investigated the kinetics of field annealing $Co_{58}Ni_{10}Fe_5Si_{11}B_{16}$ isothermally at a range of different temperatures and for varying times at a given temperature. Curves of the form shown in figure 1.9 were observed.

The magnitude of the induced anisotropy, K_u, depends upon the sample composition and annealing temperature but is typically in the range $10-10^3$ J/m^3 in metallic glasses.

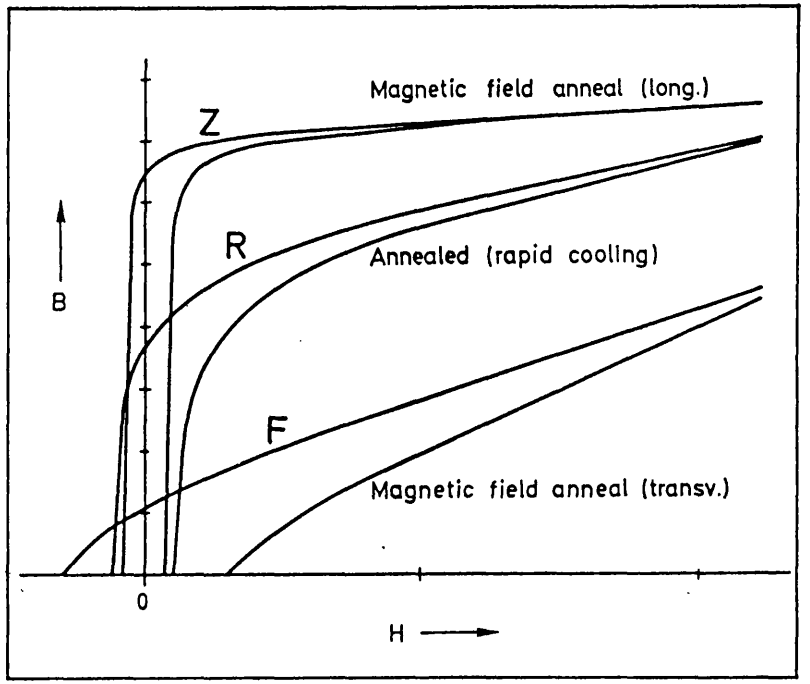

Figure 1.8 THE EFFECT OF INDUCED ANISOTROPY ON THE M-H LOOP

(after Boll et al)

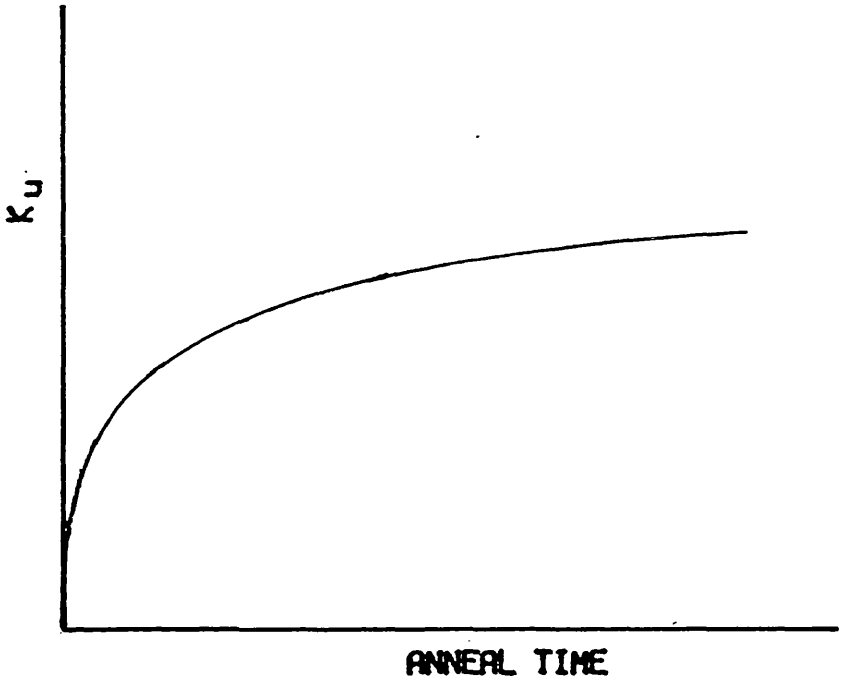

Figure 1.9 A SCHEMATIC OF THE KINETICS OF INDUCED ANISOTROPY (after Kronmuller et al)

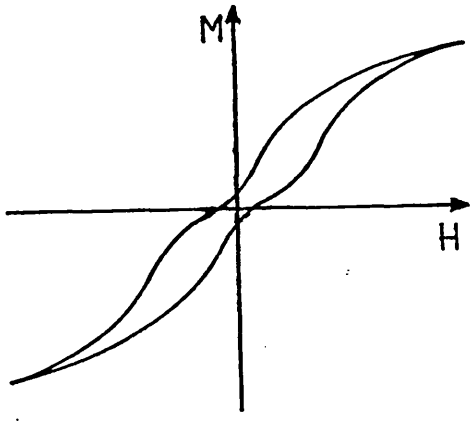

Figure 1.10 THE PERMINVAR LOOP

Extending this argument, if a sample which will respond to magnetic field annealing is annealed below its Curie point in the absence of any external field, then each domain and domain wall present will define local directions of magnetisation which will locally field anneal. Provided that other mechanisms do not interfere, the result of this will be a sample with local easy directions determined by the domain structure of the material at the anneal temperature. In other words, the sample will magnetically self-anneal. The effect of this is to produce a wasp waisted (Perminvar) loop similar to that shown in figure 1.10 (Graham,1958). If a single domain wall is considered, it can be seen that the self annealing process produces local easy axes in the directions of the individual moments within the wall itself. Thus the spin geometry and local easy axis geometry are the same. This implies that the anisotropy energy associated with the wall is a minimum with the wall in this position. As the wall is moved by an external field, the spins have to rotate away from the local easy axis and thus the wall energy increases. This effect therefore adds to the domain wall pinning by stress centres and inhomogeneities and can therefore have the effect of increasing the coercivity. This has been observed by Fujimori, Yoshimoto, Masumoto and Mitera (1981).

Note that the presence of directional order associated with induced anisotropy in no way implies the presence of crystallographic order.

A primary effect of a longitudinal field anneal is a further reduction in the number of walls present in the sample (Chen,1983). Secondary effects include a decrease in the domain wall width (since d_w depends on the anisotropy (Cullity,1972)), and a decrease in the sample magnetostriction (section 1.4.2). The reduction in the number of walls present is likely to increase the ac loss still further (see section 1.7.1). This is confirmed by the results of Yamaguchi, Yoshizawa and Nakajima (1988). These authors reported the effect of increasing the magnitude of the longitudinal component of anisotropy on the core losses of a Co-based metallic glass sample. They showed a correlation between the induced anisotropy, the resulting domain width and the subsequent core loss. The effect of the decrease in the magnetostriction has obvious consequences for the core vibration and is thus likely to significantly affect the ac behaviour of the core, particularly at high excitation frequencies. The effect of a decrease in the domain wall width on the domain wall dynamics is not known.

1.8 Other post production treatments

In addition to those described above, there are a number of other widely used treatments which are used to affect the magnetic properties of metallic glass samples. These are described in sections 1.8.1 to 1.8.3.

1.8.1 Stress annealing

In glasses with a non zero-magnetostriction a similar effect can be obtained by annealing the sample under mechanical stress (Fujimori,1983). This again causes an induced uniaxial anisotropy which affects the ease of magnetisation in a given direction. There have also been reports in the literature of the effects of stress annealing non-magnetostrictive alloys. The origin of the anisotropy induced in such a case can be attributed to the plastic and anelastic deformation of the sample (Nielsen,1985). The component due to the plastic deformation is permanent whilst the latter can be reversed by a stress relief anneal.

1.8.2 Surface treatments

Mechanical surface treatments have also been reported to have a significant effect on the dc magnetic properties of metallic glass ribbons. Small pits, bumps and scratches on the surface of a metallic glass can have a detrimental effect on the dc magnetic characteristics of a sample. The stresses introduced by surface scratching act as pinning centres impeding domain wall motion. Small strongly pinned domains are often found at these surface irregularities. The demagnetising effects caused by surface irregularities may also act as pinning sites. Mechanical and chemical polishing techniques (Luborsky,1983) have been shown to have a significant effect on the coercivity in amorphous ribbons, due to the removal of pinning sites. In contrast to this, in some cases the benefits of domain refinement and the introduction of domain wall nucleation sites, by surface scribing, can outweigh the disadvantages of an increased number of pinning centres. Core loss reductions of up to 25 percent have been reported for mechanically and laser scribed Metglas 2605-S2 excited at 60 Hz (Tan,1986).

The reported core loss reductions have all been reported on highly magnetostrictive materials. It is possible however, that the demagnetising fields

centered around surface scratches or bumps may act as wall nucleation sites in non-magnetostrictive metallic glasses. It is known, however, (Cullity,1972) that the grooves produced by surface scratching are unlikely to produce a suitable demagnetising effect. Bumps on the surface of a sample are more likely to produce the desired effect. The reason for this can be seen in figure 1.11. The demagnetising field produced around a groove is such that if a reverse field is applied to the sample, the stray field is in such a direction as to reduce the effect of the applied field to the material around the scratch and thus the scratched area is not likely to be the point at which reversal begins. The stray field caused by a protrusion from the surface, on the other hand, is in the same direction as an applied reverse field and the bump is therefore likely to reverse at a much lower field than the rest of the sample. For this reason, localised surface melting by either laser scribing or spark ablation may be more successful in producing domain refinement in this material since this type of treatment is likely to lead to small bumps on the ribbon surface as the material solidifies. Bumps and surface protrusions, however, are likely to be undesirable in high frequency applications. Under these conditions, the inter-lamina eddy current losses can be substantial and inter-lamina insulation is

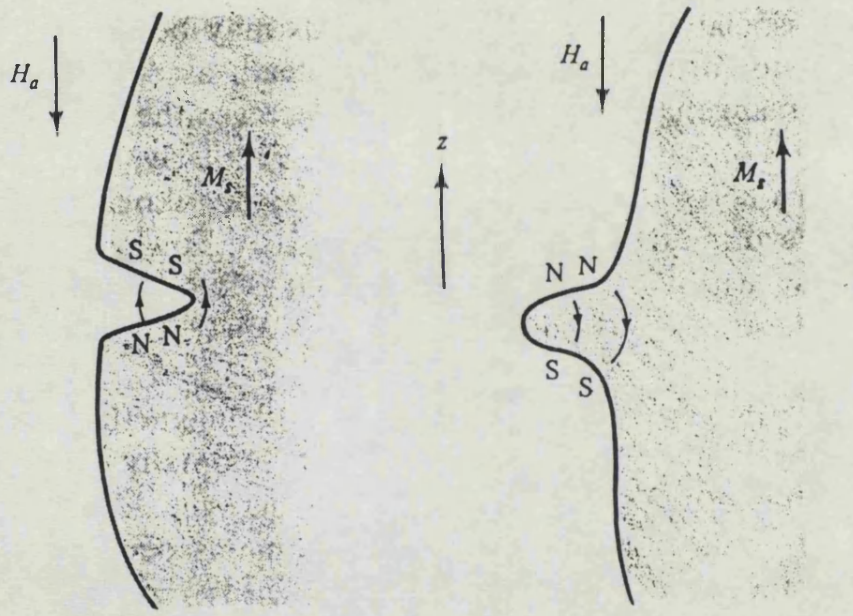

Figure 1.11 THE STRAY FIELD AROUND SURFACE FEATURES

(after Cullity)

often included. The increase in electric field intensity around a surface protrusion may exceed the breakdown field of the insulator.

1.8.3 Local crystallisation

If the annealing process is continued, eventually the material will start to crystallize. When this occurs local stresses from the amorphous/crystalline interfaces increase the dc coercivity and dc loss. The effect of the crystallite content on the ac behaviour of metallic glasses seems to depend upon the precise sample treatment. There are several reports in the literature (Datta, DeCristofaro and Davis,1981; Krause and Werner,1981; Narita, Jamasaki, Fukunago and Hata,1981; Hasegawa, Ramanan and Fish,1982) which discuss the effect of small volume fractions of crystallinity on ac performance. The results of Datta et al, (1981) and Hasegawa (1982) were obtained on several Fe-rich alloys at an induction of 0.1T and at a drive field frequency of 50kHz. Both of these papers report a decrease in the ac loss and a decrease in the exciting power required. Both also report that if the crystallinity is increased beyond an optimum, the ac loss started to increase again.

The results of Krause and Werner (1981) were

obtained under conditions which more closely approximate to those used in this investigation, namely higher induction (0.4-1.4T) and lower frequency (0.06-10kHz). At three frequencies in the range given above, the authors reported a lower ac loss at 0.4T for the sample which had started to crystallise than for a similarly treated sample annealed at a slightly lower temperature. At 1.4T, however, the loss of the partly crystallised sample was higher than that for the amorphous sample. These results were, however, obtained on transversely field annealed samples. Hasegawa et al (1982) concluded that the morphology of the crystalline precipitates is not important but the structural symmetry and magnetic characteristics of the crystallites are.

Narita et al (1981) reported a reduction in the ac loss of Fe-Co based metallic glass ribbon after local crystallisation at a measurement frequency of 20kHz and up to 1.4T. These results were obtained on ribbon which had been locally crystallised by drawing a 50 micron diameter red-heated tungsten wire across the surface. The improvement observed depended upon the spacing of the lines.

The following explanation of the effect of crystallisation on the ac behaviour of metallic glass

toroids is generally accepted. The reduction in low induction loss is due to domain refinement caused by the strain field around the crystallite sites. The additional walls introduced into the sample reduce the average wall velocity and hence the eddy current loss (section 1.7.1). The increase in observed loss as the induction level is increased, however, has not been satisfactorily exlained but may be caused by the additional energy required as the walls introduced by the crystallites are broken free of their pinning sites during the magnetisation process. The volume fraction of crystallites required for a reduction in loss is determined by the balance between the reduction in eddy current losses and the increase of the hysteresis losses (Hasagawa et al, (1982)).

1.9 Applications

Many potential applications for amorphous metals exist. The initial interest in the mechanical properties of these materials has now been superseded by the potential magnetic applications. These include magnetic field sensors, transformers, switched mode power supplies, magnetic amplifiers, switches, magnetic shields and record/playback heads. The advantages offered by amorphous materials for these applications are summarised below.

1.9.1 ac applications: transformers

The high electrical resistivity and general physical form of metallic glass strips lead to low ac eddy current losses in transformers. The advantage gained over conventional alloys increases with increasing frequency. An additional advantage is the moderately high flux swings available compared to the ferrite materials.

1.9.2 Saturating applications: switches and switched mode power supplies

Again the high electrical resistivity and thin strip form of amorphous alloys are the main advantages in this type of application. The relatively high flux swings available and the ability to easily induce a uniaxial anisotropy are, however, also very important.

1.9.3 Sensors: hydrophones and read/write heads

The main advantages of metallic glasses in these area are the ability to induce a user defined anisotropy and, particularly for read/write heads, the mechanical hardness and wear resistance exhibited by some of these alloys.

CHAPTER 2

2 Pulse Compression and Fast Magnetisation Reversal

This chapter is concerned with the use of saturable inductors in a pulse compression line. This is fundamentally a magnetic switching application. The abrupt change in permeability, and hence electrical impedance, of a ferromagnetic-cored inductor, on saturation of the core material, can be used as an electrical switch (Mathias and Williams,1955). The concept of pulse compression for use in radar pulse modulators and particle accelerators was first proposed by Melville in 1951 using a 50/50 grain oriented Ni-Fe alloy as the core material. This type of pulse generator had significant advantages over the discharge devices of the day, including greater power handling capability, higher repetition rates and the absence of shock waves (VanDevender and Reber,1981). However, improvements in thyratron and spark gap techniques coupled with the prohibitive size and cost of the magnetic switches (Stockton, Neau and VanDevender,1982) meant that until the advent of ferromagnetic metallic glasses, the potential of magnetic switches was left relatively unexplored. The advantages offered by metallic glasses include potentially low losses due to high electrical

resistivity, a large change in impedance on saturation and the ability to tailor the loop shape (see chapter 1).

This chapter will introduce the concept of the saturable inductor pulse compression technique. The associated terminology will be discussed and previous work in this field, including magnetic models, material studies and applications will be reviewed.

2.1 Pulse compression

A schematic of a possible pulse compression system is shown in figure 2.1. This arrangement is referred to as a Pulse Compression (or Melville) Line and its operation in the ideal case of perfect circuit elements is outlined in section 2.3. First, however, the transfer of charge between adjacent capacitors, in such a system, will be discussed. This process is termed 'resonant charging'.

2.2 Resonant Charging

Consider the capacitor-inductor network shown in figure 2.2. If the capacitor C_1 is charged to V_1 volts, and the switch S is then closed, the response of the circuit is described by the

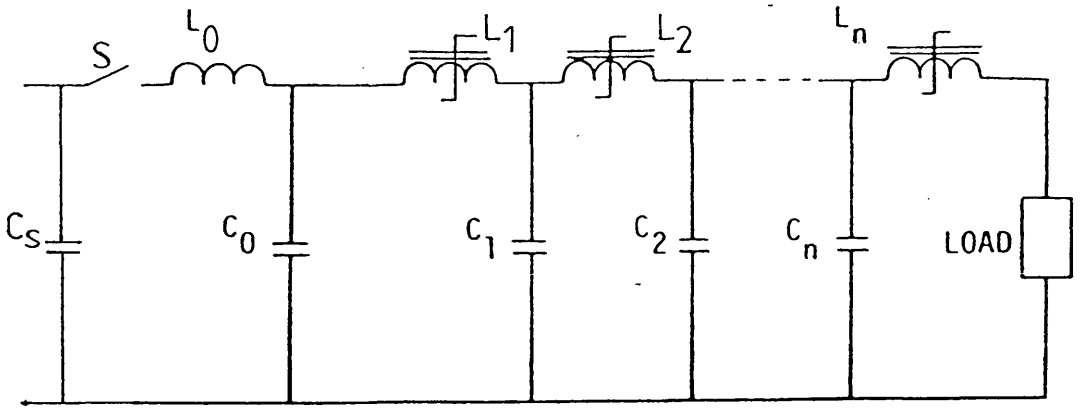

Figure 2.1 A SCHEMATIC OF A PULSE COMPRESSION (MELVILLE) LINE

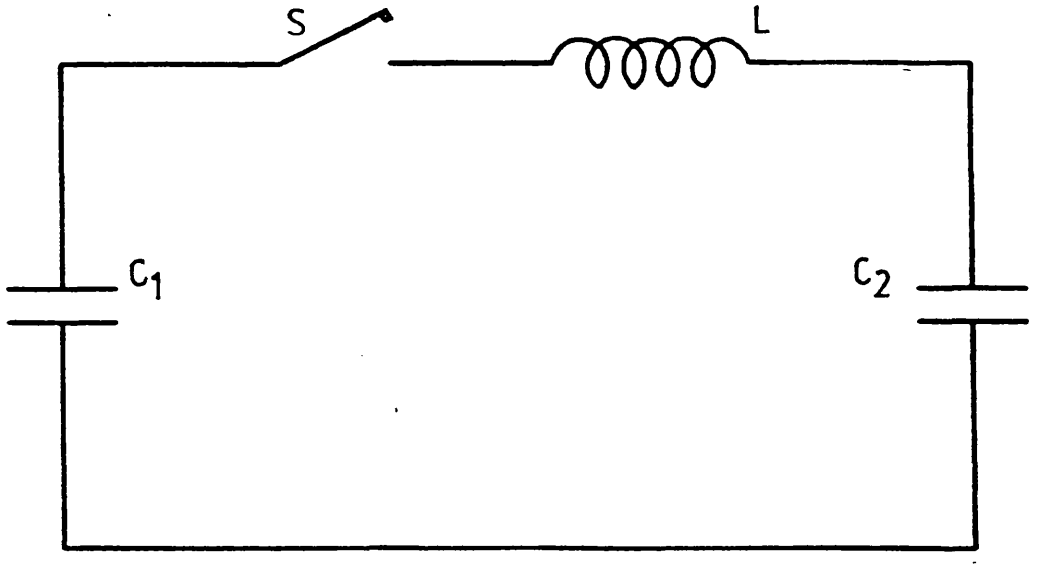

Figure 2.2 A SCHEMATIC OF THE RESONANT CHARGING CIRCUIT

differential equation

$$LdI/dt+q_1/C_1 = q_2/C_2 \qquad ..(1)$$

where q_1 is the charge initially on C_1, L is the value of the inductor and C_1 and C_2 are the capacitor values. It can easily be shown, that if the capacitors are identical, ie, $C_1=C_2=C$, this equation has the oscillatory solution

$$V_2 = V_1(1-\cos\pi t/T)/2 \qquad ..(2)$$

Where V_2 is the voltage measured across C_2. Thus when S is closed, C_1 discharges completely through L and C_2 charges fully. When the charging is complete, the process reverses and C_2 discharges fully onto C_1. The transfer of charge from C_1 to C_2 is called resonant charging and the charge oscillation will continue indefinitely if ideal circuit elements are assumed. The quantity

$$T = \pi/\omega = \pi(LC/2)^{0.5} \qquad ..(3)$$

is the resonant charging time.

If the capacitors and inductor in figure 2.2 are non-ideal, ie, they contain some resistive component

to their impedance, then equation (1) is modified as follows

$$L dI/dt + RI + q_1/C_1 = q_2/C_2 \quad ..(4)$$

and the solution is somewhat more complex

$$V_2 = V_1 [1 - e^{-R/2L} (\cos \pi t/T + (RT/2\pi L) \sin \pi t/T)]/2 \quad ..(5)$$

where T, now is given by

$$T = \pi/\omega = 2\pi [(R/L)^2 + 8/LC]^{-0.5} \quad ..(6)$$

This is a damped oscillation: eventually the total charge becomes evenly distributed between the two capacitors. Figure 2.3 shows the voltages on the capacitors C_1 and C_2 under resonant and damped resonant charging conditions. In each case, $C_1 = C_2 = 10\mu F$ and $L = 5\mu H$. In the damped case, a series resistor of 0.3Ω is included. These values were chosen to coincide approximately with those used in the experimental arrangement described in chapter 3. Note that both the resonant charging time and the form of the charging waveform are affected by the additional resistance.

By simply including extra terms in equation (4), this analysis can be extended to include the effects

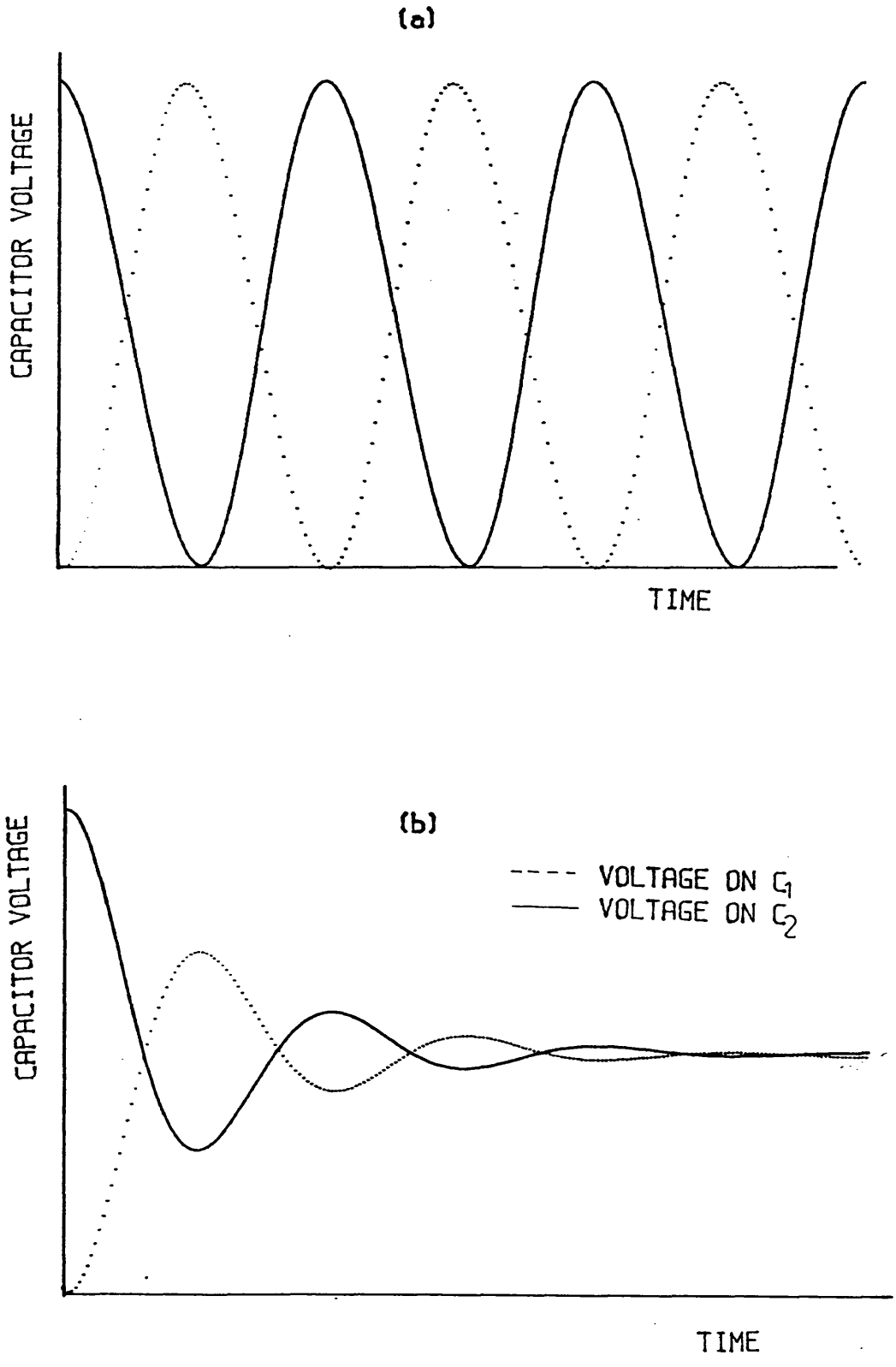

Figure 2.3 RESONANT (a) AND DAMPED RESONANT (b)

CHARGING WAVEFORMS

of lead inductance and the parasitic capacitance of both the leads and the inductor. The parasitic capacitance is generally small compared to C_1 and C_2. The lead inductance, however, cannot normally be ignored and has the effect of increasing the charging time.

2.3 The Pulse Compression Line

Consider now the circuit shown in figure 2.1, assuming again, ideal circuit elements. C_s is initially charged to V_0 volts and the switch, S, is then closed. As described above, C_s will then discharge through L_0 into the next stage of the compression line at a rate determined by the switch S and the value of L_0. As the capacitor C_0 charges, the infinite initial permeability, and therefore infinite impedance of L_1, allows no current to flow until the voltage on C_0 reaches a peak. This is the equivalent of the switch, S, in figure 2.2 being open. The design of L_1 is such that at this point the inductor saturates (S closes) and C_0 resonantly discharges into C_1 at a rate determined by the saturated inductance of L_1. Since the saturated inductance of L_1 is chosen to be much less than that of L_0, C_1 charges much more quickly than did C_0. L_2 is chosen to saturate when the voltage on C_1 reaches a maximum and C_1 discharges into

C_2. Since the saturated inductance of L_2 is smaller than that of the previous inductor, C_2 charges more quickly than did C_1. In this way, the pulse applied at the input to the line is gradually shortened and the peak power transferred increases. This process continues down the line until the n^{th} capacitor discharges into a capacitive load or pulse forming network. In an ideal line the capacitor values are all identical but the losses present in 'real' inductors force the use of slightly larger capacitors in each successive stage (Mathias and Williams, 1955).

The design of a real compression line based on the above analysis will be presented in section 2.5. First, we will consider the switching characteristics of a single core.

2.4 Magnetisation Reversal

Under ideal low field conditions, ($H \simeq H_c$), magnetisation reversal is thought to take place by the movement of a single, planar, strip-spanning domain wall (Barker,1960). At higher fields this simple picture is no longer applicable, and,

i) many walls contribute

ii) nucleation is likely to be at the surface and the walls are, therefore, not strip spanning and not planar.

(Rodbell and Bean,1955).

The first attempt to model the fast magnetisation reversal of a saturated ferromagnetic core, however, ignored the domain structure entirely. This approach, the so-called saturating wave theory, is simply a solution of Maxwell's equations in a constant or infinite permeability medium. There is some confusion as to who originated this theory although credit is usually given to Ganz (1946).

The main points and conclusions of this theory are given below.

2.4.1 Saturating Wave Theory

In the ideal case for both pulse transformer and magnetic switching applications, the core material would exhibit infinite permeability (up to saturation) and zero loss so that the loop shape is as shown in figure 2.4. In practice, this is not possible. However, a theory based on these assumptions does prove to be informative.

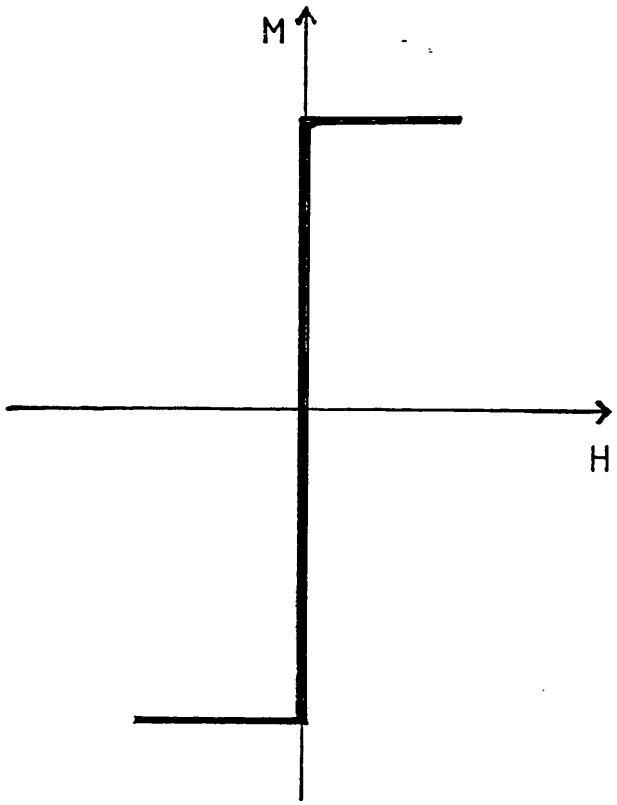

Figure 2.4 A SCHEMATIC OF THE IDEAL (INFINITE PERMEABILITY) LOOP

Consider a toroid consisting of N turns of ferromagnetic tape of width w, thickness d and having a uniformly distributed primary winding of N_p turns. If the permeability of that material is infinite then the only possible values of magnetic flux density are $\pm B_s$. Now, assuming perfect circuit elements and assuming the core to be initially at $-B_s$, if a voltage source applies a voltage V_0 to the primary windings of the core at time t=0, then the total magnetic flux in the core will change linearly with time at a rate given numerically by V/N_p. Assuming that this is uniformly distributed in the radial direction of the toroid, then for any given lamination the total flux is given by Faraday's law to be

$$d\phi/dt = V_0/(N.N_p) \qquad ..(7)$$

Thus, the flux density at the surfaces of the tape will immediately jump to the value B_s on application of V_0 and, in accordance with equation (7), a 'wave' of amplitude $2B_s$ will then advance into the material until the whole of the material is saturated. As the two wavefronts advance, localised eddy currents are set up due to the changes in flux density in the material and it can be shown that the primary current therefore increases with time to counterbalance the effect of these eddy currents. At time $t=t_s$, the walls

meet at the centre of the material and the primary current, I, will then discontinuously jump to that value which would be applicable if the toroid were replaced by a non-magnetic material of the same dimensions and electrical conductivity (σ). It can be shown by simple algebra (Field,1985) that the time required to saturate the lamina t_s is given by

$$t_s = 2wN_p dNB_s / V_0 = 2(N_p / V_0) AB_s \quad ..(8)$$

where A is the effective cross sectional area of the toroid. It can also be shown (using Faraday's law and Ampere's law) that although the material's intrinsic permeability is assumed to be infinite, the effect of the eddy currents is to produce an effective 'saturating wave pulse permeability' which can be defined as

$$\mu_p = (4B_s / \sigma d^2)(dB/dt)^{-1} \quad ..(9)$$

where dB/dt is rate of change of the mean flux density over the cross sectional area, ie, the mean flux reversal rate in the material. Therefore, for a given dB/dt, the quantity $4B_s / \sigma d^2$ can be regarded as a measure of the best possible performance which can be achieved with a particular material. Due largely to its very low conductivity and thin strip form (20μm

thickness), this quantity can be as high as three orders of magnitude greater for metallic glass than for 100μm, 3% Si-Fe and more than twice as large as that for 20μm Ni-Fe. Note, however, that this expression is independant of the dimensions of the toroid and of all magnetic parameters except the saturation induction.

It was concluded by Field (1985) on the basis of the above theory that the narrow square hysteresis loops, generally held to be the ideal shape for magnetic switching applications confer little or no practical advantage and that it is the 'figure of merit', $B_s/\sigma d^2$, alone which is important. This, however, is a dangerous conclusion since the theory which yields this figure of merit itself requires the narrow square hysteresis loop.

The saturating wave theory is a very idealised model assuming perfect magnetic properties and perfect circuit elements. Losses and ΔB-H curves similar to those predicted by the saturating wave theory have, however, been reported by several authors, both in Ni-Fe alloys and metallic glasses, particularly at high flux reversal rates (Jones,1982,1983; Smith, 1988a,b,c). In general, however, fast magnetisation reversal yields ΔB-H curves which are considerably

more complicated than the S.W. behaviour. Figure 2.5 shows a typical ΔB vs H result obtained with a real core material; the dotted line shows the predicted S.W.T. behaviour. The largest deviations from the ideal behaviour occur at the two extremes of the magnetisation curve, these being reversal initiation and the approach to saturation. Several attempts to explain the form of the pulse reversal curve have been reported and these will be described below. Particular attention will be paid to the initial part of the curve since it is in this region that the domain configuration responsible for the reversal is being formed.

It is generally accepted, that region III of the reversal curve shown in figure 2.5 corresponds to saturating wave-type behaviour. The regions I and II are generally associated with the development of an appropriate domain structure. Although the exact form of the initial rise in field seen in region I is not entirely magnetic in origin and may be stray inductance limited, it is thought to be caused by either domain wall nucleation or expansion of existing domains. This will be discussed in more detail later in this chapter. Region II is usually associated with reversal by strip-spanning bar domains which bow under the influence of localised eddy currents to eventually

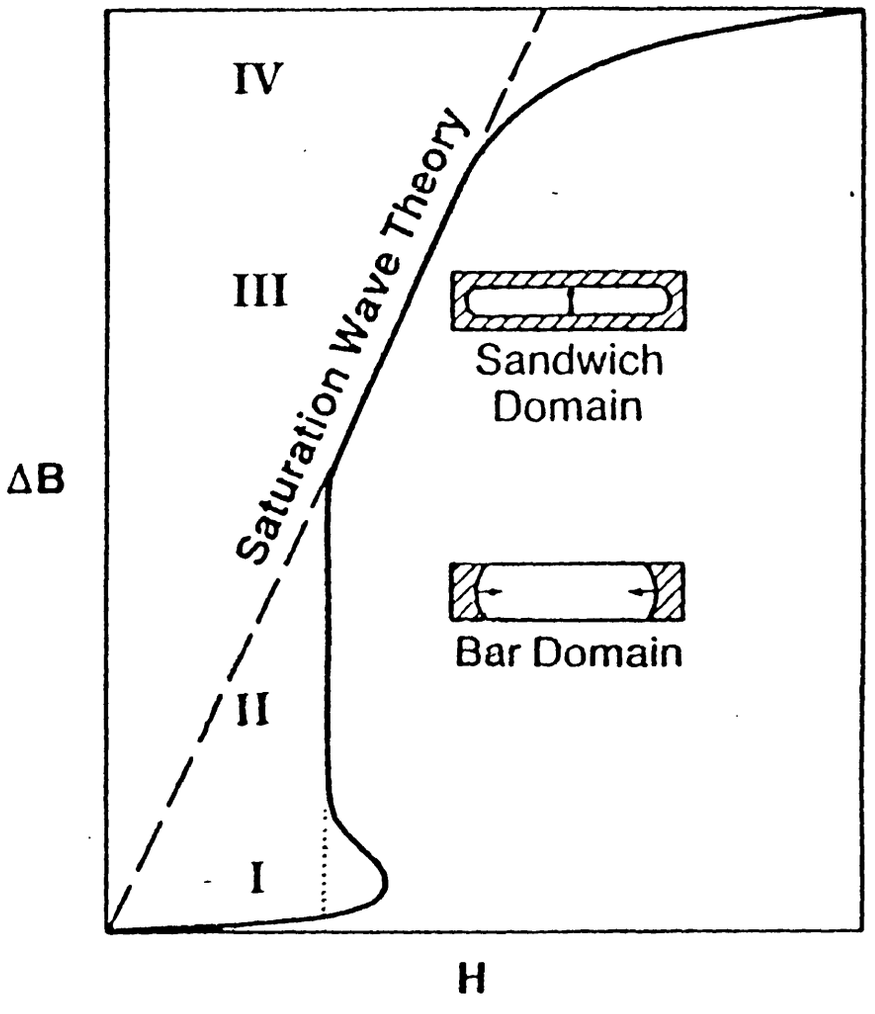

Figure 2.5 A SCHEMATIC PULSE REVERSAL CURVE

(after Smith)

form one or more sandwich domain regions (Williams, Shockley and Kittel, 1950). This is supported by the experimental observation that this region is responsible for a greater fraction of the reversal in thinner materials and for lower magnetisation rates. These conclusions are based upon a comparison of calculations of the expected driving field required for the two limiting cases of bar domains and sandwich domains (see section 2.6.1) and the observed reversal curve. The first true mathematical model of the initial stages of magnetisation reversal, based upon realistic starting conditions, was that of Friedlaender (1956). The model adopted here was one of expanding rigidly hemicylindrical domains.

2.4.2 Expansion of a rigid hemicylindrical domain

Friedlaender (1956) proposed that flux reversal in grain oriented Ni-Fe cores can be modelled by considering the expansion of hemicylindrical domains nucleated at the surface of the tape. This assumption is supported by the calculations and experimental observations of Menyuk and Goodenough (1954) and Rodbell and Bean (1955). Several cases were considered including random and evenly spaced reverse domains. The expansion was considered to be impeded by macroscopic (classical) eddy currents, microscopic

eddy currents, spin relaxation damping, an inertia term, the wall surface energy and the coercive field. On the basis of some experimental evidence, and in order to simplify the mathematics, Friedlaender, assumed that the influence of microscopic eddy currents and spin relaxation damping were dependent only upon the wall velocity and that classical eddy currents were unimportant in the early stages of flux reversal. In addition, the inertia term was ignored and the wall surface energy simply assumed to have an inverse dependence on the domain radius. The results obtained from this model were compared with step H and sinusoidal B measurements of Ni-Fe cores. Using the number of reverse domains participating in the reversal process, and a quantity dependent on the spin relaxation damping and the microscopic eddy currents as adjustable parameters, the times to saturation under step magnetomotive force and trends under sinusoidal voltage were in reasonable agreement with experiment. In addition, the density of reverse domains used was found to be the same order of magnitude as that reported by Menyuk and Goodenough (1955). In a subsequent paper Friedlaender and Leliakov (1961) concluded, on the basis of experimental results, that flux reversal did indeed initiate at the ribbon surfaces. They also obtained evidence to support both the assumption that the field

required to initiate expansion of small domains was larger than that required to continue the expansion and that the field required is related to the domain radius. Depending upon the tape thickness and reverse domain spacing, it is easy to see how the model adopted can lead to both bar and sandwich domain configurations. However, the assumption of no domain distortion, leads to difficulties in explaining the transition from one regime to the other as seen in figure 2.6.

A more realistic attempt at modelling the behaviour has been made by Bishop (1971,1973,1974 and 1976). In a series of papers, he has attemped to describe the bowing of a planar wall due to the local balance between eddy current screening and domain wall surface tension forces. The segmented wall model developed by Bishop is outlined below.

2.4.3 Bowing of a planar wall

The first attempts to model the flux reversal under conditions where severe wall bowing is expected was made by Bishop in 1971. Bishop represented a 180° Bloch wall by 2N moving segments of equal size perpendicular both to the direction of magnetisation and the direction of wall motion (figure 2.7). The

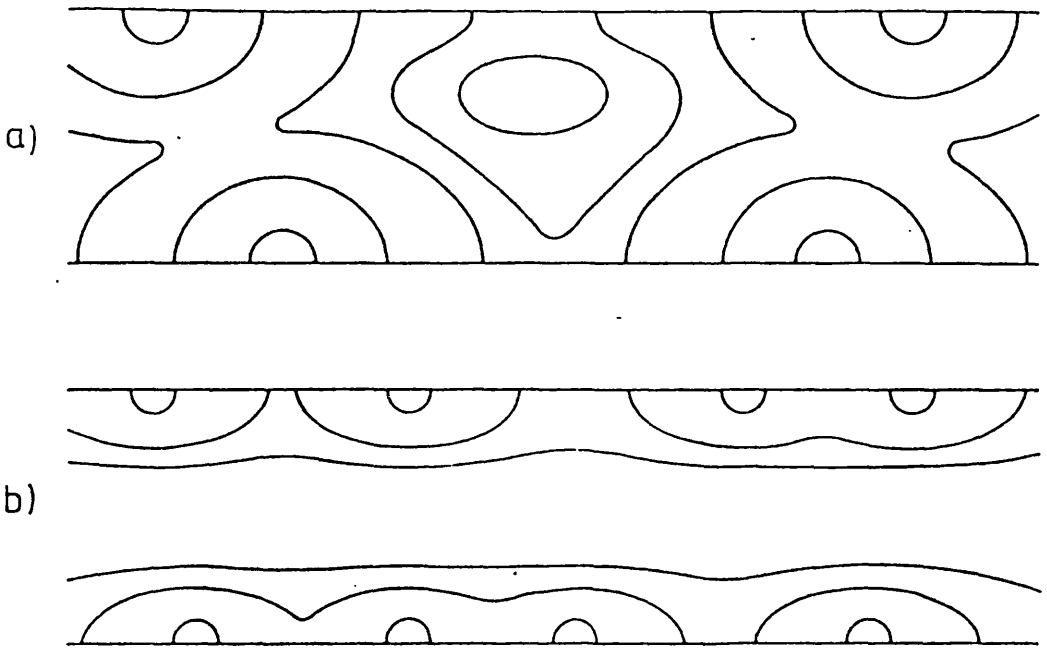

Figure 2.6 A SCHEMATIC SHOWING THE DEVELOPMENT OF BAR (a) AND SANDWICH (b) DOMAINS

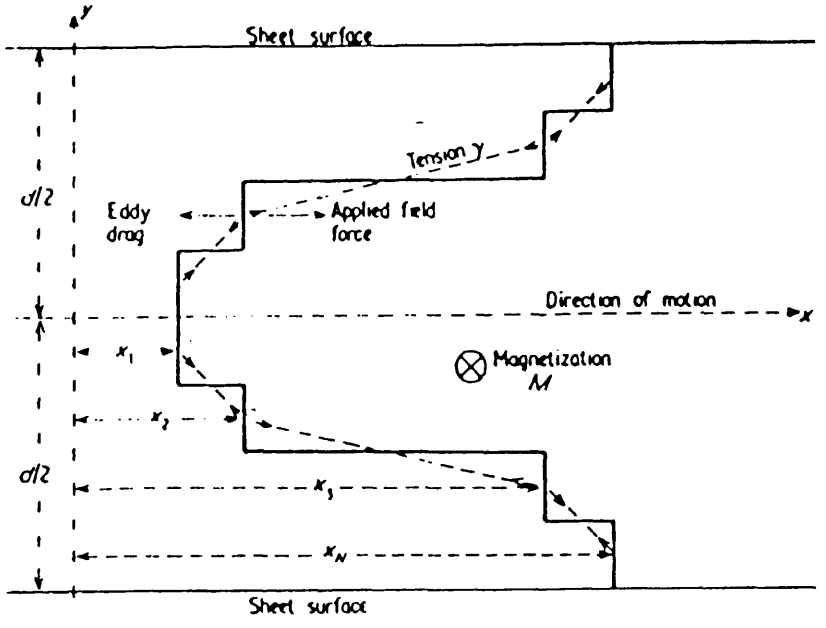

Figure 2.7 A SCHEMATIC OF A BOWED (SEGMENTED) DOMAIN WALL (after Bishop)

horizontal links play no part in the calculations and can therefore be ignored. The magnetisation process is modelled as follows. Each wall segment is assumed to be acted upon by three forces:- a driving force due to the applied field (F_H), a retarding force due the the eddy currents associated with the individual moving wall segments (F_E) and a wall surface tension force (F_T). The latter is assumed to act in the line joining the centres of neighboring wall segments. The development of the wall configuration is calculated from

$$F_H + F_E + F_T = 0 \qquad ..(10)$$

As a result of the computing time required, direct solution of the resulting equation is impractical and a technique of 'dynamic wall stabilisation' is employed. This involves the extrapolation of the previous n positions of a given wall segment to determine the $(n+1)^{th}$ position. When all 2N segment positions have been determined in this way, an iterative adjustment of these positions is carried out until the force calculated on each element is 'sufficiently close to zero'. Bishop compared his steady state results to the experimental observations of Helmiss (1969) obtained in a single crystal 'picture frame' of 3.5% Si-Fe. Significant differences

existed between the two sets of results. These were attributed to the evolution of the domain wall profile in the results of Helmiss compared to the steady state approximation of Bishop and that, in the experimental results, two walls were responsible for the reversal and these were observed to meet at the centre. In a later paper, Bishop (1973) presented results based upon the same model but modified to take account of the evolution of wall shape as the reversal developed and to allow for wall coalescence and separation. Comparison with experiment now showed good agreement. Application to sinusoidal flux conditions showed that wall bowing significantly reduces the energy loss per cycle compared to the rigid planar walls described by Pry and Bean (1958). In addition, it was shown that the field required for a given wall speed is proportional to the square root of the domain wall velocity and hence to $(dB/dt)^{1/2}$. This is compared (Bishop, 1974) to the results of Winter, Kuenning and Berg (1970) who found that, under step dB/dt conditions, the initial step in field is proportional to $(dB/dt)^{1/2}$ over a range of reversal rates spanning two orders of magnitude. These papers, however assumed that flux reversal began with a domain wall spanning the ribbon width. This was observed by Helmiss in the picture frame samples but is unlikely to be the case in tape wound toroidal samples of either metallic

glass, Ni-Fe or Si-Fe (see section 2.4.2). In a subsequent paper, Bishop (1976) addressed the problem of the eddy current limited expansion of a small hemi-cylindrical domain at the surface of a ferromagentic tape. This is essentially the same problem as that tackled by Friedlaender (1956) described above. Bishop's approach, however, was based upon more realistic assumptions and allowed for wall bowing. This is now discussed.

2.4.4 Expansion of a small hemicylindrical domain

The treatment presented here is similar to that described above, only the wall geometry has changed. Here an initially hemicylindrical geometry is asssumed. Expansion of these domains under the influence of some driving force will lead to reversal progressing as shown in figure 2.6 (as before). If wall bowing is now allowed, however, it will be shown that the dominant reversal mechanism is determined not only by the spacing of the nucleation sites and the ribbon thickness but also by the reversal rate. In order to model the reversal process Bishop (1971) constructed a segmented domain wall (figure 2.8). As in the case of the planar wall, the domain wall motion is assumed to be governed by three forces, the applied field, the wall surface tension and the local eddy

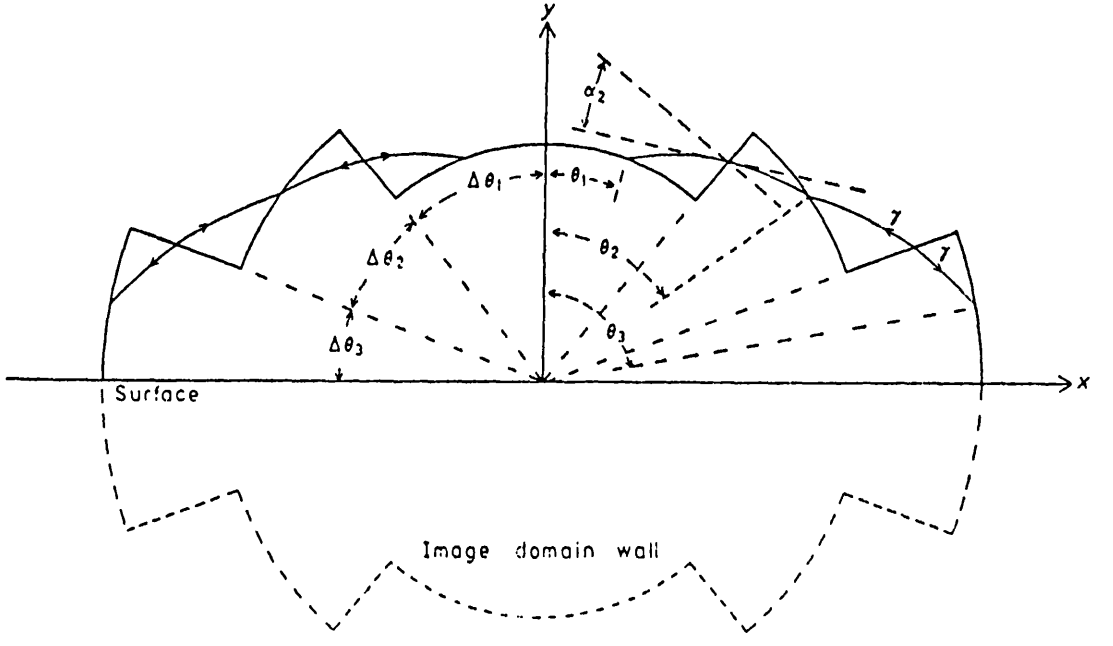

Figure 2.8 A SCHEMATIC SHOWING A SEGMENTED HEMICYLINDRICAL DOMAIN WALL (after Bishop)

currents generated by the moving wall segments. The surface tension forces are again assumed to act between adjacent segment centres but are deemed to act along the curves dR/dθ=constant. The reason for this choice is related to the need, in the limiting case of $R_{i-1}=R_i=R_{i+1}$, for the surface tension forces to act only along the wall surface and thus exhibit no dependence upon the choice of $\Delta\theta$. The effect of the material surface is simulated by assuming a mirror image of the real domain which produces eddy current forces such that at the boundary y=0, the net result of the eddy currents due to the real and mirror domain walls cancel to zero. The technique of dynamic wall stabilisation is again used to predict the wall expansion. Bishop (1976) showed that under a fixed reversal rate, the field required for the growth of such a domain is inversely proportional to the cross sectional area to the power 0.191 and to $(dB/dt)^{0.618}$. The smaller the initial domain, therefore, the larger the field required to expand it at any given reversal rate. This confirms the assumption made by Friedlaender and Leliakov (1961) - see section 2.4.2. The dependence of the required field on the reversal rate should be compared with the square root dependence found for an initially planar wall (section 2.4.3). Note that this treatment is for a single domain wall and that no wall interactions are

considered. The dependence of required drive field on the domain cross-sectional area has the following consequence. During the initial stages of flux reversal, the reverse domain areas are small and a large initial field is therefore required. As the reversal proceeds, the continued expansion of the reverse domains requires successively smaller applied fields. Thus an 'overshoot' in H is often seen (regions I and II (full line) in figure 2.5). The magnitude of the overshoot depends on many factors including the area of the extant domains, the reversal rate and the number of reverse domains present. In many cases, no overshoot will be seen and a simple initial rise in field is observed (regions I and II (dotted line) in figure 2.5).

In a subsequent paper, Bishop and Williams (1977), compare the predictions of both the strip-spanning bar domain and the surface domain models with measurements made on HCR (50% Ni-Fe) tape wound cores of different tape thicknesses. Kerr magneto-optic studies of the tape surface were also used. Bishop showed that the transition from region II (figure 2.5) to region III corresponded, within the experimental accuracy, with the saturation of the tape surface. Region III can thus be described by the saturating wave theory. Regions I and II were both then modelled with the bar

and surface domain treatments. It was found that in order to model the behaviour satisfactorily, the simple steady state motion of bar domains could not be used and that a transient approach was needed. This allows the walls to start in a planar configuration and bow as the reversal proceeds - see also Bishop (1973) and the comparison with the results of Helmiss (1969). This is more important in the case of the faster switching rates. When this was taken into account, the reversal curve could be modelled and the surface saturation point predicted. The expansion of surface domains was also used to model the reversal behaviour seen. Again reasonable agreement was obtained. In both of these models, the number of reverse domains active is an adjustable parameter. The number required to give good fit to the data, however, was the same in both models.

In a real material, except at the material edges, reversal is likely to begin with small surface domains expanding. As the reversal continues, both of these reversal mechanisms are likely to be operative. In thinner material at lower reversal rates, the bar domains are likely to be established earlier as less severe bowing is expected. In thicker samples at higher reversal rates, fewer bar domains are expected since severe bowing due to differential eddy current

screening is expected. In this case, a transition from surface domains to sandwich domain is expected. In all of these calculations, Bishop ignored spin relaxation damping arguing that in materials more than a few microns thick, this would be insignificant compared with the eddy current screening. This is in conflict with the conclusions of Jones, Collins and Cleaver (1981). However, the form of such a term would be similar to that due to the eddy currents.

The observations that

i) the overshoot is most notable in square loop materials (Smith,1984)

ii) in amorphous alloys, S.W. type behaviour is only seen in relatively thick ribbons or for short reversal times

iii) in thin ribbons or for slow reversal rates (Smith,1983) the bar domain structure may be present right up to saturation

are all consistent with the Bishop argument. Point (i) will be discussed further in section 2.6.1 and in chapter 4.

The above summarised the main works published on the modelling of fast flux reversal as well as

contemporary experimental observations. The sections 2.5-2.8 will concentrate on the design of a pulse compression line and reports of the use of metallic glasses in pulse compression and magnetic switching applications.

2.5 Design Considerations

In section 2.2, the principles of resonant charging and the basic operation of a Melville line were discussed. In this section, the factors affecting the design of a pulse compression line will be presented.

Consider again, the circuit shown in figure 2.1, assuming, again, that all the capacitors are identical. It was shown in section 2.3, that, for pulse compression, the i^{th} inductor must saturate as the charge on the $(i-1)^{th}$ capacitor reaches a maximum. ie., the resonant charging time of the $(i-1)^{th}$ capacitor must be the same as the voltage hold-off time of the i^{th} inductor

$$N_i A_i \Delta B_i = [\int V dt]_i = V_0 T_i / 2 \qquad ..(11)$$

where N_i is the number of turns, A_i is the cross sectional area and ΔB_i is the available flux swing of the i^{th} inductor.

$$T_i = (CL_{i-1,s}/2)^{0.5} \quad ..(12)$$

is the resonant charging time of the $(i-1)^{th}$ capacitor and $L_{i-1,s}$ is the saturated inductance of the $(i-1)^{th}$ inductor given by

$$L_s = \mu_{r,s}\mu_0 N^2 A/l \quad ..(13)$$

$\mu_{r,s}$, in equation (13), is the saturated permeability of the inductor. Ideally $\mu_{r,s}$ =1, but a slow approach to saturation gives an effective value higher than this.

If we define the gain, g_i, of the i^{th} stage of the compression line as the ratio of the charging time of consecutive capacitor banks,

$$g_i = T_{i-1}/T_i \quad ..(14)$$

then, substituting for the resonant charging time from equation (12) gives

$$g_i = (L_{i-1,s}/L_{i,s})^{0.5} \quad ..(15)$$

Thus the gain is determined by the ratio of the saturated inductances of the consecutive stages.

Combining equations (11) and (12), gives

$$L_{i-1,s} = 4(N_i A_i \Delta B_i)^2 / (0.5 C V_0^2) \quad ..(16)$$

Thus, if we write the volume of the i^{th} inductor, v_i, as the product of the core cross sectional area and mean magnetic path length,

$$v_i = A_i l_i \quad ..(17)$$

then the gain of the i^{th} stage can be seen to be

$$g_i = [v_i 4\Delta B^2 / \pi^2 (CV_0/2) \mu_0 \mu_{i,s}]^{0.5} \quad ..(18)$$

Hence, for any given gain, the core volume required is inversely proportional to the square of the flux swing available (Chu, 1983). In a pulse compression system, therefore, a high flux swing is very important. Smith (1982) and Chu (1983) describe several reset arrangements designed to increase the available flux swing. It should be noted, however, that the hold-off time of any given core and hence the core volume can be reduced considerably (the latter by up to 40%) without significantly affecting the efficiency of the system (Chu, 1983).

Equation (18) relates the gain of a single stage to known parameters, it now remains to determine how the values of the capacitors and successive inductors are chosen and how many stages to use. These are determined by the overall circuit requirements. For example, the total gain, G, required is usually set by the initial pulse available and the pulse required at the output. In addition, the final core geometry is determined by the load requirements. If we consider a simple case where the gains per stage are all identical, then, if the same material is used in each core, the core volumes required per stage are also the same (equation (18)). If, in addition, the core geometry is kept the same for each stage, then the $L_{1,s}$ is changed simply by altering the number of turns on the core. Thus,

$$g_1 = N_{1-1}/N_1 \qquad ..(19)$$

(Avery, 1987b).

Now, the optimum number of stages, for any given application, depends upon what is to be minimised. For example, depending upon the application, it may be the total system volume, the system cost or weight which is most important. Chu (1983) and Mathias and Williams (1955) both derived expressions for the optimum number

of stages for any given overall gain assuming that only the core volume was to be minimised. This treatment is summarised below.

If a total gain G is equally divided over n stages, the the gain per stage is given by

$$g = G^{1/n} = [v_i 4\Delta B^2 / \pi^2 (CV_0/2)\mu_0\mu_{i,s}]^{0.5} \quad ..(20)$$

The total core volume, then, is given by

$$v_{tot} = nv = G^{2/n} / [4\Delta B^2 / \pi^2 (CV_0/2)\mu_0\mu_{i,s}]^{-1} \quad ..(21)$$

This is a minimum when

$$n = 2\ln(G) \quad ..(22)$$

For total volume minimisation, it is only necessary to add to equation (21), the capacitor volumes. Other optimisation conditions, for example total weight or cost, can easily be obtained using suitable weighting factors for the core and capacitor values.

Having fixed the total number of stages, the core volume and geometry are determined from equation (18), and the number of turns from equation (19).

Smith (1982) noted that, since the saturated inductance of a core is proportional to the square of the number of turns but only to the first power of core area, and the voltage hold-off time is proportional to the first power of both, then in order to obtain a higher hold-off time, it is better to increase A than N. This considerably complicates the compression line design but could lead to a more efficient use of materials.

The above outlines the basic procedure for constructing a pulse compression line to drive a given load. In such a system, the repetition rate is governed only by the time to discharge and charge the first capacitor bank. In a real system, practical points, such as the core losses affect the circuit design and operation. Some of these will now be discussed.

2.6 Amorphous alloys for saturable inductors

Smith (1982) summarised the potential advantages of metallic glasses over conventional crystalline alloys. The points noted included:-

i) ability to control the material anisotropy (and therefore the loop shape)

ii) high intrinsic resistivity

iii) thin strip form

iv) high mechanical strength

v) high saturation induction (cf the ferrites)

vi) large change in permeability on saturation

vii) ability to modify the high frequency losses by partial crystallisation, scribing etc.

Some of these points have already been mentioned in chapter 1. It is the purpose of this section to describe the use of metallic glasses in pulse compression and magnetic switching applications. Many of the points discussed here apply not only to amorphous materials but to flux reversal in any magnetic material.

2.6.1 The Effects of Core Loss

The core loss associated with a magnetic material under fast reversal conditions has several effects on the pulse compression system. The most obvious effect is that of core heating. As the pulse repetition rate is increased, the energy dissipated in the core per second increases and the core temperature will rise. This has two main effects:

i) a reduction in the available flux swing - the law of corresponding states (Cullity,1972), compounded by the low Curie temperatures found in metallic glasses.

ii) possibility of re-annealing the sample and thus destroying any post production tailoring of the core behaviour; even crystallisation in extreme cases (maximum continuous working temperature, around 120°C (Allied Chemicals data sheet)).

Core heating thus limits the maximum repetition rate. In addition, core losses decrease the value of the unsaturated permeability $H/\Delta B$ (Smith, 1983), and, in order to maintain maximum energy transfer, force the use of successively higher valued capacitors in consecutive compression stages (Mathias and Williams, 1955).

It is therefore very important to understand the source of, and minimise, the losses in any core. Losses in magnetic materials under flux reversal were discussed in chapter 1. In general, the losses can be reduced by appropriate control of the material's domain structure. In a strip wound core, however, one major source of loss, which can be eliminated, is that

due to interlaminar eddy currents. These can be reduced by interlamina insulation of which there are several types Smith (1982). At reversal rates of order 1T/us, core loss improvements, due to interlamina insulation, of a factor of 5 have been observed (Smith, 1985).

Insulation types can be divided roughly into three categories - dip or spray coatings, vapour deposition coating and polymer ribbons. These are discussed briefly below.

Dip coatings (eg SiO) can typically only stand a few volts per lamination and are therefore prone to electrical breakdown at high reversal rates. These can be annealed with the ribbon although care has to be exercised to ensure that the ribbons are not stressed by different thermal expansion rates. In addition, chemical compatibility may be a problem - water based coatings for example may cause rusting in some cores.

Vapour deposition treatments in general are very expensive and may fail at the ribbon edges.

Polymer ribbon eg MYLAR or KAPTON are the most popular insulation materials. MYLAR cannot be annealed and therefore must be used either with an unannealed core

or must be rewound with the core after the annealing treatment. The first option may be unsatisfactory in many applications; the second may cause degredation of the core properties on rewinding. Smith and Nathasingh (1984) noted that the higher the longitudinal anisotropy of a given core, the less degredation occurred on rewinding.

KAPTON can be annealed with the core material but may stick to ribbon surface after the anneal (Smith and Nathasingh,1984) degrading the properties of the core. This material is also expensive.

In order to further minimise the core losses, it is important to get the correct domain structure for reversal. The saturating wave theory presented in section 2.4.1 is generally regarded as describing the best possible pulse performance. It is not clear, in practice, how to achieve the correct domain structure or how to interpret the observed ΔB-H curves in terms of the material domain structure. Smith (1988a) indicated that the initial increase (and, where observed, overshoot (see section 2.4.4)) in applied field, shown in figure 2.5, was greater in square loop materials and was due to the nucleation of bar domains. Smith, however, presented no evidence to support this claim. In contrast, Jones, Collins and

Cleaver (1983) concluded that, when observed, the overshoot can be attributed to the excess field required to initiate expansion of small reverse domains. An explanation which they justified with the observation that increasing the reset field increased the maximum field of the overshoot but only slightly affected the rest of the reversal diagram. This corresponds to reducing the size of the reverse domains present thus requiring a larger starting field (see section 2.4.4).

Smith and Barberi (1985) discuss the use of 5 field annealed METGLAS alloys under step dB/dt reversal conditions with and without interlamina insulation over a range of reversal rates. This work was analysed using the two extremes of magnetisation reversal:- saturating wave type behaviour and the results of Rodbell and Bean (1955) concerning flux reversal by strip spanning bar domains. These two theories lead to following expressions for the field required for flux reversal:-

$$H_{bd} = H_c + 0.54(d^2/4\rho)(2a/d)(dB/dt) \quad A/m \qquad ..(23)$$

and

$$H_{sw} = H_c + (d^2/4\rho)(\Delta B/2B_s)(dB/dt) \quad A/m \qquad ..(24)$$

leading to energy losses

$$E_{bd} = (H_c + 0.54(d^2/4\rho)(2a/d)(dB/dt))\Delta B \quad J/m^3 \quad ..(25)$$

and

$$E_{sw} = (H_c + (d^2/8\rho)(\Delta B/2B_s)(dB/dt))\Delta B \quad J/m^3 \quad ..(26)$$

where the subscripts 'bd' and 'sw' signify reversal by bar domains and sandwich domains respectively. In the case of bar domains, Smith (1988) points out that the effect of dB/dt on the number of walls active must also be taken into account. Haller and Kramer (1970) showed that the number of walls present is proportional to the square root of dB/dt. Thus the losses under bar domain reversal are expected to be proportional to the square root of dB/dt. This should be compared with the results of Winters and Kuenning (1970) and Bishop (see section 2.4.4). Smith and Barberi (1985) found that their results did not show the dependence on dB/dt expected of either saturating wave type or bar domain behaviour. Neither did the results show the expected dependence on the thickness of the ribbon, d. These authors concluded that the regime studied was probably close to the transition between these two regimes. It would, however, seem more likely that, in the early parts of the reversal process, expanding surface domains dominate and as reversal continues, depending on the ribbon thickness and the reversal rate, bowed bar domains are formed which then may develop into sandwich domains. Note

that the energy losses observed under bar domain reversal can only be less than those under S.W. reversal if 'a', the domain spacing, is less than d/2. This violates the assumptions used to obtain equation (23), (Smith,1988c).

In addition, the effect of core geometry is important. Jones (1982,1983) has shown that the effects of using a practical toroid with an outer to inner diameter ratio significantly greater than unity increases the observed loss due to non-uniform reversal. As one layer saturates, a higher dB/dt is impressed upon the remaining layers. Avery, (1987b) demonstrated this by considering the case of two single wrap cores of different diameters seperated by a non-magnetic spacer (figure 2.9). On application of a reversing field, the reversal curve shown in figure 2.10 was observed. This clearly shows the saturation of the inner core before the outer one. One possible solution to this is that of Drabovich and Krishtafov (1978) - to wind the core in the form of a Möbius strip so that the inner and outer pathlengths are the same (figure 2.11).

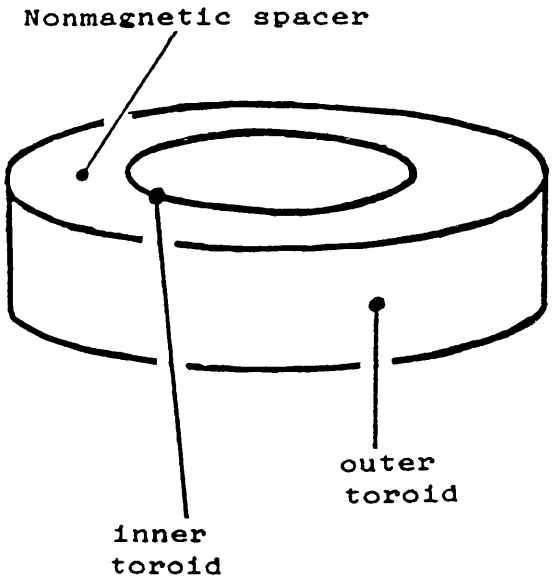

Figure 2.9 TWO CONCENTRIC TOROIDS (after Avery)

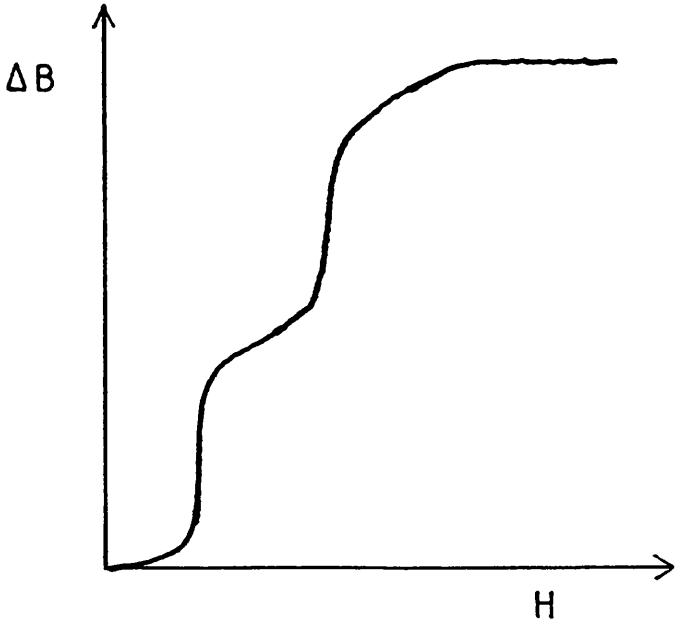

Figure 2.10 THE REVERSAL CURVE OF THE SAMPLE SHOWN IN FIGURE 2.9 (after Avery)

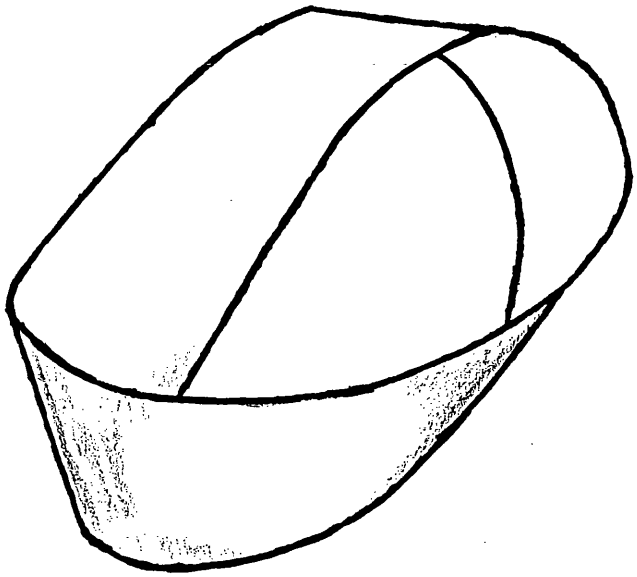

Figure 2.11 A MOBIUS STRIP

In all of the above treatments, a step dB/dt voltage pulse has been assumed. As discussed in section 2.2, however, in a pulse compression line, a $1-\cos\omega t$ waveform is used. The form of this reversal waveform has an effect on the core losses. Smith (1988c) reported that the $1-\cos\omega t$ waveform increased the observed losses by 20% in the bar domain case and by 70% under saturating wave conditions.

In summary therefore, for an efficient and practical pulse compression line, the following are required. A thin material with a high electrical resistivity in order to reduce intralamina eddy current losses. Interlamina insulation is needed in order to reduce interlamina eddy current losses. A high flux swing is required in order to reduce the core volume needed for any given overall gain and to ensure a small, compact system. The ribbon must also be smooth in order to increase the packing density and to avoid bumps and pits on the surface as these can lead to a locally increased electric field intensity which may exceed the interlamina insulation breakdown limit. The material must also retain many small reverse domains under the chosen reset conditions. Many of these conditions are contradictory. For example, interlamina insulation often precludes the heat treatment which is required to obtain a high

available flux swing. The presence of small reverse domains again reduce the ΔB available. In addition, one method of retaining reverse domains is the production of small bumps on the material surface. This then violates the condition that the ribbon be smooth. The design of a core for a pulse compression system is therefore a series of compromises. The final section in this chapter will present very briefly, some of the attempts to construct such a system using metallic glass cores.

2.7 Pulse compression systems

There have been several reports published on the use of metallic glasses in magetic switching applications particularly in particle beam accelerators (Birx, Cook, Hawkins, Poor, Reginato, Schmidt and Smith,1983; Neau,1983; VanDevender and Reber,1983; Stockton, Neau and VanDevender,1983). These reports all confirm the potential of metallic glasses as saturable inductors in pulse compression systems. Without exception, the above papers report the use of as received materials (METGLAS 2605-SC and 2605-CO). No attempt is made at material optimisation although in some cases, interlamina insulation is used. Neau (1983) reported that the switches were reliable with no deterioration apparent after 100

shots. VanDevender and Reber (1983) also concluded that this system was a practical one but that at current material prices, magnetic switching was not economically competitive. That there is still considerable interest in this technology, particularly in the USA, seems to indicate that the advantages offered by this technique outweigh the financial considerations.

This project was concerned with the optimisation of metallic glasses for pulse compression applications. The emphasis here, in contrast to much of the work presented above, was placed upon understanding the effects of various material characteristics on the pulse behaviour of these materials. To this end two metallic glass compositions were chosen, one magnetostrictive and one non-magnetostrictive. Samples of both of these alloys were subjected to various heat and mechanical treatments and each sample studied, was observed under three distinct measurement regimes - dc, ac and pulse conditions. The dc and ac data obtained give information regarding the effects of each treatment on the fundamental magnetic properties of the material, for example, the sample anisotropy, domain wall pinning, domain wall kinetics etc. The pulse results were then analysed in the light of the information gained from the ac and dc measurements.

Chapter 3 of this document describes the measurement systems used and Chapters 4 and 5 present and discuss the results obtained.

CHAPTER 3

3 Experimental Details

The majority of the work reported here was carried out on two metallic glass compositions - Allied Corporation's METGLAS 2605-SC and Vacuumschmelze's VAC 6030. The manufacturer's data on these alloys (and on other commercially available compositions) are shown in table 3.1. The reason for the choice of these two alloys was mentioned briefly in section 2.7 and will be discussed in more detail in chapters 4 and 5. This chapter will describe sample preparation and the measurement systems used.

3.1 Sample preparation

In order to ensure the validity of direct comparison of results from one sample to another, two standard sample geometries were decided upon - rectangular straight strip and 3cm diameter toroids

The straight strip samples were 20cm x 25mm x 16μm for METGLAS 2605-SC and 20cm x 20mm x 22μm for VAC 6030. It should be noted that the dc hysteresis loop of a straight strip sample of this size is not governed by the material properties alone, the

TRADE NAME	COMPOSITION									Max.oper.temp.	Tx	Tc	L	Density	Resistivity	E	Exp.coeff.	Bs
	Fe	Ni	Co	Mo	Mn	Cr	Si	B	C	C	C	C	ppm	kg/cu.m.	microhm m.	GPa	ppm/K	T
VAC 0040	40	40						20		200	400	400		7750	1.25	140	12	1.0
VAC 4040	39	39		4			6	12		120	450	260	8	7800	1.35	150	12	0.75
VAC 6010	5	10	58				11	16		80	500	270	<0.5	7700	1.3	150	12.5	0.35
VAC 6025	4		66	2			16	12		80	500	250	<0.3	7700	1.35	150	12.5	0.55
VAC 6030	x		x	x	x		x	x		90	450	350	<0.3	7600	1.3	150		0.8
VAC 7505	x									120	500	420	30	7100	1.3	150	8	1.5
METGLAS 2605SC	81						3.5	13.5	2	125	480	370	30	7320	1.25			1.61
METGLAS 2605CO	67		18				11	14			430	415	35	7560	1.3			1.8
METGLAS 2605S2	78						9	13		125	550	415	27	7180	1.3			1.58
METGLAS 2605S3A	77					2	5	16		125	535	358	20	7280	1.25			1.58
METGLAS 2826MB	40	38		4				18		125	410	353	12	8020	1.6			0.88

TABLE 3.1 COMMERCIALLY AVAILABLE METALLIC GLASS ALLOYS

demagnetising effect is still important. However, by choosing all the samples to have the same length, demagnetising effects can be ignored. 20cm was chosen as a convenient size which could easily be annealed in either the box or hot air furnaces (section 3.2) with little temperature variation along the length.

Toroidal samples were always prepared from 1m lengths of metallic glass and which were wound to form 3cm diameter cores. These were supported, in the as-received state, by a 25SWG tinned copper band around the core circumference. The band was usually removed after annealing and replaced by a small piece of tape. The magnetic measurements were, however, found not to be affected whether or not the band was removed.

The cross sectional area of the toroidal samples was determined by weighing the material and calculating the area from the known length and the manufacturer's quoted density. This method was significantly more repeatable than measuring the thickness with a micrometer and width with a ruler or travelling microscope.

All samples used were cleaned with acetone before weighing and were subsequently handled with gloves to

avoid grease on the sample surface which may, particularly if present during an anneal, stress the surface of the material (by oxidation) and thus affect the magnetic properties of the sample.

3.2 The annealing facilities

As-received metallic glass ribbon can be treated in a variety of ways in order to enhance certain aspects of its behaviour (section 1.7). The simplest and most commonly used of these is a heat treatment usually carried out between the Curie temperature and the crystallisation temperature, sometimes under the influence of an externally applied field.

A 6kW Carbolite box furnace controlled by a Eurotherm '810' temperature controller and a hot air tube furnace (figure 3.1) heated by a Karl Leister 3.4kW 'Hotwind S' Type 921 hot air blower were used in this investigation. In both furnaces, a thermocouple was rested in contact with (one of) the samples being annealed in order to determine the anneal profile of the material itself. This was found to be necessary since the furnace temperature (particularly on short anneals) can differ considerably from the sample temperature. The relative advantages of the two furnaces are discussed below.

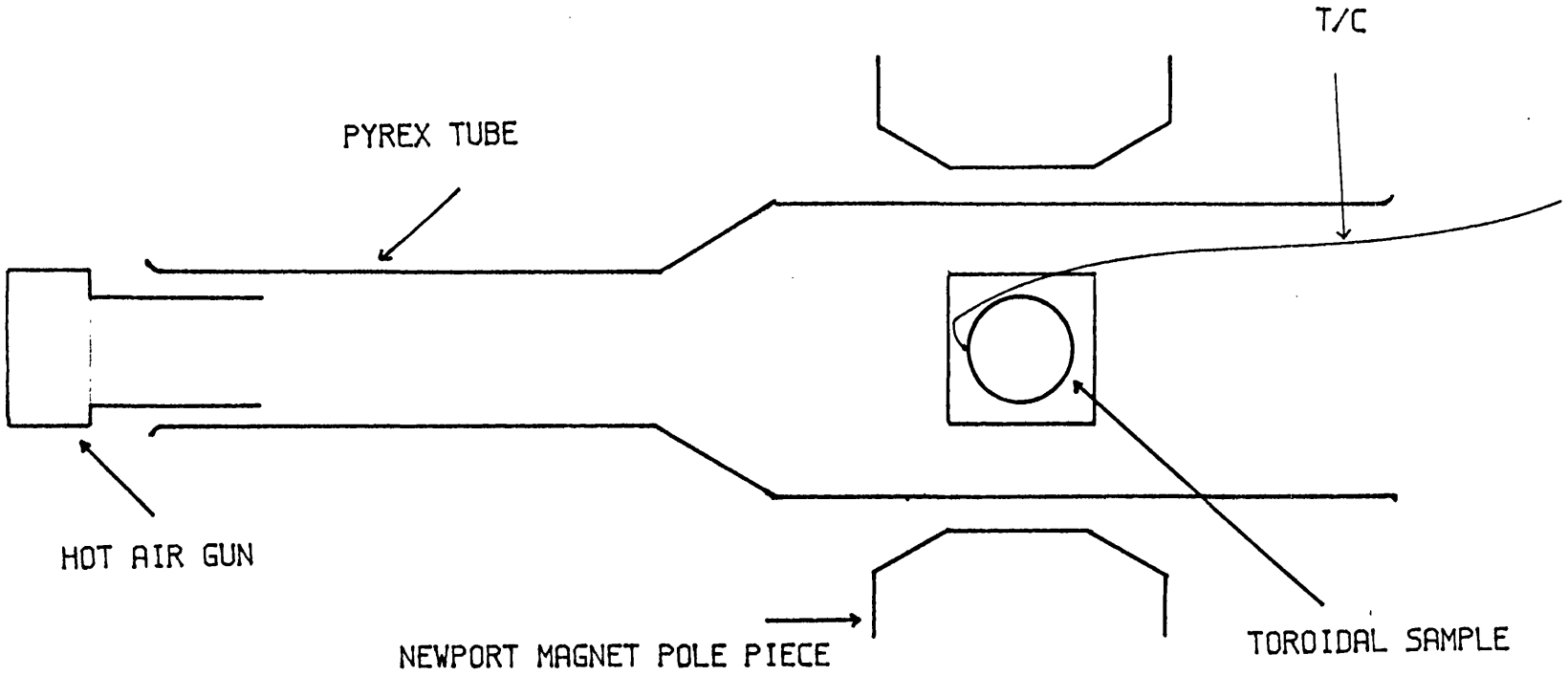

Figure 3.1 THE HOT AIR FURNACE

The hot air furnace was used in cases when a controlled cool from the anneal temperature was required. This was achieved by manually adjusting the air gun output temperature (maximum 600° C) throughout the cool to give the desired cooling rate. This kind of controlled cool is not practical using the box furnace. Very low cool rates were, however, achieved in the box furnace by simply turning the furnace off with the samples inside and allowing to cool naturally (at less than 0.1° C/s). Very high cool rates could also be achieved when using the box furnace by removing the cores from the oven directly into water or liquid nitrogen or simply allowing to cool in air. Cool rates in the range 100° C/s to 0.1° C/s can thus be obtained using the box furnace and in the range 5° C/s to 0.5° C/s in the tube furnace.

The tube furnace, however, was found to introduce a temperature variation around the circumference of the core. The side of the toroid closest to the heat gun output heated up very much more rapidly than the side furthest away. During the approach to the anneal temperature, this difference was observed to be as high as 100° C. A reduction to approximately 30 degrees was seen as steady state conditions were approached, less if the furnace is lagged. Figure 3.2 shows a typical temperature profile of a core annealed in the

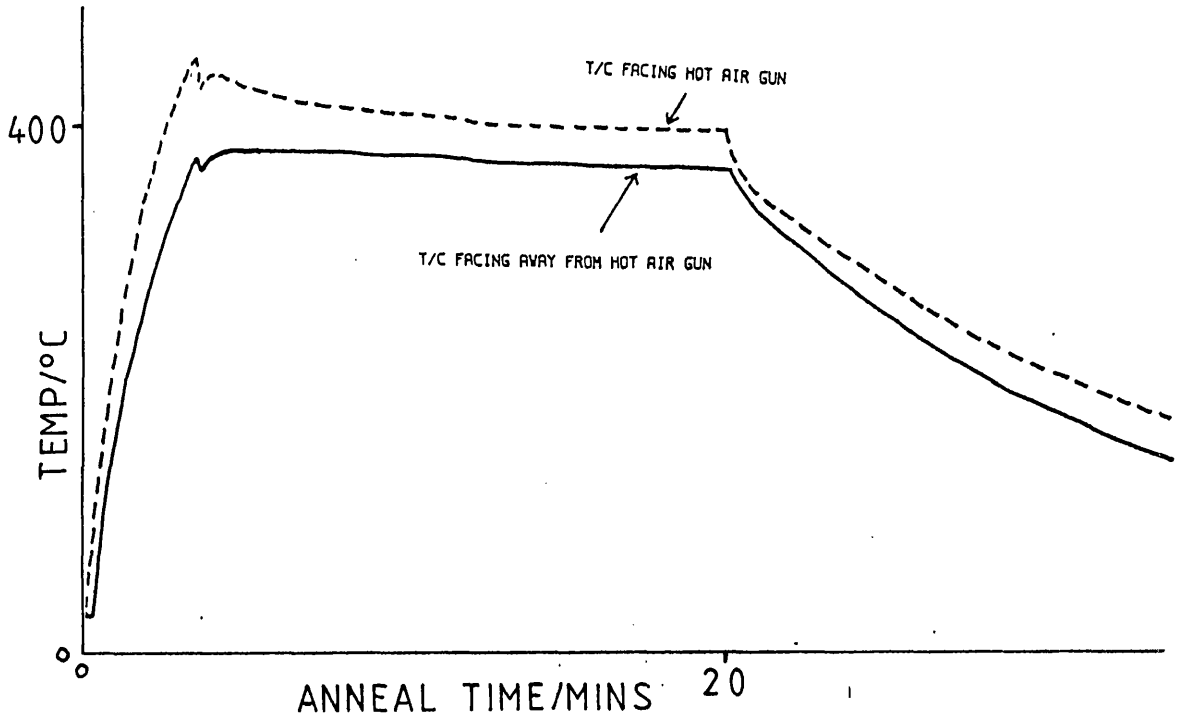

Figure 3.2 TEMPERATURE DIFFERENCE ACROSS A TOROIDAL SAMPLE ANNEALED IN THE TUBE FURNACE

tube furnace. The two traces were obtained from thermocouples in contact with opposite sides of the core; one directly facing the hot air gun and one facing away.

In the Co-based material studied, this temperature difference had no noticeable effect on the sample properties. In METGLAS 2605-SC, however, careful control of the toroid temperature was neccessary to avoid crystallisation. This will be discussed further in chapter 5.

Longitudinal field annealing (section 1.7.2), under either ac or dc conditions, was carried out in both the box and tube furnaces simply by winding a few turns (typically 5 or 10) of fibre-glass sleeved copper wire to form an exciting winding. A Coutant (dc) or Variac (ac) power supply can then used to provide the required field. Care was needed to avoid stressing the core. A remountable pyrophillite former, similar in design to the test former discussed in section 3.3.5, was constructed and used for field annealing METGLAS 2605-SC. This eliminated completely the danger of the windings stressing the sample during the anneal.

Transverse field annealing was carried out using

the tube furnace between the pole pieces of a Newport Instruments watercooled 4 inch type 'A' electromagnet. The magnet is capable of producing fields of up to 300kA/m with a 7cm pole piece separation.

All of the annealing treatments described above were carried out in air. This decision was taken in the light of the results of Avery (1986) which indicated that in both of the alloys used here, stress relief was possible in air with little visual indication of surface oxidation. This will be discussed further in chapter 5.

Having prepared a toroidal sample either thermally or mechanically, the sample was then subjected to three types of magnetic measurement: dc, ac and pulse characterisation. Straight strip samples were only dc looped. The three measurements are, in principle, very similar but the different excitation frequencies and waveforms involved lead to very different circuit configurations. The systems will therefore be described seperately.

3.3 The dc measurement system

The principles of operation of the dc magnetometer can best be explained with reference to the simple arrangement shown schematically in figure 3.3a. The system consists of a single solenoid, 1.5m long and of 7.5cm internal diameter. It is made up of four 18 SWG coils in parallel which can be driven either together or independently. Using the four coils together allows magnetic fields in excess of 10kA/m to be generated.

Two search coils wound of 47 SWG each of 40000 turns and of length 8.2cm are mounted symmetrically inside the field coils on a sliding aluminium frame with their centres 44cm apart. These coils are connected 'back to back' so that, in the absence of a sample, the sum of the voltages induced in the search coils when subjected to an applied field cancels to zero. In practice the two search coils can never be made identical and the potential divider network seen in figure 3.3a is used to 'balance' the search coils so that with no sample present there is no resultant output.

A ferromagnetic sample is placed symmetrically in one of the search coils and subjected to a slowly ramped magnetic field (less than 0.1Hz period in order

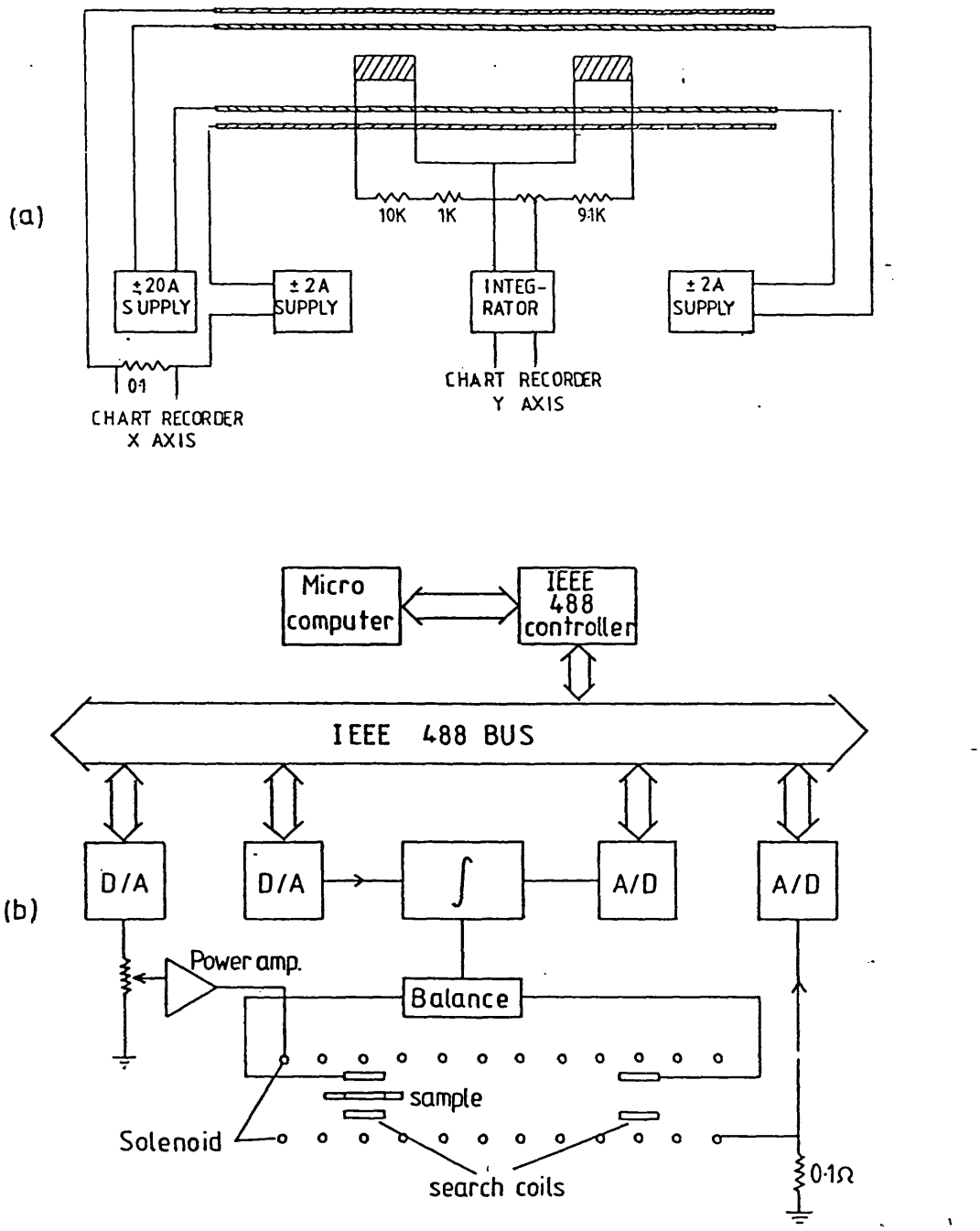

Figure 3.3 THE DC MEASUREMENT SYSTEM (a) MANUAL (b) COMPUTER CONTROLLED

(after Squire et al)

to ensure that eddy current effects are not significant). The voltage induced in the search coil containing the sample is given by Faraday's law as

$$V_1 = -N_s (d\phi/dt) \qquad ..(27)$$

where N_s is the number of turns in the coil and ϕ is the flux linking the coil. Also, the flux density B is given by

$$\underline{B} = \mu_0 (\underline{H}+\underline{M}) \qquad ..(28)$$

and

$$\phi = \underline{B}.\underline{A} = \mu_0 (A_c H + A_s M) \qquad ..(29)$$

where μ_0 is the permeability of free space, $\underline{H}$ and $\underline{M}$ are the applied field and the magnetisation of the sample respectively and A_c and A_s refer to the coil and sample cross sectional areas. It is assumed in this argument that the coil cross sectional area is very much greater than A_s. In practice A_c is approximately $100A_s$.

Substituting for ϕ in (27) from (29) gives

$$V_1 = -N_s \mu_0 d(A_c H + A_s M)/dt \qquad ..(30)$$

Similarly, the second search coil which contains no

specimen will produce and induced voltage V_2 which is given by

$$V_2 = -N_s \mu_0 d(A_c H)/dt \quad ..(31)$$

The voltage, V_0, output from the potentiometer network is therefore given by the difference of the equations (30) and (31), ie,

$$V_0 = -N_s \mu_0 d(A_s M)/dt \quad ..(32)$$

This voltage is then integrated electronically and the integrator output V_y, given by

$$V_y = N_s \mu_0 A_s .M/RC \quad ..(33)$$

is used to drive the vertical axis of the chart recorder (a Philips PM8143). RC in the above equation is the integrator time constant. The voltage measured across the 0.1 ohm resistor is directly proportional to the field applied to the sample and is used to drive the horizontal axis of the chart recorder. The resulting trace is therefore directly proportional to the M-H loop of the sample. The proportionality constant for the H axis is easily calculated from the number of turns on the solenoid and the voltage across the 0.1 ohm resistor. The calibration of the vertical

axis is somewhat more involved. From equation (33), it can be seen that the integrator voltage is linearly related to the magnetisation of the sample. It is therefore a simple scaling factor that is required. However, although a value can be obtained for A_s, and μ_0 is known, the integration time constant RC and the number of search coil turns N_s, can only be estimated. Two methods are available to calibrate this axis. The first method can only be used on material for which saturation magnetisation, M_s, has been quoted by the manufacturer. The sample placed in the magnetometer in the usual way and is subjected to a very large field - high enough to saturate the specimen. The vertical axis is then simply scaled so that the maximum M achieved is the manufacturers quoted value of the saturation magnetisation. This simple technique relies on a knowledge of what the saturation magnetisation 'should be' and on the fact that M_s changes little with the post production history of the glass (see section 1.4). A more fundamental method of calibration is available if necessary. This is described below.

A coil of N_{pr} turns is wound onto a piece of 10BA brass studding and the cross sectional area of the coil (A_{pr}) is carefully measured. This test coil is then placed in that search coil which is usually used to hold the sample and a small current is passed

through the coil via the 0.1 ohm resistor. The rest of the circuit is as usual with the X axis of the chart recorder driven from across the standard resistor and the vertical axis driven from the integrator output. The field produced by the stud, which is assumed to entirely enclose the search coil, is given by

$$H = N_{pr} I \qquad ..(34)$$

and the flux density within the search coil can therefore be written

$$B = \mu_0 H = \mu_0 I N_{pr} \qquad ..(35)$$

The flux linking the coil, ϕ, is therefore given by

$$\phi = \mu_0 N_{pr} I A_{pr} \qquad ..(36)$$

and from this the voltage induced in the search coil of N_s turns can be seen to be

$$V = \mu_0 N_s N_{pr} A_{pr} (dI/dt) \qquad ..(37)$$

This voltage is then integrated to give

$$V_0 = N_{pr} A_{pr} I (N_s \mu_0 / RC) \qquad ..(38)$$

Since the chart recorder is plotting V_0 vs I and, since N_{pr} and A_{pr} are known, the quotient $N_s \mu_0 / RC$ can be obtained from the gradient of the chart recorder output and thus using equation (33), the M axis of the loop can be calibrated. In this project, however, usually, it was only changes in the loop shapes of any given material which were important and the M axis calibration was therefore rarely used.

The above serves to illustrate the principles of the magnetometer system, this particular arrangement, however, exhibits several serious limitations including chart recorder slew rate problems and more importantly integrator drift. The latter is a common problem in dc or quasi-dc applications and is not easily overcome. In this project various integrator designs have been tried to minimise the problem. Even using a chopper stabilised OP-AMP and a user-variable dc offset to balance out the drift does not eliminate the problem.

A novel magnetometer arrangement has been developed (Squire, Sheard, Carter and Gibbs,1988) which reduces the problems described above and facilitates the calculation of various important magnetic parameters. A schematic diagram of this system is shown in figure 3.3b. The solenoid arrangement itself is no

different to that described above but the shape of the H field waveform and the data collection and display are now under computer control. In addition, the integration is performed by a computer resettable, hybrid digital/analogue technique.

3.3.1 The drive (H) field

At frequencies low enough to approximate dc conditions the shape of the applied field waveform as a function of time, H(t), does not have a significant influence on the shape of the hysteresis loop. In the arrangement described above, the solenoid is driven using a linear ramp. The response of a 'square loop' sample to such an applied field, however, is almost zero except very close to H=0 where it has the appearance of a delta function. This is illustrated in figure 3.4 which shows the H and dM/dt waveforms for a well stress-relieved metallic glass sample. This makes the digitisation of the loop impractical.

Ideally we would like to drive the solenoid with a waveform which would spread out the M(t) peaks in such a way that the digitised points occur equally spaced along the M-H curve. This would, however, involve an iterative procedure since a particular H(t) would have to be chosen for a given M(H) and M(H) is not known in

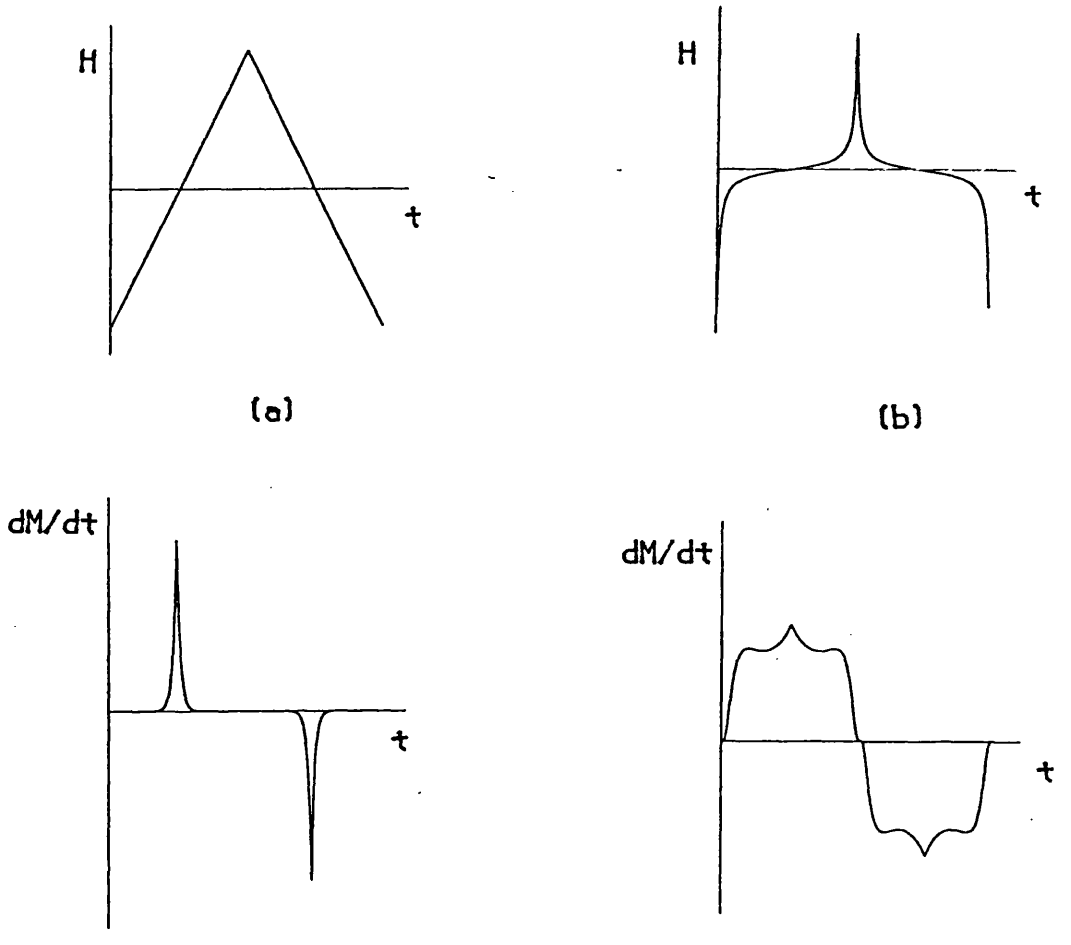

Figure 3.4 A SCHEMATIC DIAGRAM APPLIED FIELD AND TYPICAL CORRESPONDING dM/dt WAVEFORMS

(after Squire et al)

advance. In practice this is unnecessary and any function that spreads the peaks sufficiently is acceptable. The function we have chosen is a truncated tangent of the form

$$H = \tan(2bt/T)/\tan(b/2) \qquad ..(39)$$

where b is an adjustable shape parameter in the range zero to one. Low values of b produce a near-linear ramp; high values of b produce a sharply peaked function. Figure 3.5 shows this function plotted for several values of b, using symmetry to produce the second half-cycle. Values of b between 0.9 and 0.999 are commonly used for metallic glass samples. In general, the 'squarer' the M-H loop the larger the value of b required.

A typical loop will contain 256 points and will have a loop time of not less than 70s. Thus the time between steps is about 250ms. Each individual step however takes a much shorter time. The time constant of the input to the power amplifier is 1ms and the step in H is therefore effectively complete (more than 99%) after 5ms.

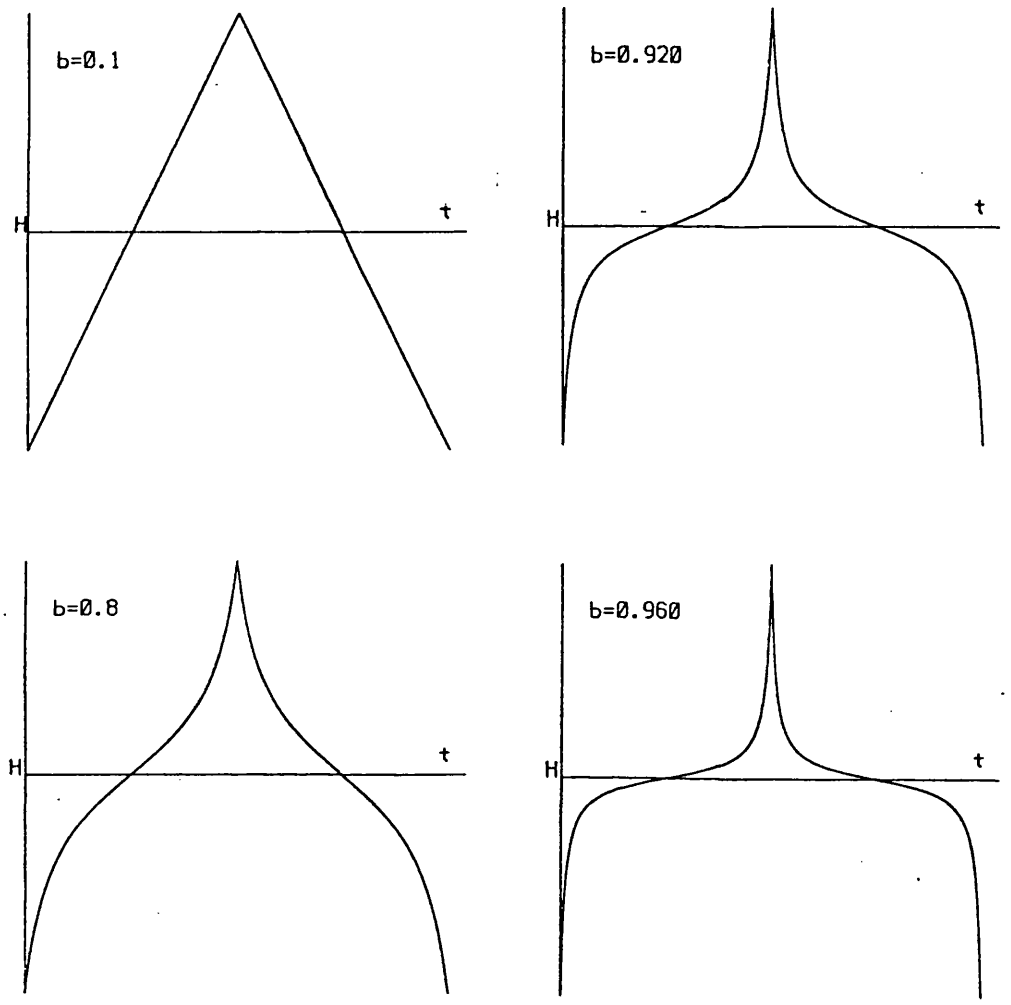

Figure 3.5 THE TRUNCATED TANGENT WAVEFORM PLOTTED FOR VARIOUS VALUES OF 'b'

(after Squire et al)

3.3.2 Integration and Data Collection

It was noted in section 3.3, that, at low frequencies and with small samples, the weak signals induced in the search coils make drift-free integration very dificult using conventional integrators. For loop times of greater than 100s even the best analogue integrators are unable to produce drift-free operation. Two alternatives remain: numerical integration or a hybrid design. The resolution and speed of the A/D converter which would be required for the former have led us to choose the latter. This hybrid integrator combines the advantages of both the analogue and the digital techniques.

The details of the integrator are shown in figure 3.6. It can be divided into three main units: the integrator proper, an output sample-and-hold circuit, and a control interface. The integrator is based on an OP77 IC; it incorporates offset nulling and a remote reset by means of the JFET across the feedback capacitor. The control interface takes the 0/10V control signal from the D/A convertor and derives from it suitable signals to reset the integrator and the sample-and-hold. The D/A converter used was a CIL Microsystem Ltd, model PCI 6380.

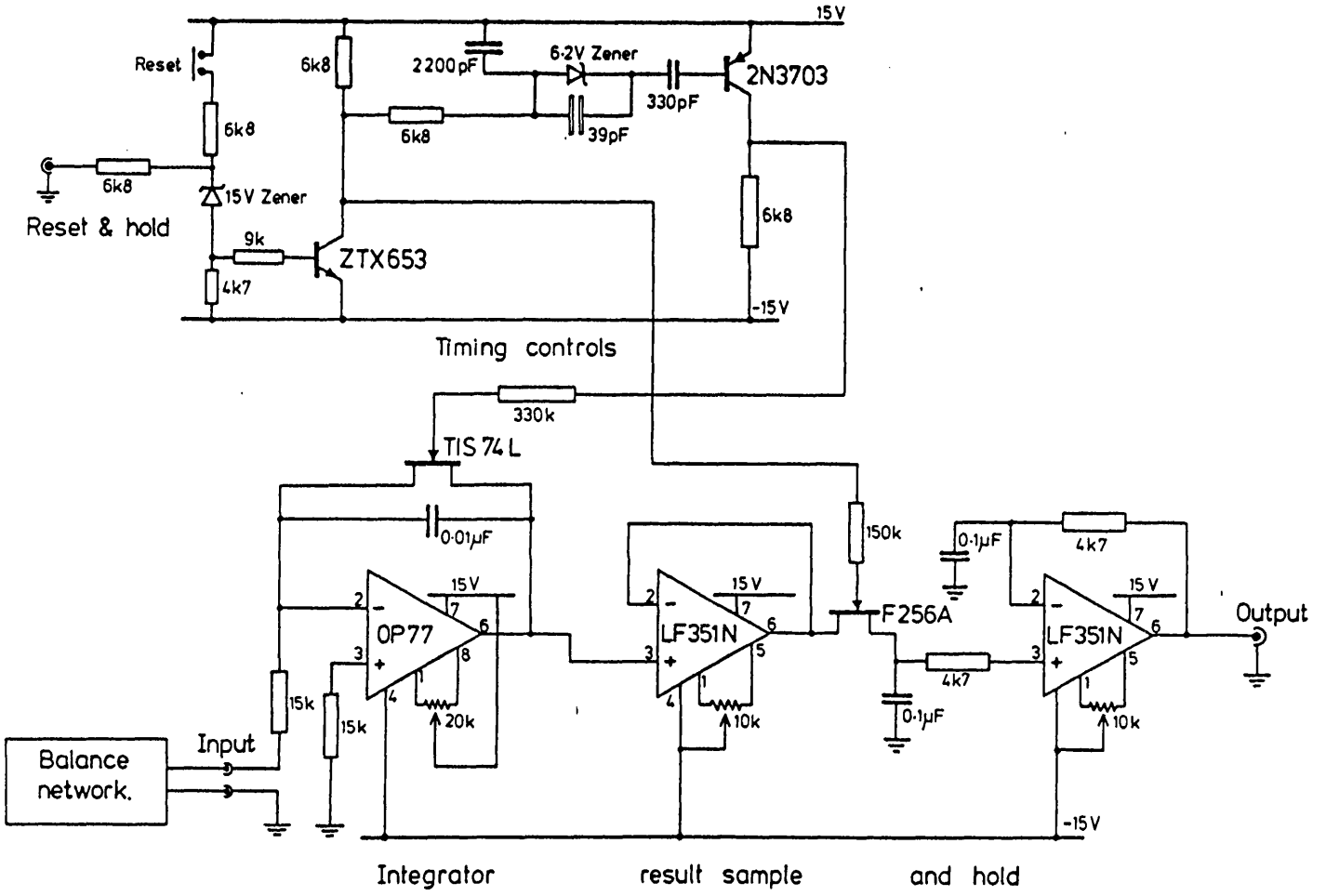

Figure 3.6 A SCHEMATIC OF THE HYBRID INTEGRATOR (after Squire et al)

In contrast to the analogue integrator system, the hybrid integrator is not required to continuously integrate dM/dt around the complete loop. As explained in section 3.3.1, the H field is changed in a series of small steps (typically 256). During each of these, the signal reaching the integrator is a sharp spike which is proportional to dM/dt. This is integrated to produce a voltage output proportional to the total change in magnetisation due to this small field step. This is stored in a sample and hold circuit and in turn read by the CIL. The integrator is then reset (by means of the JFET across the feedback capacitor), the sample and hold circuit is flushed and the whole process is repeated. The timing sequence is shown in figure 3.7.

Since the integrator is only required to integrate over a very short time, the drift is correspondingly small and, more importantly, it is approximately the same over each integration period. Thus the residual drift in the M-H loop will be equally distributed amongst the 256 points and a linear drift correction can be applied in the software.

This system was conceived and designed and the original control software written by Mr.P.T. Squire. The construction and testing of the hardware was

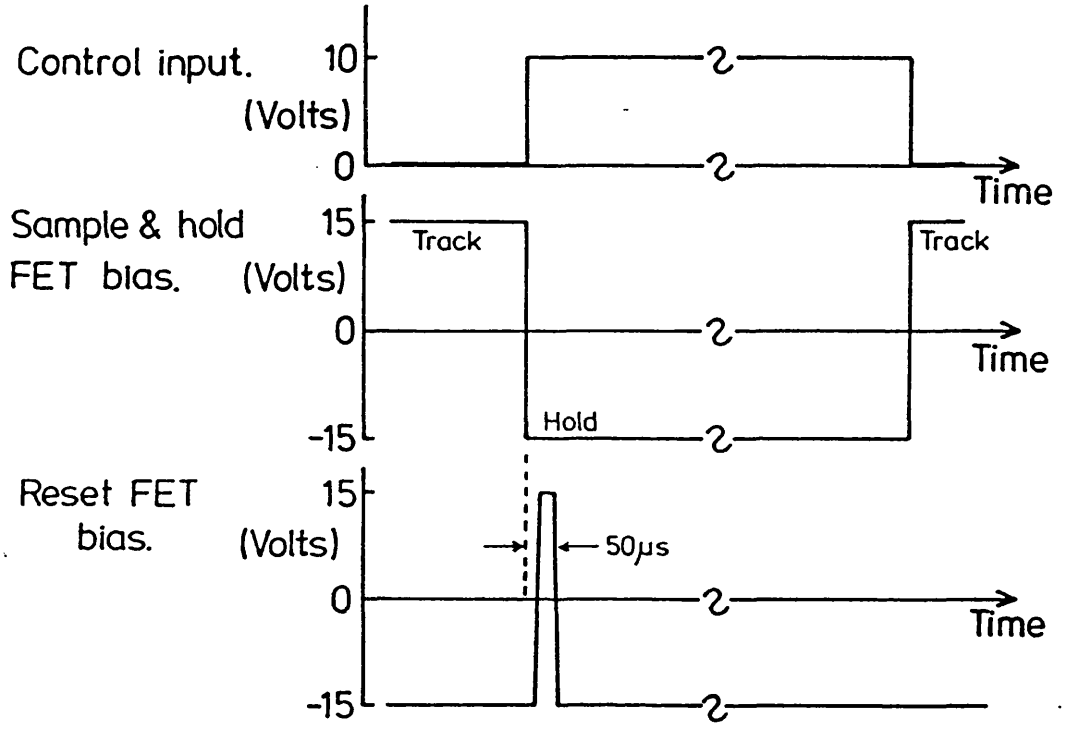

Figure 3.7 A SCHEMATIC SHOWING THE TIMING SEQUENCE OF THE HYBRID INTEGRATOR (after Squire et al)

performed by C.H. Carter. The parameter calculations, described below, and the production of the existing control software is my own work.

3.3.3 Parameter calculation

Four parameters are calculated from the loop data: the coercive field H_c, the remanence ratio M_r/M_s, the magnetisation energy E_m, and the energy loss per cycle ΔE. The two energy parameters cannot be calculated in absolute units without additional information (the saturation magnetisation). This is often unimportant because it is only the relative values for a particular sample or series of similar samples that are required in this investigation.

In the analogue system described briefly in section 3.3, the sample coecivity H_c and the remanence ratio M_r/M_s were obtained by measuring the distance between two chart recorder pen lines, which, in many cases, were only a few millimeters apart. The maximum accuracy of these measurements was, therefore, limited to a few percent regardless of the precision and sophistication of the magnetometer itself. In addition, the magnetisation energy, E_m, and the static loss, ΔE, were previously obtained by digitising the M-H loop and then employing a numerical integration

routine implemented on a microcomputer to calculate the areas enclosed. Again the accuracy of these measurements was limited not by the magnetometer but by the errors introduced in obtaining the required data from the chart recorder plot. The digital system eliminates this type of error completely allowing the required parameters to be calculated to the precision of which the magnetometer itself is capable.

The parameter calculation software which is currently in use is described below. Some possible improvements which have not yet been fully implemented are suggested.

3.3.3.1 The Coercivity

The variable b, which is used to adjust the shape of the drive waveform (section 3.3.1), facilitates the calculation of the H_c, E_m and ΔE by ensuring that regardless of the loop shape, with an appropriate choice of b, a sufficient number of points will be digitised on the rapidly changing portions of the M-H loop. It is, however, very rare for there to be points digitised at exactly M=0. Indeed, in some very square loop samples, there may only be 4 or 5 points on each edge even when using a very high shape factor. In order to calculate H_c, therefore, the zero crossing

points must be determined by some method of interpolation. This is currently achieved by performing a simple linear regression calculation using a few points either side of the M=0 axis. When the true zero crossing points have been calculated, equation (39) can be used to determine H_c. However, because different samples can produce very different M-H curves, it is not possible to fix a given number of points, for the regression analysis, over which the curve is known to be linear. An iterative procedure has therefore been adopted. The program initially calculates H_c using only 3 points in each regression line, the coercivity is then re-calculated using 5 points and the two values are compared. This is repeated using successively more points in the regression lines until the values of two consecutive calculations agree to within a preset tolerance, typically, 0.01% of the maximum applied field. If this is not achieved before the number of points in the regression line exeeds 11, then the whole process is repeated with a higher agreement tolerence. Coercivities of less than 0.5A/m have been measured reproduceably using this technique.

A more sophisticated and potentially more accurate method of extracting H_c from the stored data which is being considered at the moment exploits the symmetry

of the M-H loop (Squire,1988). The decremental changes in magnetisation ΔM resulting from the decreases in applied field can be shown to be the inverse of the ΔM's obtained as H is increased, shifted slightly along the H axis. This shift is a direct measure of the coercivity. Hence H_c may be obtained by reversing and inverting the second half of the ΔM array and then shifting this relative to the first half until a maximum in the correlation between the two sets of values is reached. The shift required to obtain this maximum is then used to calculate H_c using equation (39).

3.3.3.2 The Remanence Ratio

Ideally, in a loop of X points, M_r/M_s could be obtained simply as the ratio M(X/4)/M(X/2) since H(X/2)=H_m and H(X/4)=0. Several factors including the horizontal component of the Earth's field along the direction of the solenoid axis and a slight drive waveform asymmetry have the effect of displacing the loop along the H axis and the 'true' H=0 points must therefore be deduced from the hysteresis loop obtained. This is achieved using the zero crossing points obtained in the H_c calculation - the value of H midway between these points is taken to be the 'true' H=0. The corresponding value of magnetisation at this

H is then calculated using a linear interpolation between the two nearest digitised points and this value is then divided by $M(H_m)$ to yield the remanence ratio.

3.3.3.3 Loss and Magnetisation Energy

The static loss is obtained using a simple trapezium rule numerical integration routine to calculate the total area enclosed by the hysteresis loop. The value obtained for ΔE is then used to obtain an approximate value of the magnetisation energy E_m.

Strictly, E_m can only be obtained from the normal induction curve. In low coercivity samples, however, if the locus of the average value of H for any given positive M is plotted, then the area enclosed between the resulting curve and the M axis is approximately Em. This area is obtained by calculating the area enclosed between the M axis and that portion of the hysteresis loop H=0 to $H=H_m$ (again using the trapezium rule) and then subtracting one quarter of the total area enclosed by the loop itself, ΔE.

3.3.4 System Limitations

Although this sytem is a significant improvement over the analogue system described, certain limitations are imposed by the effects of noise and by the form of the drive waveform chosen. These are discussed below.

3.3.4.1 Noise

The most important and most obvious source of error in this system is due to the effects of noise particularly on the drive waveform near H=0. Here the H field step size is very small and may correspond to a change of only a few bits (out of 64000) in the CIL output. Mains noise (50Hz) is by far the largest component of this noise and is thought to originate in the CIL or associated leads. Two methods of reducing the effects of this noise have been considered and may be implemented sometime in the future. The first of these is simply to use a higher resolution A/D converter in place of the CIL. The second method is somewhat more complicated but could be used in conjunction with either the present CIL or a higher resolution replacement if required. The basis of this method would be to use a computer controllable potential divider network to allow the A/D to work

over as much as possible of its full range throughout the M-H measurement. The operation of such a network is best described by means of an example. Note that, although this example is specific to the CIL used at present, a similar arrangement could be used with a different A/D unit.

Consider that the CIL output is in the range ±10V and that initially the potential divider allows ±5V to reach the amplifier input which in turn provides a peak current of 5A. As the current required decreases below 0.5A, the CIL output is less than 1V. The potential divider network would now be adjusted so that a CIL output of 10V would allow 0.5V to reach the power amplifier input thus allowing the CIL to work over its full range again. This would result in better H-step resolution and, therefore, a higher signal/noise ratio.

At present a simple RC filter is included in the circuit and although far from perfect, the signal/noise ratio is acceptably high on the materials and sample geometries measured to date.

3.3.4.2 Shape factor and point distribution

Section 3.3.1 described the reasoning behind the adoption of the variable shape factor H waveform. The ideal drive waveform would be one which produced equally spaced points along the actual M-H curve. In order to achieve this in practice, an iterative procedure would have to be adopted. This is unecessarily complicated and the shape factor method described is satisfactory. A consequence of this method, however, is a clustering of points around H=0 not at $H=\pm H_c$. Materials with a very square loop shape but non zero coercive field can therefore present some difficulties - it is not possible to obtain more and more points on the $-M_s$ to M_s transition simply by increasing the value of b. Indeed this can actually reduce the number of points in the required region by clustering them more tightly around H=0. The shape factor system is therefore not ideal and must be used with care.

3.3.4.3 Repeatability

The accuracy of the calculation of magnetic parameters (section 3.3.3) will obviously be affected by noise in the system and to some extent by the distribution of digitised points around the loop. A

set of readings were taken on an as-received METGLAS 2605-SC toroid with a maximum applied field of approximately 500A/m and a shape factor of 0.99. The vertical axis of these measurments is therefore B and not M (see section 3.3.5). These results showed a ±1% variation in H_c from run to run, a variation of less than ±5% in the remanance ratio and the magnetisation energy and a ±10% variation in the loss. The effect of changing the shape factor was also studied using a METGLAS 2605-SC core. All calculated parameters except E_m were found to vary as above as b was alternated between 0.99 and 0.97. The magnetisation energy variation, however, increased to ±10%. The results summarised above can be understood if one considers which part of the loop dominates a given parameter and what effect noise/shape factor has on that part of the loop.

The dc loss is the most susceptible parameter to the effects of noise because it is on the $-B_r$ to $+B_r$ transition that the effects of noise are most pronounced and it is this region which contributes most to the loss. Similarly the magnetisation energy E_m is dominated by the region B_r to B_s and the effect of increasing b is to reduce the number of points on this portion of the curve hence affecting the calculation of E_m.

3.3.5 Toroidal samples

With the exception of the last section, all of the above has been dedicated to the measurement of the dc properties of straight strip material. The solenoid and search coil arrangement can, however, be replaced with a toroidal sample wound with exciting and sensing coils. In this case no air flux compensation is used and the resulting curve is therefore a B-H not an M-H loop. A remountable test former consisting of 10 primary and 20 secondary turns has been constructed (figure 3.8). This has the advantage that in the both the dc and ac measurements, each individual core is measured under exactly the same conditions with the same winding distribution, the same air flux component and without the stress which is so difficult to avoid when simply winding wire around a toroidal sample.

This former is also used to mount the cores during the ac characterisation described below.

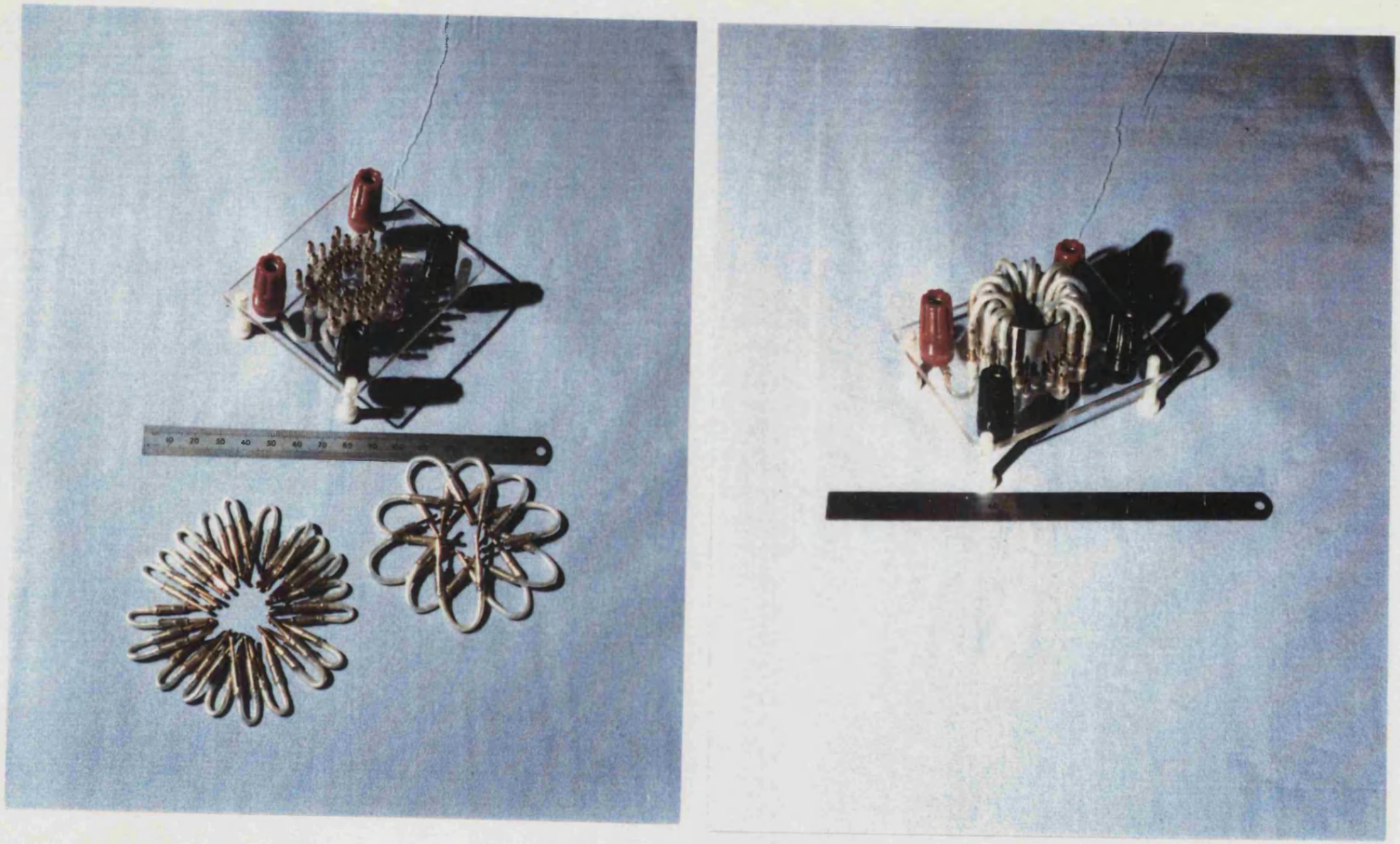

Figure 3.8 THE REMOUNTABLE TEST FORMER

3.4 The ac measurement system

At drive frequencies above a few tenths of one hertz, the shape of the drive (H) waveform becomes an important factor in determining the shape of the B-H loop of a sample. If the magnetic properties of samples treated in different ways are to be compared by comparing their respective B-H loops, it is imperative that those loops are produced under as near identical drive conditions as possible. It is primarily this consideration which leads to the differences between the ac and dc measurement systems.

The ac system is shown in figure 3.9. It consists of a Crown M-600 power amplifier driven by a Philips PM5134 function generator. The core is mounted as described in section 3.3.5 and the primary current is monitored using an Alrad current transformer (model 411 or 2877) details of which are given in table 3.2. The feedback circuit and 5 ohm series resistor are included in the circuit in order to maintain a sinusoidal drive field (section 3.4.1). The signal from the current coil (proportional to H) and the voltage induced in the secondary winding of the core (proportional to dB/dt) are simultaneously stored on a Gould 1425 digital storage oscilloscope. These

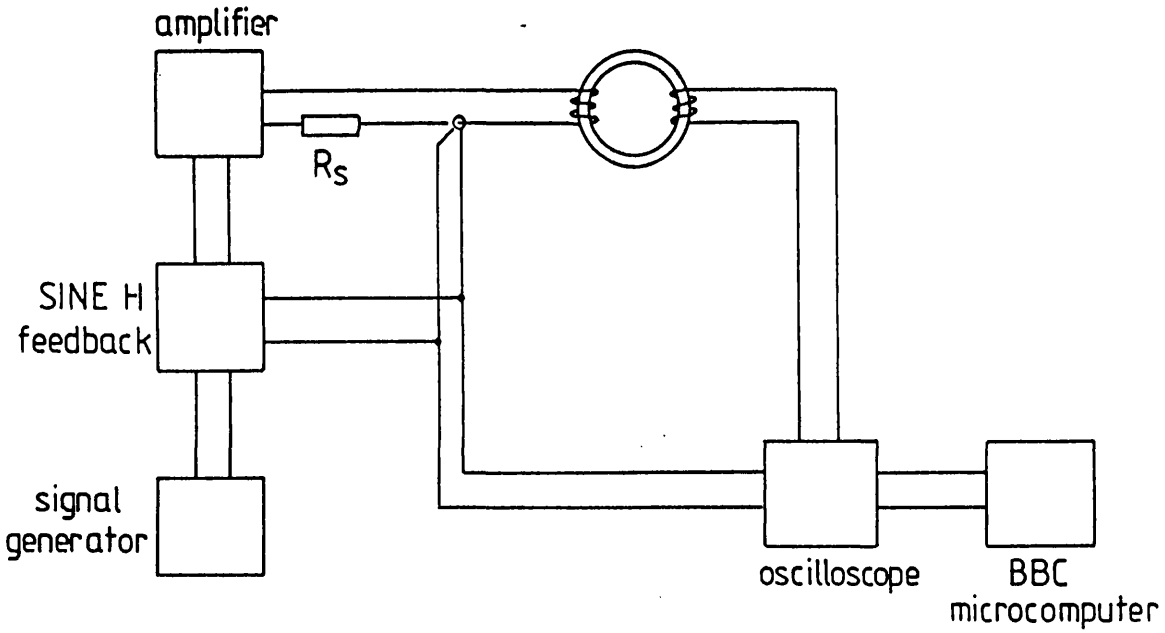

Figure 3.9 THE AC MEASUREMENT SYSTEM

Model Number	2877	411
Output/V/A	1.0	0.1
Max peak current/A	100	5000
Droop (%/μs)	0.2	0.0009
Useable risetime/ns	2	20
$(IT)_m$ /As	0.0004	0.2
Lower -3dB freq./Hz	300	1
Upper -3dB freq./MHz	200	20

TABLE 3.2 ALRAD CURRENT COIL SPECIFICATIONS

waveforms are then downloaded to a BBC microcomputer via the RS423 interface. This data along with other necessary information is stored on floppy disc for later analysis and the oscilloscope is then released ready for the next set of data. This apparatus was originally set up and the control/analysis software written by R.K. Avery (Avery,1986). Considerable modifications to both the hardware and software, however, have since been made.

3.4.1 The primary circuit and the drive waveform

In the dc case described above, the metallic glass core has no effect on the drive waveform. The windings of the test rig can be regarded as a resistance small enough compared with the other circuit elements to be neglected. This is not true under ac excitation where the core must be regarded as an inductor of magnitude

$$L = \mu_0 \mu_r A N_p / l \qquad ..(40)$$

where μ_r is the relative permeability of the core, A is the cross sectional area, l is the mean magnetic path length and N_p is the number of windings on the primary coil. μ_r in an unsaturated core can reach values approaching 10^6 but falls to unity when the core saturates. The impedance of the core can

therefore change by as much as 6 orders of magnitude as the B-H loop is traced out and it is this non-linearity of the core impedance which gives the hysteresis loop its characteristic 'S' shape and it is also the magnitude of this switch relative to the total primary circuit impedance (Z_p) which determines the shape of the drive field. The apparatus shown in figure 3.9 can be used to provide either sinusoidal H or sinusoidal B conditions or any state between the two depending on the relative values of Z_p and the core impedance. If Z_p is very much greater than L, the impedance change of the core with applied field will not be important and SINE-H conditions will result. If, however, Z_p is small compared with the core impedance then the sinusoidal voltage output of the amplifier will be dropped almost entirely across the core and sinusoidal B conditions will be realised. Note that in this case, the current in the primary circuit (and hence H), will be non-sinusoidal. In addition, it can be seen from equation (40) that L increases as the square of the number of turns on the primary coil. Now, N_p must be as large as possible to enable the production of large fields but this is limited by the maximum output power of the Crown amplifier which can deliver up to 10A, only into loads of less than 12 ohms. When winding a core therefore, these three constraints must be considered. As

described in section 3.1, the cores used in this project are 3cm in diameter and contain one metre of metallic glass. The test rig (figure 3.8) allows up to 10 primary turns and 20 secondary turns to be used. In practice, the rig is only rarely used with less than this maximum number.

In practice it is never possible to fulfill exactly the conditions required for either SINE-B or SINE-H conditions and the distortion can be considerable even at moderate flux densities. For this reason, feedback circuits which allow operation under sinusiodal B or sinusoidal H conditions have been designed and built. These circuits are shown schematically in figures 3.10 and 3.11 and their operation is described below.

3.4.2 SINE-B

For SINE-B, several feedback circuits have been published (Blundell, Overshott and Graham,Jr,1979; McFarlane and Harris,1958; Baldwin,1970) designed to reduce the harmonic distortion of the B waveform to less than 1 percent. These circuits all employ either B or dB/dT feedback and, although they may work at low frequencies over a limited frequency range, they suffer from severe phase and stability problems at higher frequencies. A slightly different approach is

outlined below.

In the circuit shown in figure 3.10, a sinusoidal voltage, $V_0 \sin\omega t$, is applied across a circuit of varying impedance and hence a non-sinusoidal current will flow. The voltage across the core is therefore

$$V_c = V_0 \sin\omega t - I(t)Z \qquad ..(41)$$

where I(t) is the current in the primary circuit and Z is the total lumped impedance of this circuit if the core were not present. Thus, the second term on the right hand side of the above equation is the origin of the distortion and the problem can be solved approximately by modifying the applied waveform by an amount proportional to this term. This is acieved in practice by including in the primary circuit a resistor (approximately 0.5 ohm) which dominates Z. The voltage dropped across this resistor is scaled and added to the function generator output to form a distorted sinusoidal input to the power amplifier. Figure 3.12 shows two dB/dt waveforms for a single core both with and without the SINE-B feedback.

3.4.3 SINE-H

Although most of the literature dealing with losses

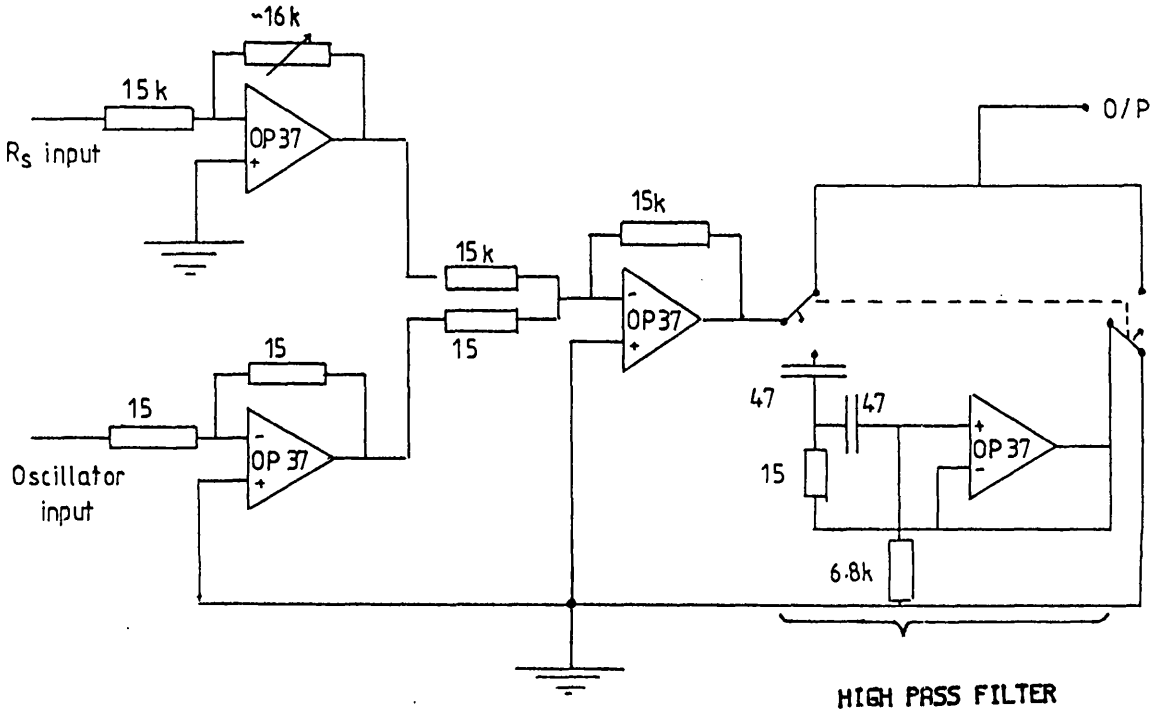

Figure 3.10 A SCHEMATIC OF THE 'SINE-B' FEEDBACK CIRCUIT

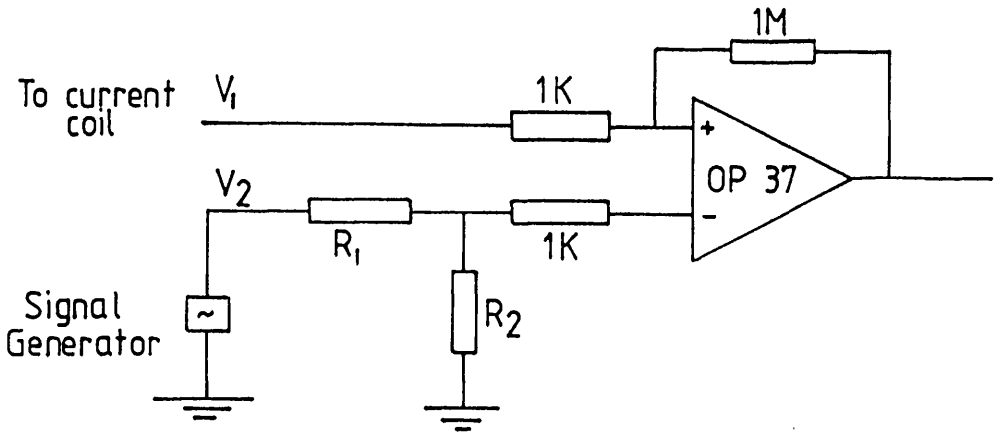

Figure 3.11 A SCHEMATIC OF THE 'SINE-H' FEEDBACK CIRCUIT

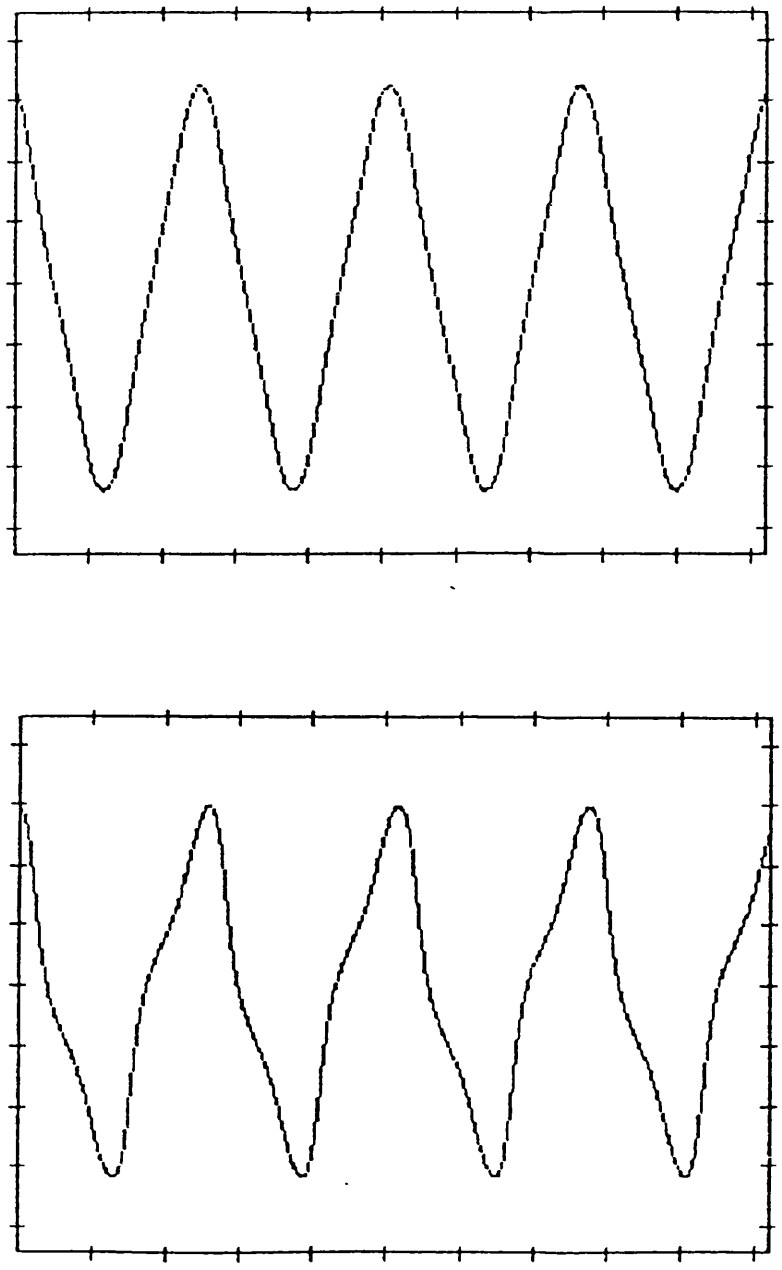

Figure 3.12 A dB/dt WAVEFORM OBTAINED UNDER IDENTICAL DRIVE CONDITIONS (a) WITH AND (b) WITHOUT FEEDBACK.

in amorphous materials has been carried out under controlled B conditions, it is more satisfactory from an analysis point of view to fix the drive conditions (H) and observe the resulting behaviour of the core (B) rather than try to analyse the H waveform required to produce a given B response. Hence the decision was made to operate under a contolled H regime. The feedback circuit required is shown in figure 3.11. Here, the departure of the H waveform from the ideal (ie the voltage waveform output by the signal generator) is sensed and the input waveform to the power amplifier is modified in such a way as to lessen this distortion. The resistor, R, is also included in the circuit to help maintain a sinusoidal current. R presents a fixed impedance to the amplifier output which is of the same order of magnitude as the core (at a few kilohertz) and thus renders the impedance change of the core on saturation, a lower fraction of the total circuit impedance (see section 3.4.1). This circuit operates satisfactorily up to frequencies of approximately 5kHz. The upper frequency limit being imposed by the phase response of the Amcron. All the results quoted here have been obtained with a third harmonic distortion of less than 3.5%.

3.4.4 Data processing

The data processing involved on the ac loops is essentially the same as that already described for the dc system with two important additions - the digital integration of the dB/dt signal and the calculation of the harmonic content of the B-H loop.

The two voltage waveforms digitised on the oscilloscope are transferred in the form of two strings of 1024, 8 bit numbers to a BBC microcomputer. The waveform from channel 1 of the oscilloscope is then scaled by the output response of the particular Alrad current coil in use and by the oscilloscope sensitivity setting to obtain H(t). The channel 2 waveform is integrated numerically using a trapezium rule integration routine before scaling to obtain B(t). One full cycle of the digitised data is then isolated and the waveforms are zeroed and then plotted as H vs B. The values of ac coercive field and remanent induction are calculated from the zero crossing points. No interpolation is used (cf dc case). This will lead to some errors in this calculation of these parameters, see section 3.4.5 where the errors and limitations of the ac system are discussed in greater detail. The ac loss is calculated using trapezium rule integration around the loop in

exactly the same way as the dc loss.

Having obtained the H and B waveforms, their harmonic content is calculated (up to the 10th harmonic) using a Fast Fourier Transform chip in the BBC microcomputer. The phases of the harmonics of both the H and B waveforms can be referenced to the fundamental of the H waveform and hence the loss can be calculated as

$$\text{Loss} = \sum H_m B_m \sin(m\omega t + \phi_m) \qquad ..(42)$$

In practice, however, this program is usually only used to check the levels of distortion in the H waveform. The program has been checked against a Hewlett Packard HP3561A signal analyser. Good agreement was found.

3.4.5 Errors and limitations

There are several sources of error inherent in this measurement system including errors in the digitisation and numerical integration and errors incurred in the measurment of the toroid dimensions and the current waveforms.

The effect of the inaccuracy of the oscilloscope is

somewhat different in the case of the H and B waveforms. For H, the ±3% uncertainty in the vertical deflection of the oscilloscope will be reflected directly in a ±3% uncertainty in the absolute value of H at any given time.

This is also true for the dB/dt waveform, but this is not directly reflected in the B waveform errors. Assuming that the errors in the vertical deflection of the oscilloscope traces are random, then the numerical integration of dB/dt will progressively reduce the error associated with consecutive points in the B waveform due to the vertical deflection uncertainty. The first point will have a maximum error of 3%, the second point will, on average, have a maximum error of 3 over root 2 percent, the third, 3 over root 3 percent and so on. In addition to these errors, the calculation of B from dB/dt requires a knowledge of the sweep speed of the oscilloscope and hence an extra 3% error is possible in the B waveform from the horizontal deflection uncertainty of the oscilloscope. Thus the error in B varies from point to point between 6% at the start of the loop $B(0^+)$ to little above 3% at the end of the loop $B(0^-)$.

The second category of errors are those present due to the numerical integration routine required to

calculate the area enclosed by the B-H curve using the formula

$$\text{Loss} = \int HdB = \int BdH \qquad ..(43)$$

A simple trapezium rule integration is used to calculate this loss and, tests on known computer generated ellipsoids have shown that the errors incurred in this routine are approximately 1%.

The errors incurred in the measurement of the toroid dimensions and those due to the current transformers can be estimated to be less than one percent giving a total error in the loss calculations of approximately 10%. In practice, the oscilloscope's own averaging routine is used to reduce the random errors in the H and dB/dt waveforms. Tests on both VAC 6030 and METGLAS 2605-SC cores have been shown to be repeatable to within 6% for all of the magnetic parameters calculated.

Two final points should be noted with respect to the ac measurements:-

i) It is known that the response of a ferromagnetic core to an ac field depends upon the core temperature. In addition, under

certain conditions, the heat generated in the core in the course of the ac measurements maybe sufficient to raise the core temperature. In order to ensure that the measurements made as part of this project were not subject to error arising from core heating, the core temperature was periodically checked and found not to increase by more than 1°C on any core, even under the most severe drive conditions.

ii) Although the Alrad current coil accuracies are rated by the manufacturer at ±1%, a calibration of one against the other revealed small but noticeable phase and amplitude differences. However, since the VAC 6030 data set was obtained using the Alrad 2877 transformer only, and the METGLAS 2605-SC data set was obtained using the Alrad 411 transformer only, the data sets are internally consistent.

3.5 Pulse Testing

The pulse testing arrangement is shown schematically in figure 3.13. The two capacitors (C_1 and C_2) are each composed of ten, one micro Farad, 250V polyester capacitors connected in parallel. The switch S is a mercury wetted relay and L_0 is a toroidal air cored inductor constructed in the same way as the remountable core former. L_0 has a mean diameter of approximately 0.03m, a cross-sectional area of order $10^{-3} m^2$ and the number of turns can be varied between one and twenty. The value of R (2.4kΩ) is chosen such that the time constant RC is small compared with the 1/(repetition frequency) (approximately 1s) but large compared with the discharge time of C through the saturable inductor (L).

To set up the standard test conditions, the core (L) is replaced with a resistor of value 2.4kΩ. This allows the second capacitor bank (C_2) to discharge between successive 'shots' but does not allow sufficient current to flow during the charging process to distort the charging waveform. Under these conditions (and assuming ideal circuit elements), the voltage rise across C_2 should be

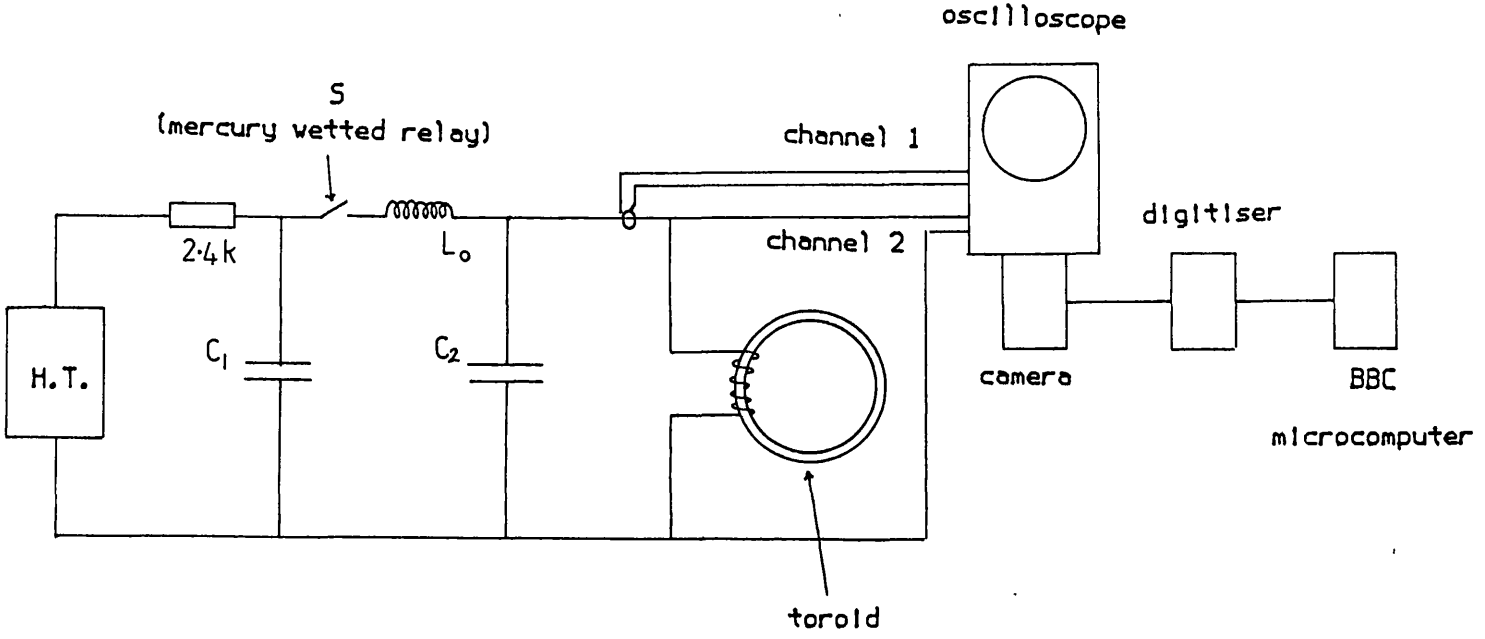

Figure 3.13 THE PULSE MEASUREMENT SYSTEM

$$V = V_0 (1-\cos\pi t/T) \quad ..(43)$$

(section 2.2). In practice, however, non-ideal circuit elements lead to a damped oscillation (section 2.2). The H.T. supply is adjusted so that the peak voltage of this waveform is approximately 20V. L_0 is chosen so that, assuming ideal core behaviour, the resonant charging time of the capacitor-inductor network is approximately the same as the hold-off time of the core to be measured. The resistor is then replaced by the core to be tested.

The core is reset between pulse 'shots' using an additional winding on the core (usually of one turn) and a dc bias supply. Inductors of 0.85mH and 5mH are included in the reset circuit to give it a high impedence at all frequencies of interest.

Note that in this arrangement, it is the dB/dt (and hence B) waveform of the core which is controlled and not the drive waveform.

3.5.1 Data collection and analysis

As in the case of the ac circuit, the primary current is monitored using an Alrad current transformer (model 411) whose signal V_1 is directly

proportional to the applied H field. In contrast to the ac case, however, the dB/dt (V_2) waveform is measured directly across the primary windings and not across the secondary. These two signals are applied to channels one and two of a Tektronix 7844 dual beam oscilloscope. V_2 also provides the oscilloscope triggering. The signals displayed on the oscilloscope screen are digitised using a Thomson TSN 1151 MIDAScope (10-bit) screen digitiser and the digitised signals are then transferred to a BBC microcomputer. In general the only part of the B-H loop of interest is the reversal from the reset value B ($\Delta B=0$) to positive saturation and hence only this part of the loop is displayed on the oscilloscope.

The software used to produce the reversal curve from these digitised traces is very similar to that on the ac system with one important difference. In the ac case at least one full waveform is digitised. Thus H=0 and dB/dt=0 are easy to determine. This is not true in the pulse system where only a part of the waveform is captured. Hence a 'baseline' is required for both the H and dB/dt waveforms. This is achieved by grounding both inputs to the oscilloscope and digitising the $V_1=0$ and $V_2=0$ traces. Each successive run is then referenced to these baselines. If any of the oscilloscope controls are changed (including the trace

brightness), the baselines must be re-measured.

The pulse testing arrangement described above was designed and the associated software (GOLD (Avery, 1987)) produced by Dr. R.K. Avery. A hard-wired pulse measurement box (connected as in figure 3.13), however, had to be built as repeatability was found to be a problem with the original system. With the exception of the 'pulse box', this equipment is situated at the British Aerospace site at Filton.

3.5.2 Errors and limitations

The errors associated with this measurement are largely the same as those described with reference to the ac system (section 3.4.5), namely errors in the numerical integration routine, in the core dimensions and inaccuracies in the digitisation of the H and dB/dt signals. Little technical data, however, is available for the Thomson digitising camera and hence a calculation of the absolute error involved in this measurement is not possible. The pulse performance parameter (which will be defined in section 4.3.1), however, shows a variation of less than ±6% from shot to shot.

In addition to the measurement errors listed above,

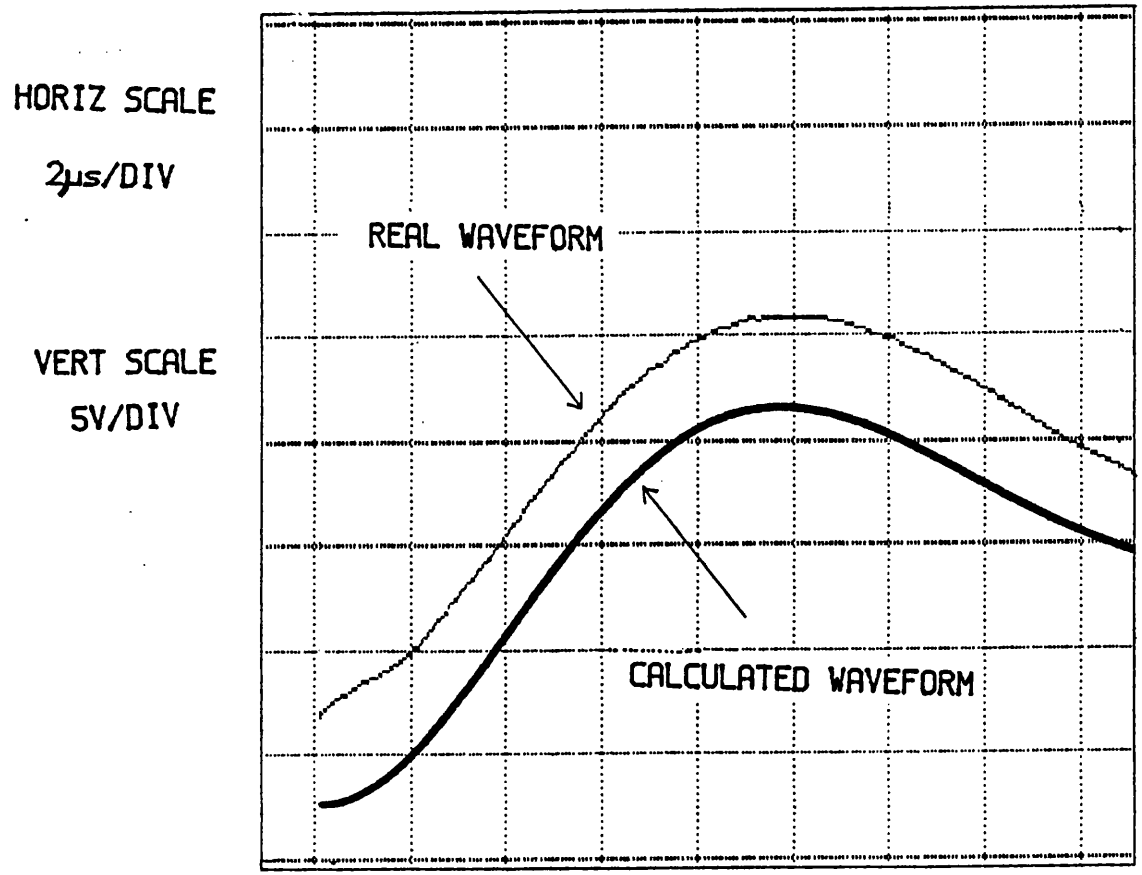

Figure 3.14 DAMPED RESONANT CHARGING WAVEFORMS

it can be seen from figure 3.14, that, although the applied voltage waveform can be approximated very closely using the damped resonant charging solutions presented in section 2.2 (assuming a series resistance of 0.3 ohms), a small deviation from ideal damped behaviour is exhibited by the real system in the initial part of the curve. This is thought to be due to the electrical behaviour of the mercury wetted relay as it closes and could not be eliminated either by changing the relay or the circuit layout.

3.6 Other measurements

After the above measurements have been made, two further tests were available if neccessary:- X-ray diffraction and ferrofluid domain observation. Since both of these are destructive tests, they were rarely used. No domain observation results are reported in this document and this technique will therefore not be described here. The X-ray diffraction work was carried with the following equipment

i) Philips PW 1730/10, 4kW X-ray generator
ii) Philips PW 2273/20 long fine focus, 2kW, copper target X-ray tube.
iii) Philips PW 1820/00 computer controlled vertical diffractometer goniometer

iv) Philips Xe proportional counter PW 1711/10 with graphite monochromator and automatic divergence slit assembly

v) Philips PW 1710 diffractometer control

vi) Philips PM 8203A chart recorder.

Each measurment was taken with a target potential of 40kV and an electron current of 30mA. The scan range was 40-50° at a 2θ scan speed of 0.008°/s.

3.7 Summary

This chapter has described the measurements systems used in this project, the principles of their operation and the errors and limitations associated with each. The following two chapters will present the results obtained with these systems.

CHAPTER 4

4 The effects of post production treatments on the magnetic properties of VAC 6030

In section 2.5 it was shown that for any given total compression ratio (gain), the volume of core material required in a pulse compression line is proportional to the reciprocal of the square of the flux swing available. In general, the iron based metallic glasses have the largest ΔB of all amorphous alloys and are therefore the logical choice for pulse compression systems. It is also true, however, that the iron based glasses are highly magnetostrictive (λ_s typically greater than 25ppm). In a high repetition rate pulse compression line, the magnetostrictive response of the core could, however, be detrimental to the core's behaviour. The stress generated in the core as the material is magnetised may obscure the effects of any careful post production tailoring of the magnetic properties of the core. Consider, for example, a material with a Young's modulus of 10^{11}Pa and a magnetostriction of 30ppm. The stress anisotropy developed as the material is magnetically saturated can be shown to be of order $100J/m^3$. This is comparable in magnitude with the anisotropy which can be introduced by field annealing ($10-1000J/m^3$,

depending on material composition).

In addition, at frequencies above a few hundred Hertz, it is possible that the magnetostrictive expansion of the core may excite vibration at one of the core's natural resonant frequencies and magneto-mechanical resonances may then dominate the core's magnetic behaviour (this will be discussed further in chapter 6). It is therefore possible that the magnetostrictive response of the iron-based metallic glasses may render these alloys unsuitable for pulse applications. In order to effectively remove magnetostrictive effects, a non-magnetostrictive alloy (VAC 6030) was used; this allows control of K_u but avoids the influence of K_σ. VAC 6030 was chosen in preference to other available 'low lambda' alloys solely because of its high saturation induction (see table 3.1).

4.1 The effects of post production treatments on the quasi-dc magnetic behaviour of VAC 6030 cores

The dc magnetic response of a given alloy can provide useful information regarding the effects of post production treatment on that material (sections 1.7-1.8). For this reason, every sample was first tested under dc conditions. These measurements

were performed at several maximum H fields in order to ensure a major loop was obtained. The following sections (4.1.1-4.1.3) summarise the dc magnetic responses of the VAC 6030 alloy after a variety of post production heat treatments.

4.1.1 As-Received and Stress Relief Annealed Cores

The dc measurements on as-received and stress relief annealed samples are divided into two categories - straight strip and toroid. This differentiation between sample geometries is important since the lower cooling rates (from the anneal temperature) exhibited by the toroidal samples were found to have a significant effect on the magnetic properties of this material.

It was noted, in section 1.7.1, that the dc response (in particular the dc coercivity) of an amorphous alloy in the as received state is affected by stresses introduced by the rapid quench, and that the strength of this effect depends on the material magnetostriction. Therefore, even given that VAC 6030 is a near zero magnetostriction material (λ_s <0.2ppm), a small decrease in H_c is expected after annealing due to the relief of the quenched-in (and in toroidal form, wound-in) stresses. A small drop in the value of

H_c is indeed observed (figure 4.1) on 20cm straight strip samples of VAC 6030 annealed at 425° C (75° above T_c ; 25° below T_x). The increase in H_c seen after annealing for approximately 60 minutes can be attributed to an increase in domain wall pinning at stress centres, this time generated by the onset of crystallisation.

Toroids annealed under the same furnace conditions, however, did not show a decrease in coercivity. As figure 4.2 shows, the coercivity of these samples was actually seen to increase after this heat treatment, their remanence ratio fell and their magnetisation energy increased. This change was observed following an anneal of 1.5 minutes. A plateau was then reached until anneal times in excess of 60 minutes. The increase in coercivity at long anneal times can, again, be attributed to the onset of crystallinity.

The initial changes observed in the dc loop shape are contrary to the stress relief arguments outlined above. In order to understand why these changes should occur, we have to examine in detail the annealing cycle and determine how it differs between the two sample geometries in question.

Firstly let us consider the anneal of a straight

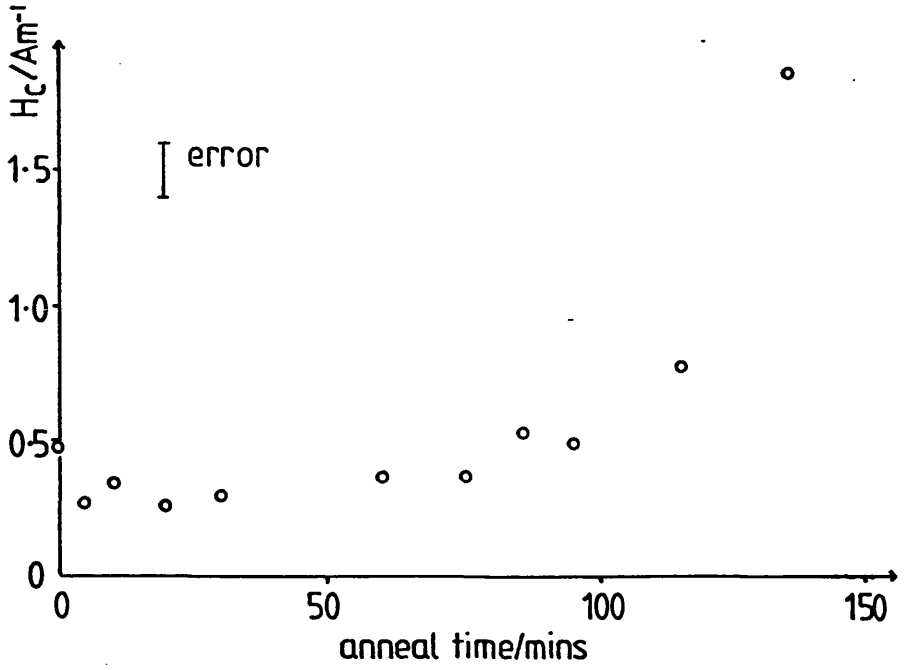

Figure 4.1 COERCIVITY vs ANNEAL TIME FOR STRAIGHT STRIP VAC 6030

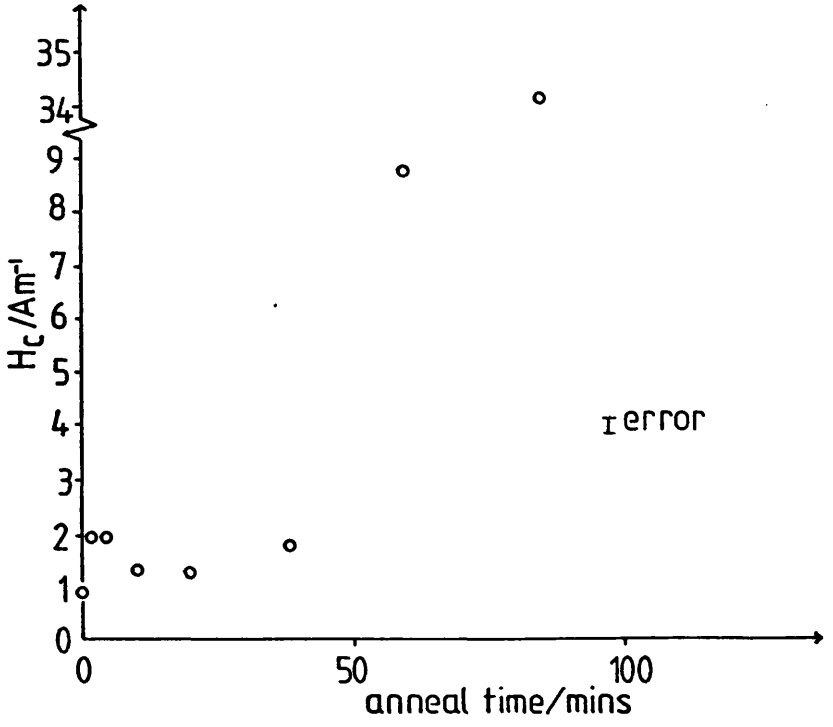

Figure 4.2 COERCIVITY vs ANNEAL TIME FOR TOROIDAL VAC 6030 SAMPLES

strip sample. A sample of this type assumed the oven temperature immediately on contact with the furnace base and, since the entire anneal was carried out above the Curie temperature, the sample was in the paramagnetic state throughout the treatment. On removal from the oven, the sample was quickly transferred onto a flat aluminium plate (at room temperature) and was therefore cooled almost instantaneously to room temperature. By contrast, the toroidal sample, because of its larger thermal mass and smaller contact area (with the furnace floor and aluminium cooling plate), heated and cooled more slowly than the straight strip sample. The lower heating rate proved to be unimportant, it is the cool rate from the anneal temperature which holds the key to understanding the response of the toroidal samples to the annealing treatment.

As noted above, during the anneal, the core temperature was 75° C above the material's Curie temperature. The core was therefore paramagnetic throughout the anneal. As the core was cooled through T_c, however, it returns to the ferromagnetic state and, again, divides into domains. Now, whilst the material is below the Curie point but still at a sufficiently high temperature for atomic re-arrangement to take place, localised self-

annealing can take place and local anisotropy is developed in the region of the domain walls and within individual domains (see section 1.7.2). This has two important effects. Firstly, the sample produced after the anneal has a complicated set of anisotropies determined by the domain configuration present just below the Curie temperature. Secondly, since the effect of the self anneal is to minimise the domain wall energy, the spin geometry matches that of the local easy axes and the magnetic self annealing, therefore, produces small potential wells in the vicinity of the domain walls. Now, the coercivity of a magnetic material, in a simple model, is directly proportional to the maximum energy gradients encountered by a domain wall as it traverses the sample (section 1.5 and Cullity,1972). It is therefore possible that in a particularly soft material with a low magnetostriction, where there is little domain wall pinning, the energy gradients caused by these potential wells may be large enough to have a significant effect on the coercivity. To test that this mechanism could be responsible for the observed increase in H_c, a straight strip sample was alternately annealed above and below the Curie temperature and H_c measured after each anneal. Figure 4.3 shows the results of this experiment. The value of H_c measured alternates between approximately

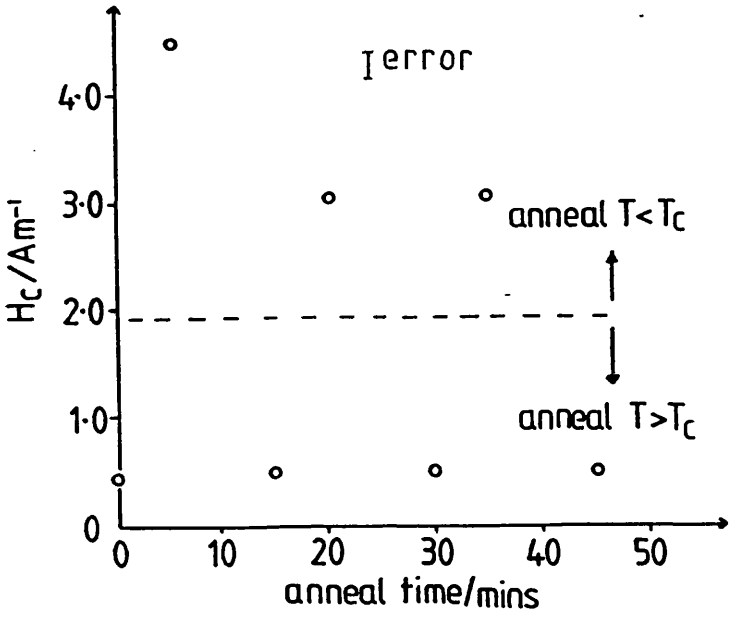

Figure 4.3 COERCIVITY vs ANNEAL TIME FOR A VAC 6030 SAMPLE ALTERNATELY ANNEALED ABOVE AND BELOW THE CURIE POINT

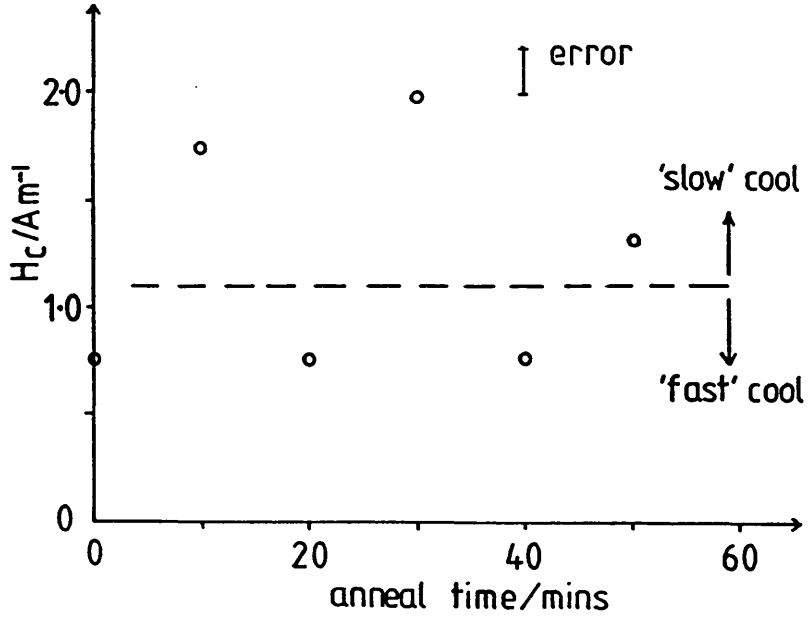

Figure 4.4 COERCIVITY vs ANNEAL TIME FOR A VAC 6030 SAMPLE ALTERNATELY FAST AND SLOW COOLED

0.5A/m for those samples annealed above T_c and 3.0A/m for those annealed below the Curie temperature.

This confirms that magnetic self annealing can produce the behaviour shown in fig 4.2. A second experiment was performed in order to verify that this was the mechanism involved. Anisotropy induced by field annealing is a kinetically controlled process and must occur below the Curie temperature. Thus, if magnetic self annealing is the cause of the observed behaviour, it should be possible to suppress the increase in H_c simply by cooling the core rapidly from the anneal temperature. Figure 4.4 shows the cyclic variation in H_c of a single toroid annealed above T_c and alternately cooled 'slowly' (2° C/s) in air and quickly in water (100° C/s). These results confirm the conclusion that the observed increase in H_c on annealing is due to the development of local induced anisotropies in the region of the sample domain walls.

Toroids were also cooled in liquid nitrogen but tests have shown (figure 4.5) that toroids cooled in water (at 20° C) exhibit a higher cooling rate than those cooled in liquid nitrogen. This can be attributed to the formation of a gaseous boundary layer at the surface of the material cooled in nitrogen which inhibits heat transfer to the liquid

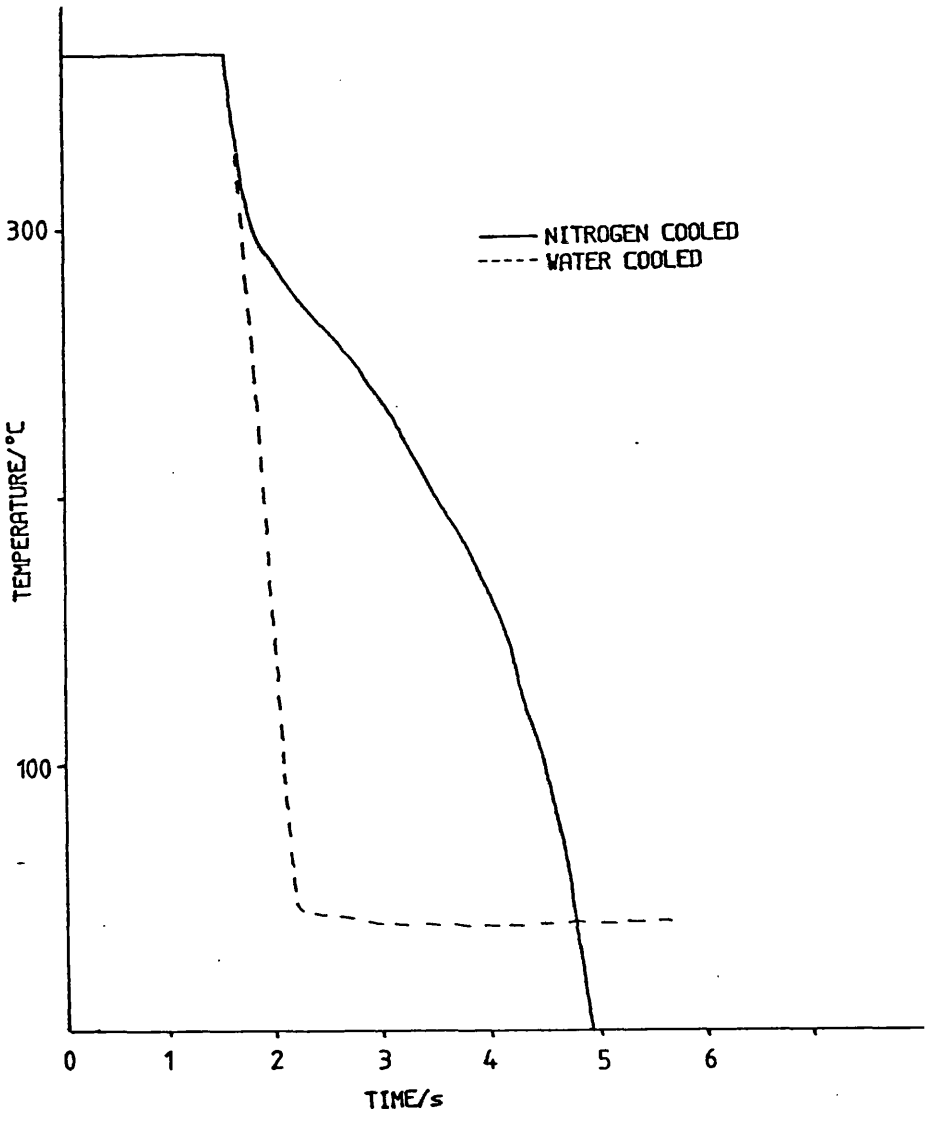

Figure 4.5 COOL RATES OF SAMPLES QUENCHED IN WATER AND LIQUID NITROGEN

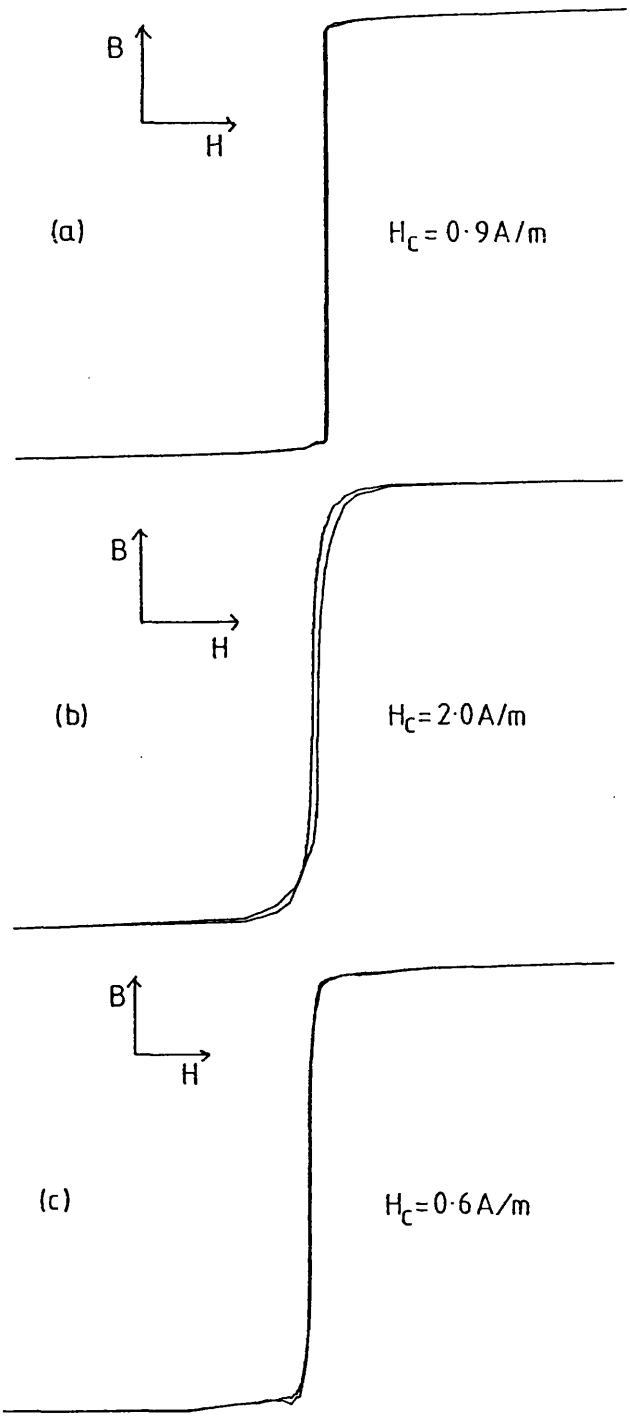

Figure 4.6 DC LOOPS OF (a) AS-RECEIVED (b) STRESS RELIEF ANNEALED AND (c) FAST COOLED TOROIDAL VAC 6030 SAMPLES

$H_{max} = 110\ A/m$

and thus decreases the cooling rate.

Figure 4.6 shows typical dc hysteresis loops of as-received, stress-relief annealed and fast-cooled toroid. In addition to their low coercivity, it should be noted that the fast-cooled samples show a slightly slower approach to saturation than the as-received samples. The reason for this is unclear at present but may be connected with stress generated in the core due to the fast cool.

4.1.2 Field Annealed Cores

An alternative method of eliminating this development of local induced anisotropy in the region of the domain walls is to magnetically saturate the sample throughout both the anneal and the cool. In this way, even below T_c, no domains are present in the sample and hence no local anisotropy is developed. A long range uniaxial anisotropy, however, is induced. Three different types of field anneal were used - a transverse dc field, a longitudinal dc field and an ac longitudinal field. In each case, the samples were annealed at 425°C for 4.1 minutes. This was chosen since the results presented in fig 4.2 indicate that this is sufficiently long to allow any stress relief to take place but short enough to avoid any

crystallinity. However, for each type of anneal, one toroid was annealed for 15 minutes and compared with a toroid annealed for 4.1 minutes under the same conditions. In all cases, the duration of the anneal was found to be unimportant thus confirming that the samples were fully stress relief annealed but not crystallised.

In the following sections, references will be made to the cool rates of the toroids from the anneal temperature. It should be noted that the cool rates were not held constant thoughout the cool. The values quoted were measured from the time-temperatures plots at the sample Curie temperature. Figure 4.7 shows a typical time-temperature plot.

4.1.2.1 Transverse Field

The transverse field anneals were carried out in the hot air furnace between the poles of the Newport electromagnet as described in section 3.2. The samples were heated as quickly as possible using the hot air gun giving an initial heating rate in excess of 5°C/s. After 4.1 minutes at 425°C, the hot air gun output temperature was decreased to minimum giving a forced air cool. The cool rate was approximately 4°C/s. The applied field was 300kA/m.

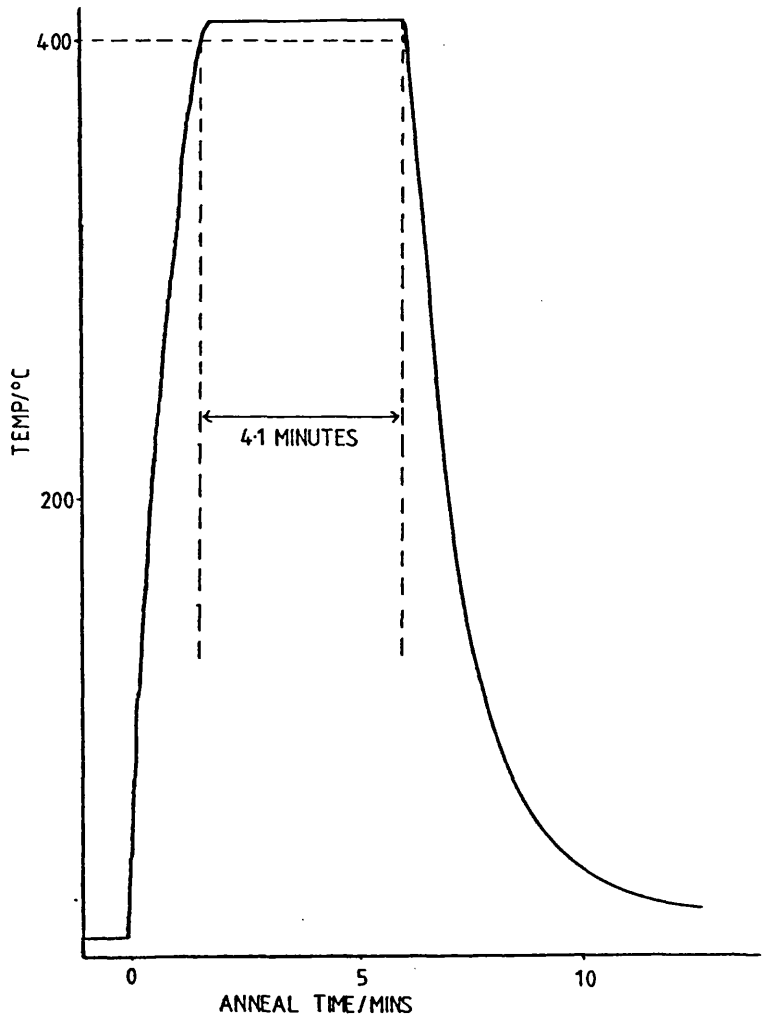

Figure 4.7 TIME-TEMPERATURE PLOT FOR THE TUBE FURNACE

Figure 4.8 shows the dc hysteresis loop of a transversely field annealed toroidal sample. The sample shows the linear B-H loop and low H_c characteristic of a moment rotation system with transverse anisotropy (Jakubovics,1987).

4.1.2.2 dc Longitudinal Field

The longitudinally field annealed samples were heat treated as described in section 3.2. In all cases a circumferential field of 210A/m was applied. Since the samples were annealed above the Curie temperature, it was only during the cool $T<T_c$, that any long range anisotropy was induced. The magnitude of the induced anisotropy therefore depends on the cool rate (see section 1.7.2 regarding the kinetics of induced anisotropy). A series of identical toroids were annealed under the same furnace conditions and then cooled at various rates in the range 0.3-100°C/s. The magnitude of the induced anisotropy was expected to increase with decreasing cool rate.

Figure 4.9 shows dc loops of several longitudinally field annealed samples cooled at different rates. It can be seen that all of the samples exhibited a low coercivity (less than 0.8A/m) and exhibited a very square dc loop. Because the loops are so square, even

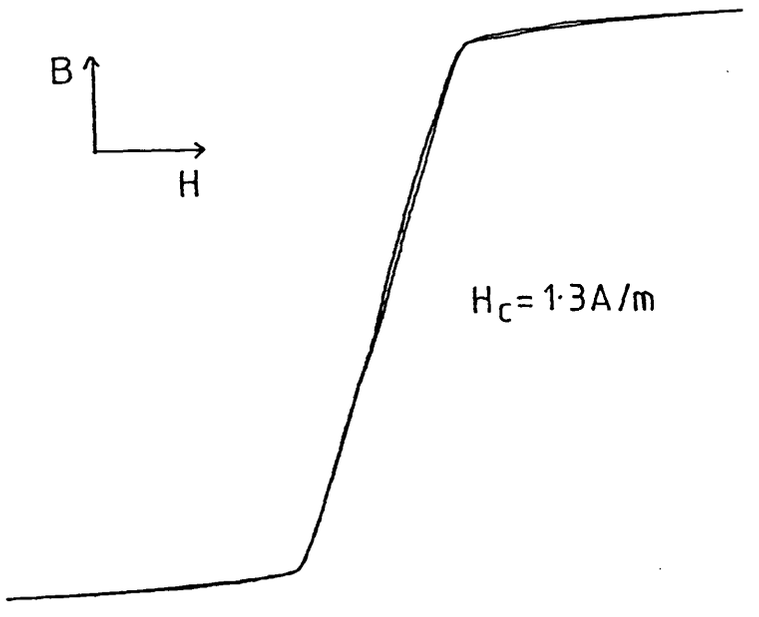

Figure 4.8 DC LOOP OF A TRANSVERSELY FIELD ANNEALED SAMPLE

$H_{max} = 110 A/m$

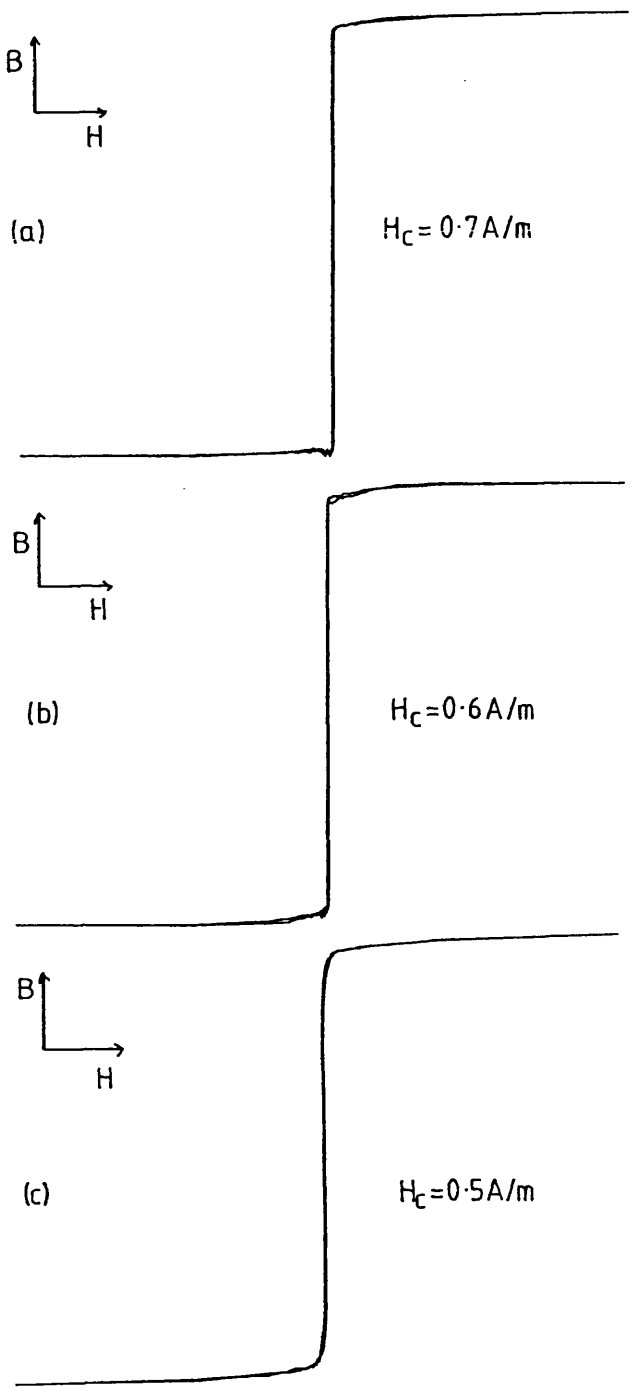

Figure 4.9 DC LOOPS OF LONGITUDINALLY FIELD ANNEALED SAMPLES COOLED AT DIFFERENT RATES (a) 0.5°C/s (b) 5.8°C/s AND (c) 30°C/s

$H_{max} = 110 A/m$

when using a very high shape factor on the dc measurement system (section 3.3.4.2), very few points were digitised on the rapidly changing portion of the B-H curve. The parameters calculated from these measurments are therefore to be treated cautiously. The dc measurements obtained can only reliably be used to indicate that the loops exhibited by all of the samples treated in this way were very square and that the sample coercivities were low.

It should be noted that the highest cool rate quoted here was obtained by cooling the core in water. This is the same as the treatment given to the stress relieved samples in order to suppress the development of local anisotropy. It should also, therefore, suppress the induction of long range anisotropy and these two samples should exhibit very similar magnetic responses. This can be seen to be the case (compare figures 4.6 and 4.9).

4.1.2.3 ac Longitudinal Field

Under ac field annealing conditions, a long range uniaxial anisotropy will be induced in the direction parallel to the applied field provided that the alternating field is sufficiently large to saturate the sample for a significant fraction of the ac cycle

(Graham,1958). If the ac field applied during the anneal is small, then little or no long range anisotropy will be induced. However, the ac field will keep the domain walls in the sample mobile throughout the cool and thus self annealing of the domain wall structure itself may be avoided. Local anisotropies within the domains themselves, may, however, still develop. The toroidal form of the samples (via the shape anisotropy) ensures that the domain structure assumed by the sample on cooling through T_c will be one in which most of the atoms have their magnetic moments aligned along or close to the ribbon axis. Thus the anisotropies developed within the domains will have a significant longitudinal component.

Figure 4.10 shows the dc loops of two ac field annealed samples. Fig 4.10a shows a sample annealed in a RMS field of 210A/m; fig. 4.10b shows a sample annealed under the same thermal cycle with an applied RMS field of 21A/m. Figure 4.10b should be compared with the dc field annealed sample shown in fig. 4.10c which was cooled at a similar rate. Little difference in the dc properties can be seen. The low-field, ac-annealed sample also exhibited a low coercivity but showed a more rounded dc-loop. The small ac field used here, however, is, again, almost sufficient to saturate the sample at 50Hz and interpretation of

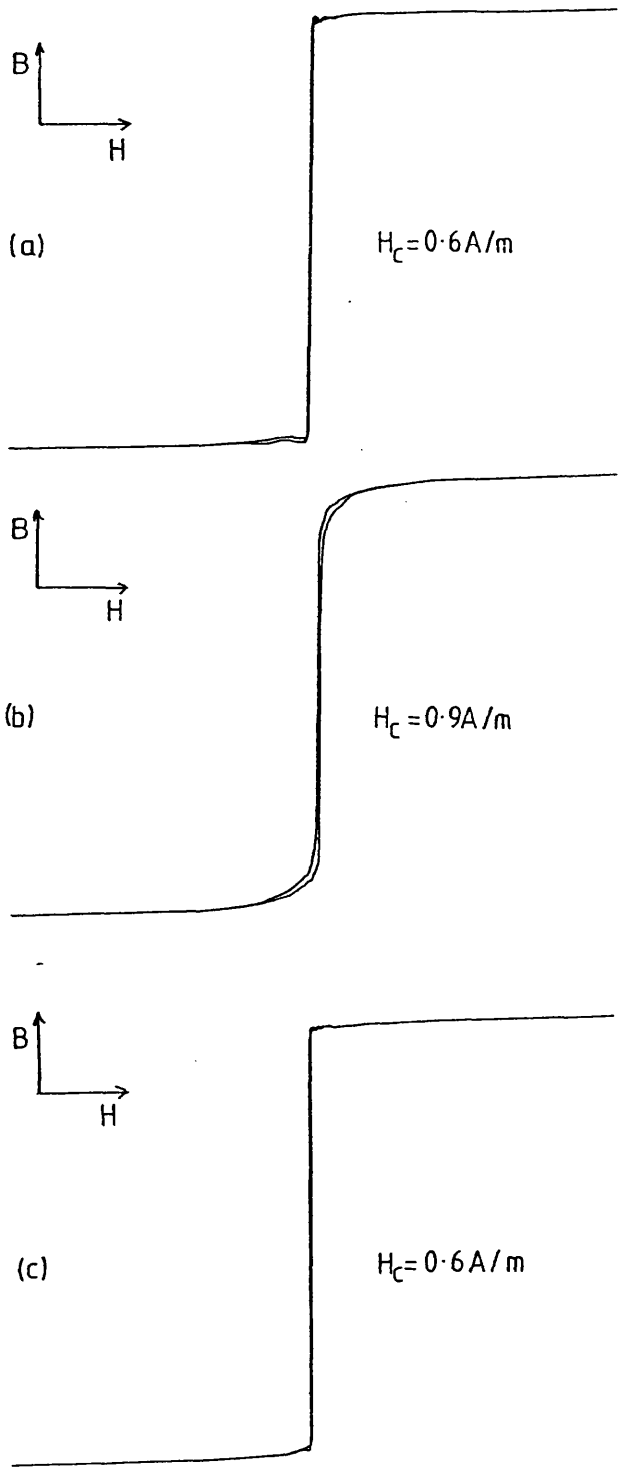

Figure 4.10 DC LOOPS OF SAMPLES FIELD ANNEALED UNDER SEVERAL CONDITIONS

(a) SATURATING AC FIELD (b) LOW AC FIELD (c) SATURATING DC FIELD

H_{max} =110A/m

these results is therefore difficult. One possible explanation of the results obtained on this sample is as follows. The ac field may have introduced a significant longitudinal anisotropy as the moving walls saturated a large fraction of the sample volume (this is supported by the very high initial susceptibility seen from the B-H curve). An off-axis anisotropy, may, however, have developed in the parts of the sample which were not affected by the field or around domain walls which were moved little by the applied ac field.

4.1.3 Scribed samples

In addition to the thermal treatments described above, a mechanical surface treatment of the cores was also investigated.

Several cores were scribed in different ways, some with fine grade 'wet and dry' paper (SiC 400) with the scratches running parallel to the ribbon direction, others with tungsten carbide and diamond scribes. Of the cores which were scratched with the tungsten carbide scribe some had the scratches parallel to the ribbon axis, some perpendicular, some were scratched on one side and some on both. On all of these cores, the scratch spacing was approximately 1mm. The dc loop

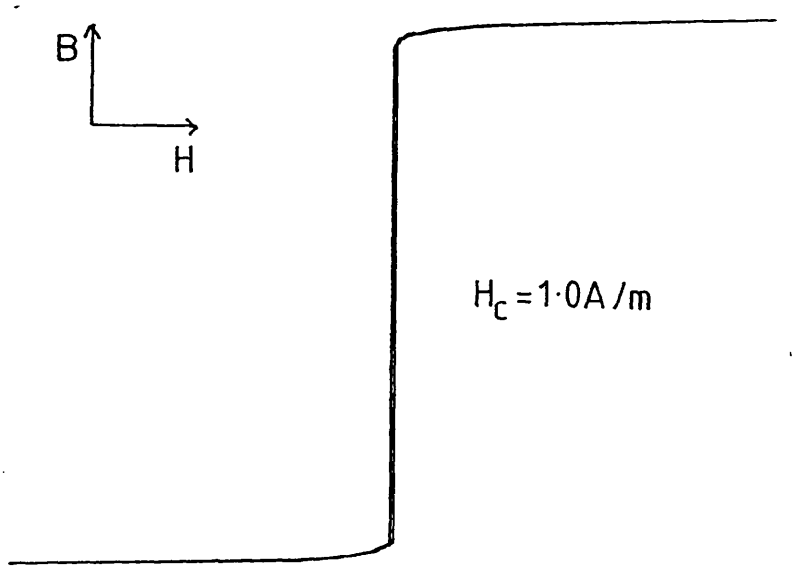

Figure 4.11 DC LOOP OF A SCRATCHED CORE

$H_{max} = 110 A/m$

shown in figure 4.11 is that obtained on a sample of VAC 6030 scribed perpendicular to the ribbon axis on both sides. The loop differs little from the loop shown in figure 4.6 which was obtained with an as-received sample of VAC 6030. This core is typical of all of the cores scratched in any way and indicates that, although in some cases the cores were severely mechanically deformed, the stress induced by the scratching process couples only weakly or not at all to the dc magnetic properties of this material.

4.1.4 Summary of the dc results on VAC 6030

The dc results presented in sections 4.1-4.1.3 can be summarised as follows.

The deterioration of the dc magnetic properties of VAC 6030 after stress relief annealing can be attributed to self annealing of the core during the cool from the anneal temperature. This can be avoided by either fast cooling the core from the anneal, by magnetically saturating the core thoughout the anneal and cool or by applying a small ac field to the core in order to keep the domain walls in constant motion.

The saturating field annealed cores exhibited very square dc loops with a low dc loss and high remanence

ratio. According to the simple SWT picture of fast flux reversal presented in section 2.4.1, this would appear to be ideal for pulse compression applications.

Core scribing appears not to affect the dc properties of this material. This can probably be attributed to the low magnetostriction of VAC 6030.

4.2 The effect of post production treatments on the ac magnetic behaviour of VAC 6030

Although the dc hysteresis loop of a ferromagnetic material can yield useful information on some aspects of the magnetisation process (domain wall pinning, domain wall motion, moment rotation etc), it can give no information regarding the dynamics of flux reversal. Ac measurements under accurately reproducible conditions are required to determine how a given sample will behave under rapid flux reversal conditions. Section 3.4.3 described the experimental arrangement used for SINE-H ac measurements in the frequency range 0.5-4.0kHz. This section will present the ac responses of the samples whose dc behaviour was described above.

All the ac results presented here were obtained at 1kHz with an applied field of approximately 60A/m. All

were obtained with the third harmonic distortion of the H waveform was less than 3.5%. It should be noted that, under these drive conditions, the core material approached saturation.

Similar results were also observed at excitation frequencies of 0.5,2 and 4kHz and over a range of applied fields at each frequency thus indicating no frequency dependence of these results.

4.2.1 As-Received and Stress Relief Annealed Cores

In the as-received state, VAC 6030 exhibits a very 'square' dc magnetic characteristic (section 4.1.1) and this is reflected directly in its ac response (shown in figure 4.12a). Again the loop is very square with a remanence ratio greater than 0.9. This coupled with the high ac coercivity (17A/m) results in an ac loss of 52J/m^3/cycle.

Figure 4.12b shows a typical ac loop of a stress relieved VAC 6030 toroid. It can be seen that the remanence ratio and the ac loss have decreased but the ac coercive force remains unchanged. The decrease in remanence ratio is expected from the dc loop; the off-axis anisotropy developed by the localised field annealing led to a more rounded dc magnetisation loop.

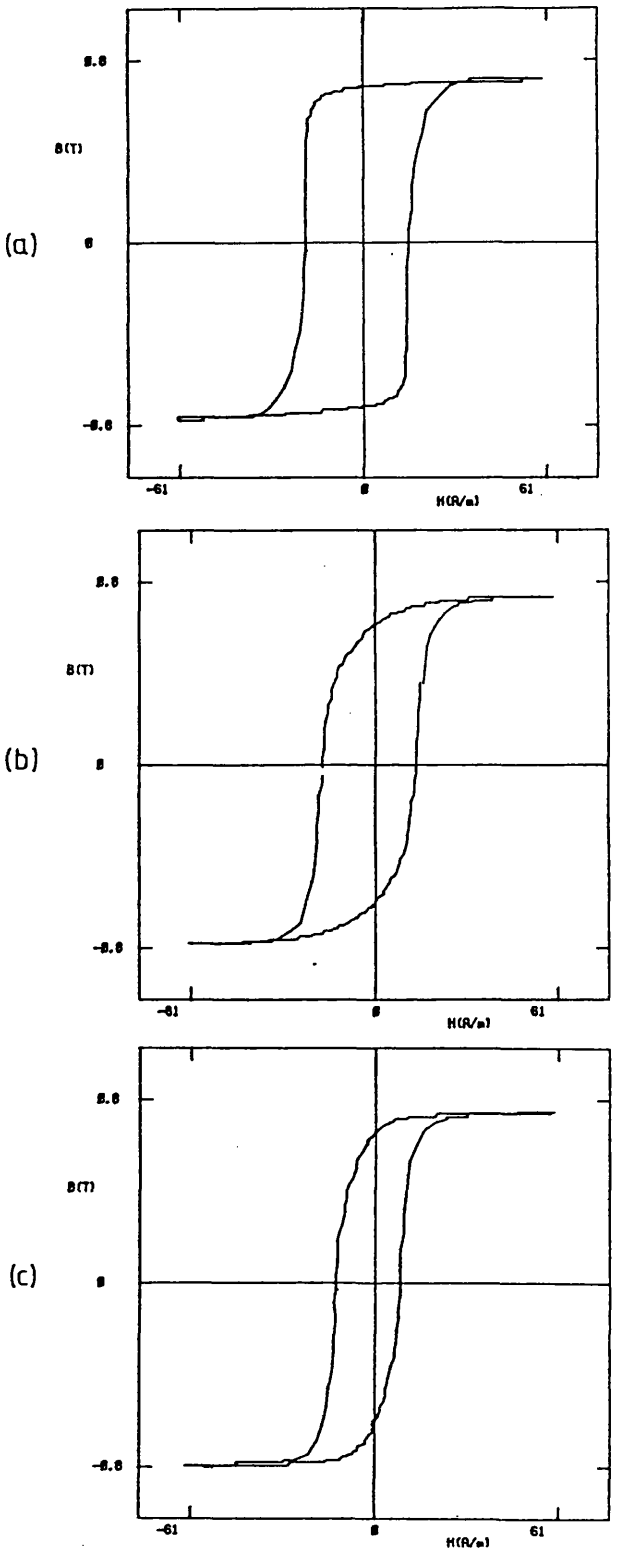

Figure 4.12 AC LOOPS OF (a) AS-RECEIVED (b) STRESS RELIEF ANNEALED AND (c) FAST COOLED TOROIDAL VAC 6030 SAMPLES

The reduction in ac loss observed after annealing occurs despite an increase in the domain wall pinning (H_c) and the dc loss. This result can be explained by considering a modification to the domain structure responsible for the magnetisation reversal. More specifically, a reduction in the ac eddy current loss associated with moving domain walls. It was reported, in section 1.7.1, that the eddy current loss due to a moving domain wall is proportional to the square of the wall velocity. It was also noted (in section 1.7.2) that an increase in the longitudinal component of anisotropy is likely to result in an decrease in the number of walls available. It is clear from the dc data that the as-received samples exhibit a larger component of longitudinal anisotropy than do the stress-relieved cores and the lower losses of the stress relieved toroids are therefore probably due to an increase in the number of active walls. This is also consistent with the results of Tan (1986) and Beckley, Snell and Lockhart (1985) who reported a reduction in ac loss after surface treatments which increased the number of walls active within the samples and with the partial crystallinity studies presented earlier (see sections 1.8.2 and 1.8.3)

At long anneal times, the effects of crystallinity again start to dominate the magnetic response of the

cores with the ac loss and coercive force increasing and the remanence ratio decreasing further (figure 4.13). This will be discussed further in chapter 5.

The fast-cooled toroids (figure 4.12c) exhibit a very different ac characteristic to both the as-received and stress relieved, slow-cooled samples. The ac loss of the fast-cooled toroids is $27J/m^3$/cycle, the remanence ratio, 0.87 and the ac coercivity, 8.7A/m. By the same argument cited above, the reduction in ac loss is probably due to an increase in the number of domain walls available. This again is supported by the larger dc magnetisation energy exhibited by these toroids, indicating a lower longitudinal component of anistropy and therefore more domain walls. The reduction in loss over the stress relieved cores may be related to the reduction in domain wall pinning in the fast cooled toroids.

The ac magnetic behaviour of these toroids, therefore represents a considerable improvement on both the slow-cooled toroids and the as-received. This has been achieved by supressing the development of local anisotropy in the region of the domain walls and reducing the magnitude of the longitudinal component of anisotropy.

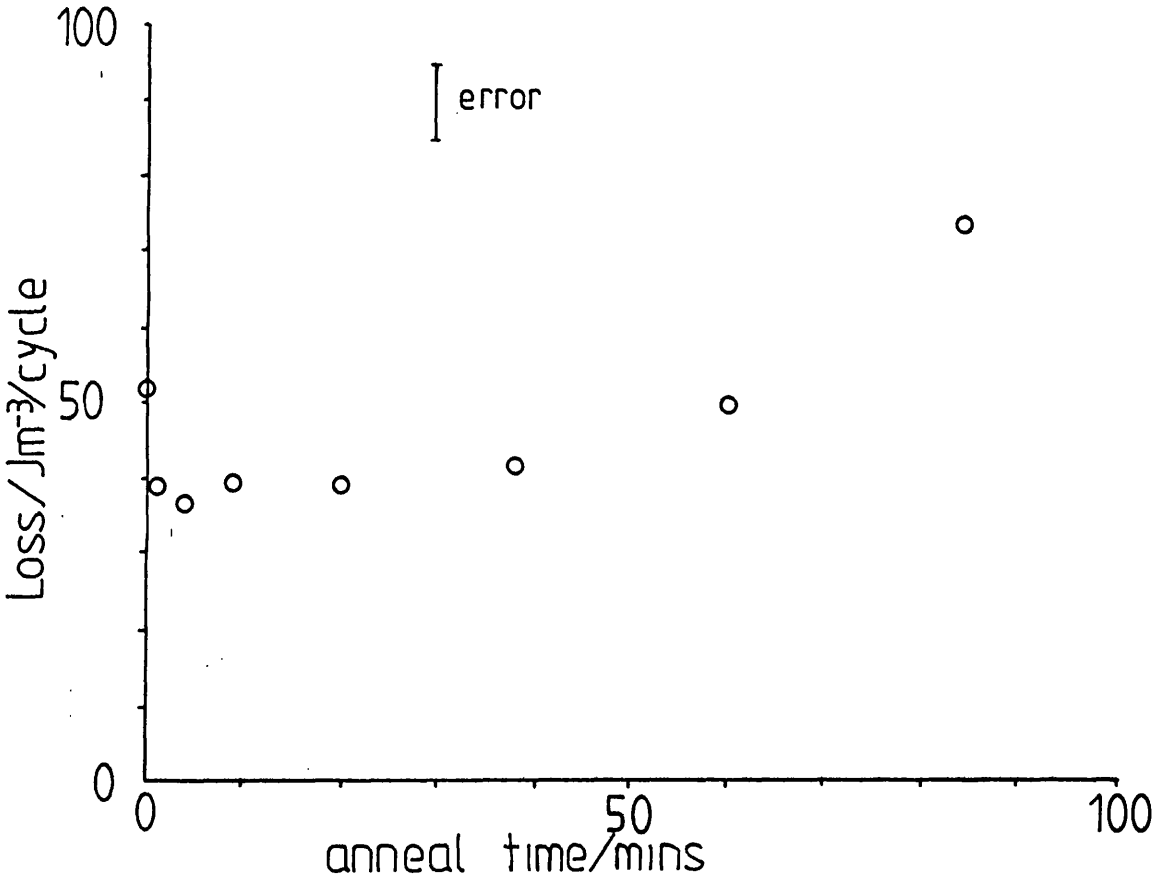

Figure 4.13 AC LOSS vs ANNEAL TIME

4.2.2 The effect of field annealing on the ac properties of VAC 6030 cores

Sections 4.1.2.1-4.1.2.3 described how a longitudinal field anneal can be used to avoid the problems associated with local induced anisotropy. The following sections will present the ac results obtained on the field annealed cores.

4.2.2.1 Transversely field annealed cores

In an ideal transversely field annealed sample, magnetisation reversal takes place by moment rotation alone and there is therefore no wall motion. Thus the eddy current loss associated with moving domain walls is entirely absent and the observed ac loss therefore expected to be lower than that seen in samples where the reversal takes place by domain wall motion. A significant reduction in the ac loss was observed in the transversely field annealed sample ($10J/m^3$/cycle), lower even than that observed in the fast-cooled samples when driven with the same field ($27J/m^3$/cycle). It should be noted, however, that the flux swing obtained for any given field was lower for the transversely field annealed material (until saturation).

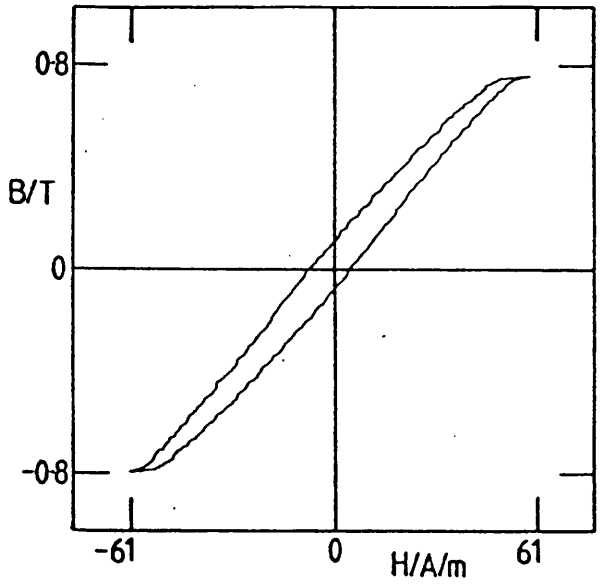

Figure 4.14 AC LOOP OF A TRANSVERSELY FIELD ANNEALED CORE

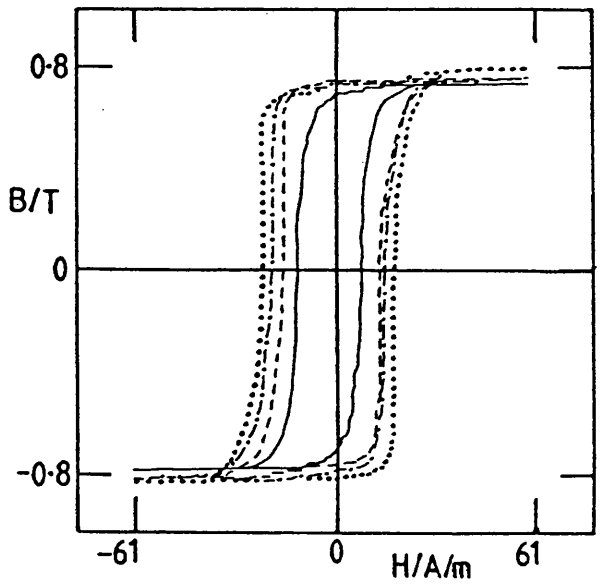

Figure 4.15 DC LOOPS OF SEVERAL LONGITUDINALLY FIELD ANNEALED CORES COOLED AT ····· 0.5°C/s ----0.9°C/s ----5.8°C/s AND —— 30°C/s

Figure 4.14 shows a typical loop obtained on a transversely field annealed sample.

4.2.2.2 dc Longitudinal Field

Under dc conditions, it was seen that, except at very fast-cool rates, the longitudinally field annealed toroids all showed low coercivities and high remanence ratios. The very fast-cooled sample again showed a low H_c but a somewhat more rounded loop giving a lower remanence ratio and higher magnetisataion energy. Under ac conditions, a very square loop is again seen in all of the toroids except the water-cooled sample. There is however a systematic increase in ac loss with decreasing cool rate. In other words, the ac loss increases with the increasing magnitude of the longitudinal component of anisotropy (figs 4.15 and 4.16). This is consistent with the argument presented above to explain the losses obtained with the stress-relieved samples. The increase in ac loss can be explained by considering a successive reduction in the number of walls available for reversal, with increasing longitudinal component of anisotropy.

The fast-cooled sample annealed in the presence of a dc field shows very similar ac magnetic properties

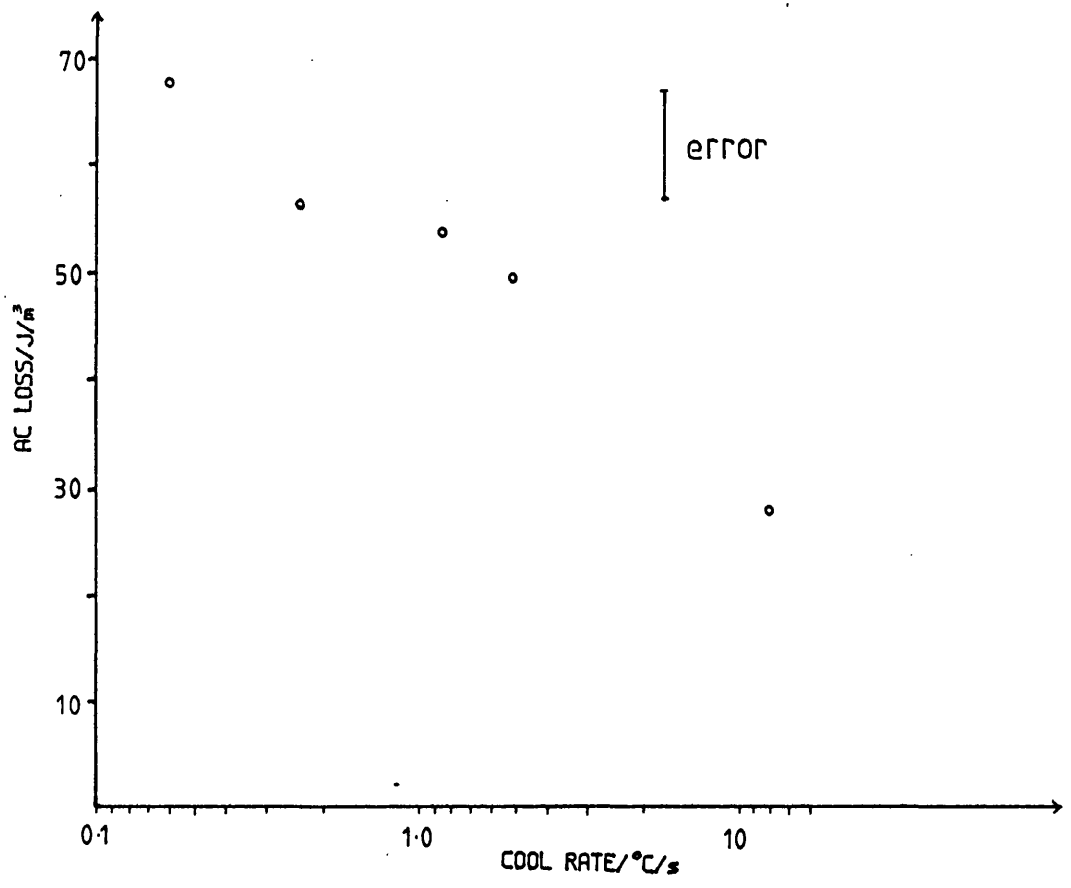

Figure 4.16 AC LOSS vs COOL RATE

to the toroid fast-cooled from a simple stress relief anneal confirming that at this rate of cool, insufficient time is available at elevated temperatures (below T_c) for pair ordering to take place.

4.2.2.3 ac Longitudinal Field

The ac hysteresis loop of a VAC 6030 toroid annealed with a saturating ac field is very similar to that exhibited by a sample annealed in a saturating dc field and cooled at the same rate (figure 4.17). This is as expected (section 4.1.2.3).

The low-field ac-annealed core also exhibits a similar ac loss to the dc field annealed toroid although the ac loop shows a somewhat slower approach to saturation, as did the dc loop of this core. Without more information, for example, similar treatments at different cool rates, it is not possible to definitively explain this result. However, the high ac loss again indicates that the flux reversal is carried out with only a few walls, and the slow approach to saturation indicates a significant component of moment rotation. This is consistent with the explanantion of the dc results given in section 4.1.2.3.

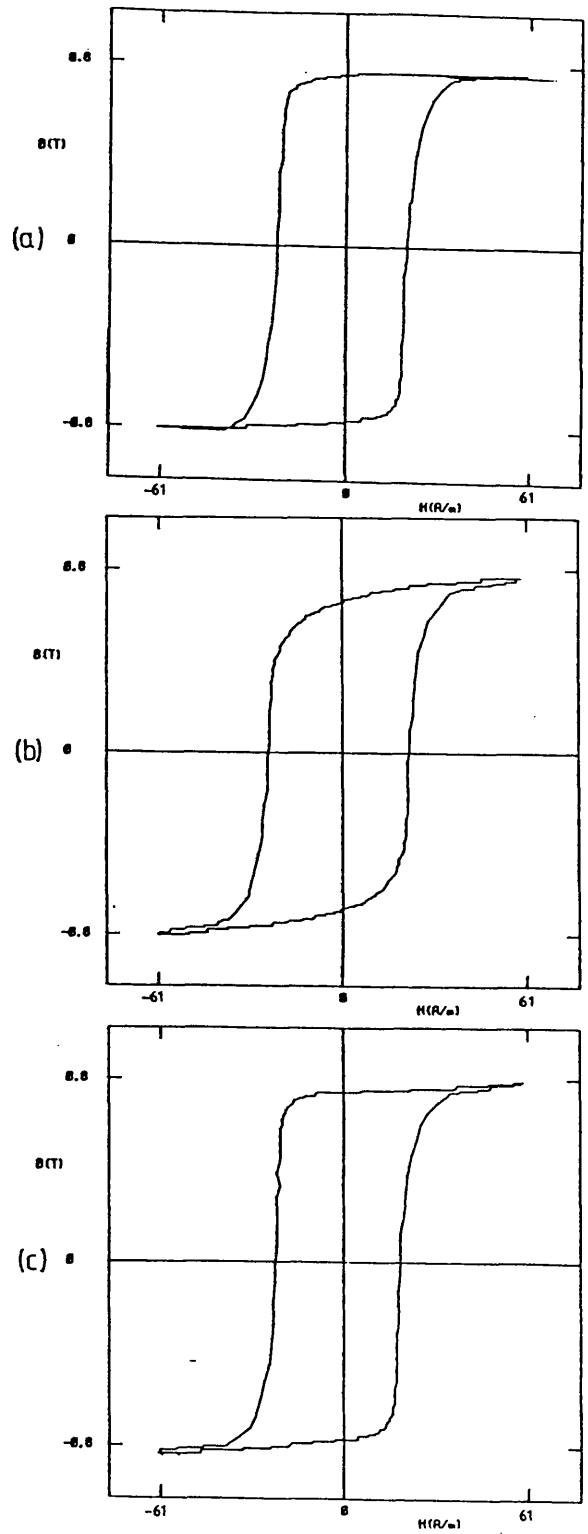

Figure 4.17 AC LOOPS OF SAMPLES FIELD ANNEALED UNDER SEVERAL CONDITIONS
(a) SATURATING AC FIELD (b) LOW AC FIELD (c) SATURATING DC FIELD

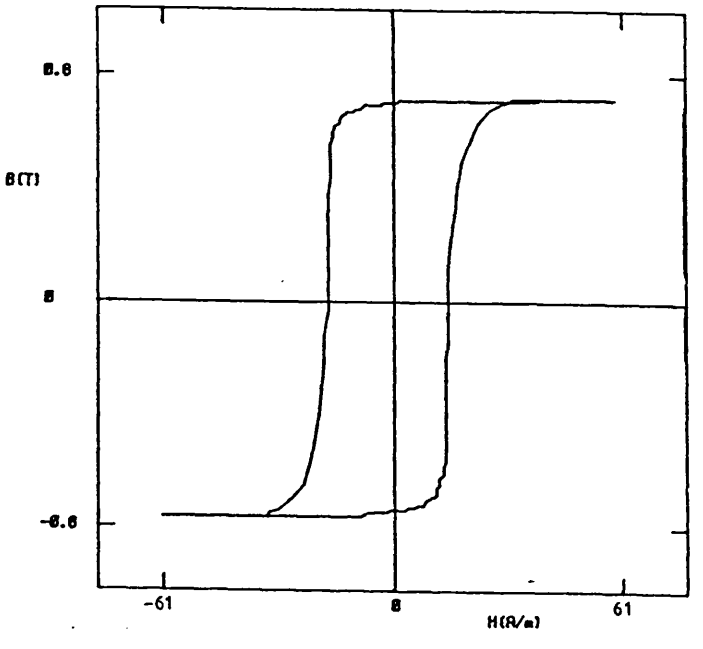

Figure 4.18 AC LOOP OF A SCRATCHED CORE

4.2.3 Scribed Samples

Figure 4.18 shows the ac hysteresis loop of the scratched VAC 6030 core whose dc loop was shown in figure 4.10. The form of the ac loop obtained on this sample is very similar to the as-received case with no improvement in the ac loss. Indeed, none of the scratched cores showed any improvement in their ac behaviour. This indicates either, that the mechanism by which scribing has previously been reported to improve ac performance is stress-magnetostriction coupling or that the scribing technique used here failed to produce the necessary surface modification for production of demagnetising fields suitable to help reverse domain nucleation (section 1.8.2).

4.2.4 Summary of ac results on VAC 6030

The as-received and longitudinally field annealed VAC 6030 core, exhibit a large component of longitudinal anisotropy and thus a widely spaced domains. This is reflected in the high ac loss exhibited by these samples. The loss of the longitudinally field annealed samples has been shown to increase with increasing component of longitudinal anisotropy. The losses measured on these samples are in reasonable agreement with those quoted in the

Vacuumschmelze data sheets.

The stress relieved samples, despite their higher dc loss, exhibit a lower loss under ac conditions than either the as-received or the longitudinally field annealed samples. This has been attributed to the presence of more walls available to take part in the magnetisation reversal. This is also the case for the fast cooled toroids, with the addition that the domain wall pinning is also lower in this sample.

The ac results obtained on the surface scribed cores are not significantly different to those exhibited by the as-received toroids.

It should also be noted in this section that after annealing some of the cores could be heard vibrating despite their low magnetostriction. This needs further investigation.

4.3 The effects of post production treatments on the pulse behaviour of VAC 6030

Having annealed and characterised a core under dc and well controlled ac conditions, the core was then taken to the British Aerospace site at Filton and measured under resonant charging pulse conditions. The pulse testing arrangement was described in section 3.5.

In an ideal pulse compression line, the resonant charging time of any given compression stage is fixed (by choosing an appropriate value for the saturated inductance of L_i) such that L_{i+1} saturates as the voltage on the capacitor C_i reaches a maximum (figure 2.1). This corresponds, in our test line (figure 3.13), to choosing the values of V_0 and L_0, such that L_s saturates as the voltage on the second capacitor bank reaches a maximum. In all of the measurements presented here, the peak voltage measured on C_2 under the set up conditions (section 3.5) was 20V and L_0 was a 20-turn air cored inductor of order $10^{-3} m^2$ cross sectional area, giving a resonant charging time of order 10μs.

When the 2.4kΩ resistor is replaced by a core then, ideally, the resonant charging voltage waveform on the

second capacitor bank should follow that observed under the set-up conditions regardless of the current drawn by the core. With real circuit elements, this is not possible since the current drawn by the core discharges the capacitor bank and therefore reduces the voltage across the core. The voltage waveform applied to the core therefore depends to some extent on the behaviour of the core itself. In general, however, the leakage current through the core is too small to significantly affect the charging waveform until the core approaches saturation. As the core saturates, the impedance of the core tends towards that of a similar core wound without any magnetic material present and the current drawn by the core therefore increases rapidly. At this point, the voltage waveform on the second capacitor bank departs from the ideal $1-\cos\omega t$ form (figure 4.19). The point at which this happens depends on both the core treatment and, in some of the samples, on the reset field applied. In most of the VAC 6030 cores, this break-off point is around 17V. The important point is that, until this point, each core is measured under the same dB/dt conditions.

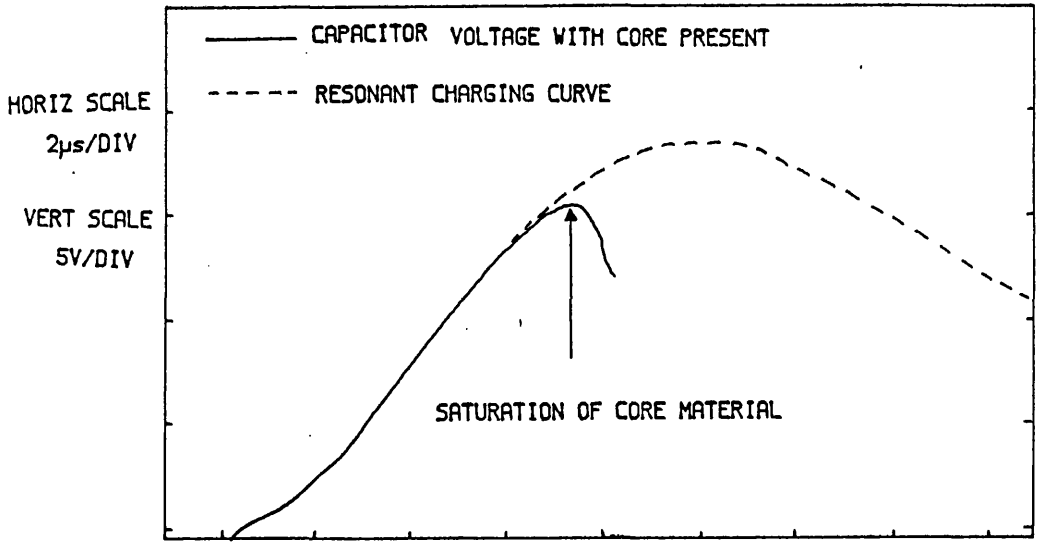

Figure 4.19 THE DEVIATION OF THE dB/dt FROM RESONANT CHARGING

4.3.1 As-Received and Stress Relief Annealed Cores

In the as-received state, the VAC 6030 alloy exhibited a very square ac and dc loop. The corresponding pulse curve is shown in figure 4.20. From a given reverse reset field (10.6,31.8 or 53.1A/m given by 1,3,or 5 amps through a single turn reset coil), the pulse curve exhibits a significant initial rise in field (H) for little flux change. The magnitude of this initial step increases with increasing reset current (since a larger positive current is required to counteract the negative reset) - figure 4.21. This initial rise corresponds to a leakage current through the core during the reversal process and its cause can be viewed in two distinct ways. If the core is regarded simply as a variable inductor, the initial rise in H can be attributed to the cores low permeability (and hence low impedance) in the reverse saturated state thus allowing a significant current flow for even a small applied voltage. In this sample, as the voltage applied across the core increases, the H field (or leakage current) does not increase further until saturation is approached. This indicates an increase in the core's impedance as the flux reversal curve is traversed. A quite different, but not contradictory, way of explaining the observed curve is as follows. Suppose

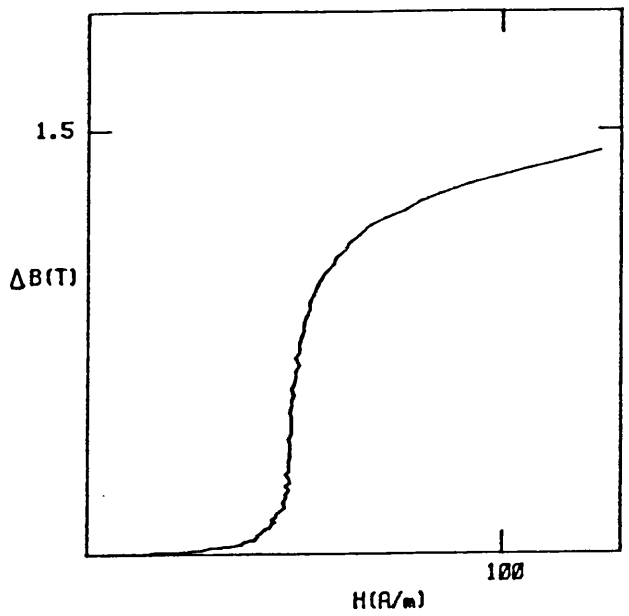

Figure 4.20 PULSE RESPONSE OF AS-RECEIVED VAC 6030

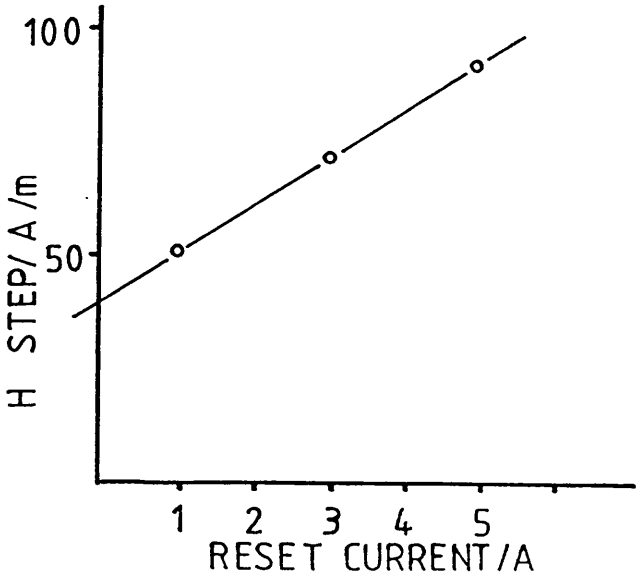

Figure 4.21 INITIAL H STEP vs RESET FIELD

that the material is initially reverse saturated (or nearly so), then the voltage applied across the core corresponds to an applied dB/dt. ie the area under the voltage curve corresponds to a change, ΔB, in the core's magnetic state. If we consider first that any flux reversal occurs by domain wall motion, then in order for this to occur, domain walls have to be nucleated and/or existing reverse domains expanded. The initial rise in H is simply the field required to nucleate the required domains and/or drive the domain wall motion of the small domains already present. As the reversal process proceeds, dB/dt increases as $1-\cos\omega t$ but the field remains approximately constant (in the as-received sample) indicating that the wall movement is becoming successively easier as the reversal progresses either because more mobile walls are involved and/or because the cross sectional area of each individual domain increases (see section 2.4.4). This point will be discussed further when the longitudinal field anneal results are presented.

In order to quantify the pulse behaviour of any given core, a pulse performance parameter (PPP) will be defined. The most obvious way of quantifying the pulse behaviour of a core is in terms of its pulse loss. It is, however, difficult to define a loss under pulse conditions for 2 reasons. Firstly, only a half

loop is obtained and secondly, the position of this half loop is determined not only by the materials' response but also by the reset field.

Now, for a sample starting from negative saturation, the effect of the reset field has been shown to be a simple shift along the H axis linear in H_r and, although the pulse curve cannot be measured with no reset field applied, an effective H=0 can be defined by extrapolation. However, in a sample which is not completely saturated by the reset field or a sample for which there is no initial H step, then the definition of an effective H=0 would result in a reduction in 'available' ΔB (figure 4.22). The definition of an effective H=0 to eliminate the effect of the reset field on loop position is, therefore, not a useful way of eliminating the problem. It is best, where possible, to compare cores measured from the same reset field noting, where appropriate, whether or not the core was reverse saturated with this particular reset field.

From a given reset, for a 'square loop' sample, it is possible to estimate the half cycle pulse loss by measuring the area enclosed by the curve, the H axis, the B axis and the line $B=2B_s$. This is, however, a dangerous practice for the following reason. The area

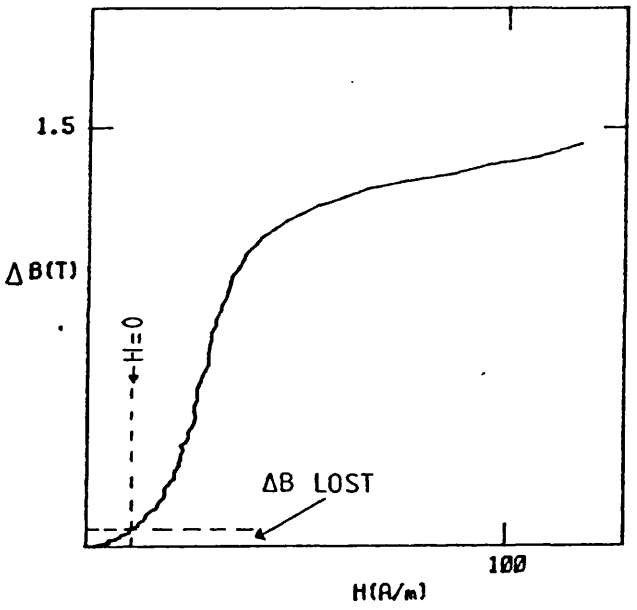

Figure 4.22 PULSE REVERSAL CURVE SHOWING EFFECTIVE H=Ø

enclosed by the B axis and by that part of the B-H curve where B tends to $2B_s$ can dominate the measured 'loss'. This is the part of the curve where core permeability decreases and the geometry of the core windings therefore becomes important. It is also the point at which the resonant charging waveform begins to deviate from the ideal due to current drain on the capacitors (section 4.3.1).

For this reason and because of the difficulty of identifying precisely where a sample becomes saturated, a calculation of the pulse loss as described above can be misleading. A more useful way of evaluating the performance of a material under pulse conditions is to choose an arbitrary flux swing $\Delta B=B_a$, ideally as close to $\Delta B=2B_s$ as possible but avoiding the problems identified above, and evaluate the area enclosed by the axes, the curve and the line $\Delta B=B_a$. It should be noted that although this is indicative of the half cycle pulse loss under a given set of reversal conditions for a square loop sample, it is not a measure of the half cycle pulse loss nor even proportional to it.

The pulse performance parameter will be defined for VAC 6030 to be the value of this half loop integral with 1T chosen as the ΔB limit. The values of PPP

quoted in this chapter are obtained from a reset current of 1A and using the true H=0 axis. The PPP evaluated for as-received VAC 6030 under these conditions is 50J/m^3. This compares well with the value of approximately 50J/m^3 obtained by extrapolating the results of Herzer and Hilzinger (1987), to the reversal rate of 0.3T/μs used in this investigation.

After stress relief, the pulse response of VAC 6030 shows marked differences from the as-received. The initial step in H (at 1A reset) has disappeared entirely and the pulse curve is more rounded than in the as-received case. Figure 4.23 shows the pulse curves of VAC 6030 toroids annealed for a range of times at 425°C and figure 4.24 shows the variation of the PPP as a function of the anneal time. It should be noted that the sample annealed for 85 minutes exhibited a flat pulse curve which never reached 1T. This is because a reset field of 10.6A/m was not large enough to reset the sample. Increasing the reverse bias current from 1A to 3A was sufficient to restore a stable pulse trace. The PPP plotted for this core is the value calculated from the 3A reset condition with the reset artificially reduced to 1A. This value therefore is not strictly comparable with the lower anneal time points.

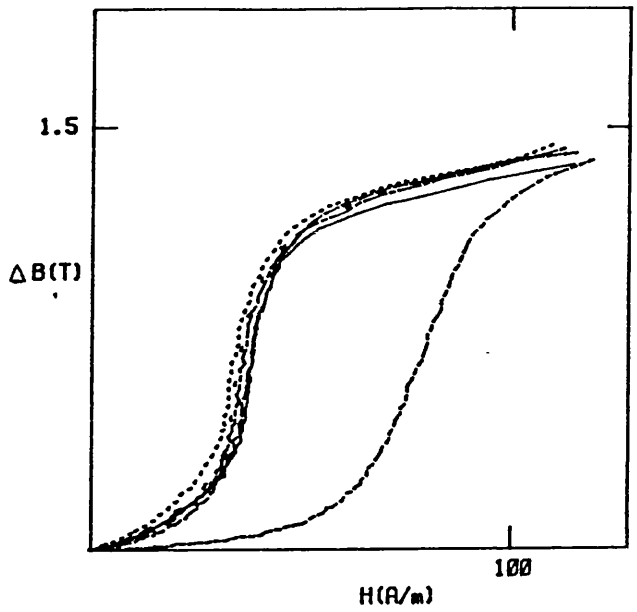

——— VAC 6030 SR ANNEALED 1.5 MINUTES
---------- VAC 6030 SR ANNEALED 4.1 MINUTES
. - . - VAC 6030 SR ANNEALED 9.1 MINUTES
——— VAC 6030 SR ANNEALED 21 MINUTES
——— VAC 6030 SR ANNEALED 60 MINUTES
——— VAC 6030 SR ANNEALED 85 MINUTES

Figure 4.23 PULSE RESPONSE OF VAC 6030 vs ANNEAL TIME

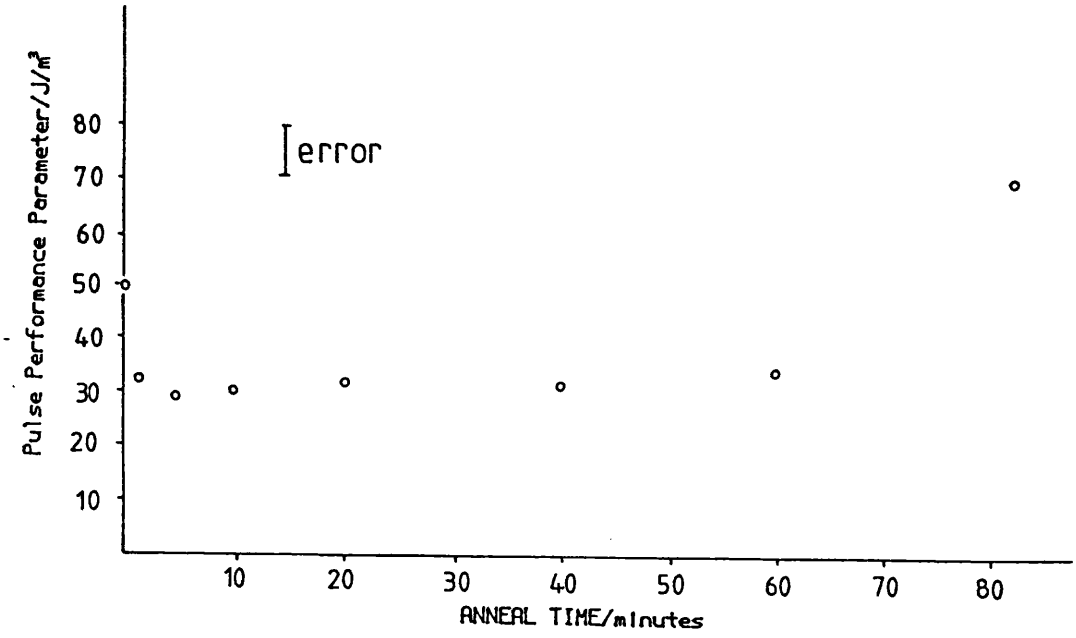

Figure 4.24 PPP vs ANNEAL TIME

The pulse performance of a fast-cooled toroid is shown in figure 4.25. Again, no initial step in H is seen and the PPP can be seen to be approximately 25.5J/m^3/cycle, lower than either the as-received or simple stress relief annealed cores.

Thus, the pulse loss trend and the pulse curve shapes shown in these figures are exactly as would be expected from the ac and dc measurements.

4.3.2 Field Annealed Cores

The following sections will report the effects of various field annnealing treatments on the pulse behaviour of the VAC 6030 alloy.

4.3.2.1 Transversely field annealed cores

In section 4.1.2, it was reported that the transversely field annealed toroid exhibited an almost linear dc hysteresis loop with a low permeability. From the dc results, it can be seen that the field required to saturate the sample is approximately 60A/m. Even the maximum pulse reset current of 5A is therefore insufficient to reverse saturate a sample treated in this way. For completeness, however, figure 4.26 shows the pulse behaviour of a

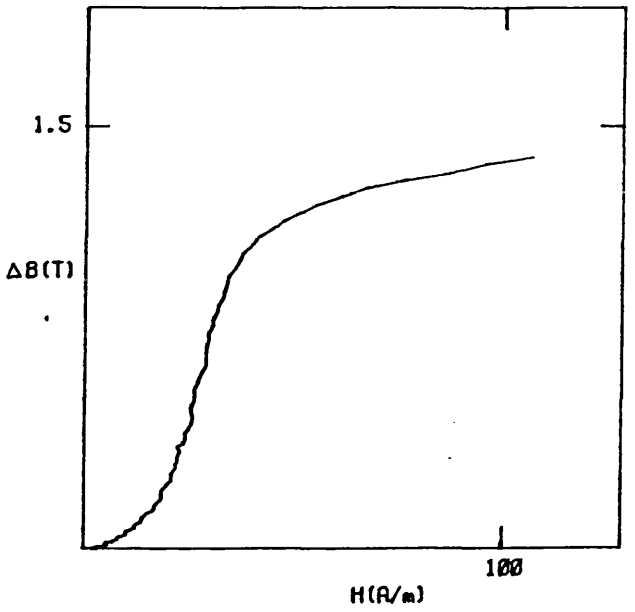

Figure 4.25 PULSE RESPONSE OF A FAST COOLED CORE

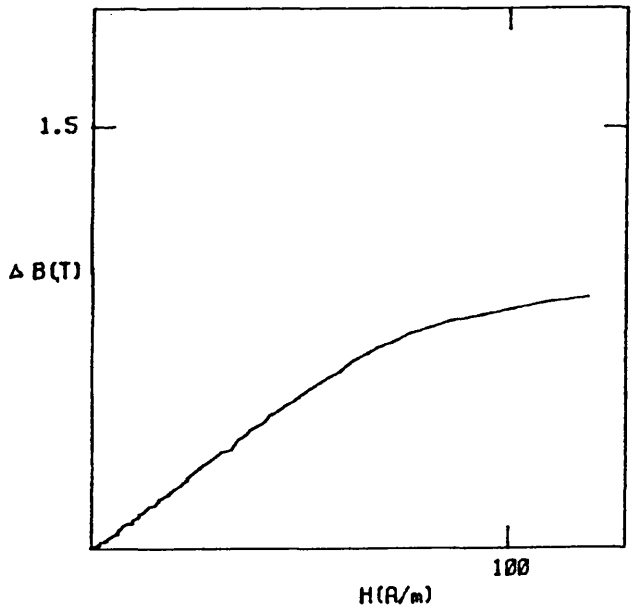

Figure 4.26 PULSE RESPONSE OF A TRANSVERSELY FIELD ANNEALED CORE

transversely field annealed sample reset with a 1A reset current. The low permeability seen under ac and dc conditions is also seen in the pulse behaviour. In addition to the large reset current requirements of this core, this low unsaturated permeability renders it unsuitable for pulse applications since a low permeability means a low impedance and hence, in the unsaturated part of the reversal diagram when the core is ideally an open circuit, cores treated in this way act as very poor insulators.

It was noted when defining the pulse performance parameter, the PPP, that this parameter was only valid for square loop materials. This is simply because in a square loop sample, the remanence ratio, by definition, is high and the part of the loop from $B=2B_s$ to $B=B_s+B_r$ can be replaced by a straight line $B=2B_s$ with little error. In the case of a loop such as that exhibited by the transversely field annealed sample, this is not true and hence the PPP as defined above is not meaningful. Such samples, as described in the ac results section, exhibit low ac loss and hence low pulse loss but for the reasons discussed above are not suitable for magnetic switching applications.

4.3.2.2 dc Longitudinal Field

The pulse response of the longitudinally field annealed samples cooled at various rates are shown in figure 4.27. The initial step in H for little increase in B is again evident in these samples with the peak initial current increasing with decreasing cool rate.

The pulse performance parameter, PPP, plotted in figure 4.28 as a function of cool rate from the anneal temperature, is much larger than the stress relieved and fast-cooled cores and is comparable with the as-received sample. In addition, the PPP can clearly be seen to increase with increasing induced anisotropy. This should be compared with the ac loss measured on this set of samples, where the same trend is seen.

Using the same type of argument as with the as-received, this behaviour can be explained as follows: the initial step in field corresponds to the driving force required to initiate flux reversal. This may be either the energy required to nucleate reverse domains and/or initiate domain wall movement in small reverse domains already present. The decrease in H seen in some of these curves after the initial step occurs either because the field required to expand a

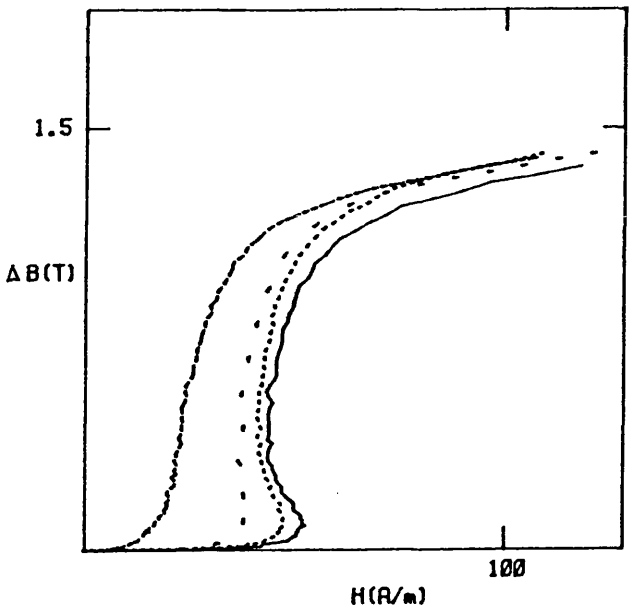

Figure 4.27 PULSE RESPONSE OF LONGITUDINALLY FIELD ANNEALED CORES

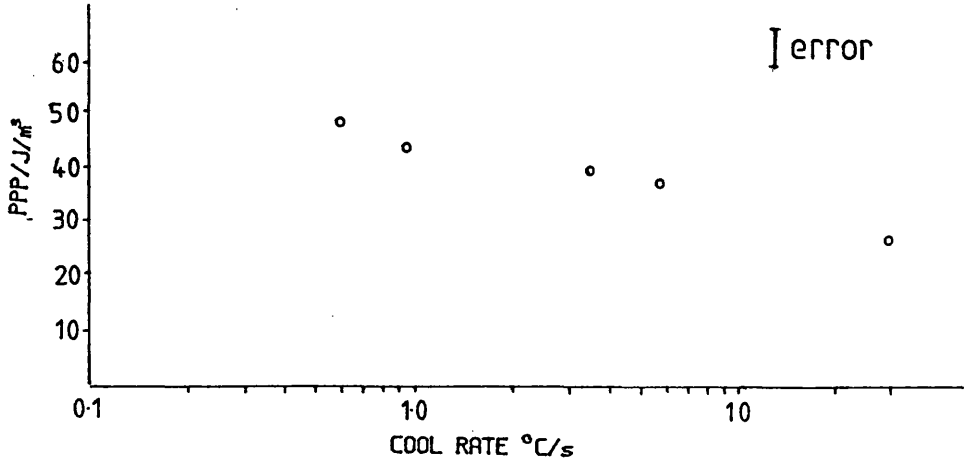

Figure 4.28 PPP vs COOL RATE

reverse domain is less than that needed to nucleate that domain or simply because the field required to continue domain expansion decreases as the domain cross-sectional area increases.

In order to determine whether domain nucleation or domain expansion is responsible for the initial H step, it is first necessary to examine exactly how domain nucleation takes place.

Let us consider a metallic glass sample which is completely reverse saturated. If a forward field is then applied to the sample, the effect of this field will be to rotate some of the magnetic moments near to the surface of the sample. This rotation of moments will continue until a complete domain wall is formed seperating the bulk of the material from an infinitesimal domain. This will occur in many places along the surface of the ribbon. Flux reversal will then continue by wall movement ie, by expansion of these small domains.

Consider, now, the work of Bishop described in chapter 2. Let us assume that even in the reset condition, the samples are not completely reverse saturated and that small reverse domains are still present. The work of Fähnle and Kronmüller (1978)

indicates that at the low reset fields used in this work, this is likely. If this is the case, then, firstly, the samples with the larger component of longitudinal anisotropy are likely to be closer to saturation in a given field than are the samples with a lower K (ie the reverse domains are smaller for the higher K samples) and secondly, because of the more widely spaced domain configuration associated with the higher K, fewer of these reverse domains are likely to be present. Now, according to the results of Bishop, the smaller the domain cross-section, the larger the field required in order to expand that domain. In addition, under conditions of fixed macroscopic dB/dt, the fewer the domains available for flux reversal, the higher the wall velocity required from any given domain. This again will require a larger field.

Thus, if reversal is considered to take place only be expansion of the reverse domains present in the reset VAC 6030 samples, then the samples with a higher K will need a larger initial field to begin the reversal process and will also exhibit higher pulse losses. This is consistent with the results shown in figures 4.27 and 4.28.

Of course, flux reversal will not only take place by the expansion of existing domains, additional

domains will be nucleated. The volume of these domains, however, will be very small and the field required to expand them will be large. Thus reversal will continue primarily by expansion of existing domains. The smaller reverse domains will merge into the larger expanding domains as the reversal process proceeds.

In section 4.2.1, it was implied that the increase in ac loss was due to a reduction in the number of walls available. The reasoning above does not contradict this argument. The ac results must, however, be divided into two regimes:-

i) Small field excitation: here, the widely spaced domain configuration produced by a larger K will increase the loss as described earlier.

ii) Near-saturating excitation: this can be viewed in the same way as the pulse results. The only difference between the two cases is the form of the excitation. Under ac conditions the field is constrained to be sinusoidal, it thus cannot decrease as the reversal process continues. No overshoot is, therefore, seen in the ac loops. Hence, the larger field required to initiate the reversal is still present

once the reversal process is well underway. This leads to an increased domain wall velocity and hence higher ac loss.

There is no distinct dividing point between these two regimes, the second will become more important as the drive field approaches that needed to saturate the sample.

4.3.2.3 Ac Longitudinal Field

The pulse response of the saturating ac field annealed sample is very similar the dc field annealed samples presented in the previous section. The sample annealed under a low field ac anneal, however, shows a completely different loop shape figure 4.29. The PPP of this sample is comparable to the other field annealed samples but the form of the curve is different. The initial rise in field for no significant ΔB is replaced by a more gradual increase in H as ΔB increases from zero. Instead of the sharp peak in H exhibited by some of the dc LF samples, the low field ac annealed sample shows a broad nose with H decreasing to a minimum at approximately B=0.25T.

Given that the annealing treatment has produced a sample with widely spaced domains, the form of the

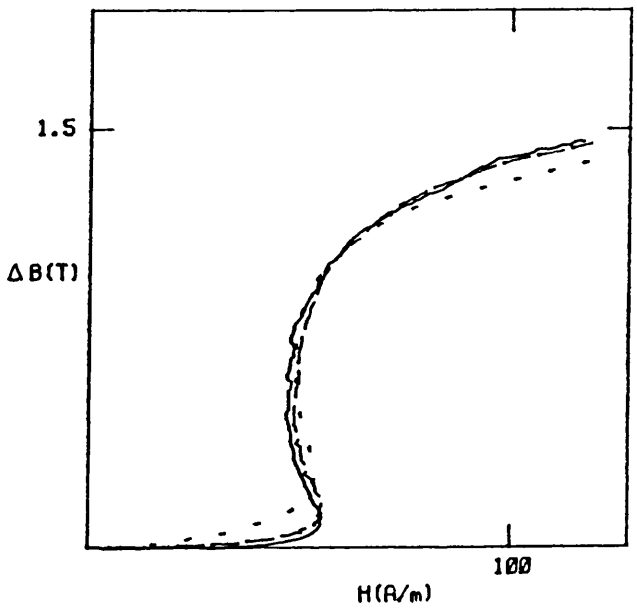

Figure 4.29 THE PULSE RESPONSE OF CORES SUBJECTED TO VARIOUS FIELD ANNEALS

flux reversal diagram can be understood as follows. As in the case of the longitudinally field annealed material, the material exhibits a large initial step in field and an overshoot. This corresponds to the the field required to initiate domain wall movement in the small reverse domains present. The decrease in H as the reversal process proceeds, again indicates, that the field required to drive the reversal decreases as the area of the reverse domains increases. Superimposed upon this behaviour, however, is a component of flux reversal by moment rotation. That moment rotation is important in the flux reversal of this sample was indicated by the rounded dc hysteresis loop shown in figure 4.10. Looking at the reversal process from the alternative viewpoint of a variable inductor exposed to an increasing applied voltage, the observed behaviour can be explained as follows. As the applied voltage is increased from zero, the core immediately begins to reverse (by moment rotation) this increases the impedence of the core and causes the current through the core to increase slower than that seen in the longitudinally field annealed cores. As the reversal progresses, existing reverse domains expand, the impedence of the core becomes larger still and the current decreases slightly even as the voltage increases. Just before saturation is approached, the flux reversal of the both the dc and low field ac

longitudinally field annealed cores is similar and then as saturation is approached, the current in the ac annealed core increases first. This is again the effects of moment rotation. Here the core impedence falls as moment rotation again becomes the dominant flux reversal mechanism.

4.3.3 Scribed Samples

As expected from the dc and ac results presented on cores which had been mechanically scribed, the scribing has no discernable effect on the pulse performance of this material. This may be due in part to the method of scribing used here or may be due simply to the low magnetostriction of this material. See section 4.1.3

4.3.4 Summary of pulse results on VAC 6030

The as-received cores and longitudinally field annealed cores all exhibit a large initial rise in field and consequently a high value of the pulse performance parameter. This corresponds to a large leakage current during the initial stages of the resonant charging process. The initial step in field increases with increasing longitudinal component of anisotropy. An overshoot is seen in some of the slower

cooled samples. The stress relieved and fast cooled cores do not show the initial increase in H and exhibit lower values of the PPP. The stress relieved sample, however, shows a significantly slower approach to saturation. The scratched cores, again, show no change from the as-received state.

The trend in the pulse performance of these toroidal cores can be predicted from their ac and dc responses. The loss trend exhibited under resonant charging conditions are precisely those seen under ac conditions.

CHAPTER 5

5 The effects of post production treatments on the magnetic properties of METGLAS 2605-SC

Currently, research in magnetic switching applications is focussed on the high saturation induction alloys despite the problems of high magneto -striction discussed in section 4. A survey of commercially available alloys indicates that the Allied Corporation alloy METGLAS 2605-CO exhibits the largest saturation induction of any amorphous alloy and would therefore be the obvious choice for pulse compression applications.

In our study, we decided against using this alloy for two reasons.

i) Heat treatment of METGLAS 2605-CO is difficult. The problem lies in the small gap between the Curie and crystallisation temperatures of this alloy (415° C and 430° C respectively). This renders stress relief annealing above T_c, without introducing crystallisation, very difficult.

ii) A preliminary study of Allied Corporation's METGLAS range for this project (Avery,1986)

indicated that this alloy alone, of all those available, failed to show a decrease in coercivity on annealing.

Indeed, over a range of anneal temperatures (265° C to 365° C) and times (0 to 100 minutes), Avery (1986) observed an increase in dc coercivity and a decrease in the remanence ratio (figure 5.1). This he attributed to surface oxidation - a conclusion reinforced by the tarnished appearence of this alloy after annealing. However, in the light of the disaccommodation effects observed in VAC 6030 annealed below T_c, it was decided to anneal METGLAS 2605-CO above its Curie point.

Although the annealed samples still tarnished, these additional anneals did show that, contrary to the results of Avery (1986), it is possible to obtain a reduction in the dc coercivity of METGLAS 2605-CO (figure 5.2) by a simple stress relief anneal. This indicates that the increase in H_c observed by Avery (1986) was probably due to magnetic self-annealing of the alloy. This was confirmed by annealing a sample below and then above the Curie temperature. Initially, an increase in H_c was seen. When the same sample was then annealed above the Curie point, the coercivity decreased. The cyclic behaviour

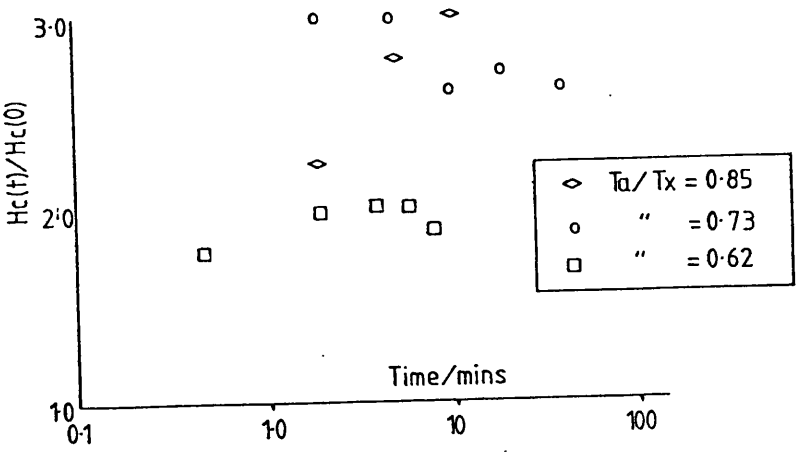

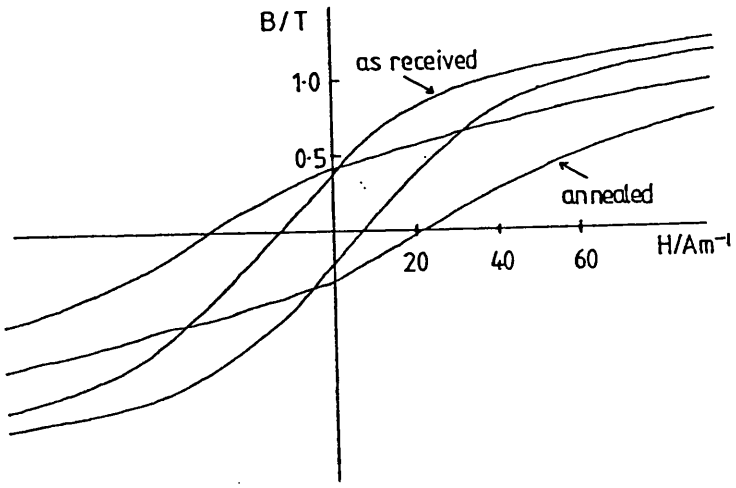

Figure 5.1 STRESS RELIEF BEHAVIOUR OF METGLAS 2605-CO (after Avery)

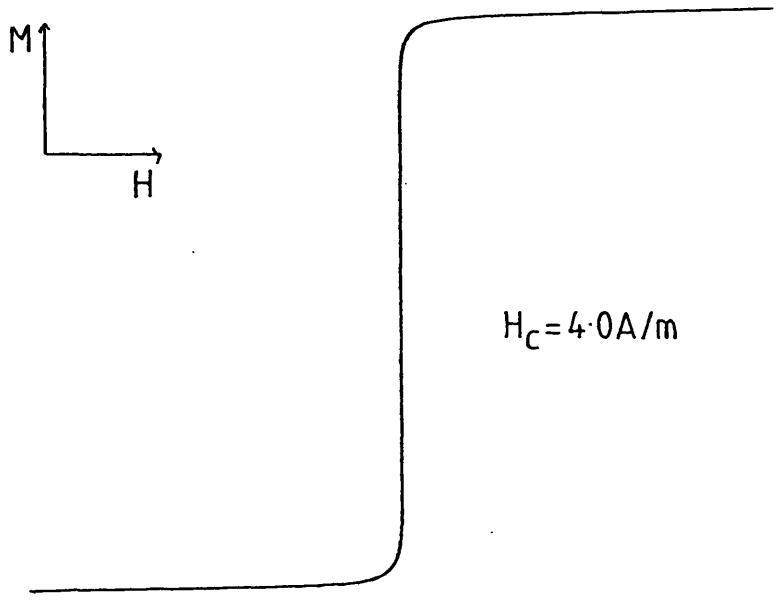

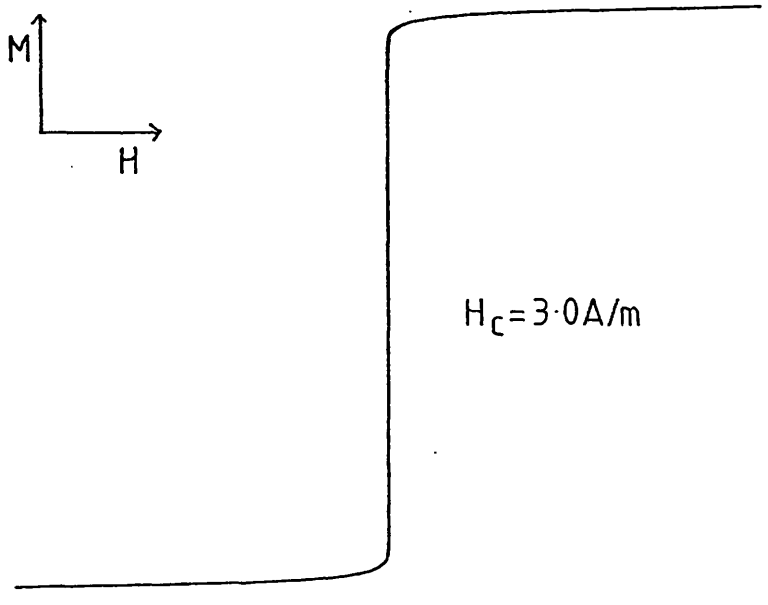

Figure 5.2 STRESS RELIEF IN METGLAS 2605-CO.
$H_{max} = 3{\cdot}7 kA/m$

seen in VAC 6030 was not observed in this alloy because after the second anneal, the sample crystallised.

Despite these results, the combination of having to anneal above the Curie temperature in order to avoid problems due to the development of local anisotropy and the small gap between T_c and T_x renders repeatable annealing treatments difficult, particularly if low cool rates are required. In addition, in order to avoid the severe surface oxidation seen in this alloy, the heat treatments may have had to have been carried out in an inert atmosphere. For these reasons, METGLAS 2605-CO was not used in this investigation.

On the basis of requiring the largest flux swing available, METGLAS 2605-SC was the next obvious choice for invesigation. The results obtained by Avery (1986) indicated that the dc magnetic characteristics of this alloy responded well to a simple stress relief anneal. METGLAS 2605-SC was therefore chosen for our investigation of a magnetostrictive alloy. Further tests were, however, undertaken in order to confirm that self annealing was unimportant in this alloy.

5.1 The effect of cool rate on H_c

The initial results taken on this alloy were a series of stress relief anneals on straight strip and toroidal samples cooled at different rates. Two anneal temperatures were chosen - one above and one below the Curie temperature. The purpose of these anneals was to determine whether or not the effects of the development of local induced anisotropy due to magnetic self annealing are important in this alloy.

It is well known (Brugel, Gibbs and Squire,1988) that METGLAS 2605-SC responds to field annealing treatments. Since the mechanism for the development of local induced anisotropy is the same as that for induced long range anisotropy, then any alloy which responds to the former is likely to affected by the latter (section 1.7.2). It was therefore expected that METGLAS 2605-SC would show signs of magnetic self annealing.

Several toroids were annealed above T_c and then cooled at different rates. The annealing conditions used were, 20 minutes at 390°C. Of the fast cooled toroids, some were quenched in water and some in

liquid nitrogen. The water cooled toroids were dried in a stream of warm air to avoid rusting (this was not necessary with the VAC 6030 samples as this material showed no signs of surface corrosion). The water cooled METGLAS 2605-SC toroids, however, rusted severely even after this drying treatment. The results on the toroids treated in this way are therefore not presented. The toroids annealed and then fast cooled in liquid nitrogen did not show any signs of rusting. Nor was there any significant difference in the dc properties of these toroids and those that were slow cooled. This, however, is not conclusive proof that magnetic self annealing is not important in this material. The stresses generated in the core during the rapid cool are also likely to affect the magnetic behaviour of the sample

Thus the fast cool data is not easy to interpret. The straight strip data on samples consecutively annealed above and below T_c are a more reliable guide. Figure 5.3 shows the results of a single straight strip sample annealed successively above and below T_c. No significant change in the measured value of H_c is seen nor any change in the shape of the dc loop. Since, as discussed above, any material that will respond to field annealing will also magnetically self field anneal, the only conclusion which can be drawn

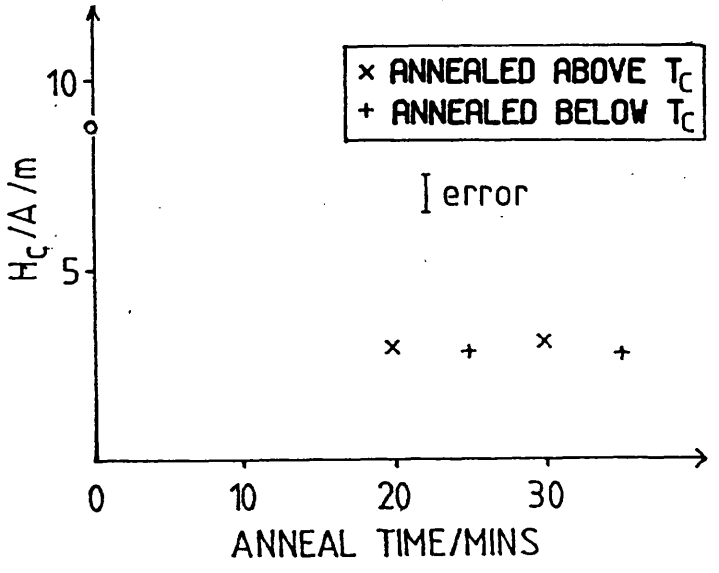

Figure 5.3 COERCIVITY vs ANNEAL TIME FOR METGLAS 2605-SC ANNEALED ABOVE AND BELOW T_c

from these results is that the effects of the stress-magnetostriction interaction as the sample is magnetised dominate any magnetic self annealing effect present. A possible explanation of why METGLAS 2605-CO shows evidence of self annealing whilst the alloy METGLAS 2605-SC (despite its lower magnetostriction) does not, concerns the magnitude of the induced anisotropy in both of these alloys. It has been reported (Smith,1988) that the anisotropy energy is an order of magnitude higher in METGLAS 2605-CO than in METGLAS 2605-SC. Thus, the effect of local self annealing may be expected to be significantly greater in this material.

In addition, it should be noted, in this section, that, although a slight surface discolouration was seen in the annealed METGLAS 2605-SC samples, this material did not show significant surface oxidation.

5.2 Effects of annealing on the magnetic and mechanical properties of METGLAS 2605-SC

Several of the treatments which were performed on VAC 6030 were chosen with the intention of eliminating the effects of magnetic self annealing. Having established that the effects of magnetic self annealing in METGLAS 2605-SC are unimportant under the

annealing conditions used, some of the treatments which were performed on VAC 6030 were deemed unnecessary in the study of METGLAS 2605-SC. The fast cooling of toroids, as described above, is not a useful technique in this alloy and was therefore not pursued. Transverse field annealing was found, in VAC 6030, to produce a low incremental permeability unsuited for switching applications. This treatment was therefore omitted from the study of METGLAS 2605-SC as was the ac field annealing treatment.

Two sample treatments were investigated: stress relief annealing and longitudinal field annealing. Initially, the annealing conditions were as follows. Eight samples were annealed at 390° C for times ranging from 1 minute to 3 hours. All of the toroids stress relieved in this way were allowed to cool slowly (approximately 5° C/s) to room temperature. The field annealed toroids were all heat treated for 20 minutes at 390° C and then cooled to room temperature at different rates (see section 4.1.2.2).

All of these samples were dc, ac and pulse measured and then the top layer of each toroid was removed (in 2cm lengths) for X-ray analysis. This revealed two problems which are discussed in section 5.2.1 and

5.2.2.

5.2.1 Oxidation and surface corrosion

It has already been noted that, after an anneal, the surface layer of the METGLAS 2605-SC toroids became slightly discoloured. This was attributed to surface oxidation caused by annealing in air. When the samples were unwound to enable the X-ray analysis, however, corrosion of the material was noticed. The deeper layers of the toroid which were exposed as the toroid was unwound showed small light brown spots (figure 5.4). The presence of these spots can be attributed to rusting of the toroid caused as follows. As the toroid is cooled from the anneal temperature, any moisture in the air circulating around and through the toroid windings may condense onto the toroid surfaces. Any small droplets condensing onto the surface layer will quickly evaporate and thus no rust develops on the top layer. Moisture on the deeper layers of the toroid, however, is trapped and cannot easily evaporate. It is these trapped droplets which over a period of time will lead to the small rust spots seen. This is supported by the following observation.

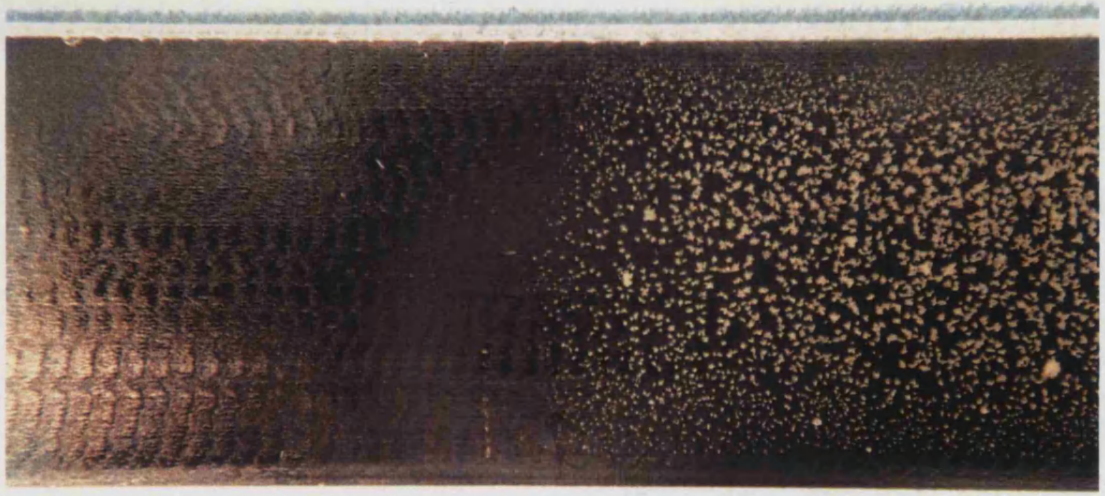

Figure 5.4 RUST SPOTS SEEN ON METGLAS 2605-SC SAMPLES

Before the rust spots were first seen, it had already been noted that if the dc coercivity of the toroids were measured immediately after the anneal, values of approximately 1A/m were recorded. The same toroids measured several days later may exhibit values of H_c much larger that this, in some cases greater than 3A/m. This can be attributed to domain wall pinning at the stress centres caused by the rust spots. The change in H_c over a period of days corresponds to the time taken for the moisture trapped in the core to corrode the sample surface.

5.2.2 Stress relief vs crystallisation

A further problem encountered with this alloy concerns the temperature gradient measured across the core during annealing in the tube furnace. This problem was discussed in section 3.2 but was found to present no problem with the VAC 6030 alloy.

It was, however, found to be important when annealing METGLAS 2605-SC cores. The H_c-time data obtained on box-furnace annealed METGLAS 2605-SC toroids indicated that an anneal of 20 minutes at 390° C is required to completely stress relieve METGLAS 2605-SC. The first signs of crystallisation were detected in the magnetic response of the material

after 60 minutes anneal. This was confirmed by X-ray analysis of the top layer of these stress relieved toroids (figure 5.5). To enable a wide range of cool rates from the anneal temperature, however, some of the field annealed toroids were heat treated in the tube furnace.

The results on VAC 6030 showed a distinct correlation between the cool rate from the anneal temperature and the ac loss exhibited by the resulting cores. This was not found to be the case for this set of METGLAS 2605-SC cores. Differences in the ac magnetic behaviour of the cores were observed but no correlation with annealing conditions was obvious (figure 5.6). It was for this reason that the decision was taken to X-ray the cores. All of this set of cores exhibited the same inner-wrap rusting discussed above. This had been held responsible for the high values of H_c observed. In addition to this, however, the X-ray data on these cores indicated the presence of some crystallinity. Two X-ray measurements were performed on the cores annealed in the box furnace - one on the shiny side and one on the reverse (dull) side of the ribbon. Five X-ray measurements, equally spaced around the toroid circumference were made on the tube annealed cores (shiny side only). Figure 5.7 shows the results of the X-ray work. The differences in the

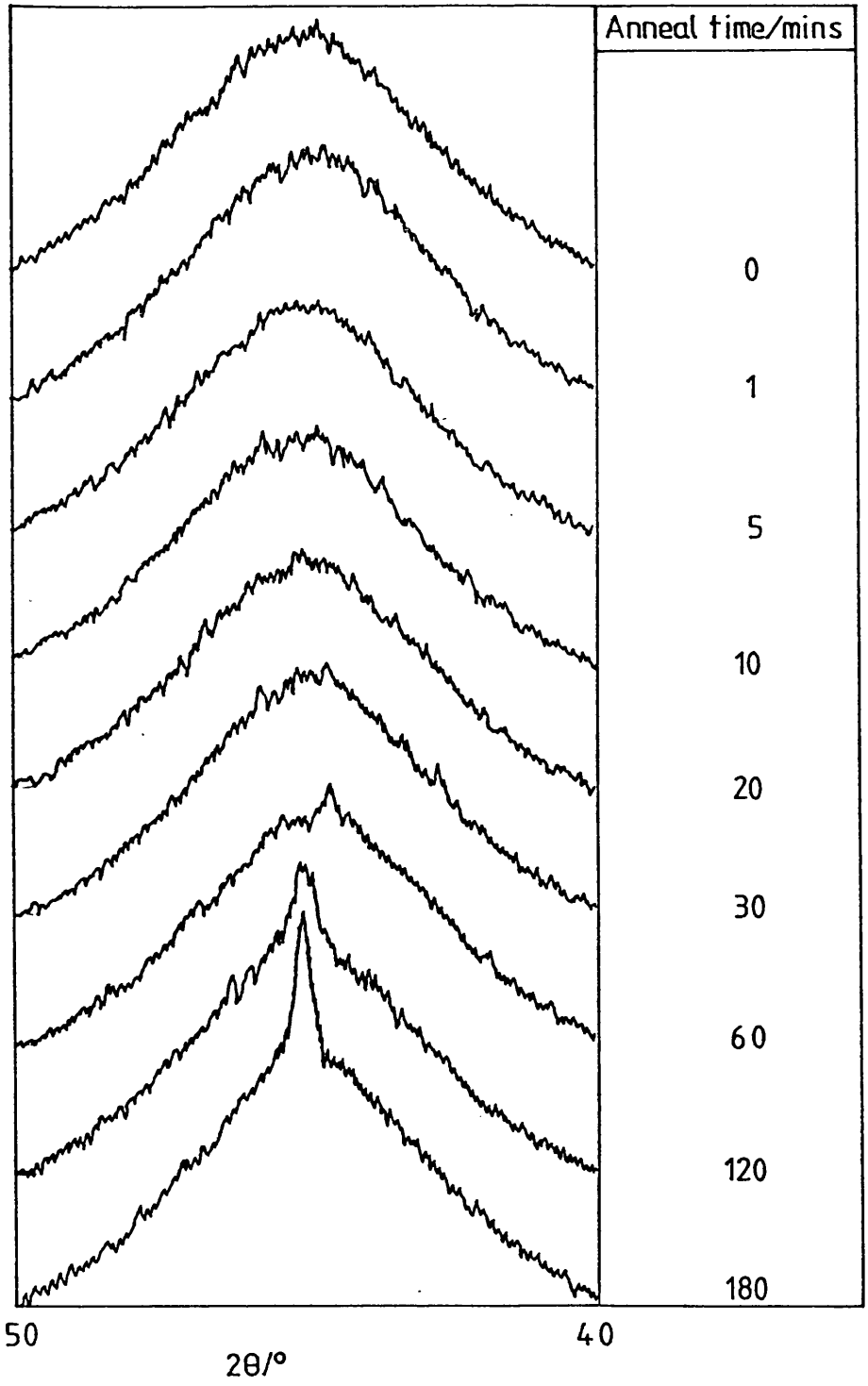

Figure 5.5 X-RAY TRACES FOR SEVERAL CORES ANNEALED IN THE BOX FURNACE

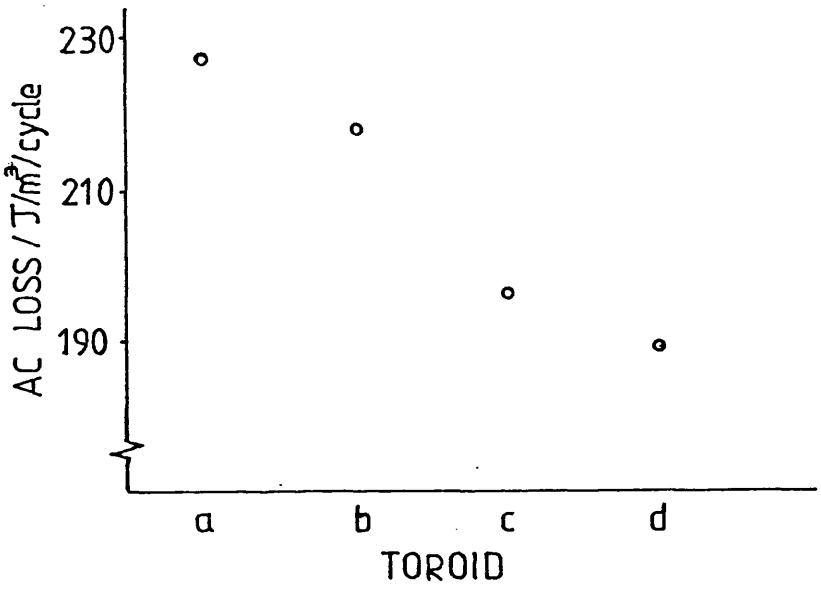

Figure 5.6 AC LOSS OF THE CRYSTALLISED SAMPLES SHOWN IN FIGURE 5.7

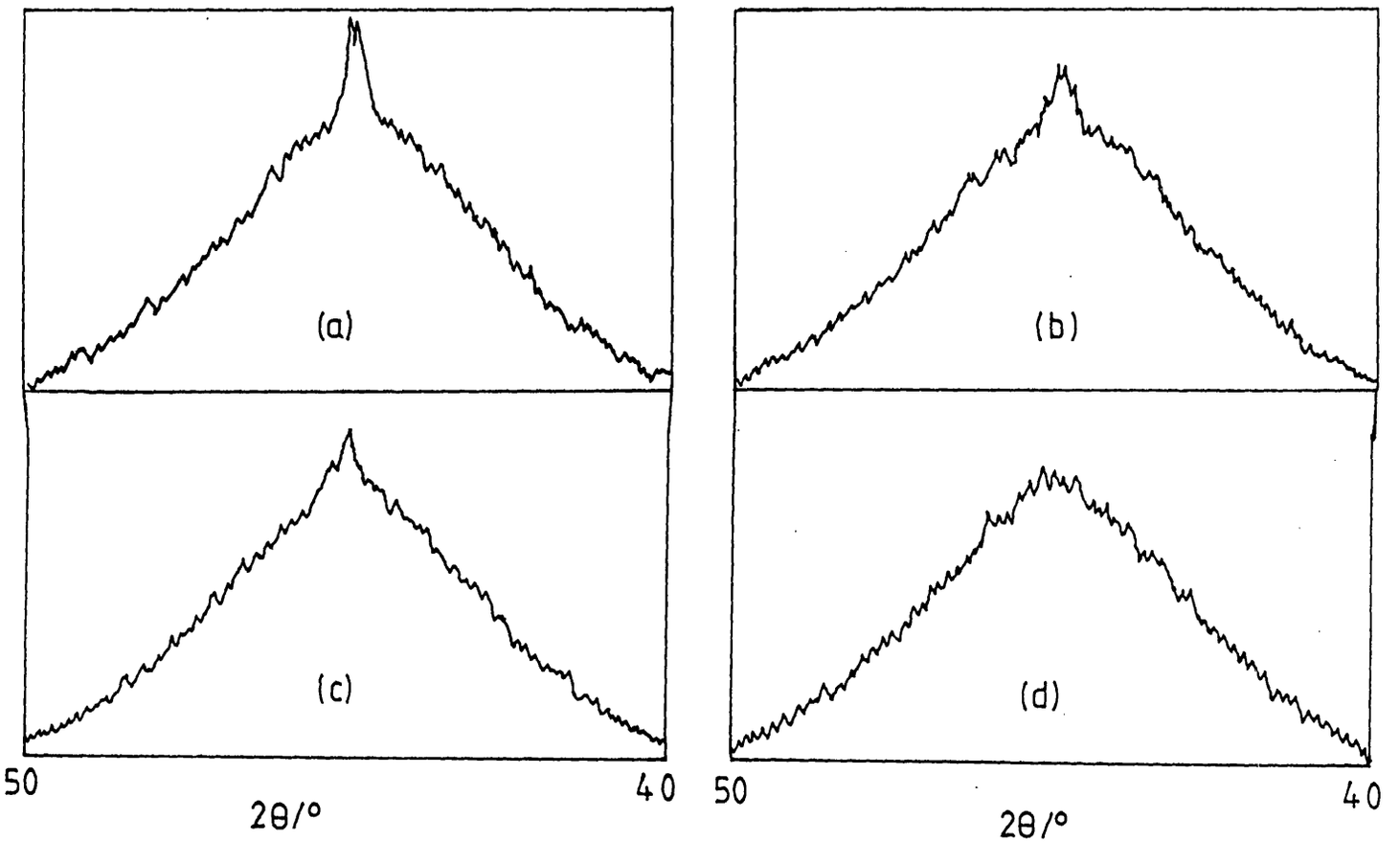

Figure 5.7 X-RAY TRACES FOR FOUR CORES ANNEALED IN THE TUBE FURNACE

crystallinity around the circumference of the tube annealed toroids, as revealed by the X-ray data, are due to the difference in temperature across the core throughout the annealing process. It was shown (section 3.2) that the steady state temperature difference between the 2 sides of a toroid annealed in the tube furnace could reach 30°C. The crystallisation of the METGLAS 2605-SC cores annealed in this way can be ascribed to some parts of the core being annealed at a significantly higher temperature than that part of the core in contact with the thermocouple.

If the X-ray data is compared with the ac data shown in figure 5.6, some evidence for a correlation can be seen. The ac loss of longitudinally field annealed toroids increases with increasing crystallite content. This will be discussed further in section 5.5.

In subsequent anneals in the tube furnace, the thermocouple used to record the core temperature was always placed at the hottest part of the sample. In addition, to avoid the rust problem described above, all future toroids were placed in a dessicator immediately after the anneal and were replaced in the dessicator as soon as possible after each measurement. The dc coercivity of samples treated in this way was

found not to change with time and, when the samples were unwound (several weeks after the annealing treatment), no signs of surface corrosion were seen.

Having established and eliminated the causes of the sample crystallisation and surface corrosion, a third series of toroids were wound and annealed. The results obtained on these toroids are described in the following sections.

5.3 The effect of post production treatments on the quasi-dc magnetic behaviour of METGLAS 2605-SC

In contrast to the measurements on VAC 6030, the results obtained on the METGLAS 2605-SC material were found to depend very strongly on the precise annealing conditions to which the alloy was exposed. Thus the slight differences in the time-temperature profiles of the box and tube furnaces had a significant effect on the magnetic properties of the cores. The results presented here are therefore divided into 4 groups - box furnace stress relief annealed, box furnace longitudinally field annealed, tube furnace stress relief annealed and tube furnace longitudinally field annealed. Sections 5.3.1 and 5.3.2 summarise the dc response of METGLAS 2605-SC after these various anneals. It should be noted that in each anneal, the

timing commenced as the toroid temperature increased above 370°C. The reason for this lies in the arbitrarily slow approach to the anneal temperature exhibited by the toroids treated in the box furnace (figure 5.8). For all but the very shortest anneal times, however, the average core temperature throughout the anneal was approximately 390°C.

5.3.1 As-received and stress relief annealed

Seven samples were stress-relief annealed at 390°C in the Carbolite box furnace. These samples were placed directly on the furnace base and their temperature was monitored with a chromel-alumel thermocouple placed in contact with the toroid itself. A typical time-temperature profile is shown in figure 5.8.

Figure 5.9 (open circles (o)) shows the variation in dc magnetic properties of these samples with anneal time. The reduction in H_c seen is due to the relief of quenched-in and wound-in stresses. The change is much larger for METGLAS 2605-SC than in the case of VAC 6030 because of the higher value of magneto-striction (section 1.7.1). The results indicate that full stress relief under these annealing conditions

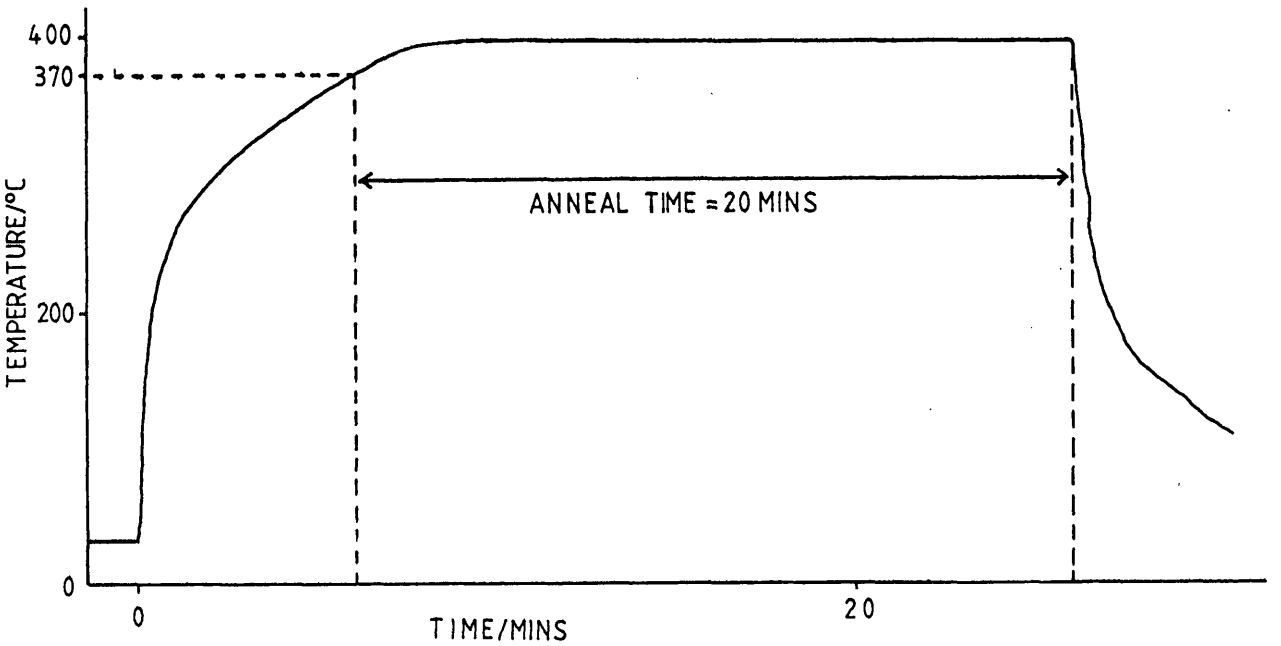

Figure 5.8 A TYPICAL ANNEAL PROFILE FOR THE BOX FURNACE

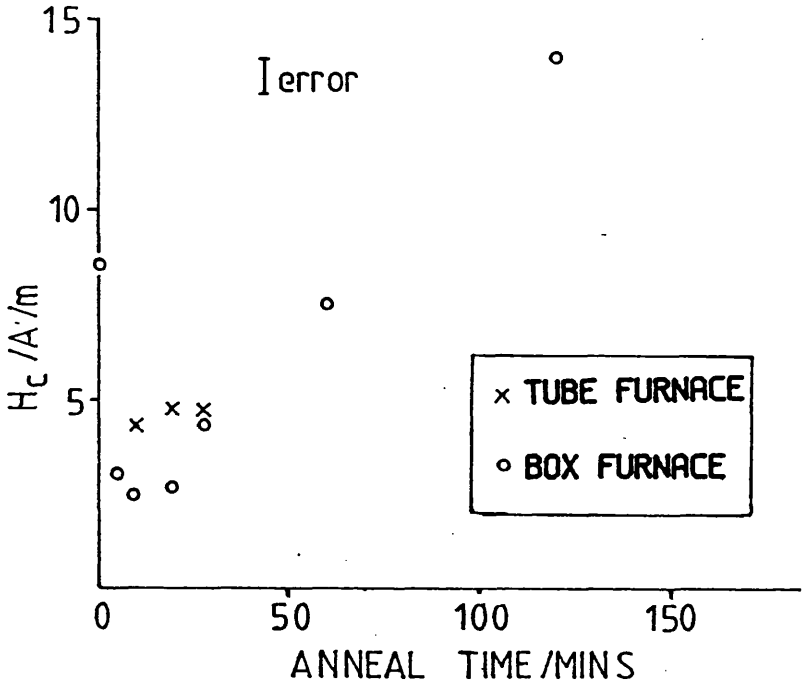

Figure 5.9 COERCIVITY vs ANNEAL TIME

occured between 10 and 20 minutes.

Three samples were then stress relief annealed in the tube furnace. These samples were placed on a pyrophilite holder in the air stream. A typical time-temperature plot for the tube-furnace annealed toroids is seen in figure 5.10.

The dc results on the tube annealed samples showed a constant value of H_c over the anneal time range 10 to 30 minutes. The much higher value of coercivity seen in these samples (figure 5.9, crosses (x)) compared with the box furnace annealed material (figure 5.9, circles (o)) can be attributed to either increased surface oxidation caused by annealing in a hot air stream or the thermal gradient across the core during the anneal. The first of these is unlikely as examination of the toroid surface still indicates little surface discloration (see also chapter 6). The latter has two effects. Firstly, the lower temperature experienced by the cooler side of the core may not be sufficient to fully stress relieve the material. Secondly, stresses generated in the core by the temperature gradient across the sample may contribute to the higher observed H_c. A sample subjected to a stress-relief anneal for 20 minutes at 360°C in the box furnace showed a similar value of dc coercivity to

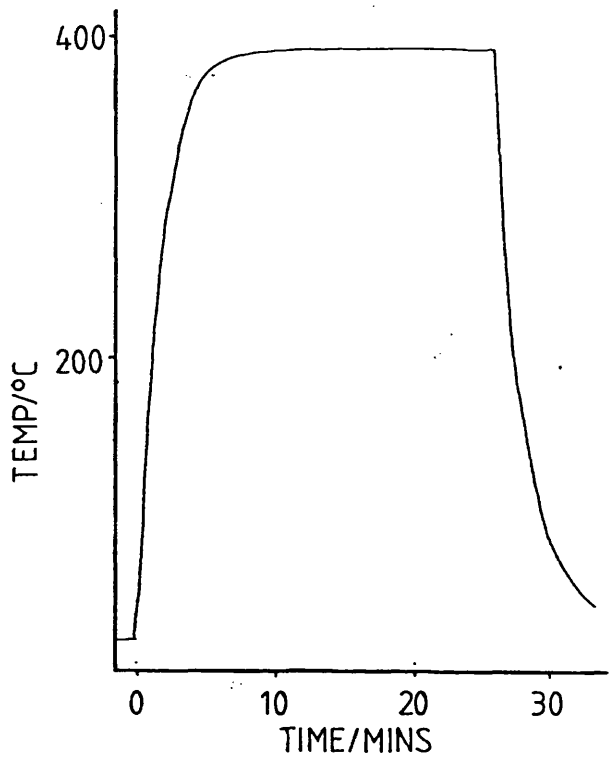

Figure 5.10 TIME-TEMPERATURE PROFILE FOR THE TUBE FURNACE

that exhibited by the tube annealed cores indicating that incomplete stress relief is likely to be a significant factor in the higher coercivities of the tube-furnace samples.

5.3.2 Longitudinal Field Annealed Cores

Several samples were then longitudinally field annealed, some in the box furnace and some in the tube furnace.

In the box furnace, samples were longitudinally field annealed for 10, 20 and 30 minutes. These toroids were placed on a pyrophilite holder with 10 turns of 20 SWG copper wire around the toroid to form a primary winding. A current of 4A was passed through these turns generating a longitudinal field of 420A/m. The samples were cooled by removing the holder and toroid from the furnace and cooling in a cold air stream produced by a hairdryer.

Only the 10 minute anneal sample prepared in this way exhibited a low coercivity. The 20 and 30 minute anneals yielded samples with coercivities in excess of 4A/m signalling the onset of crystallinity. The reason for the increase in H_c in the longitudinally field annealed samples treated for 20-30 minutes is not

clear but can probably be attributed to lower heating rate of these samples (compared with the stress relieved samples annealed in this furnace) caused by the need to include the pyrophilite holder and windings. This has the effect of slightly increasing the time spent at elevated temperature for any given anneal time and may, therefore be responsible for the observed behaviour.

The toroids which were longitudinally field annealed in the tube furnace were annealed under the same time-temperature conditions as the samples stress relieved in this furnace. The pyrophilite holder was present in each case and so the heating rate was also identical. Three toroids were annealed under the influence of an external field and each was cooled at a different rate from the anneal temperature.

In all three samples treated in this way, a low coercivity and a low dc magnetisation energy are seen. Lower than any of the stress relief annealed cores despite the high coercivity and dc magnetisation energies seen in cores stress relieved in this furnace. The low coercivity indicates good stress relief with no crystallisation and the low magnetisation energy confirms that these toroids exhibit a large longitudinal component of anisotropy.

5.4 The effect of post production treatments on the ac magnetic behaviour of METGLAS 2605-SC

As in the case of VAC 6030, the dc results presented above give indications of the domain wall pinning and the material anisotropy, but give no indications of the domain wall dynamics. The data presented in this section describes the ac response of this material after post production stress relief and longitudinal field annealing.

5.4.1 As-Received and Stress-Relief Annealed Cores

Because of the differences in the tube and box furnace treatments discussed in section 5.3, the ac response of cores annealed in these two ovens differs considerably and these results will therefore be discussed seperately.

5.4.1.1 Box furnace annealed

Figure 5.11 (open circles (o)) shows the variation in ac loss, maximum induction, remanent induction and ac coercive field with anneal times from zero to 180 minutes. These measurements were made at frequency of 1kHz and with an excitation field of approximately 150A/m. The decrease in dc magnetisation energy and

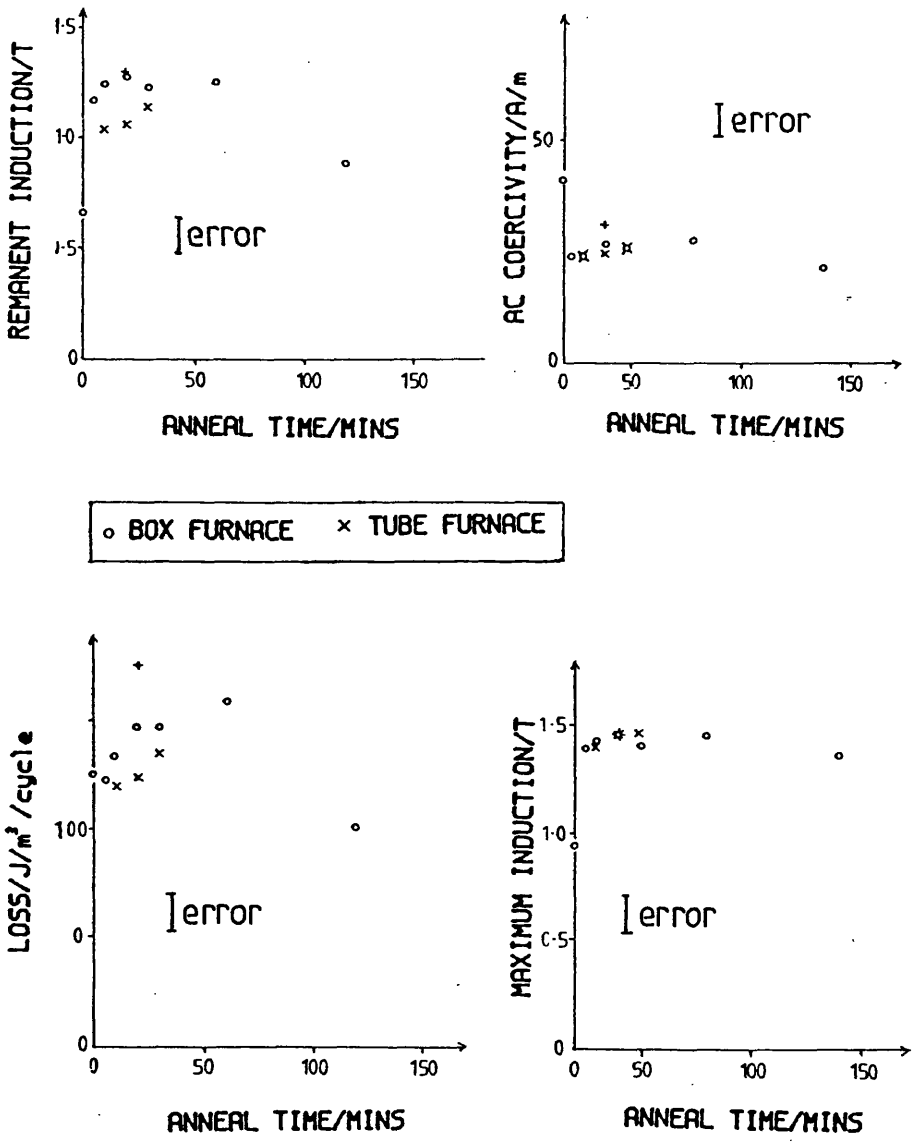

Figure 5.11 AC RESPONSE OF METGLAS 2605-SC TO STRESS RELIEF ANNEALS

coercivity for anneal times less than 30 minutes is reflected in an increase in the ac loss, maximum induction and remanent induction and a decrease in the ac coercive field.

Consider first, the ac loss. The increase in loss seen on annealing can be attributed to two causes. Firstly, after the stress relief anneal, the induction level reached in a given applied field is much higher than was achieved in the as-received state. Thus, the domain walls in the sample must sweep out more of the sample volume. This in itself would cause an increase in the loss observed. In addition, however, the stress anneal simplifies the domain structure resulting in a sample with fewer domain walls (see section 1.7.1 and chapter 4) and this again will result in an increased loss.

The increase in remanence can be attributed to an increase in the maximum induction reached and to the reduction in sample stresses (and the consequent modification of the domain structure). The change in ac coercivity is also the result of two factors; a decrease caused by a reduction in domain wall pinning and an increase due to a reduction in the number of walls available.

The decrease in loss seen for large anneal times is accompanied by a reduction in the remanence ratio and a slight decrease in the maximum induction reached. This is the opposite of the results presented in section 5.2.2 where an increase in ac loss was observed with increasing crystallite content. This will be discussed further in section 5.5.

5.4.1.2 Tube furnace annealed

The ac response of the tube furnace stress relief annealed samples is also shown in the graphs in figure 5.11 (crosses (x)). The ac loss exhibited by these toroids is, in all cases, lower than the samples annealed in the box furnace. The generally lower loss exhibited by these toroids is consistent with the idea that more domain walls are present in these samples due to the increased level of residual internal stresses (see section 5.3.1). The maximum induction reached in these cores is comparable to that seen in the box furnace annealed material indicating that the material is still magnetically soft. The remanent induction, however, has decreased. This, again, can be attributed to the presence of the residual stresses, and the consequent off-axis anisotropy. The unchanged ac coercive field probably represents a balance between the increased domain wall pinning and the

change in the domain structure.

5.4.2 Longitudinally field annealed cores

Figure 5.12 shows the ac results obtained on the longitudinally field annealed samples. The tube annealed results are plotted as a function of cool rate (crosses (x)). In all cases the ac loss and coercivity are significantly higher than the stress relieved samples annealed under the same time-temperature conditions. The increase in loss is greater than 40% and the increase in ac coercive field greater than 30%. The remanence ratio is also increased (20%), although the maximum induction remains approximately the same (almost saturation). Indeed, the results obtained on these samples indicate a significantly higher loss than even the worst of the stress relieved samples already presented (60 minutes stress relief in the box furnace, plotted on figure 5.12 (vertical cross (+)) for comparison. The final data point on this figure (o) is that for the 10 minute longitudinally field anneal sample treated in the box furnace. This core exhibits losses and coercive fields which are larger again than the tube furnace toroids.

These results should be compared with the results

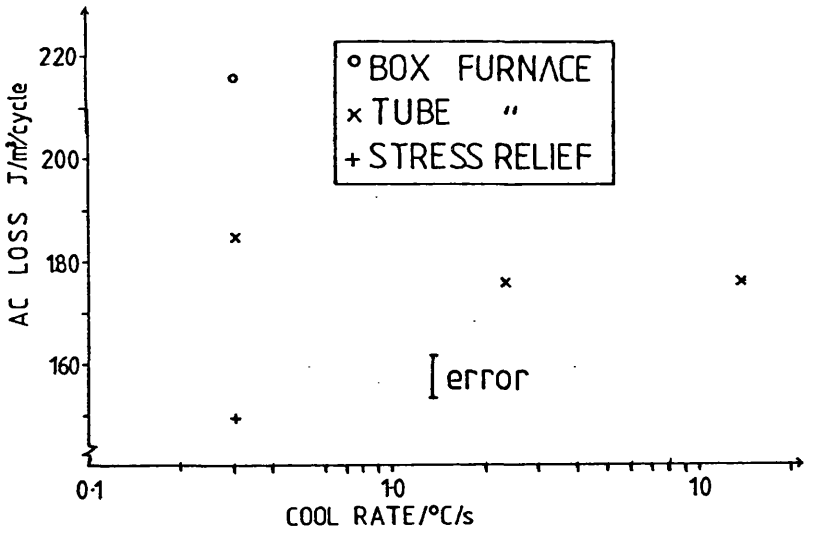

Figure 5.12 AC LOSS vs COOL RATE FOR LONGITUDINALLY FIELD ANNEALED METGLAS 2605-SC

on longitudinally field annealed VAC 6030 presented in section 4.2.2.2. A similar result was found in this material. In contrast to the Co-based material, however, no correlation between cool rate and ac magnetic behaviour is observed in the magnetostrictive alloy. Several possible reasons exist for this behaviour. Firstly, it is known from the tube annealed, stress-relieved toroids that the time-temperature anneal profile is insufficient to fully relax these toroids. Local disruption of the overall longitudinal anisotropy by the residual stress centres in the samples may therefore obscure this effect. The anisotropy induced by field annealing METGLAS 2605-SC is known to be low (approximately 100 J/m^3 cf METGLAS 2605-CO where K_u is of order 1000 J/m^3 (Smith,1988)). Secondly, it is possible that the even at the highest cool rate used here, the induced anisotropy approaches the maximum possible in this particular alloy and the lower cool rates, in contrast to the behaviour of VAC 6030, increased the induced anisotropy little or not at all (see section 1.7.2). A third possibility is that the stresses generated by the magnetostrictive response of the core during the magnetisation process itself may obscure the effect of a slight increase in the induced anisotropy.

Whichever of the causes may be dominant, it is

clear from the above results that the introduction of a uniaxial anisotropy increases the observed ac loss. The increase seen can be explained in terms of a modification of the domain structure by annealing (cf VAC 6030), more specifically, a reduction in the number of domain walls.

5.4.3 Magnetostriction and its effect on the ac behaviour of METGLAS 2605-SC

A simple model of magnetostriction in metallic glasses was presented in section 1.4.2. According to this model, the magnetostrictive response of a specimen is greatest if all of the individual atomic moments are initially aligned perpendicular to the magnetisation direction and are subsequently rotated through 90° to lie along the direction of the applied field. In a real material, it is never possible to achieve this - the moment fan angle (Melamud, Swartzendruber, Bennet, Cullen and Wun-Fogle, 1987) and inhomogeneities in the sample both produce deviations from the ideal. It is true, however, that the maximum magnetostriction is measured in samples in which a transverse anisotropy has been induced, and a minimum when the anisotropy is longitudinal (Squire, Gibbs and Thomas; to be published: see also section 1.4.2). Thus the toroids annealed in a

saturating longitudinal field would be expected to exhibit less core vibration than the as-received or stress-relieved cores.

The magnetostrictive response of a core depends upon the functional form of M(t). For cores excited with a 'SINE-H' drive waveform, M(t) is not a simple function. It is however periodic with the same fundamental frequency as the applied field and a component of the magnetostriction would therefore be expected at twice this frequency. For typical excitation frequencies of 0.5-1kHz, the mechanical excitation of the core would be expected to contain frequencies in the audible range. All of the cores measured did indeed produce audible emmissions of varying pitch, quality and intensity. In addition, these were clearly less intense in the case of the longitudinally field annealed samples.

It should be noted that the mechanical vibration of the core can affect the ac magnetic loop shape. Further details on this phenomena and its effect on high rep-rate pulse measurements will be presented in chapter 6.

5.5 Effects of crystallinity on ac performance

In sections 5.2.2 and 5.4.1.1, the effects of crystallinity on the ac performance of longitudinally field annealed and stress relieved toroids were reported. There are several reports in the literature (Datta et al,1981; Krause and Werner,1981; Narita et al;,1981; Hasegawa,1986) which discuss the effect of small volume fractions of crystallinity on ac performance. These were discussed fully in section 1.8.3. Briefly, however, the results of Datta et al (1981) and Hasegawa (1986) were obtained on several Fe-rich alloys at an induction of 0.1T and at a drive field frequency of 50kHz. Both of these papers report a decrease in the ac loss and a decrease in the exciting power required. Both also report that if the crystallinity is increased beyond an optimum, the ac loss started to increase again.

The results of Krause and Werner (1981) were obtained under conditions which more closely approximate those used in this investigation namely higher induction (0.4-1.4T) and lower frequency (0.06-10kHz). At three frequencies in the range given above, the authors reported a lower ac loss at 0.4T for the sample which had started to crystallise than for a similarly treated sample annealed at a slightly

lower temperature. At 1.4T, however, the loss of the partly crystallised sample was higher than that for the amorphous sample. These results were, however, obtained on transversely field annealed samples.

In order to verify that the results of Krause and Werner (1981) are not peculiar to transversely field annealed samples, one sample of METGLAS 2605-SC (core A) was stress-relief annealed (20 minutes at 390° C) and a further toroid (core B) annealed for 45 minutes at the same temperature. The ac behaviour of both of these samples was measured at 2kHz over a range of inductions. dc measurements on these toroids indicated a low coercivity in the stress relief annealed core (3.8A/m) and a higher value of 10.6A/m in core B. Figure 5.13a shows the reponse of these 2 cores to an ac field at 2kHz. The core loss is plotted against the magnetic induction. It can be seen that at all inductions (up to 1.1T), the partially crystallised core exhibits a higher loss than the stress relieved core. Core B was then re-annealed for a further 45 minutes at 390° C and re-measured. The dc H_c of this core had now increased to 16A/m and the ac loss characteristic had changed considerably (dashed line in figure 5.13a). The ac loss of core B is now lower than the stress-relieved at low inductions but higher as B_m is increased above 0.4T. This is similar to the

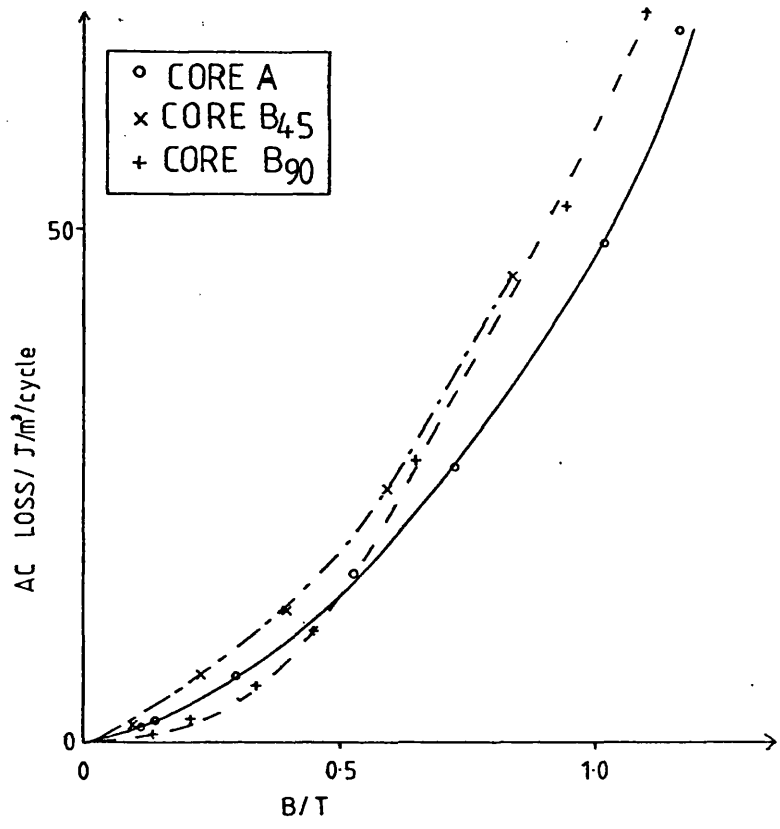

Figure 5.13a AC LOSS vs INDUCTION FOR CORES (A) AND (B)

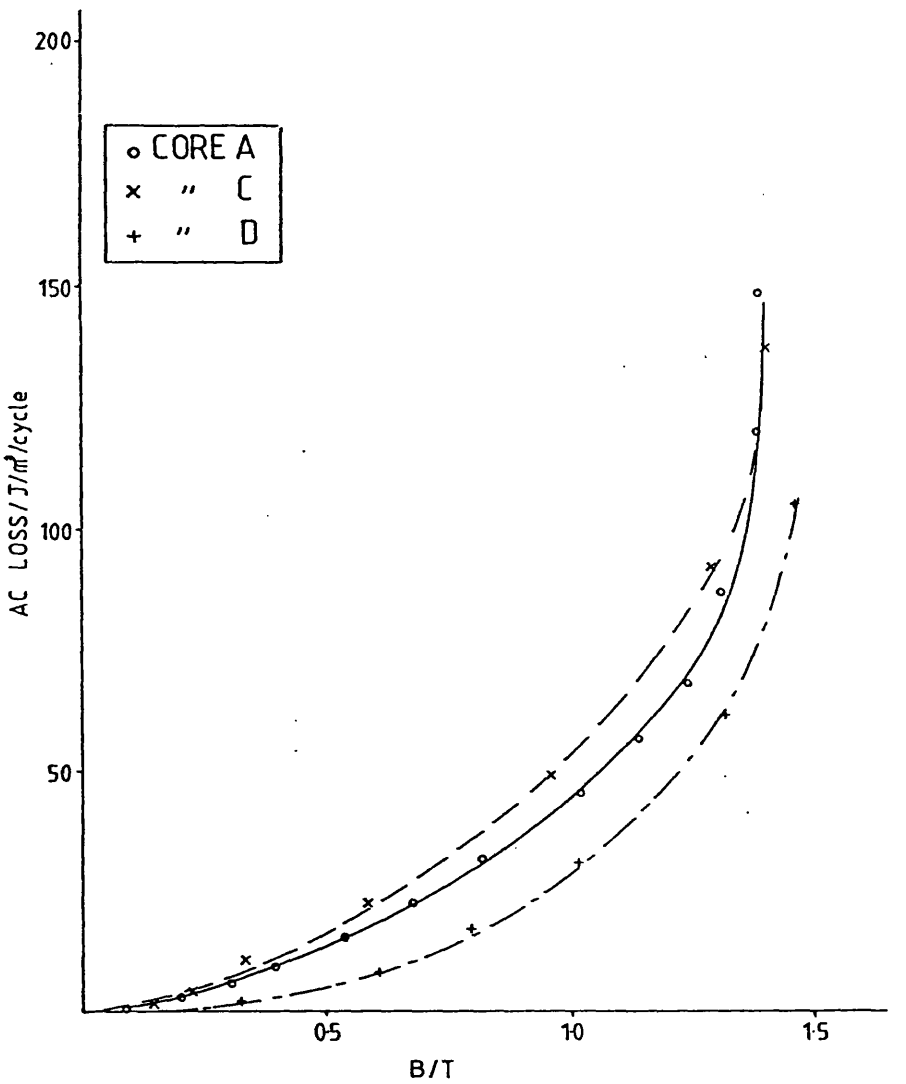

Figure 5.13b AC LOSS vs INDUCTION FOR CORES (A) (C) AND (D)

results presented by Krause and Werner (1981) and is consistent with those of Datta et al (1981) and Hasegawa (1986).

The loss vs induction characteristics of the cores annealed for 120 (core C) and 180 (core D) minutes (figure 5.11; section 5.4.1.1) were then measured and compared with the 20 minute stress relief annealed core (core A). Figure 5.13b shows the results of this comparison. It can be seen that the core annealed for 120 minutes (dc coercivity of 15A/m) showed a higher loss than the stress relief annealed toroid at inductions of less than 1.35T. Above this value, the uncertainties in the measured flux density and in the measured loss, coupled with the steepness of the loss-induction curve at this point, make it difficult to determine the whether or not the curves cross. The sample annealed for 180 minutes showed a lower loss at all induction levels although a greater field was required to reach any given induction. Figure 5.14 shows the ac loops at a driving field of 150A/m for cores A,C and D.

It should be noted that although the cores B and C received slightly different annealing treatments, their dc coercivities were similar. Their ac response, however was not. This indicates the sensitivity of the

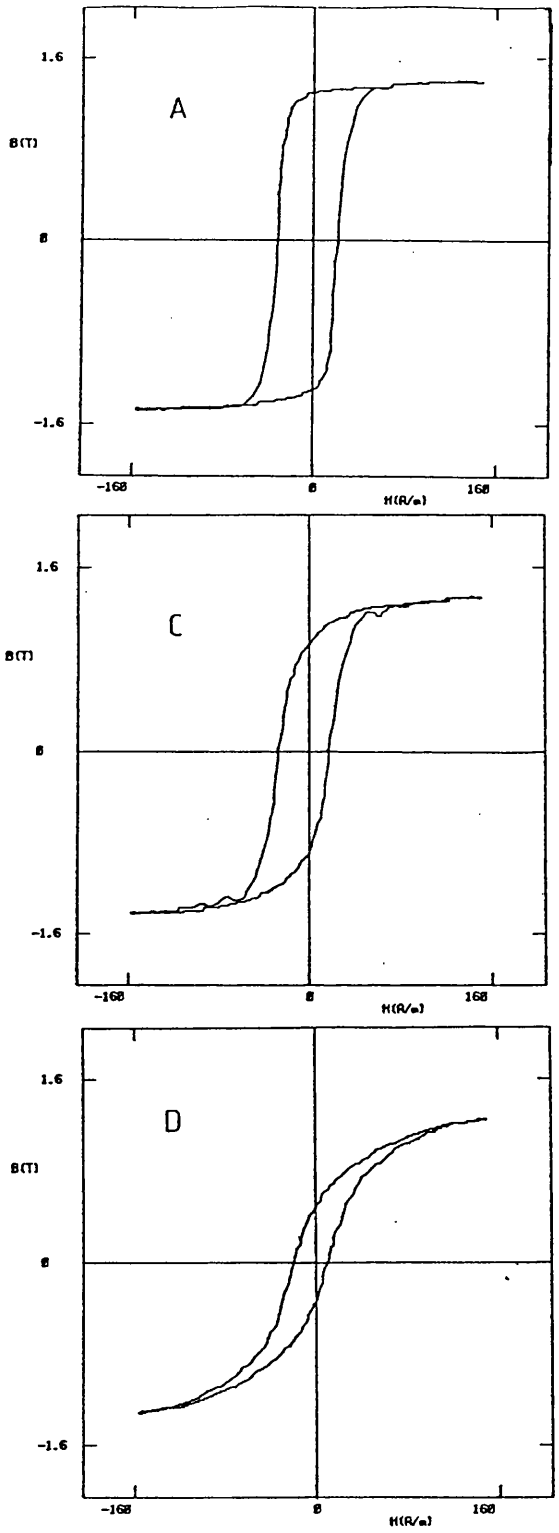

Figure 5.14 THE AC LOOPS OF CORES (A) (C) AND (D)

ac behaviour to the crystallite structure, composition and/or distribution.

The following explanation of the effect of crystallisation on the ac behaviour of metallic glass toroids is generally accepted. The reduction in low induction loss is due to domain refinement caused by the strain field around the crystallite sites. The additional walls introduced into the sample reduce the average wall velocity and hence the anomolous loss. The increase in observed loss as the induction level is increased, however, has not been satisfactorily exlained but may be caused by the additional energy required as the walls introduced by the crystallites are broken free of their pinning sites during the magnetisation process.

This section has demonstrated that the ac magnetic properties of METGLAS 2605-SC can be changed significantly by the introduction of some crystallites and has indicated that in some cases and under certain excitation conditions, this can be beneficial. The effect, however, is very sensitive to the heat treatment parameters. More work is needed to determine how this affects the concentration, orientation, morphology and magnetic properties of the crystallites themselves and how these in turn affect the magnetic

performance of the core.

5.6 The effect of post production treatments on the pulse behaviour of METGLAS 2605-SC

Section 4.3.1 described the pulse measurement arrangements and limitations for the testing of the VAC 6030 cores. It was stated there that in the ideal case, the saturation of the magnetic material occurs when the charge on the preceeding capacitor bank has reached a maximum. In the case of the VAC 6030 toroids, with the value of L_o chosen, saturation occurred at approximately 85% of the maximum - before the voltage on C_2 peaked (figure 4.18).

The time required to saturate a core depends upon the voltage-time product applied to the primary windings (Faraday's Law). For a given voltage waveform, the larger the flux swing available, the longer the material takes to saturate. Thus METGLAS 2605-SC would require a longer resonant charging time in order to ensure saturation of the material as the voltage on C_2 reaches a maximum. If the same value of L_o used for the Co-rich alloy is also used for the METGLAS material, it is found that for all but the as-received and heavily crystalline samples, saturation occurs approximately at the

maximum (figure 5.15). In order to keep the results on the two materials comparable, it was, therefore decided to make the pulse measurement on this material with an unchanged resonant charging time. The results presented in the following sections are therefore on the METGLAS 2605-SC alloy, measured under resonant charging conditions, with a resonant charging time of approximately 15μs and a maximum applied voltage of 20V.

5.6.1 As-received and stress relief annealed cores

The pulse results on the stress relieved METGLAS 2605-SC are summarised in figures 5.16 and 5.17. The pulse performance parameter (PPP) for this alloy is calculated for a reset current of 3A and for a flux swing of 2.0T. Some samples, notably the as-received and highly crystalline cores, did not reach this induction level at this value of reset and are therefore not included in figure 5.17. The results presented here are consistent with the ac results presented in section 5.4. The pulse loss increases as the anneal time increases (ie as stress relief is maximised) and then decreases as crystallisation in the material begins to dominate the magnetic performance of the core. Note, however, that the lower

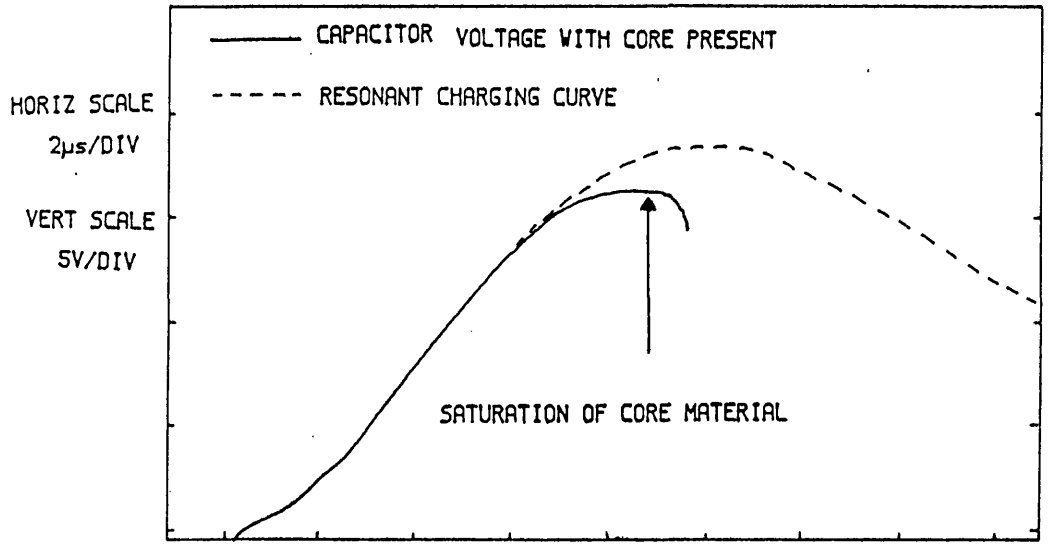

Figure 5.15 THE CAPACITOR VOLTAGE WAVEFORM FOR A METGLAS 2605-SC CORE

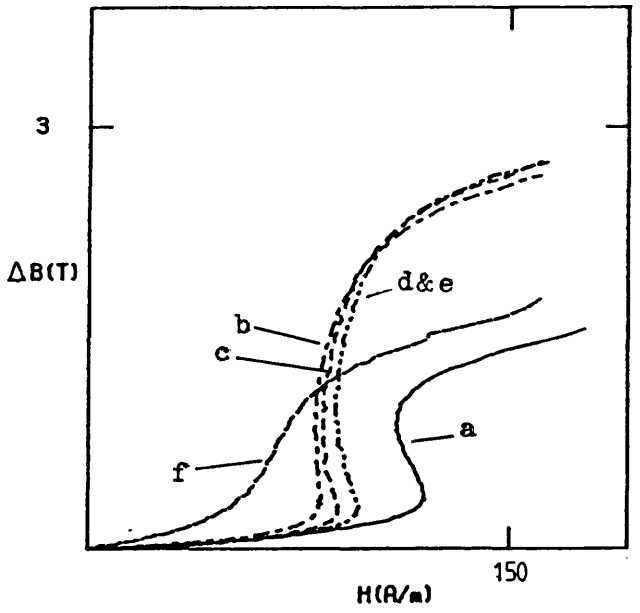

a ——— AS RECEIVED
b - - - - - - - ANNEALED 5 MINUTES
c - - - - - - - ANNEALED 10 MINUTES
d . - . - . ANNEALED 20 MINUTES
e ..... ANNEALED 30 MINUTES
f ——— ANNEALED 180 MINUTES

Figure 5.16 THE PULSE RESPONSE OF STRESS RELIEF ANNEALED METGLAS 2605-SC

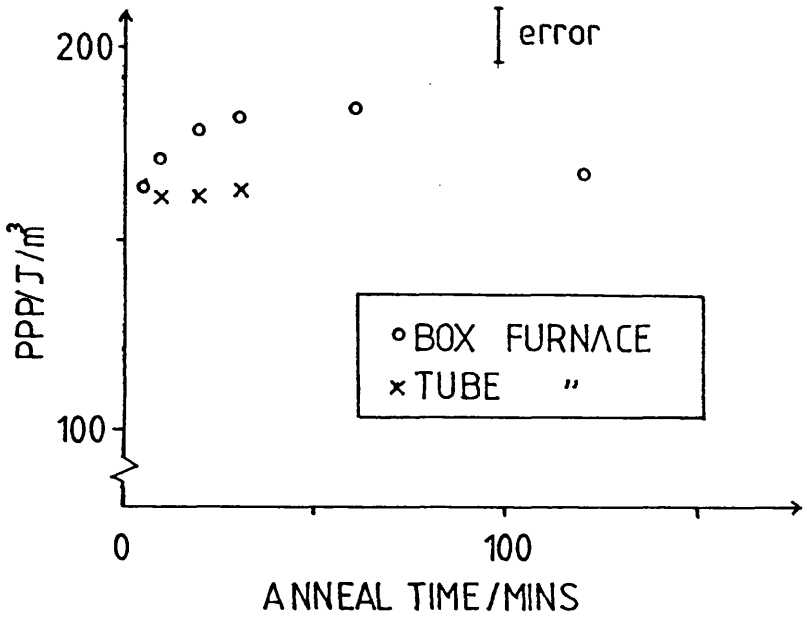

Figure 5.17 PPP vs ANNEAL TIME FOR METGLAS 2605-SC

loss exhibited is accompanied by a reduction in the useful flux swing and that consequently, a larger reset field is required for even a modest ΔB.

The pulse performance parameter is lower for the tube annealed toroids than the box annealed. This is as expected from the ac results and can be attributed to the effects of residual stresses in the material producing a more mobile domain walls. Additional pinning also caused by the residual stresses, however, decreases the flux swing available from a given reset condition.

Note that the pulse perfomance parameter, PPP, is related to the pulse loss of the material. Given the difficulties in defining a true pulse loss (section 4.3.1), the values presented here are comparable to the METGLAS 2605-SC pulse loss values quoted by Smith (1988) of approximately 200J/m^3 at a reversal rate of 0.3T/μs.

5.6.2 Longitudinal Field Annealed Cores

The pulse results (figures 5.18 and 5.19) again confirm the ac measurements on the field annealed samples. The samples annealed in the tube furnace and cooled at different rates to room temperature all show

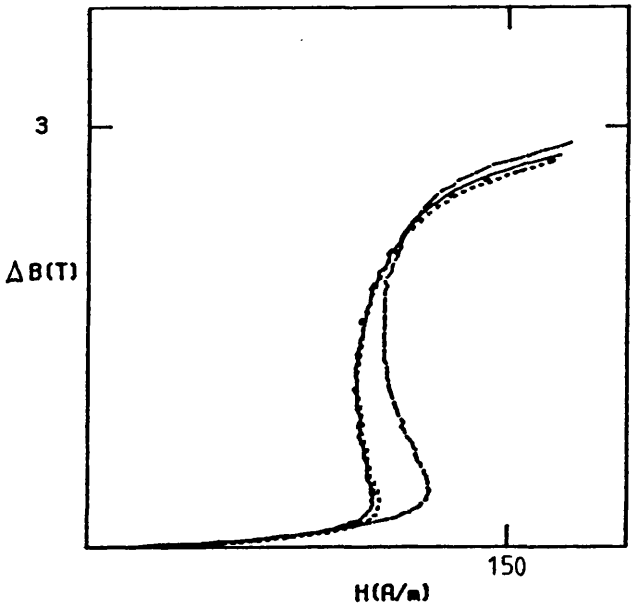

Figure 5.18 THE PULSE RESPONSE OF FIELD ANNEALED METGLAS 2605-SC

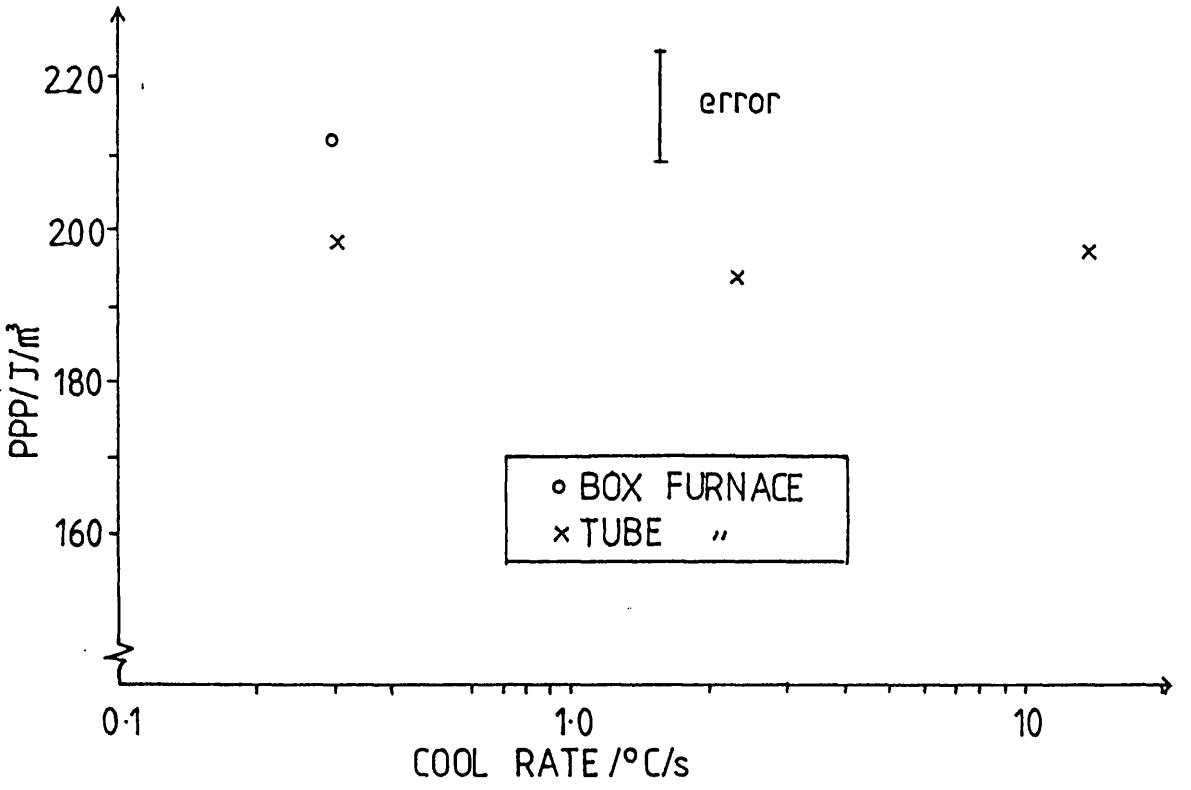

Figure 5.19 PPP vs COOL RATE FOR LONGITUDINALLY FIELD ANNEALED CORES

a higher PPP than the cores stress relieved under these furnace conditions. The cool rate, however, has no significant effect on the pulse performance of these cores. In addition, the flux swing exhibited by this set of cores is greater than that shown by the stress relieved set. This also can be inferred from the ac and dc results.

The longitudinally field annealed sample treated in the box furnace showed a significantly higher PPP than any other toroid. This is also consistent with the ac results presented in section which showed a higher ac loss for this sample than any other.

5.7 Summary of results on METGLAS 2605-SC and comparison with VAC 6030

The above results, as in the case of the Vacuumschmelze alloy, indicate that the dc and ac magnetic characteristics can be used to predict the pulse response of a given material. In the case of the alloy METGLAS 2605-SC, the results indicate that the stresses present in the as-received material reduce the useful flux swing and therefore render it ill-suited to pulse compression applications. The stress relief annealing treatment in the box furnace, slightly increases the loss (under both ac and pulse

conditions) but also significantly increases the available flux swing. The residual stresses (and therefore lower longitudinal component of anisotropy) after stress relief in the tube furnace serve to increase the number of active walls in the material and therefore produce a material with a high flux swing but with ac and pulse losses lower than the box furnace annealed material. Longitudinal field annealing increases the losses still further. This was also seen in the VAC 6030 cores. The systematic increase in the PPP with decreasing cool rate presented in chapter 4, is, however, not seen in METGLAS 2605-SC. This is probably related to either the kinetics of anisotropy development or the stress effects present in this alloy. It is clear from the above, however, that in both magnetostrictive and non-magnetostrictive metallic glass cores, the production of a uniaxial anisotropy is detrimental to the pulse performance of the core.

CHAPTER 6

6 Discussion of the effects of the magnetostriction, controlled crystallisation and surface oxidation

In the course of this work, several topics were investigated which were directly relevent to this study. These were discussed in chapters 4 and 5. In addition, there were some topics which, although of some relevence, were not studied in detail due to lack of resources or time. The purpose of this chapter is to record some of these additional studies. Four topics will be presented:-

i) a simple model to explain the odd ac behaviour of magnetostrictive cores under certain drive conditions
ii) the effects of high repetition rates on the pulse response of the magnetostrictive alloy METGLAS 2605-SC
iii) the effects of controlled surface and bulk crystallisation on the dc magnetic properties of VITROVAC 0040
iv) the effects of controlled surface oxidation on the dc magnetic properties of METGLAS 2605-S2 and VITROVAC 6010

The unusual loop shapes often observed in magnetostrictive toroids under ac excitation will be discussed first.

6.1 The effect of magnetostriction on the ac magnetic behaviour of amorphous alloy cores

Thottuvelil (1983,1984) has reported unusual magnetic behaviour in amorphous alloy, tape wound cores under both sinusoidal and step dB/dt conditions. Similar behaviour has also been seen in some of the cores used in this project (figure 6.1). Thottuvelil (1984) showed a correlation between this type of behaviour and the natural resonant frequencies of the cores but did not attempt to explain specific loop shapes. It is the purpose of this section to propose a simple model to explain the general forms of some of these odd B-H curves.

It is useful for the sake of clarity to divide the following argument into two distinct cases - controlled B (or dB/dt) and controlled H. In each case, the basic mechanism is the same but the effect on the B-H curve is different. The reasons for this will become apparent.

Sinusoidal drive field (SINE-H), will be considered

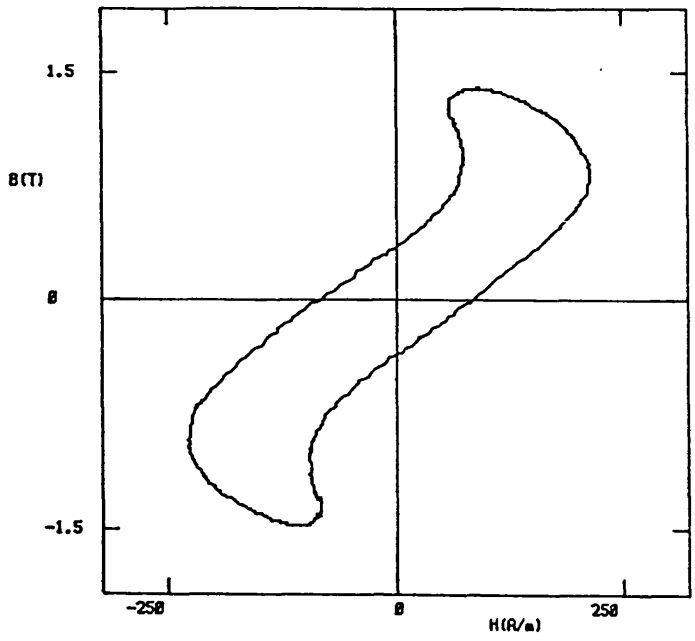

Figure 6.1 A 'STRANGE' B-H LOOP

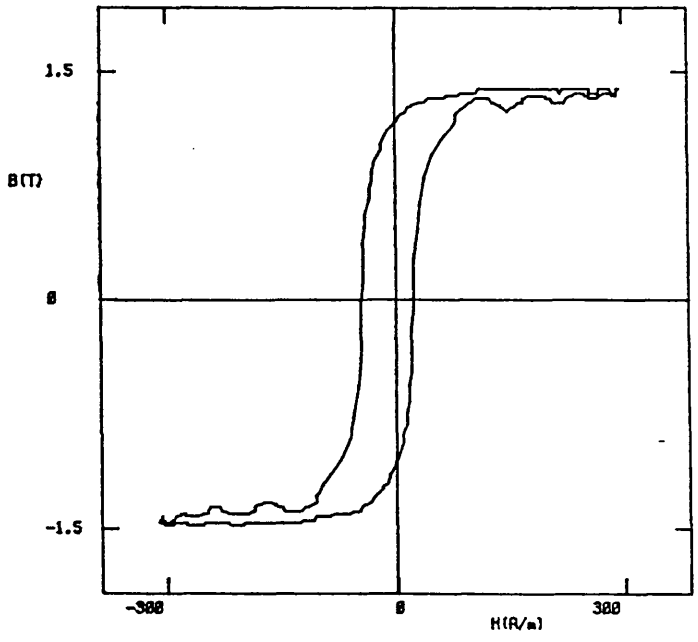

Figure 6.2 A B-H LOOP SHOWING HIGH FREQUENCY RIPPLE

first.

6.1.1 Controlled H

Consider two samples, identical in every way (physically, electrically and magnetically), except that in one the magnetostriction is zero and in the other it has some finite value. Under the same conditions of applied field, the flux density in the second sample will differ from that in the first by an amount which depends upon the magnetostriction characteristics of the material. For example, if we take a material with positive magneto- striction, λ, and Young's Modulus E, then in a given applied field, the first sample will reach an induction, B. The stress in the second sample, due to its own expansion will be

$$\sigma = E(\Delta l/l) = E\lambda \qquad ..(44)$$

Taking $E=10^{11}$ Pa and λ=30ppm, the stress generated by the material's own expansion can be shown to be of order 3×10^{5} Pa. Now, in a positive magnetostriction sample, the effect of a tensile stress, is to increase the induction achieved for any given applied field. Rees (1987) showed that the effect of a constant, longitudinally applied stress on the dc magnetic

behaviour of METGLAS 2605-SC was to increase the magnetisation, M, achieved by approximately 0.01 A/m/Pa. ie B was increased by 10^{-8} T/Pa. Thus, the induction in the magnetostrictive sample will be of order 0.03T greater than that in the zero magnetostriction material.

Under ac conditions, the core's behaviour is more complex. Under SINE-H excitation, M(t) is not a simple function of time and includes many high frequency terms. $\Delta l(t)$, will therefore include frequencies other than the fundamental, and the effect on the B-H loop of the magnetostrictive vibration of the core must also include these higher order terms, although the amplitude of the frequency components higher than the fundamental may be expected to be small. Under certain drive conditions a frequency component of the magnetostrictive response of the core may be sufficiently close to one of the cores natural resonant frequencies to excite a resonant vibration. If this is the case, then the amplitude of this component of vibration will increase and the effects of this oscillation may be seen on the B-H curve. If the resonant frequency is much higher than the excitation frequency, this would take the form of high frequency 'ripple' on the B waveform. This can be seen in the loop shown in figure 6.2. These results were

obtained on a stress relief annealed core of METGLAS 2605-SC. The ripple amplitude is approximately 0.1T and is at a frequency of approximately 45kHz. This was found not to change in frequency when the excitation frequency was varied over the range 0.5-5kHz. This implies a low Q-factor for the core. This is not surprising since the core is not a solid ring and will, therefore, not have a well defined resonant frequency.

The frequency of the fundamental extensional mode of vibration of a toroidal is given as

$$f = (E/\rho)^{0.5}/2\pi r \qquad ..(45)$$

where r is the core radius and ρ, the material density (Thottuvelil (1984)). Taking $E=10^{11}$ Pa and the density as 7.32×10^{3} kg/m^{3}, then for a 3cm diameter toroid, this resonant frequency can be calculated to be approximately 40kHz. This therefore, confirms that the model proposed is realistic and can explain the effects of core vibration under the simple conditions of sinusoidal field. The following section will attempt to explain the odd loop shapes reported by Thotuvellil (1983,1984) by simple application of this model.

6.1.2 Controlled B

Under the controlled field conditions described above, the effect of core vibrations is to alter the induction achieved for a given applied field. Under conditions of controlled flux density, the field, H, takes whatever value is necessary to produce the required B. Thus the effect of the magnetostrictive response of the core is not directly on B but must be reflected in the field (H) waveform. The magnitude of the change in H is difficult to estimate since it requires a knowledge of the precise shapes of both the B-H and λ-B curves. However, the previous section on SINE-H indicated that the effect is, at least, of the right order of magnitude. This section will illustrate that given an effect of sufficient magnitude, the loop shapes reported by Thottuvelil (1983,1984) can be reproduced by considering the stress-induction argument presented above.

Let us first assume that $B \simeq \mu_0 M$ so that Δl will follow approximately the periodicity of B. Therefore,

$$M = M_1 \sin\omega t \qquad ..(46)$$

and

$$H = \sum H_n \sin(n\omega t + \phi_n) \qquad ..(47)$$

The modification to the H waveform due to the magnetostrictive strain in the material will, therefore, be of the form $A\sin(\omega t+\theta)$. With appropriate choices of A and θ, the 'normal' loop (figure 6.3), can be modified (figure 6.4) to appear similar in form to the loops reported by Thottuvelil (1984), figure 6.5.

The loop shown in figure 6.1 above, and reported by (Thotuvellil, 1984 however, cannot be reproduced regardless of the choice of A and θ. In order to explain how this shape can come about it is necessary to consider the possibility that higher frequency components of the core vibration may be significant under SINE-B conditions. In the case of the loop shown in figure 6.1, it is the third harmonic component which is primarily affected by the core vibration. If the third harmonic of $\Delta l(t)$ is at or near one of the core's natural resonant frequencies, then the core may vibrate at this frequency in preference to the drive frequency. In this case, the H waveform is mainly affected by $A_3 \sin(3\omega t+\theta_3)$. Choosing arbitrary values for A_3 and θ_3, the loop shape shown in figure 6.1 can be reproduced (figure 6.6).

This argument is supported by the observation that,

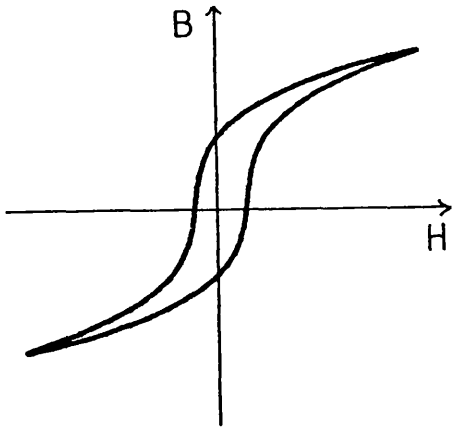

Figure 6.3 A NORMAL B-H LOOP OBTAINED UNDER SINE-B CONDITIONS

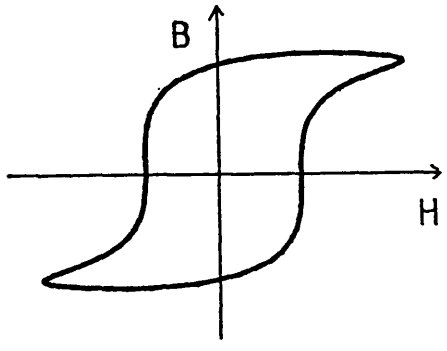

Figure 6.4 THE LOOP SHOWN IN FIG. 6.3 MODIFIED BY CORE VIBRATION

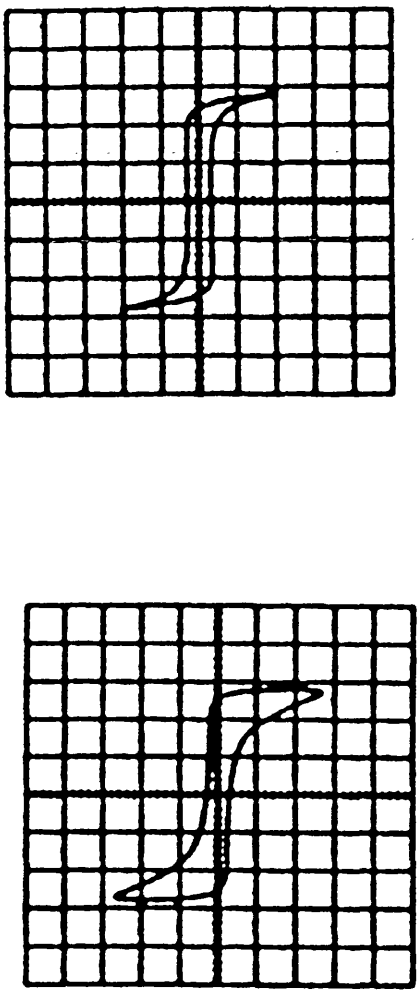

Figure 6.5 B-H LOOPS OBTAINED ON A TOROIDAL SAMPLE AT DIFFERENT FREQUENCIES (after Thottuvelil et al)

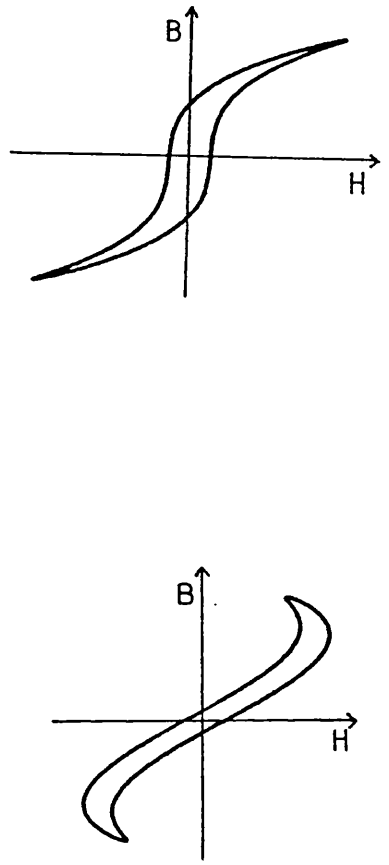

Figure 6.6 A NORMAL B-H LOOP OBTAINED UNDER SINE-B CONDITIONS (a) AND MODIFIED BY CORE VIBRATION (b) TO GIVE A LOOP SIMILAR TO THAT SHOWN IN FIG. 6.1

when this loop was observed, the core was quiet. This indicates that either the core was not vibrating or that the vibration frequency was outside the audible range. The first of these is unlikely and it must therefore be concluded that the primary core vibration was at a frequency outside the audible range. As the drive level was increased, the B-H characteristics returned to normal and the audible output of the core returned.

In summary, therefore, the unusual ac behaviour of some magnetostrictive cores can be explained by considering the effect of the core vibration on the drive field required or the induction achieved. This section has demonstrated that under SINE-B conditions, the strange loop shapes observed can easily be modelled. In addition, it is easy to see how this explanation can be extended to explain the loop shapes reported under square dB/dt excitation conditions (Thottuvelil, 1983). Examples are shown in figure 6.7. The model presented here provides at least order of magnitude agreement with experiment. Further work, however, is obviously required.

The above is relevent not only to ac excitation of cores but also to magnetic switching applications if high repetition rates are used. Section 6.2 reports a

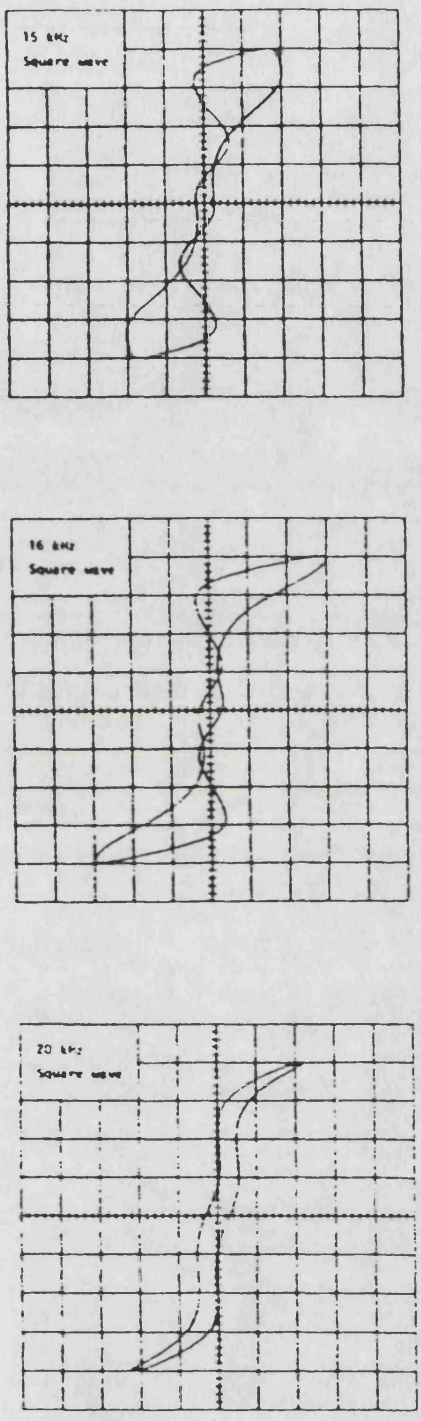

Figure 6.7 LOOPS OBTAINED UNDER SQUARE dB/dt CONDITIONS (after Thotuvellil et al)

short investigation into the high repetition rate behaviour of a single magnetostrictive pulse compression element. This work was carried out at British Aerospace, Filton with Dr Nigel Seddon.

6.2 High repetition rate pulse measurements

The pulse results presented in chapters 4 and 5 were obtained using a voltage waveform of the form which would be experienced in a real compression line. The pulse repetition frequency (PRF), however, was only 1Hz and core resonances were, therefore, unimportant. In a real pulse compression system, the PRF required is likely to be much higher than this; in some applications over 10kHz, the maximum PRF, is often limited by core heating (section 2.6.1). In magnetostrictive materials, problems associated with core vibration and core resonances may also limit the operating frequencies. In order to investigate the effect of increased PRF on the pulse response of a magnetic core, a variable width bipolar pulse generator was designed and built at British Aerospace. The circuit diagram is shown in figure 6.8 and the experimental arrangement used is shown in figure 6.9. Briefly, a laboratory pulse generator was used to trigger the bipolar pulse box at rates varying between 20Hz and 20kHz. The pulse was amplified by an Amcron

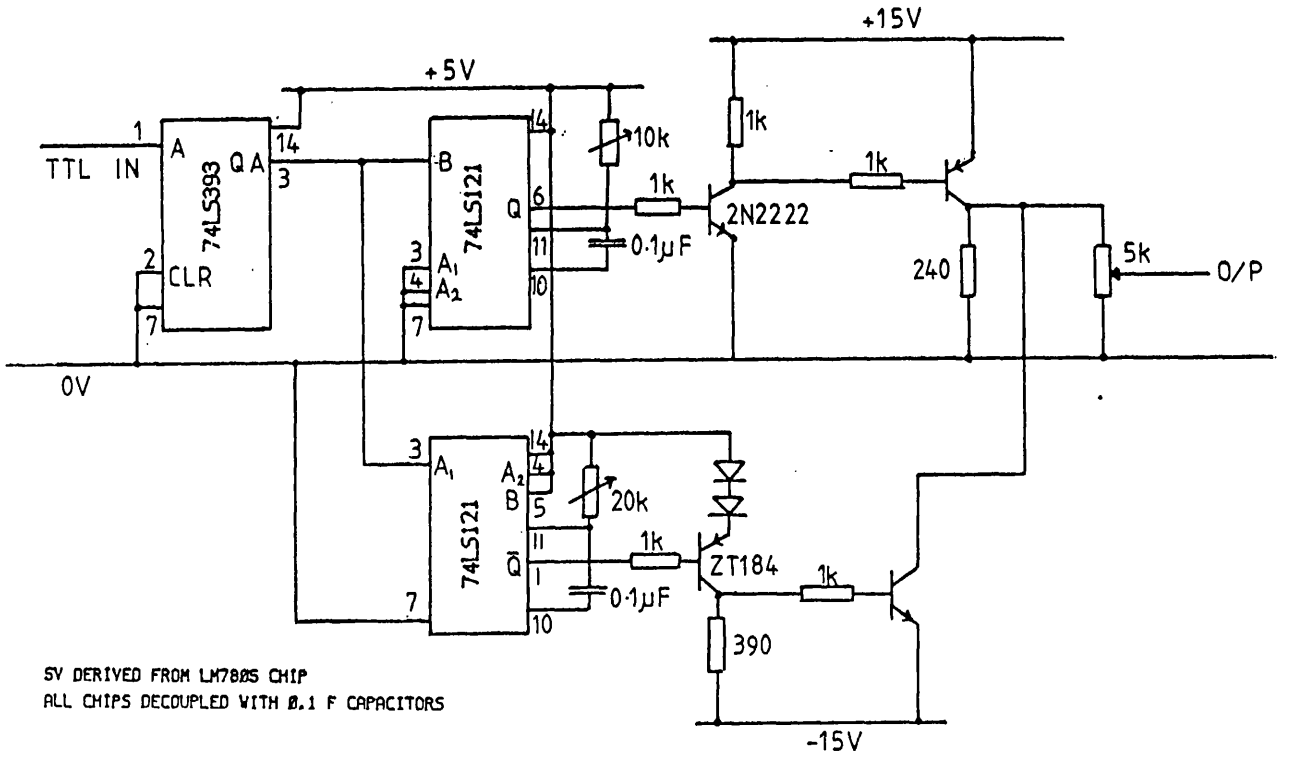

Figure 6.8 THE BIPOLAR PULSE BOX

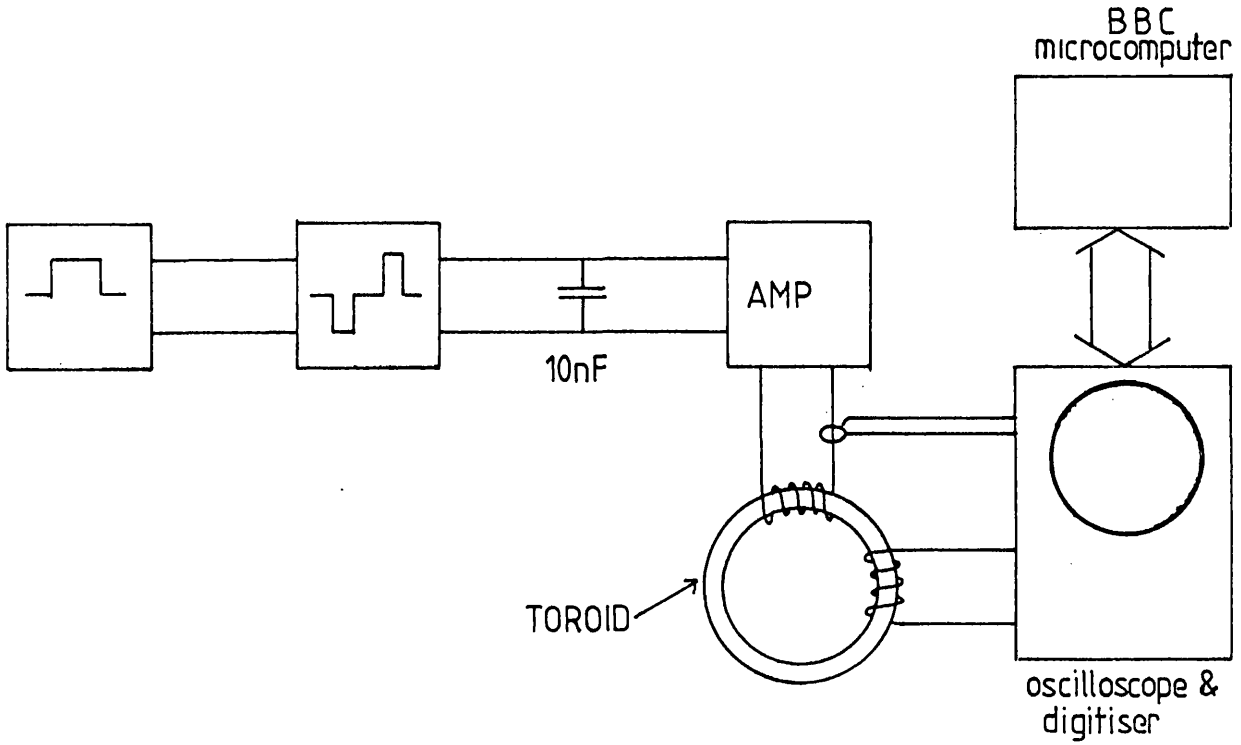

Figure 6.9 A SCHEMATIC OF THE HIGH PRF MEASUREMENT SYSTEM

power amplifier and applied to the core. The current in the primary windings was monitored using an Alrad 411 current transformer and the voltage induced in the secondary was monitored using a Tektronix x10 oscilloscope probe. The signals were then stored and analysed as described in section 3.5.1 for the pulse measurements. The 10nF capacitor in parallel with the bipolar pulse generator output was included to increase the rise time of the power amplifier input pulse. This is necessary because the Amcron input stages can be damaged by slew rates in excess of 32V per microsecond.

The sample used was a 10 wrap longitudinally field annealed METGLAS 2605-SC core wound with a 6 turn primary winding and a single turn secondary. The core cross-sectional area was measured as $3.9 \times 10^{-6} m^2$. The voltage pulse used was of 10 microseconds duration and of variable amplitude.

Assuming a maximum flux swing of 3.2T, therefore, a primary voltage of 7.5V was required. This was provided by adjusting the Amcron gain and the input pulse amplitude. Measurements were then made over a range of pulse repetition frequencies (20Hz to 20kHz). PRFs of 5kHz, 11kHz, 13kHz, 14.5kHz and 17.9kHz were chosen to correspond with maxima in the audible output

of the core. Measurements were also made at frequencies just below those at which the core began to resonate. A single control reading was taken at 20Hz. It was assumed that at this frequency, no core resonances were likely. Figure 6.10 shows the results obtained up to 18kHz. Above this frequency, the core resonances merged into a continual high frequency vibration. In addition, at frequencies above 5kHz, the response of the core to the reset pulse was not completed before the application of the forward pulse.

The core resonances can clearly be seen to have an effect on the core behaviour - the exact effect, however, depends strongly on the PRF. This is as expected from the arguments outlined in section 6.1. The effect of core resonances on the behaviour of a pulse compression element may therefore be very important. In some cases, the core vibration can actually improve the pulse reversal behaviour although, in general, a deterioration was seen when the core began to resonate.

There are two possible solutions to the problems posed by core vibration. If the working frequency of the core is known, then in many cases it may be possible to design the core itself such that core resonances are avoided. In a small toroid, this may

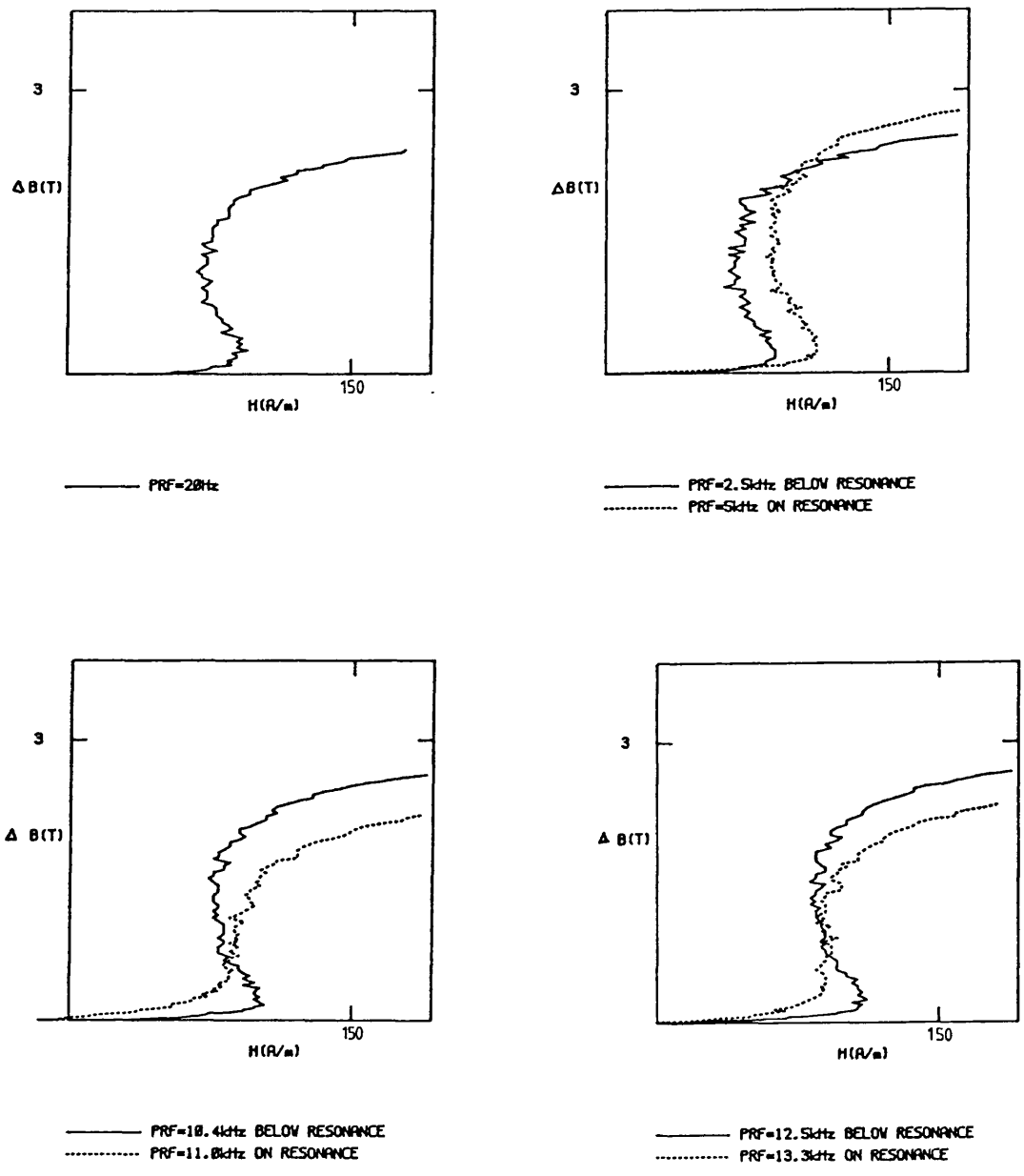

Figure 6.10 HIGH PRF PULSE RESULTS

simply be a case of adjusting the toroid diameter. In a large core, however, this may not be straightforward as the vibrational behaviour of the core will not be trivial. A second solution involves mechanical damping of the core vibrations. Ramanan, Smith and Barberi (1985) have shown that the impregnation of a toroidal core with a suitable viscosity oil, can reduce the core vibration and core losses. This technique may, therefore, be useful in larger toroids.

The final two sections in this chapter are concerned with the effects of controlled crystallisation and oxidation on the dc magnetic properties of metallic glass samples.

6.3 Controlled Crystallisation

The effects of small volume fractions of crystallinity on the magnetic properties of metallic glasses were discussed in chapters 1 and 5. It was noted there that several authors have reported improvements in the ac properties of metallic glasses after partial crystallisation. This section will present the effect of accurately controlled crystallisation on the dc magnetic properties of the Vacuumschmelze alloy VITROVAC 0040. This work was perfomed in conjunction with Mr Gao Wei and Dr Brian

Cantor. The sample preparation and non-magnetic characterisation of the samples were carried out by Gao Wei in the Department of Metallurgy and Science of Materials at Oxford University.

6.3.1 Sample preparation

All of the samples used in this study were 35mm x 7.5mm x 0.032mm. Gao and Cantor (to be published) used various combinations of three treatments to produce either controlled surface or controlled bulk crystallisation. These treatments are listed below.

i) a pre-anneal of 20 h at 350°C in air (a 'K' treatment)
ii) a surface polish with 1200 grade SiC (a 'P' treatment)
iii) subsequent anneals for various times at 390°C in air.

The P treatment was applied to both sides of the ribbon and resulted in a 5% weight loss.

For controlled surface crystallisation, the K treatment preceeded the P and for controlled bulk crstallisation, the P preceeded the K. The percentage crystallinity was varied by changing the duration of

the final anneal. The crystallisation behaviour of this alloy was studied using a combination of differential scanning calorimetry, optical and transmission electron microscopy and X-ray diffractometry (Gao and Cantor, to be published).

The following section reports the dc magnetic properties of samples subjected to various combinations of the treatments listed above.

6.3.2 Controlled crystallisation results

Figure 6.11 shows the dc properties of an as-received sample and of samples after K, P and P+K treatments. The as-received sample exhibited a coercive field of 6.7A/m. This was increased to 53.5A/m by the P treatment; the rise was due to increased stress inhomogeneity introduced by the surface polish. The pre-anneal (K) treatment also increased the coercivity (to 43.4A/m). Gao and Cantor (to be published), reported that no crystallinity was detected in the samples after the K treatment by either X-ray or TEM measurements. The increase in the sample coercivity, however, indicates that the K treatment did introduce some crystallinity. Samples subjected to the P+K treatment were found to exhibit coercivities of around 23A/m. The additional K

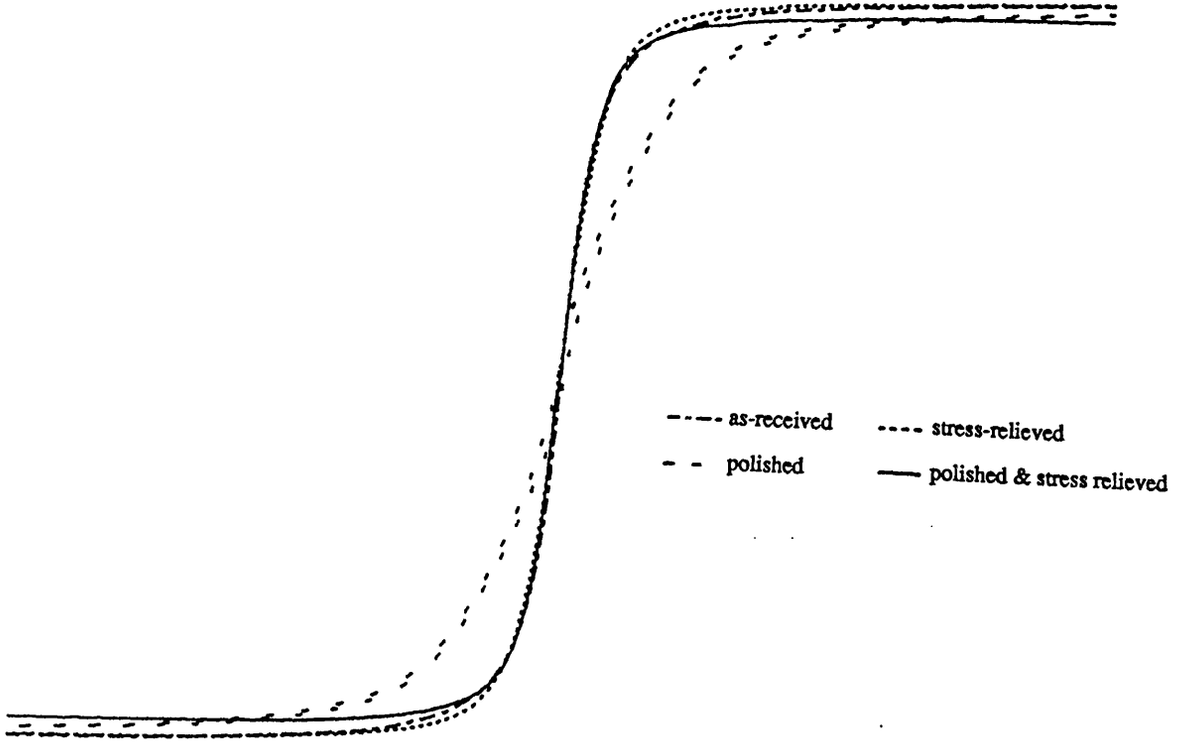

Figure 6.11 THE M-H LOOPS FOR $Fe_{40}Ni_{40}B_{20}$ (MAX FIELD 8700A/m)

treatment therefore relieves some of the stress produced by the surface polish. It is not clear, however, why the coercivity is reduced below that shown by the samples subjected to the K treatment alone.

Figures 6.12 and 6.13 show the effects increasing percentages of surface and bulk crystallinity on the dc magnetic characteristics of this material. Figure 6.14 is a plot of the coercive field of the samples as a function of the percentage crystallinity. All of these measurements were made with a maximum applied field of 8700A/m. The percentage crystallinity was determined from DSC measurements conducted by Gao Wei.

Although some small differences in the curve shapes can be seen, there appears to be little difference in the dc magnetic properties of the the bulk and surface crystallised samples up to 20% crystallinity. In both cases, the dc coercive field increases with the increasing percentage crystallinity. As the crystallinity is increased further, significant differences become apparent, particularly in the shape of the M-H curve. The surface crystallised samples exhibit lower magnetisation energies and reach a higher maximum induction in the applied field. This is

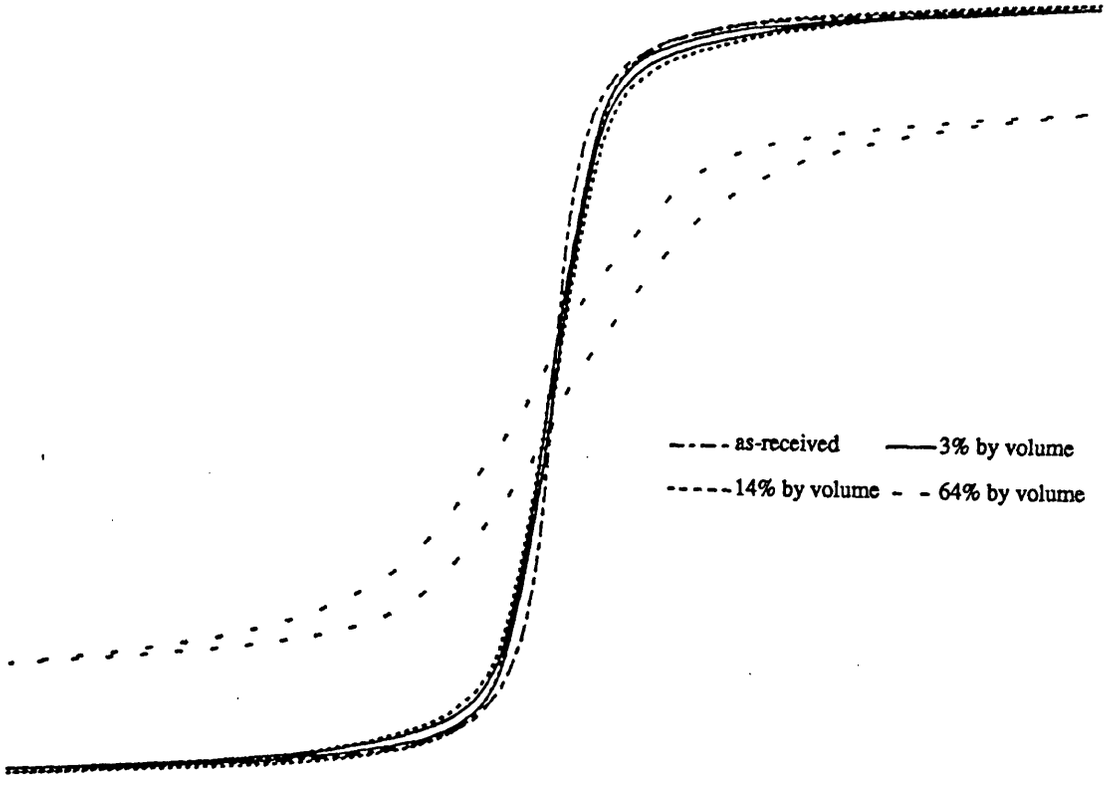

Figure 6.12 M-H LOOPS FOR SURFACE CRYSTALLISED $Fe_{40}Ni_{40}B_{20}$

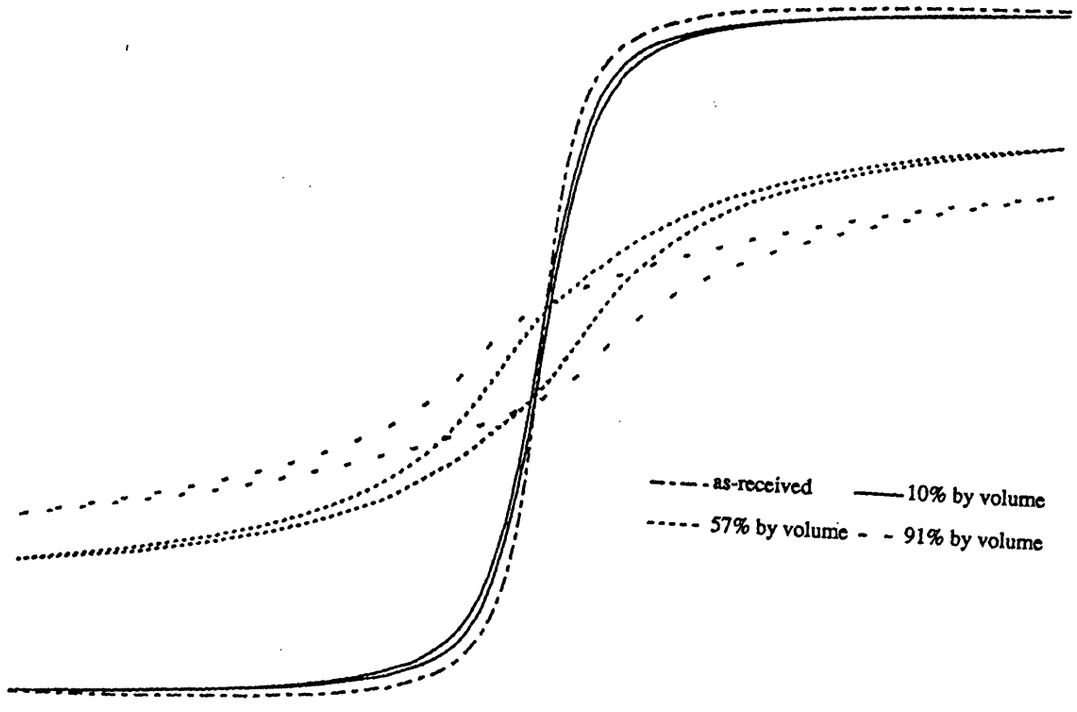

Figure 6.13 M-H LOOPS FOR BULK CRYSTALLISED $Fe_{40}Ni_{40}B_{20}$

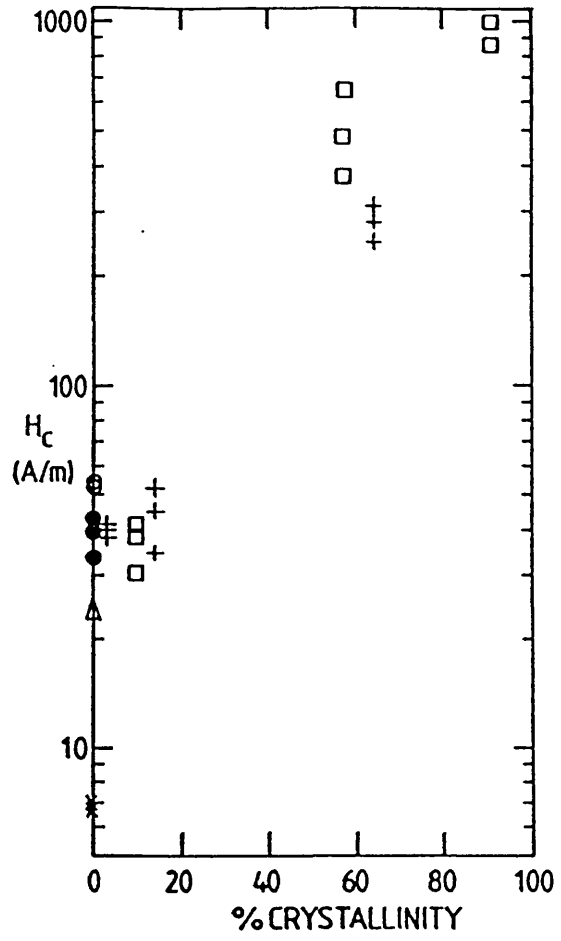

Figure 6.14 COERCIVE FIELD vs % CRYSTALLINITY FOR $Fe_{40}Ni_{40}B_{20}$

X as-received
● stress-relcived
+ surface crystallised
O polished
Δ polished & stress relcived
□ bulk crystallised

probably caused by a more coherent anisotropy distribution in these samples with the bulk magnetisation vector, on average, pointing out of the ribbon plane, Ok and Morrish (1981) and Herzer and Hilzinger (1986). In the bulk crystallised samples, the long range coherence of the moment vector in the bulk of the samples will be perturbed by the strain fields of the individual crystallites which may now be overlapping. A direct comparison of the coercive fields in samples with greater than 20% crystallinity is not useful since the samples are no longer saturated.

At low volume fractions of crystallinity, therefore, the effect of the crystallite morphology on the dc properties of this material appears to be unimportant. Note that this is probably not the case under ac conditions (see section 5.5). As the crystallite content is increased, the morphology cannot be disregarded. Further work is now required in this area to determine how the ac properties are affected by these treatments. The following section describes the effect of controlled surface oxidation on the dc magnetic properties of two metallic glass compositions.

6.4 Controlled Oxidation

The use of surface oxidation has been reported as a possible method of controlling the domain structure and hence ac properties of metallic glasses (Boll, Hilzinger and Warlimont,1983). The effect of the oxide coating on the magnetic properties is thought to be caused by stresses introduced by the oxide layer coupling to the material via the stress-magnetostriction interaction. The work presented in this section discusses the effect of a controlled oxide coating on the dc properties of two metallic glass compositions - METGLAS 2605-S2 and VITROVAC 6010. This work was also perfomed in conjunction with Gao Wei and Brian Cantor at Oxford University.

6.4.1. Sample preparation

The samples used in this study were 50mm x 12.5mm x 0.02mm (METGLAS 2605-S2) and 40mm x 10mm x 0.04mm (VITROVAC 6010). The saturation magnetostriction of these two alloys are 27ppm and <0.5ppm respectively. In both alloys, the controlled oxide layer on each sample was produced by annealing the sample in air for 200h at 300°C. The oxide layers were investigated using thermogravimetry, optical and transmission

electron microscopy and electron probe microanalysis. In the case of METGLAS 2605-S2, the oxide layer was found to be SiO_2 with embedded particles of Fe_2O_3 and Fe_3O_4 (Gao and Cantor, 1988). In the case of the low magnetostriction alloy, the oxide layer was a fine grained multiphase mixture of CoO, Co_3O_4, Co_2SiO_4, Fe_3O_4 and Fe_2SiO_4 (Gao and Cantor, to be published). A sample of METGLAS 2605-S2 was annealed under vacuum as a control.

6.4.2 Controlled oxidation results

Figure 6.15 shows the dc loops of as-received, vacuum annealed and stress relieved samples of these the first of these two alloys. The results on the magnetostrictive sample indicate a decrease in the magnetisation energy of the samples whether annealed in vacuum or air. In addition, a slight reduction in the coercivity is seen in the vacuum annealed sample (8.4A/m cf 10.3A/m for as-received). In contrast, a slight increase was seen in those annealed in air (11.6A/m). The difference in coercivity between the samples annealed in vacuum and in air, indicates that the oxide layer does have some effect on the magnetic properties of the sample. The increase in coercivity, however is small. Although this may seem surprising, the oxide layer is uniform (Gao and Cantor, to be

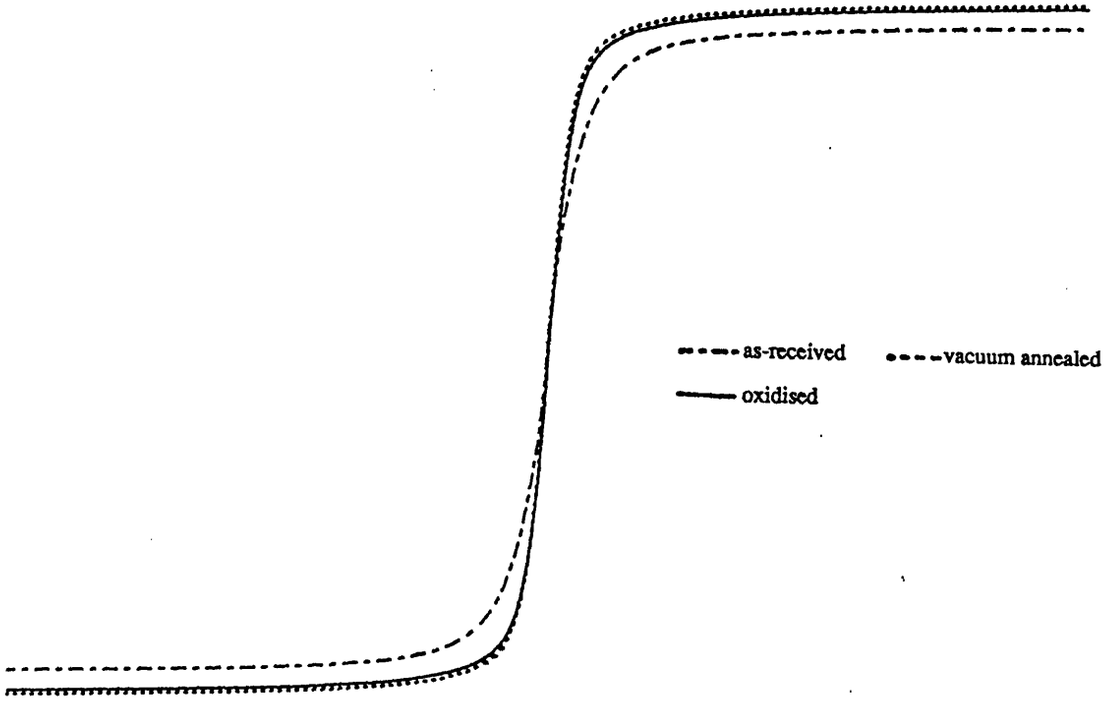

Figure 6.15 M-H LOOPS FOR $Fe_{78}Si_9B_{13}$

published) and hence the increase in the stress inhomogeneity will also be small and a small effect on the coercivity must therefore be expected. The effect of the oxide coating on the magnetisation energy will depend primarily on the differential thermal contraction of the metallic glass and the oxide layer as the sample is cooled from the anneal temperature. In this case, the effect again appears to be small.

Note that a well stress relieved sample of this alloy (10 minutes at 430°C in air) has a coercivity of approximately 2A/m. The annealing cycle used here, therefore may not have been sufficient to fully stress relieve the sample or may have introduced some crystallites (see section 6.3.2).

The oxidising anneal was found to produce no significant change in the coercivity of near-zero magnetostrictive alloy VITROVAC 6010. The coercivity was 1.8A/m in the as-received material and 2.1A/m after the anneal. This confirms that the oxide layer couples to the magnetic properties via the magnetostriction. In this material, the stress-magnetostriction coupling should be small and little change in coercivity is therefore expected due to either stress relief or the formation of an oxide coating. No vacuum annealed samples were, however,

available to enable the effects of the oxide layer to be isolated from the stress relief effects.

In summary, therefore, a surface oxide coating couples to the magnetic properties of the metallic glass via the strain-magnetostriction interaction. With a uniform coating, however, the effects of the oxide layer in these materials, were not severe.

CHAPTER 7

7 Conclusions and suggestions for further work

It has been shown in this document that magnetic measurements under dc and well controlled ac conditions can be used to indicate the behaviour of metallic glass alloys under resonant charging pulse conditions. The main results presented were obtained on two alloy compositions: VAC 6030 and METGLAS 2605 -SC. These results are summarised below.

7.1 The magnetic properties of VAC 6030: a summary

As-received samples of the zero magnetostriction alloy VAC 6030, wound into toroidal form exhibited low dc coercivites and high remanence ratios. Under ac and pulse conditions, however, these samples showed a high loss. Stress-relief of this alloy resulted in a higher dc coercivity and a lower remanence ratio. This was shown to be caused by pinning of the domain walls due to local self annealing during the cool. The ac and pulse losses of samples treated in this way were lower than those seen in the as-received alloy. However, a more gradual approach to saturation was seen.

Several treatments, aimed at eliminating the effects of local annealing, were investigated. These included fast-cooling the toroids from the anneal, and several types of field anneal. The fast cooled samples exhibited lower coercivities than the stress relief annealed and a slightly lower remanence ratio than the as-received. Under ac and pulse conditions, these samples showed the lowest loss observed after any treatment (except transverse field annealing). A rapid approach to saturation was also seen. Field annealing treatmemts, in all cases, were found to impair the pulse performance of this alloy. The transverse field anneal, although resulting low losses, produced a material with a low pulse permeability which is undesirable in switching applications. The longitudinally field annealed samples all exhibited low dc coercivities and high permeabilities but were found to show high losses under both ac and pulse conditions. Samples annealed in a saturating longitudinal field, were cooled at different rates in order to induce a varying component of longitudinal anisotropy. The ac and pulse responses of these samples were shown to exhibit a strong correlation with the cool rate. Successively slower cools lead to correspondingly higher values of ac loss. This was attributed to a reduction in the number of domain walls in the sample caused by increases in the

longitudinal component of anisotropy.

In addition to the heat treatments described above, some samples were surface scribed in an attempt to increase the number of active active domain walls in the sample. The toroids treated in this way, despite severe mechanical deformation in some cases, showed no change in their magnetic properties. This was attributed to the low magnetostriction of this material allowing little stress-magnetostriction coupling.

The fast cooled toroids, therefore, exhibited the best pulse performance achieved with this material. This treatment, however, is not feasible with practical toroids. Apart from the physical damage to the core which may occur on rapid cooling, high enough cool rates would be difficult to achieve in a practical core weighing several kilograms, or maybe a few tonnes.

7.2 The magnetic properties of METGLAS 2605-SC: a summary

In contrast to the Vacuumschmelze alloy, discussed above, local self annealing was shown not to be important in the magnetostrictve alloy METGLAS 2605-SC

despite the fact that this alloy is known to be susceptible to field annealing. This was attributed to the low value of induced anisotropy exhibited by this material coupled with the larger effects of the stress-magnetostriction interaction. This material was also found to be far more sensitive to annealing conditions and subsequent handling than the Vacuumschmelze material. In particular, great care was required in order to avoid crystallisation and post-annealing corrosion.

In the as-received state, because of this material's high magnetostriction, domain wall pinning at stress centres is of greater significance than in the VAC alloy. Some form of annealing treatment is therefore required in order to relieve the quenched-in and wound-in stresses. Although, under the annealing conditions chosen, full stress relief of this alloy was difficult to achieve without crystallising the sample, this problem could have been eliminated by annealing at a lower temperature. Stress-relief annealing was found to reduce the dc coervivity, increase the maximum induction reached and to produce a 'squarer' dc hysteresis loop. The stress relieved samples also showed improved magnetic properties under ac excitation. A higher flux swing was seen, the remanence ratio increased significantly but the ac

loss only rose slightly. Samples which were incompletely stress relieved (as seen from the dc coercivity) showed slightly better ac characteristics than the fully stress-relieved samples. Similar results were also seen under pulse conditions.

Longitudinally field annealed samples showed lower dc coercivities than the stress relieved, and higher remanence ratios. The ac and pulse losses, as with VAC 6030, were, however, higher. No trend with decreasing cool rate was evident with this material. The most likely explanation of this concerns the magnitude and the kinetics of anisotropy development in this alloy. It is known that METGLAS 2605-SC exhibits a low K_u and a high magnetostriction. It is therefore possible that any small changes in the induced anisotropy caused by varying the cool rate, are swamped by the effects of the stress-magnetostriction interaction. A further possibility is that, even at the highest cool rates used here, the induced anisotropy, K_u, reached its maximum value and that decreasing the cool rate led to no further increases in the anisotropy of this material.

In both of these alloys, therefore, the best pulse (and ac) performance was achieved after treatments which produced a significant component of off-axis

anisotropy - fast cooling in the case of VAC 6030 and incomplete stress relief in the case of the Allied Corporation material. Further sample treatments which should be investigated include rotational (Takayama, Matuda, Kudo, Tonomura and Mizoguchi,1981) and oblique angle (Fujimori, Yoshimoto and Morita,1980) field annealing. Both of these treatments result in a significant off-axis anisotropy resulting in more domain walls available for flux reversal, and consequently lower ac losses and higher ac permeabilities. Both of these treatments would avoid problems associated with self field annealing if this were important in the alloy under study.

It should be noted that, although METGLAS 2605-SC exhibits twice the saturation magnetisation of VAC 6030, the losses seen in this alloy under pulse and ac conditions were typically four times those seen in VAC 6030, ie, twice the loss per unit flux swing. However, for a given compression ratio, the volume of core material required has been shown to be proportional to ΔB^{-2}. Thus, if VAC 6030 were used, four times as much material would be required than if METGLAS 2605-SC were chosen. In addition, the price of the Co-based alloy is typically twice that of METGLAS 2650-SC. The initial cost of the core materials must therefore be offset against the reduced

losses offered by the low-magnetostriction alloy.

The above summarised the main experimental results of this project. The following indicates the properties required of a saturable inductor for use in a pulse compression system:-

i) High flux swing
ii) Many reverse domain present at reset
iii) Little domain wall pinning by stress centres or local anisotropy
iv) Square dc loop
v) Low ac losses (many walls present)
vi) Low magnetostriction to avoid core vibration

Some of these requirements, however, are contradictory. For example, if many reverse domains are present in the reset state, then the maximum flux swing which can be achieved has been reduced. The presence of many domain walls in this state also implies that the dc loop is not perfectly square. In addition, the longitudinal anisotropy required to produce a square dc loop, leads to high ac (and pulse) losses due a reduction in the walls available. In magnetostrictive materials, however, a longitudinal anisotropy may, also, be desirable for a different

reason - to reduce the magneto -strictive response of the core. The design of a pulse compression element is therefore a compromise between the above. The relative importances of core cost, losses, volume and vibration will be determined by the particular application.

The above summarises the results obtained as part of this project. The following sections will indicate areas of further work. These can be divided roughly into three areas:- comparison with flux reversal models, investigation of further treatments aimed at improving the pulse behaviour and, finally, scaling up to practical toroids and realistic repetition rates.

7.3 Comparison with flux reversal models

The ac and pulse results described in this work, have been discussed in terms of the number of moving walls in the toroidal samples, and the size of reverse domains existing in the reset state. The results obtained are consistent with reports in the literature concerning ac losses and with the segmented domain wall model developed by J.E.L. Bishop. Alternative explanations, of the initial pulse overshoot, for example, involving wall nucleation, have been discussed (Smith (1988) see chapter 2). In order to positively confirm the Bishop model, direct

observation of the domains present under the reset conditions are required. This would be difficult using the domain observation equipment presently available at Bath, particularly in toroidal samples, but may be possible, for example, using the Kerr magneto-optic technique.

7.4 Further sample treatments

In section 7.2, rotational and oblique angle field annealing were mentioned as possible treatments to enable the stress relief of metallic glass samples under conditions which would produce a domain structure suitable for low loss ac (and therefore pulse) behaviour. Both of these treatments, however produce an off-axis anisotropy with a consequent slow approach to saturation. Other treatments aimed at domain refinement, including surface oxidation and scribing, and controlled crystallisation, are likely to suffer from the same disadvantages. Some of these treatments have been investigated briefly in this project but require further investigation. Ultimately, whether or not these techniques are useful will depend upon the particular application.

7.5 A practical pulse compression element

Finally, the problems associated with the scaling up of the thin toroidal cores studied here, to practical pulse compression elements needs to be investigated. The problems which are likely to be encountered include the effects of non-uniform core reversal (see chapter 2), core heating and complex core resonances (at high PRFs). In addition, the effects of interlamina insulation on the magnetic properties of both thin and practical toroids should be studied. The inclusion of insulation after annealing is known to degrade the core response due to material stresses introduced on re-winding. This is also known to be less severe in alloys with a high longitudinal component of anisotropy (Smith and Nathasingh,1984). The inclusion of interlaminar insulation before the anneal, however requires the use of expensive insulation materials and can further complicate the already difficult process of uniformly annealing large cores.

REFERENCES

Avery R.K., B.Ae. internal report. JS 10537, (1986). Restricted: In Strict Confidence.

Avery R.K., B.Ae. Technical note 256/MATS/020D, (1987a).

Avery R.K., B.Ae. internal report. JS 10728, (1987b). Restricted: In Strict Confidence.

Baldwin, J.A.,jnr., Rev. Sci. Instr., 41, (1970), 468.

Barker, R.C., AIEE Transactions, 79, (1960), 482.

Beckley, P. Snell, D. and Lockhart, C., J. Appl. Phys., 57, (1985), 4212.Chapter 5

Birx, D.L., Cook, E., Hawkins, S., Poor, S., Reginato, L., Schmidt, J. and Smith, M., In: Digest of Technical papers; 4th IEEE Pulsed Power Conference. (M.F. Rose and T.H Martin, eds.). (1983), 231. New York: IEEE publishing services.

Bishop, J.E.L., Phys. stat. sol.(a), 7, (1971), 117.

Bishop, J.E.L., J. Phys. D: Appl. Phys., 6, (1973), 97.

Bishop, J.E.L., IEEE Trans. Mag., MAG-10, (1974), 1132.

Bishop, J.E.L., J. Phys. D: Appl. Phys., 9, (1976), 2095.

Bishop, J.E.L. and Williams, P., J. Phys. D: Appl. Phys., 10, (1977), 225.

Blundell, M., Overshott, K.J. and Graham, C.D.jnr., J. Appl. Phys., 50(3), (1979), 1598.

Boll, R., Hilzinger, R. and Warlimont, H. In: Glassy Metals: magnetic, chemical and structural properties (R. Hasagawa, ed), (1983), 183. Florida: CRC Press Inc.

Brenner, A. and Riddell, G., J. Res. Natl. Bur. Stand., 37, (1946), 31.

Brenner, A., Couch, D.E. and Williams, E.K., J. Res. natn. Bur. Stand., 44, (1950), 109.

Brill, R., Z. Kristallogr., 75, (1930), 217.

Brugel, D., Gibbs, M.R.J. and Squire, P.T., J. Appl. Phys., 64, (1988), 3149.

Buckel, W. and Hilsch, R. Z. Phys. 132, (1952), 420.

Cahn, R.W., Contemp. Phys., 21(1), (1980), 43.

Callen, E. and Callen, H.B, Phys. Rev. 129, (1963), 578.

Callen, E. and Callen, H.B, Phys. Rev. 139A, (1965), 455.

Chen, H.S. In: Amorphous Metallic Alloys (F.E. Luborsky, ed.), (1983), 169. London: Butterworths.

Chen, C-W., Magnetism and Metallurgy of Soft Magnetic Materials. (1986), New York: Dover Publications Inc.

Chu E.Y. In: Digest of technical papers; 4th IEEE Pulsed Power Conference. (M.F. Rose and T.H Martin eds.), (1983), 242. New York: IEEE publishing services.

Cullity, B.D. Introduction to Magnetic Materials. (1972), Reading, Massachusetts. Addison-Welsley.

Datta, A., DeCristofaro, N.J. and Davis, L.A., Proc. 4th Int. Conf. on Rapidly Quenched Metals, (1981), 1007.

Davis, L.A., J. Mat. Sci., 11, (1976), 711.

Drabovich, Y.U.I. and Krishtafov, I.A., USSR patent no. 626443, (1978).

Fähnle, M. and Kronmüller, H., J. Magn. Magn. Mat., 8, (1978), 149

Field, J.C.G., Private Communication, (1985).

Friedlaender. F.J., Trans. AIEE Communications and Electronics, 75, (1956), 268.

Friedlaender. F.J. and Leliakov, I.P., Trans. AIEE Communications and Electronics, 80, (1961), 269.

Fujimori, H. In: Amorphous Metallic Alloys (F.E. Luborsky, ed.), (1983),300. London: Butterworths.

Fujimori, H., Yoshimoto, H., Masumoto, T. and Mitera, T., J. Appl. Phys., 52(3), (1981), 1893.

Fujimori, H., Yoshimoto, H. and Morita, H., IEEE Trans. Mag., MAG-16, (1980), 1227.

Ganz, A.G., AIEE Transactions, 65, (1946), 177.

Gao, W. and Cantor, B., Acta Met., 36, (1988), 2293.

Gao, W. and Cantor, B. To be published in 'Acta Met.'

Gao, W. and Cantor, B. To be published in 'Int. J. of Rapid Solidification.'

Golding, E.W. and Widdis, F.C. Electrical Measurements and Measuring Instruments. (1963). London: Pittman and Sons.

Graham, C.D.,jr, In: Magnetic Properties of Metals and Alloys. (1958), 288. Cleveland: American Society for Metals.

Gubanov, A.I., Sov. Phys. Solid State, 2, (1960), 468.

Guo H.-Q., Kronmüller, H., Moser, N. and Hofmann, A., Scripta Metallurgica, 20, (1986), 185.

Haller, T.R. and Kramer, J.J., J. Appl. Phys., 41(3), (1970), 1036.

Hasagawa, R., In: Amorphous Semiconductors and Metals. (Hansen and Jaffe. eds.). 1986, 196. Oxford: Pergamon Press.

Hasagawa, R., Ramanan, V.R.V. and Fish, G.E., J. Appl. Phys., 53(3), (1982), 2276.

Helmiss, G., Z. Angew. Phys., 28, (1969), 24.

Herzer, G. and Hilzinger, H.R., In: Proc. Symp. Magnetic Poperties of Amorphous Metals. (A. Hernando, V. Madurga, M.C. Sanchez-Trujillo and M. Vazquez. eds.). 1987, 354. Amsterdam: Elsevier.

Jakubovics, J.P. Magnetism and Magnetic Materials. (1987). London: The Institute of Metals.

Jones, R.M., IEEE Trans. Mag., MAG-18, (1982), 1559.

Jones R.M., IEEE Trans. Mag., MAG-19, (1983), 2024.

Jones, R.M., Collins, A.J., and Cleaver, N.G., IEEE Trans. Magn., MAG-17, (1981), 2707.

Klement, W.,jr, Willens, R.H. and Duwez, P., Nature, 187, (1960), 869.

Kramer, J., Annln. Phys., 19, (1934), 37.

Krause, R.F. and Werner, F.E., IEEE Trans. Mag., MAG-17, (1981), 2686.

Kronmüller, H. and Fernengel, W. Phys. stat. sol.(a), 64, (1981), 593.

Kronmüller, H., Guo H.-Q., Fernengel, W., Hofmann, A. and Moser, N., Cryst. Latt. Defects and Amorph. Mat., 11, (1985), 135.

Kronmüller, H., Schäfer, R. and Schroeder, G. J. Magn. Magn. Mat., 6, (1977), 61.

Kui, H.W., Greer, A.L. and Turnbull, D., Appl. Phys. Letts., 45, (1984), 615.

Lee, D.H. and Evetts, J.E., Acta Met., 32, (1984), 1035.

Liebermann, H.H. In: Amorphous Metallic Alloys (F.E. Luborsky, ed.), (1983), 26. London: Butterworths.

Luborsky, F.E. ed. Amorphous Metallic Alloys (1983). London: Butterworths.

Luborsky, F.E. In: Amorphous Metallic Alloys (F.E. Luborsky, ed.), (1983), 1. London: Butterworths.

Luborsky F.E., Becker, J.J. and McCary, R.O. IEEE Trans. Magn., MAG-11 (1975), 1644.

Mader, S. and Norwick, A.S., Appl. Phys. Letts., 7, (1965), 57.

Mathias, R.A. and Williams, E.M. Trans. AIEE Communications and Electronics., 74(18), (1955), 169.
Mader, S. and Norwick, A.S., Appl. Phys. Letts., 7, (1965), 57.

McFarlane, J. and Harris, M.J., Proc. IEE, 105A, (1958), 395.

METGLAS is the registered trademark of Allied Corporation.

Melamud, M., Swartzendruber, L.J., Bennett, L.H., Cullen, J. and Wun-Fogle, M., J. Appl. Phys, 61, (1987), 3644.

Melville, W.S., Proc. IEE, 98(3), (1951), 185.
J. Appl. Phys., 61, (1987), 3644.

Menyuk, N. and Goodenough, J.B., J. Appl. Phys., 26(1), (1955), 8.

Moorjani, K. and Coey, J.M.D. eds. Magnetic Glasses, (1984). Amsterdam: Elsevier.

Naka, M., Nishi, Y. and Masumoto, T., Proc. 3rd Int. Conf. on Rapidly Quenched Metals,, (1978), 231.

Narita, K., Yamasaki, J., Fukunaga, H. and Hata, H., Proc. 4th Int. Conf. on Rapidly Quenched Metals, (1981), 1001.

Neau, E.L. In: Digest of technical papers; 4th IEEE Pulsed Power Conference. (M.F. Rose and T.H Martin, eds.), (1983), 246. New York: IEEE publishing services.

Néel, L., Journal de Physique et le Radium, 11, (1950), 49.

Néel, L., Journal de Physique et le Radium, 12, (1951), 339.

Nielsen, O.V., IEEE Trans. Mag., MAG-21, (1985), 2003.

O'Handley, R.C., J. Appl. Phys., 62(10), (1987), R15.

Ok, H.N. and Morrish, J. Appl. Phys. 53, (1982), 2276.

Pond, R.,jr and Maddin, R., Transactions of the metallurgical society of AIME, 245, (1969), 2475.

Pry, R.H. and Bean, C.P. J. Appl. Phys 29(3), (1958), 532.

Raskin, D. and Smith, C.H. In: Amorphous Metallic Alloys (F.E. Luborsky, ed.), (1983), 381. London: Butterworths.

Rees, D.W., Private Communication, (1988).

Rodbell, D.S. and Bean, C.P., J. Appl. Phys., 26(11), (1955), 1318.

Smith, C.H., IEEE Conf. Record 15th Power Modulator Symp., Baltimore, (1982), 22.

Smith, C.H.,IEEE Trans. Nuc. Sci., NS-30, (1983), 2918.

Smith, C.H., In: NATO ASI GLASS - current issues (A.F. Wright and J. Dupuy, eds.), (1984), 188.

Smith, C.H., J. Appl. Phys., 64(10), (1988a), 6032.

Smith, C.H., Private Communication, (1988b).

Smith C.H., IEEE Conf. Record 19th Power Modulator Symp., Hilton Head, (1988c), 336.

Smith, C.H. and Barberi, L., Proc. 5th IEEE Int. Pulsed Power Conf., Arlington, (1985), 664.

Smith C.H. and Nathasingh, D.M., IEEE Conf. Record 16th Power Modulator Symp., Arlington, (1984), 240.

Snoek, J.L., Physica, 5 (1938), 663.

Snoek, J.L., Physica, 6 (1939a), 161.

Snoek, J.L., Physica, 6 (1939b), 797.

Snoek, J.L., Physica, 8 (1941), 711.

Squire, P.T., Sheard, S.M., Carter, C.H. and Gibbs, M.R.J., J. Phys. E: Sci. Instrum. 21, (1988), 1167.

Squire, P.T., Private Communication, (1988).

Squire, P.T., Gibbs, M.R.J. and Thomas, A.P. To be published.

Stockton, M., Neau, E.L., and VanDevender, J.P. , J. Appl. Phys. 53(3), (1982), 2765.

Takayama, S., Matuda, T, Kudo, M., Tonomura, A. and Mizoguchi, T., Proc. 4th Int. Conf. on Rapidly Quenched Metals, (1981), 945.

Tan, K.S., IEEE Trans. Mag., MAG-22, (1986), 188.

Thottuvelil, V.J., Wilson, T.G., Miyazaki, I. and Owen, H.A.jnr., IEEE Power Electronics Specialists Conf., (1983), 168

Thottuvelil, V.J., Wilson, T.G. and Owen, H.A.jnr., IEEE Trans. Mag. MAG-20, (1984), 570.

VanDevender, J.P. and Reber, R.A. In: Digest of technical papers; 3rd IEEE Pulsed Power Conference. (A.H. Guenther and T.H Martin, eds.), (1981), 256. New York: IEEE publishing services.

VITROVAC (VAC) is the registered trademark of Vacuumschmelze, GmbH.

Whang, S.H. and Geissen, B.C. In: Rapidly Solidified Amorphous and Crystalline Alloys (B.H. Kear, B.C. Geissen and M. Cohen, eds.), (1982), 301. New York: Elsevier Sci. Publ.

Williams, H.J., Shockley, W. and Kittel, C., Phys. Rev., 80(6), (1950), 1090.

Winter, S.D., Kuenning, R.W. and Berg, G.G., IEEE Trans. Mag., MAG-6, (1970), 41.

Yamaguchi, K., Yoshizawa, Y. and Nakajima, S., Mat. Sci and Eng., 99, (1988), 95.